



## **Cation homeostasis in platelets**

\*\*\*\*\*

## **Kationen-Homöostase in Thrombozyten**

Thesis for a doctoral degree  
at the Graduate School of Life Sciences,  
Julius-Maximilians-Universität Würzburg,  
Section Biomedicine

submitted by

**Sanjeev Kiran Gotru**

from

Visakhapatnam, India

in

Würzburg, Germany, 2018

---

Denn Weisheit ist besser denn Perlen / vnd alles was man wündschen mag  
/ kan jr nicht gleichen. Jch Weisheit / wone bey der Witze / vnd ich weis guten  
Rat zu geben.

Die Sprüche Salomonis 08:11-12

For wisdom is better than rubies; and all the things that may be desired are  
not to be compared to it. I wisdom dwell with prudence, and find out  
knowledge of witty inventions.

Proverbs 08:11-12

జ్ఞానము ముత్యములకన్న శ్రేష్ఠమైనది విలువగల సొత్తులేవియు దానితో సాటి  
కావు. జ్ఞానమును నేను చాతుర్యమును నాకు నివాసముగా చేసికొనియున్నాను  
సదుపాయములు తెలిసికొనుట నాచేతనగును.

సామెతలు 08:11-12

---

---

Submitted on: .....

Office stamp

Members of the *Promotionskomitee*:

Chairperson: Prof. Dr. Thomas Dandekar

Primary Supervisor: Prof. Dr. Bernhard Nieswandt

Supervisor (Second): Prof. Dr. med. Guido Stoll

Supervisor (Third): Prof. Dr. Johan W. M. Heemskerk

Supervisor (Fourth): PD. Dr. rer. nat. Heike Hermanns

Date of Public Defence: .....

Date of Receipt of Certificates: .....

---

## Summary

Divalent cations are important second messengers triggering various signal transduction events in platelets. Whereas calcium channel blockers have an established antithrombotic effect and the regulation of  $\text{Ca}^{2+}$  homeostasis has been elucidated in platelets, the molecular regulation of  $\text{Mg}^{2+}$  and  $\text{Zn}^{2+}$  homeostasis has not been investigated so far.

In the first part of the thesis, the role of  $\alpha$ -type serine-threonine kinase linked to transient receptor potential cation channel, subfamily M, member 7 (TRPM7) in platelets was investigated. Using *Trpm7<sup>R/R</sup>* mice with a point mutation deleting the kinase activity, we showed that the TRPM7 kinase regulates platelet activation via immunoreceptor tyrosine-based activation motif (ITAM), hem(ITAM) and protease-activated receptor (PAR) signaling routes. Furthermore, *Trpm7<sup>R/R</sup>* mice were protected from *in vivo* thrombosis and stroke, thus establishing TRPM7 kinase as a promising anti-thrombotic target.

In the second part of the thesis, the role of TRPM7 channel in a megakaryocyte (MK) and platelet-specific knockout mouse, *Trpm7<sup>fl/fl-Pf4Cre</sup>*, was investigated. Here, we observed that depending on the type of stimulation, *Trpm7<sup>fl/fl-Pf4Cre</sup>* platelets showed either enhanced or inhibited responses. Although *Trpm7<sup>fl/fl-Pf4Cre</sup>* mice were thrombocytopenic, no differences to wildtype mice were observed in models of *in vivo* thrombosis and stroke. The above two studies highlight that inhibition of TRPM7 kinase but not the channel itself (in MKs and platelets) may be a promising anti-thrombotic strategy.

Besides TRPM7, we investigated the role of magnesium transporter 1 (MAGT1) in platelet  $\text{Mg}^{2+}$  homeostasis and found that MAGT1 primarily regulates receptor-operated calcium entry (ROCE) in platelets specifically upon GPVI activation. This physiological crosstalk is triggered by protein kinase C (PKC) isoforms. Platelets from *Magt1<sup>-/-</sup>* mice hyper-reacted to GPVI and thromboxane  $\text{A}_2$  (TXA $_2$ ) receptor stimulation *in vitro*. Consequently, *Magt1<sup>-/-</sup>* platelets were found to be pro-thrombotic in disease models of thrombosis and stroke.

To compare platelet ITAM-signaling to the immune system, we further investigated the role of MAGT1 in T and B cells. We described the primary role of MAGT1 in mice under pathogen-free conditions. *Magt1<sup>-/-</sup>* B cells showed dysregulated  $\text{Mg}^{2+}$  and  $\text{Ca}^{2+}$  homeostasis upon B-cell receptor activation, thereby altering Syk, LAT, phospholipase C (PLC) $\gamma$ 2 and PKC phosphorylation. In contrast to human MAGT1-deficient T cells, development and effector functions of mouse *Magt1<sup>-/-</sup>* T cells showed no alterations.

Finally, in the last part of the thesis, we described methods to measure intracellular free zinc [ $\text{Zn}^{2+}$ ] $_i$  in human and mouse platelets with storage pool disease (SPD). We propose to measure the [ $\text{Zn}^{2+}$ ] $_i$  status in SPD platelets as a relatively easy diagnostic to screen platelet granule abnormalities.

---

## Zusammenfassung

Zweiwertige Kationen sind wichtige sekundäre Botenstoffe, welche verschiedene Signaltransduktionsereignisse in Thrombozyten initiieren. Zwar wurde die Regulation der  $\text{Ca}^{2+}$  Homöostase in Blutplättchen bereits aufgeklärt und der Einsatz von Calciumkanalblockern zur antithrombotischen Therapie ausführlich diskutiert, die molekulare Regulation der  $\text{Mg}^{2+}$  und  $\text{Zn}^{2+}$  Homöostase in Thrombozyten und Megakaryozyten (MK) wurde bisher jedoch nicht untersucht.

Im ersten Teil dieser Thesis wurde die Rolle der  $\alpha$ -Typ Serin-Threonin Kinase des transienten Rezeptortyp Kation Kanals, Unterfamilie M, 7 (TRPM7) in Thrombozyten untersucht. Unter Verwendung von *Trpm7<sup>R/R</sup>* Mäusen mit einer Punktmutation in der Kinasedomäne, welche die Aktivität der Kinase blockiert, konnten wir zeigen, dass die TRPM7-Kinase die Thrombozytenaktivierung über Immunrezeptor-Tyrosin-basierte Aktivierungsmotive (ITAM), Hem(ITAM) und Protease-aktivierte Rezeptoren (PAR) reguliert. *Trpm7<sup>R/R</sup>* Mäuse waren vor *in vivo* Thrombose und Schlaganfall geschützt, was die TRPM7 Kinase als vielversprechendes antithrombotisches Zielprotein etabliert.

Im zweiten Teil wurde die Rolle des TRPM7 Kanals in einer Megakaryozyten (MK)- und Plättchen-spezifischen Knockout Maus (*Trpm7<sup>fl/fl-Pf4Cre</sup>*) untersucht. Wir konnten zeigen, dass *Trpm7<sup>fl/fl-Pf4Cre</sup>* Plättchen je nach Art der Stimulation erhöhte oder verminderte Reaktionen zeigten. Obwohl *Trpm7<sup>fl/fl-Pf4Cre</sup>*-Mäuse thrombozytopen waren, wurden keine Unterschiede in *in vivo* Thrombosemodellen und Schlaganfall beobachtet. Diese Studien heben hervor, dass die Hemmung der TRPM7 Kinase, aber nicht die des Kanal selbst (in MKs und Plättchen), eine vielversprechende anti-thrombotische Therapie sein könnte.

Neben TRPM7 untersuchten wir die Rolle von Magnesium Transporter 1 (MAGT1) in der  $\text{Mg}^{2+}$ -Homöostase in Thrombozyten und konnten zeigen, dass MAGT1 primär den Rezeptor-gesteuerten Calciuminflux (ROCE) spezifisch nach GPVI Aktivierung reguliert. Dieser physiologische Crosstalk wird durch Proteinkinase C (PKC) Isoformen vermittelt. Thrombozyten von *Magt1<sup>-/-</sup>* Mäusen reagierten *in vitro* hyperreaktiv auf GPVI und Thromboxan  $\text{A}_2$  (TXA<sub>2</sub>) Rezeptor Stimulation. Dementsprechend konnte auch gezeigt werden, dass *Magt1<sup>-/-</sup>* Plättchen in Modellen von Thrombose und Schlaganfall pro-thrombotisch wirkten.

Um die ITAM-Signalübertragung in Thrombozyten mit der in T und B Zellen zu vergleichen, untersuchten wir die Rolle von MAGT1 in Immunzellen. Wir überprüften die Rolle von MAGT1 in Mäusen unter pathogen-freien Bedingungen. *Magt1<sup>-/-</sup>* B Zellen zeigten eine dysregulierte  $\text{Mg}^{2+}$  und  $\text{Ca}^{2+}$  Homöostase nach Aktivierung des B Zell Rezeptors, wodurch Syk, LAT, PLC $\gamma$ 2 und PKC Phosphorylierung beeinflusst wurde. Im Gegensatz zu menschlichen MAGT1-defizienten T Zellen, zeigten *Magt1<sup>-/-</sup>* T Zellen keine Veränderungen in Entwicklung und Effektorfunktion.

---

Schließlich beschrieben wir im letzten Teil der Arbeit Methoden zur Messung des intrazellulären freien Zinks  $[Zn^{2+}]_i$  in humanen und murinen Thrombozyten mit Storage-Pool-Defekt (SPD). Wir unterbreiten in dieser Thesis, den  $[Zn^{2+}]_i$  Status in SPD Thrombozyten zu messen um nach Anomalien in den Thrombozyten-Granula zu suchen.

---

## Table of Contents

<b>1. Introduction</b> .....	<b>1</b>
1.1 Platelets and their role in blood circulation .....	1
1.2 Granule cargo in platelets .....	1
1.3 Platelet activation and thrombus formation.....	2
1.4 Central role of GPVI in platelet activation .....	4
1.5 Cation channels, stores and their role in platelet signaling .....	5
1.5.1 Calcium .....	5
1.5.2 Magnesium.....	8
1.5.3 Zinc .....	10
1.6 Roles of cations in clinical thrombosis and hemostasis .....	11
1.6.1 Calcium .....	12
1.6.2 Magnesium.....	13
1.6.3 Zinc .....	14
1.7 Thrombo-inflammation in stroke brain damage .....	15
1.7.1 Calcium .....	17
1.7.2 Magnesium.....	18
1.7.3 Zinc .....	19
1.8 Aims of the thesis.....	20
<b>2. Materials and Methods</b> .....	<b>22</b>
2.1 Materials .....	22
2.1.1 Chemicals.....	22
2.1.2 Cell culture materials .....	25
2.1.3 Kits .....	25
2.1.4 Commercially purchased antibodies .....	25
2.1.4.1 Unconjugated .....	25
2.1.4.2 Conjugated .....	26
2.1.4.3 Antibodies for immune cell analysis .....	26
2.1.4.4 Home made monoclonal antibodies.....	27
2.2 Methods.....	28
2.2.1 Generation and genotyping of mice. ....	28
2.2.1.1 <i>Trpm7<sup>R/R</sup></i> mice.....	28
2.2.1.2 <i>Magt1<sup>-/-</sup></i> mice.....	28
2.2.1.3 <i>Trpm7<sup>fl/fl-Pf4Cre</sup></i> mice .....	29
2.2.1.4 <i>Nbeal2<sup>-/-</sup>, Unc13d<sup>-/-</sup></i> mice .....	29
2.2.1.5 RNA preparation from tissues using RNeasy Kit.....	29
2.2.2 <i>In vitro</i> analysis of platelet function .....	30

2.2.2.1 Platelet preparation and washing.....	30
2.2.2.2 Aggregometry .....	30
2.2.2.3 Measurement of $[Mg^{2+}]_i$ or $[Zn^{2+}]_i$ on FACS Canto II.....	31
2.2.2.4 Measurement of $[Ca^{2+}]_i$ using fluorimeter .....	31
2.2.2.5 Flow Cytometry using FACS Calibur.....	32
2.2.2.6 Platelet life span .....	32
2.2.2.7 Measurements of second wave mediators.....	32
2.2.2.8 Mepacrine uptake and release.....	33
2.2.2.9 Adhesion under flow conditions .....	33
2.2.2.10 Determination of phosphatidylserine exposure in platelets.....	34
2.2.2.11 Spreading assay.....	34
2.2.2.12 Tyrosine phosphorylation.....	35
2.2.2.13 Confocal microscopy of platelets .....	35
2.2.3 <i>In vivo</i> analysis of platelet function.....	36
2.2.3.1 Tail bleeding and tMCAO model of stroke.....	36
2.2.3.2 Generation of BM chimera mice.....	36
2.2.4 Determination of $Mg^{2+}$ level in serum and platelets .....	36
2.2.5 Histology.....	37
2.2.6 Immune cell analysis .....	37
2.2.6.1 Flow cytometry with immune cells on FACS Canto II .....	37
2.2.6.2 B cell proliferation .....	38
2.2.6.3 Immunoblotting with immune cell lysates .....	38
2.2.6.4 Measurement of $[Ca^{2+}]_i$ in immune cells.....	39
2.2.6.5 Measurement of $[Mg^{2+}]_i$ in immune cells .....	39
2.2.6.6 Natural killer cell isolation and killing assay .....	40
2.2.7 Data analysis.....	40
<b>3. Results .....</b>	<b>41</b>
3.1 Analysis of kinase-dead TRPM7 knockin ( <i>Trpm7<sup>R/R</sup></i> ) mice.....	41
3.1.1 Platelet aggregation response upon activation .....	41
3.1.2 Calcium responses in <i>Trpm7<sup>R/R</sup></i> platelets .....	42
3.1.3 Tyrosine phosphorylation in <i>Trpm7<sup>R/R</sup></i> platelets.....	43
3.2 Analysis of <i>Trpm7<sup>fl/fl-Pf4Cre</sup></i> mice .....	44
3.2.1 Count, size, glycoprotein expression and $[Mg^{2+}]_i$ in platelets .....	44
3.2.2 Platelet reactivity in <i>Trpm7<sup>fl/fl-Pf4Cre</sup></i> mice .....	45
3.2.2.1 $Ca^{2+}$ responses.....	45
3.2.2.2 Agonist-induced platelet activation in <i>Trpm7<sup>fl/fl-Pf4Cre</sup></i> mice.....	46
3.2.2.3 PS exposure in <i>Trpm7<sup>fl/fl-Pf4Cre</sup></i> platelets .....	47



3.2.2.4 Aggregation in <i>Trpm7<sup>fl/fl-Pf4Cre</sup></i> platelets .....	48
3.2.2.5 Defective aggregate formation of <i>Trpm7<sup>fl/fl-Pf4Cre</sup></i> platelets under flow .....	50
3.2.3 TRPM7 deficiency does not affect the stroke outcome .....	50
3.3 Analysis of <i>Magt1<sup>-/-</sup></i> mice .....	51
3.3.1 Normal organogenesis and thrombopoiesis in <i>Magt1<sup>-/-</sup></i> mice .....	51
3.3.2 Platelet reactivity in <i>Magt1<sup>-/-</sup></i> mice .....	53
3.3.2.1 Increased Mg <sup>2+</sup> efflux in <i>Magt1<sup>-/-</sup></i> platelets in response to GPVI stimulation .....	53
3.3.2.2 Increased Ca <sup>2+</sup> influx in <i>Magt1<sup>-/-</sup></i> platelets upon activation .....	54
3.3.2.3 Abnormal Mg <sup>2+</sup> and Ca <sup>2+</sup> responses in <i>Magt1<sup>-/-</sup></i> platelets can be normalized by Mg <sup>2+</sup> supplementation <i>in vitro</i> .....	55
3.3.2.4 Normal integrin activation and P-selectin exposure in <i>Magt1<sup>-/-</sup></i> platelets .....	56
3.3.2.5 Partially impaired integrin outside-in activation in <i>Magt1<sup>-/-</sup></i> platelets .....	57
3.3.2.6 Increased TXA <sub>2</sub> and ATP release in <i>Magt1<sup>-/-</sup></i> platelets .....	58
3.3.2.7 TRPC6 inhibition or Mg <sup>2+</sup> supplementation normalizes aggregation in <i>Magt1<sup>-/-</sup></i> platelets .....	59
3.3.2.8 Increased thrombus formation of <i>Magt1<sup>-/-</sup></i> platelets on collagen <i>ex vivo</i> can be rescued by Mg <sup>2+</sup> supplementation or by TRPC6 inhibition .....	60
3.3.2.9 Functional crosstalk between MAGT1, PKC and TRPC6 .....	63
3.3.3 Altered hemostasis in <i>Magt1<sup>-/-</sup></i> mice .....	65
3.3.4 Enhanced susceptibility of <i>Magt1<sup>-/-</sup></i> mice towards ischemic brain infarction .....	65
3.3.5 Dispensable role of <i>Magt1<sup>-/-</sup></i> CD4 <sup>+</sup> T cells in stroke development .....	67
3.4 Investigation of T and B cells in <i>Magt1<sup>-/-</sup></i> mice .....	67
3.4.1 T cell subsets in various lymphoid organs and peripheral blood of <i>Magt1<sup>-/-</sup></i> mice .....	68
3.4.2 Magnesium and calcium responses in <i>Magt1<sup>-/-</sup></i> CD4 <sup>+</sup> cells .....	68
3.4.3 Effector function of NK cells in <i>Magt1<sup>-/-</sup></i> mice .....	69
3.4.4 B cell subsets in various lymphoid organs and peripheral blood of <i>Magt1<sup>-/-</sup></i> mice .....	70
3.4.5 Magnesium and calcium responses in <i>Magt1<sup>-/-</sup></i> B cells .....	71
3.4.6 Tyrosine phosphorylation in <i>Magt1<sup>-/-</sup></i> B cells .....	72
3.4.7 Proliferation of B cells in <i>Magt1<sup>-/-</sup></i> mice .....	73
3.5 Identification of the Zn <sup>2+</sup> store in human and murine platelets .....	73
3.5.1 [Zn <sup>2+</sup> ] <sub>i</sub> quantification .....	73
3.5.2 Defective Zn <sup>2+</sup> homeostasis in storage pool deficient human platelets .....	75
3.5.3 Effects of Zn <sup>2+</sup> supplementation and TPEN pretreatment on FluoZin-3 loaded murine platelets .....	77
3.5.4 Platelet zinc is essential for fibrin formation under flow .....	78
3.5.5 Higher total zinc content in <i>Nbeal2<sup>-/-</sup></i> platelets .....	79
<b>4. Discussion .....</b>	<b>81</b>
4.1 TRPM7 kinase controls calcium responses in arterial thrombosis and stroke in mice .....	81

4.2 Multiple roles of TRPM7 in the regulation of Mg <sup>2+</sup> and Ca <sup>2+</sup> homeostasis.....	83
4.3 Defective Mg <sup>2+</sup> transport enhances receptor-operated Ca <sup>2+</sup> entry in murine platelets and thereby results in accelerated thrombosis and stroke.....	84
4.4 Imbalanced cation homeostasis dysregulates B cell development and signaling of MAGT1-deficient B cells.....	87
4.5 Defective Zn <sup>2+</sup> homeostasis of human and mouse platelets with $\alpha$ - and $\delta$ -storage pool disorders.....	89
<b>5. Concluding remarks and future plans .....</b>	<b>91</b>
<b>6. References.....</b>	<b>93</b>
<b>6. Appendix.....</b>	<b>106</b>
6.1 List of abbreviations .....	106
6.2 Publications .....	108
6.2.1 Original articles.....	108
6.2.2 Oral presentations .....	109
6.2.3 Poster presentations.....	109
6.3 Acknowledgement.....	109
6.5 Affidavit.....	114
6.6 Eidesstattliche Erklärung.....	114

## 1. Introduction

### 1.1 Platelets and their role in blood circulation

Platelets are small, anucleate cells in the blood safeguarding hemostasis and vascular integrity. They are released from bone marrow (BM) megakaryocytes (MKs) by a process called thrombopoiesis [1]. Platelet number in humans is between 150,000 – 450,000/ $\mu\text{L}$  with a diameter of about 2-4  $\mu\text{m}$ , while in mouse, it is 1,000,000 platelets/ $\mu\text{L}$  in the circulating blood with a diameter of about 1-2  $\mu\text{m}$ . Under physiological conditions, platelets circulate in the blood surveilling the whole body for damages in the vasculature. Circulating platelets are cleared by the reticuloendothelial system in the liver and spleen after a period of 10 days in human and 5 days in mice. Under rheological forces in the circulation, platelets attach to proteins of the exposed vascular extracellular matrix (ECM) upon injury [2]. These attached platelets recruit further platelets and establish the formation of a platelet plug, which eventually seals the disrupted endothelium preventing blood loss. This function of platelets plays a role in primary hemostasis. Under certain pathological conditions like atherosclerotic plaque rupture, uncontrolled platelet activation and thrombus formation or thromboembolism can occur leading to various cardio- and cerebrovascular abnormalities [3]. Here, myocardial infarction and stroke are two major causes of death worldwide [4]. A detailed investigation into the precise activatory/inhibitory mechanisms of platelet signaling in myocardial infarction and stroke could help to develop better treatment strategies. Although divalent cations act as second messengers in various cell activation pathways during thrombosis and stroke, their regulatory role in platelets received less attention.

### 1.2 Granule cargo in platelets

Platelets contain different types of storage vesicles, i.e  $\delta$ -granules and lysosomes. The  $\alpha$ -granules contain many different proteins in their cargo ranging from growth factors [platelet factor 4 (PF4), transforming growth factor beta (TGF- $\beta$ )], adhesion molecules (P-selectin, GPIIb $\alpha$ -IX-V and GPVI) and certain factors of the coagulation cascade (factor V [5], VWF, fibronectin, zinc, fibrinogen and factor XIII [6]). On the other hand, the  $\delta$ -granules contain a rather limited number of non-proteinaceous compounds in their cargo including ADP, ATP, serotonin (5-HT) and calcium [7-10]. Lysosomal granules contain cathepsins, carboxypeptidases, acid hydrolases and many other enzymes required for various physiological activities [11].

The intracellular free  $\text{Ca}^{2+}$  concentration [ $\text{Ca}^{2+}$ ]<sub>i</sub> plays a crucial role in platelet activation. Using genetic approaches and (or) chemical inhibitors in mice, targeting specifically  $\text{Ca}^{2+}$  responses,

the pivotal role of  $\text{Ca}^{2+}$  as an important second messenger in platelet signaling has been demonstrated [8, 12, 13]. Other important divalent cations like magnesium ( $\text{Mg}^{2+}$ ), which blocks N-methyl-D-aspartate (NMDA) receptor, and zinc ( $\text{Zn}^{2+}$ ), acting as a neurotoxin beyond certain levels, are described to be important in several diseases, including stroke [14, 15], myocardial infarction [16, 17]) and in immune compromised situations [18, 19]). In comparison to  $\text{Ca}^{2+}$ , the roles of  $\text{Mg}^{2+}$  and  $\text{Zn}^{2+}$  received relatively less attention with regard to their functional relevance and the associated transport mechanisms in platelets, MKs and other cell types.

In a pilot experiment, to investigate the intracellular free magnesium  $[\text{Mg}^{2+}]_i$  store, platelets isolated from knockout mice with various granule abnormalities have been were loaded with Mag-Fluo-4 dye which is highly specific for  $[\text{Mg}^{2+}]_i$ , and flow cytometry was performed. Platelets isolated from *Unc13d*<sup>-/-</sup> mice with an abolished  $\delta$ -granule secretion and a reduced  $\alpha$ -granules release [20] showed defective  $[\text{Mg}^{2+}]_i$  release upon CRP or thrombin stimulation. On the other hand, platelets from *Nbeal2*<sup>-/-</sup> mice lacking  $\alpha$ -granules [21] showed a reduced  $[\text{Mg}^{2+}]_i$  level already in the resting stage, as well as after activation with CRP or thrombin (**Figure 1**). This result suggests that  $\text{Mg}^{2+}$  could be stored in both in the  $\delta$ - and  $\alpha$ -secretory granules and is released during platelet activation.

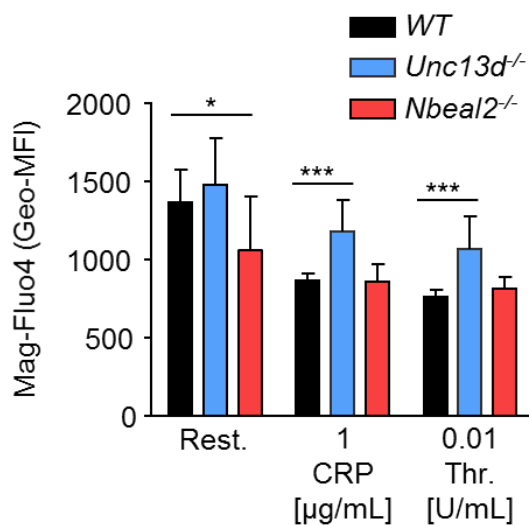


**Figure 1. Intracellular free magnesium  $[\text{Mg}^{2+}]_i$  quantification in murine platelets:** Platelets from the indicated control or knockout mouse strains were loaded with Mag-Fluo-4 dye, and fluorescence intensity was measured in the indicated conditions. Rest.: Resting; CRP: Collagen related peptide; Thr.: Thrombin. Results shown from two three independent experiments (n = 3). Student's t-test was used as a test of significance. \*P < 0.05, \*\*P < 0.01, \*\*\*P < 0.001. (S.K. Gotru, unpublished observation).

### 1.3 Platelet activation and thrombus formation

Platelet activation and adhesion to the site of injury under flow conditions is highly dependent on the prevailing rheological conditions. In larger arteries or vessels, the flow rate is faster at the center while it reduces close to the vessel wall, due to the drag between the adjacent layers of blood [22]. It is well described that under high shear stress, platelet (GP)Ib-V-IX binding to

von Willebrand factor (VWF) cause platelet tethering. Due to the fast off-rate of this interaction it is insufficient to cause stable adhesion at lower shear conditions. Nevertheless, the GPIb-VWF interaction keeps platelets in close contact to an exposed ECM during vessel wall injury; this process is called “platelet rolling” [23]. Subsequently, platelets stably attach to exposed collagen via the GPVI receptor. This interaction is of low affinity, but initiates a series of tyrosine phosphorylation events triggered by intracellular signal transduction, which shifts the platelet integrins to a high-affinity state and further causes the release of second wave mediators, adenosine diphosphate (ADP) and TXA<sub>2</sub> [24]. These mediators, along with locally produced thrombin, in addition activate G protein coupled receptors (GPCRs). These events lead to full platelet activation and thrombus growth [25] (**Figure 2**).

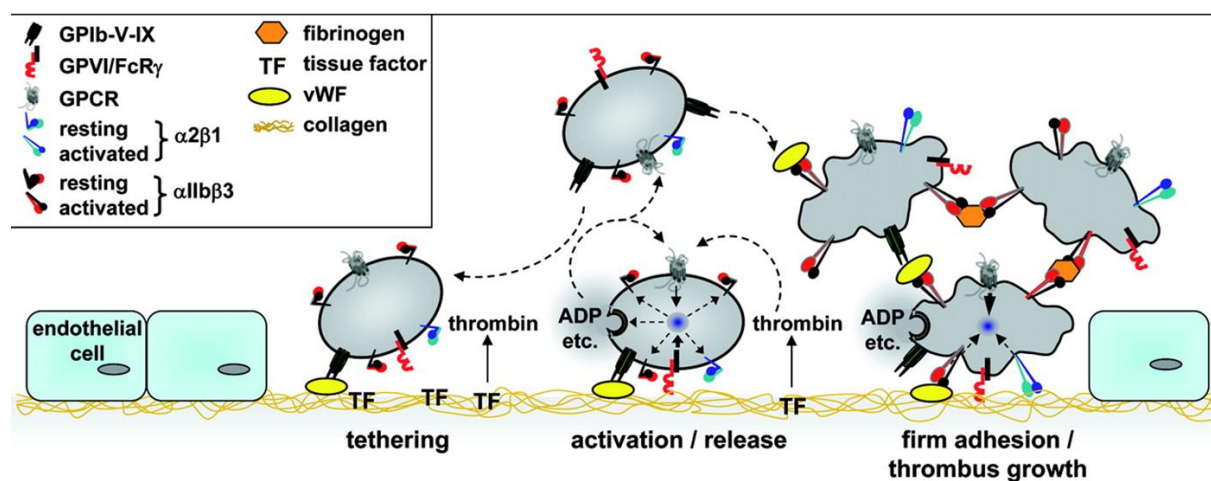


**Figure 2. Stages of platelet activation:** Graphic depicting the different steps of platelet activation. Vessel wall injury exposes extracellular matrix proteins and GPIb-V-IX interaction with VWF at high shear facilitates platelet rolling across the vessel wall. This step is followed by collagen-GPVI interactions, the release of second wave mediators (ADP and TXA<sub>2</sub>). Together with the locally produced thrombin, this reinforces further platelet activation. Subsequently, integrin  $\alpha_{IIb}\beta_3$  activation, stable platelet adhesion and aggregation induce the growth of a stable thrombus. (Graphic is taken from [2]).

Several antiplatelet agents including acetylsalicylic acid (ASA), P2Y<sub>12</sub> receptor antagonists (clopidogrel, prasugrel) inhibit platelet activation, however at the expense of an increased risk of bleeding complications. Although an increase in cytosolic Ca<sup>2+</sup> in platelets was detected in the growing thrombus *in vivo* [26], fluxes of Mg<sup>2+</sup> and Zn<sup>2+</sup> have not been investigated in this context. On the other hand, ionic Mg<sup>2+</sup> was found to be essential for platelet activation, since it regulates integrin  $\alpha_{IIb}\beta_3$  heterodimer formation [27, 28]. Ionic Zn<sup>2+</sup> is released during platelet activation and is considered to play a crucial role in hemostasis [29]. A detailed investigation of the role of different divalent cations could further help to identify new therapeutic strategies.

### 1.4 Central role of GPVI in platelet activation

Platelets express two collagen receptors, the GPVI and integrin  $\alpha_2\beta_1$ . Besides these two receptors, also integrin  $\alpha_{IIb}\beta_3$  and GPIb-V-IX allow platelet binding to collagens via immobilized VWF in an indirect manner [24, 30]. It has been shown that  $Mg^{2+}$  enhances the cleavage of ultralarge VWF by a disintegrin and metalloproteinase with a thrombospondin type 1 motif, member 13 (ADAMTS-13), thereby reducing platelet aggregation on collagen [31]. Collagen is a natural and potent platelet GPVI activator. Besides collagen, non-physiological agonists like collagen-related peptide (CRP) [32] or the snake venom toxin convulxin [33] also activate GPVI. Structurally, GPVI contains two IgG domains with sites for collagen binding, a stalk with O-glycosylation sites, a transmembrane domain and a cytoplasmic tail (**Figure 3**) [34]. The cytoplasmic tail is proline-rich and forms the site for the binding of Src-family tyrosine kinases [35]. GPVI is non-covalently associated with the immunoreceptor tyrosine-based activation motif (ITAM)-bearing IgG Fc receptor (FcR) $\gamma$ -chain [36].

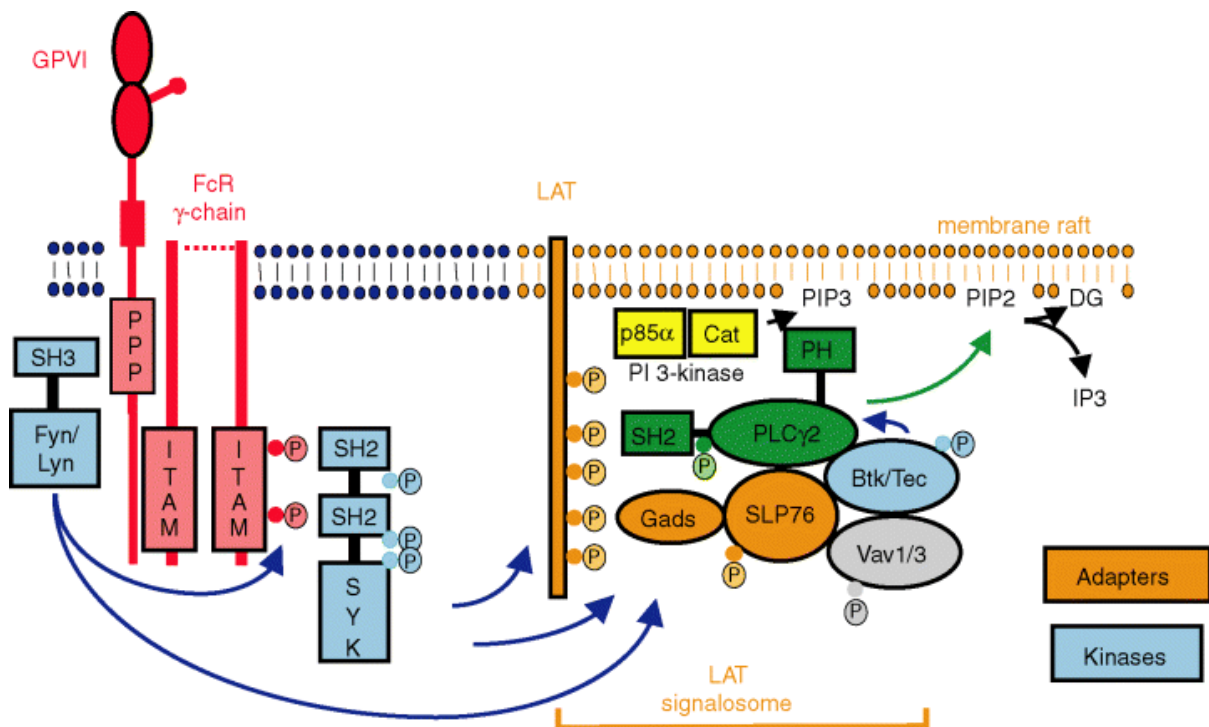


**Figure 3. The GPVI signalosome:** Graphic showing how GPVI receptor crosslinking lead to a series of signal transduction events, involving tyrosine phosphorylation by Src kinases (Fyn and Lyn) on Syk and the LAT signalosome. In addition, PLC $\gamma$ 2 phosphorylation in the LAT signalosome, other adaptor proteins and kinases like Gads, SLP76, Btk/Tec are depicted. In addition, Grb2 (not depicted). (Graphic taken from [37]). SH3: SRC homology 3 domain; Fyn, Lyn: Src-family tyrosine kinases; P: phosphorylation; ITAM: immunoreceptor tyrosine-based activation motif; SH2: Src homology 2 domain; SYK: Spleen tyrosine kinase; PI3-kinase: Phosphoinositide 3-kinase; PH: pleckstrin homology domain; Gads: Grb2-related adapter downstream of Shc; PLC $\gamma$ 2: phospholipase C  $\gamma$ 2; Btk: bruton's tyrosine kinase; Tec: Tyrosine-protein kinase; PIP3: Phosphatidylinositol (3,4,5)-trisphosphate; PIP2: Phosphatidylinositol 4,5-bisphosphate; DG/DAG: diacylglycerol; IP3: Inositol trisphosphate; GPVI: Glycoprotein VI; LAT: linker for activation of T cells.

The collagen binding to GPVI induces crosslinking of the receptor and subsequent activation of its ITAM by Src-family tyrosine kinases (Fyn and Lyn). This step further leads to the recruitment of the spleen tyrosine kinase (Syk), which is phosphorylated either by the Src-family kinases or is autophosphorylated. Syk activation is followed by tyrosine phosphorylation of linker for activation of T cells (LAT). Various adapter proteins like growth factor receptor-bound protein 2 (Grb2), Grb2-related adapter downstream of Shc (Gads) and SH2 domain-containing leukocyte protein (SLP76) together with LAT constitute the LAT signalosome [37]. Together, these signaling events culminate in the activation of the cytoplasmic enzyme phospholipase C  $\gamma$ 2 (PLC $\gamma$ 2). The signal transduction events downstream of Syk in platelets [37] show a resemblance to the T cell receptor (TCR) signaling in immune cells [38]. Mice deficient in PLC $\gamma$ 2 were found to be protected for arterial thrombosis *in vivo* through impaired GPVI signaling events [39]. In contrast, platelets derived from mice overexpressing PLC $\gamma$ 2 appeared to be hyperreactive, resulting in a pro-thrombotic phenotype *in vivo*. Platelets from these mice indeed showed an increased response to GPVI and CLEC2 agonists *in vitro* [40]. Although numerous studies described the role of GPVI signalosome in early steps of platelet activation, its role in later steps of platelet activation (subsequent to Ca<sup>2+</sup> entry and TXA<sub>2</sub> release) still remains elusive.

## 1.5 Cation channels, stores and their role in platelet signaling

### 1.5.1 Calcium

Platelet activation is mediated by increased [Ca<sup>2+</sup>]<sub>i</sub>, which enhances the enzymatic activities of calpain, calmodulin and other Ca<sup>2+</sup>-dependent enzymes, thereby facilitating actin rearrangements, integrin activation and granule secretion [41]. Two major routes for Ca<sup>2+</sup> entry mechanisms have been described in platelets, namely store-operated Ca<sup>2+</sup> entry (SOCE) and receptor-operated Ca<sup>2+</sup> entry (ROCE) [8, 42]. In platelets, the endoplasmic reticulum (ER) resident stromal interaction molecule 1 (STIM1) senses the emptying of Ca<sup>2+</sup> stores upon receptor stimulation. When the Ca<sup>2+</sup> level becomes reduced in stores, STIM1 translocates to the plasma membrane and activates Ca<sup>2+</sup> release-activated (CRAC) channels. The four transmembrane domain channel protein, ORAI1, appears to act as a major SOCE channel in platelets [43, 44]. It is the functional coupling of STIM1 to ORAI1 that induces SOCE. Consequently, *Orai1*<sup>-/-</sup> and *Stim1*<sup>-/-</sup> mouse platelets are characterized by a severely defective SOCE upon activation [13, 44]. Moreover, *Stim1*<sup>-/-</sup> platelets showed a reduced Ca<sup>2+</sup> store content. In a mouse model with constitutively active STIM1 (*Stim1*<sup>Sax/+</sup>), an increased basal [Ca<sup>2+</sup>]<sub>i</sub> level in the platelet cytoplasm was observed [45]. This suggests that hyperactive STIM1 causes a constitutive activation of SOCE, most likely through ORAI1. The increase in [Ca<sup>2+</sup>]<sub>i</sub> in

*Stim1<sup>Sax/+</sup>* platelets could not be normalized by the Ca<sup>2+</sup> pumps sarco/endoplasmic reticulum Ca<sup>2+</sup>-ATPase (SERCA) or plasma membrane Ca<sup>2+</sup> ATPase (PMCA), thus indicating a crucial role of STIM1 in regulating [Ca<sup>2+</sup>]<sub>i</sub> in both resting and activated platelets [45].

In activated platelets, PLC catalyzes the hydrolysis of phosphoinositide-4,5-bisphosphate (PIP<sub>2</sub>) resulting in the generation of inositol 1,4,5-trisphosphate (IP<sub>3</sub>) and 1,2-diacylglycerol (DAG) metabolites. IP<sub>3</sub> binds to the IP<sub>3</sub> receptor (IP<sub>3</sub>R), which in turn triggers the release of Ca<sup>2+</sup> from the endoplasmic reticulum and other IP<sub>3</sub> sensitive organelles [46]. DAG on the other hand activates protein kinase C (PKC) isoforms and binds to the transient receptor potential cation channel, subfamily C, member 6 (TRPC6) enhancing the channel activity [47]. The current literature presents contradictory results about the role of TRPC6 in platelet activation. One group showed that Ca<sup>2+</sup> influx through TRPC6 is essential for MK proliferation [48]. Yet, TRPC6 deficiency in mice did not alter platelet count or size, indicating a dispensable role of TRPC6 in megakaryopoiesis and platelet production. Another group showed that an abolished TRPC6 function in mice resulted in inhibition of the platelet reactivity. In yet another *Trpc6<sup>-/-</sup>* mouse model, no differences in platelet activation or thrombus formation were reported [42, 48-50].

To understand the functional redundancy between SOCE and ROCE, ORAI1 and TRPC6, a double knockout mouse strain (*Orai1<sup>-/-</sup>/Trpc6<sup>-/-</sup>*) was generated. In that study, thapsigargin was used as a selective inhibitor of the sarco/endoplasmic reticulum Ca<sup>2+</sup>-ATPase (SERCA). TG inhibits refilling of the Ca<sup>2+</sup> store and hence induces a continuous emptying of the Ca<sup>2+</sup> stores. In the *Orai1<sup>-/-</sup>/Trpc6<sup>-/-</sup>* platelets, a further reduction of TG-mediated SOCE was observed when compared to *Orai1<sup>-/-</sup>* platelets [8]. This suggested a physiological link between ORAI1-mediated SOCE and TRPC6-induced ROCE. In addition, it appeared that both phospholipase D (PLD) and PLC could mediate a functional crosstalk between ORAI1 and TRPC6, thereby increasing DAG production. Under certain pathological conditions, an enhanced ORAI1 activity thus can increase DAG production, which then further may enhance TRPC6 channel activity [8]. These studies implied that a more detailed analysis of TRPC6 channel function is required to understand the role of ORAI1-mediated SOCE in regulating the TRPC6 channel activity.

Yet another route of Ca<sup>2+</sup> entry in platelets is provided by the P2X<sub>1</sub> receptors. These operate as extracellular ATP-regulated Ca<sup>2+</sup> channels, inducing a rapid, short-living Ca<sup>2+</sup> influx in platelets. Members of the P2X family are encoded by seven different genes (*P2X1-P2X7*). Depending on the cell type and multimerization, these proteins can constitute an active Ca<sup>2+</sup> channel [51]. Interestingly, P2X<sub>1</sub> becomes desensitized in washed platelets, an event that can be protected by the ATP/ADP-degrading apyrase. The ATP-induced, P2X<sub>1</sub>-mediated Ca<sup>2+</sup> influx even under these conditions is lasting for upto 10-20 s [52]. Some studies showed that the P2X<sub>1</sub> channel can amplify the P2Y<sub>1</sub> receptor-mediated Ca<sup>2+</sup> influx, and that the purinergic



receptors thus synergize in calcium signaling [53, 54]. In MKs, it was found that P2Y<sub>12</sub> receptor stimulation triggers a TRP-induced cation current, in co-operation with P2X<sub>1</sub> receptors via the phosphoinositide 3 kinase (PI3K) route. On the other hand, in platelets P2X<sub>1</sub> can act in synergy with P2Y<sub>1</sub> to amplify Ca<sup>2+</sup> fluxes via the IP<sub>3</sub> and PLC route [53, 54].

Concerning Ca<sup>2+</sup> pumps, human platelets express PMCA1, PMCA4 [55] and SERCA3a, SERCA2b isoforms [56]. The released Ca<sup>2+</sup> after platelet activation is either pumped back to the intracellular stores via SERCAs, or pumped out of the cell by PMCAs, thereby decreasing the level of [Ca<sup>2+</sup>]<sub>i</sub> [53, 55-59]. The isoform SERCA3 may be specifically expressed in acidic vesicle stores. Platelets from *Serca3*<sup>-/-</sup> mice showed a partially defective Ca<sup>2+</sup> store content, indicating a specific role of SERCA3 in maintaining the Ca<sup>2+</sup> store content. Furthermore, Ca<sup>2+</sup> store release and Ca<sup>2+</sup> influx were also reduced in *Serca3*<sup>-/-</sup> platelets. Consequently, a partial inhibition of aggregation and granule secretion was observed [60]. This was accompanied by a prolonged tail bleeding time and delayed *in vivo* thrombus formation in *Serca3*<sup>-/-</sup> mice.

The predominantly expressed PLC isoforms in platelets are PLCβ<sub>2</sub>, β<sub>3</sub> and γ<sub>2</sub> [61, 62]. The PLCβ isoform is solely regulated by G-protein coupled receptor (GPCRs) activation through the α-subunit of G<sub>q</sub> and G<sub>i</sub>, whereas the PLCγ<sub>2</sub> activity is regulated via GPVI [24] and C-type lectin-like receptor-2 (CLEC-2) activation [63]. GPVI liganding induces the activation of the Syk-LAT-PLCγ<sub>2</sub> signaling cascade, which results in Ca<sup>2+</sup> store depletion [24]. Downstream of PLC, DAG also activates the Ca<sup>2+</sup> and DAG-regulated guanine nucleotide exchange factor 1 (CalDAG-GEF1) apart from PKCs and TRPC6, thereby transducing the activating signals to integrins [8, 64]. Moreover, Ca<sup>2+</sup> store-dependent activation of CalDAG-GEF1 is an important step in Rap1b and ERK activation, TXA<sub>2</sub> synthesis and granule secretion [65].

There are three classes of PKC isoforms. The classical isoforms α and β (Ca<sup>2+</sup> and DAG-dependent), the novel isoforms δ, ε, η, and θ (DAG-dependent and Ca<sup>2+</sup>-independent) and the atypical isoforms ζ and ι/λ (Ca<sup>2+</sup>- and DAG-independent) [66-69]. The role of inhibitory or activatory actions of PKC isoforms in platelet physiology is unclear. Some studies report PKCε expression in mouse platelets, but not in humans platelets [70], whilst other find translocation of PKCε in activated human platelets [71]. Some PKC isoforms can directly bind and phosphorylate TRPC6 and inhibit its channel activity, whereas other can enhance Ca<sup>2+</sup> entry mechanisms, thus suggestive of the diverse roles of PKC isoforms in Ca<sup>2+</sup> signaling.

### 1.5.2 Magnesium

Elevated  $[Ca^{2+}]_i$  was observed under conditions of hypomagnesemia in different cell types [72]. Although  $Ca^{2+}$  and  $Mg^{2+}$  homeostasis appeared to be connected and regulated, the exact molecular mechanism of how an imbalanced  $Mg^{2+}$  homeostasis can interfere with  $Ca^{2+}$  homeostasis is still unclear. Concerning platelets,  $Mg^{2+}$  can antagonize  $Ca^{2+}$  responses, whereby an excess of extracellular  $Mg^{2+}$  strongly inhibits platelet aggregation [73]. The molecular composites of  $Mg^{2+}$  channels and transporters and their regulatory roles in platelet physiology have not yet been investigated.

In mammals, primary  $Mg^{2+}$  stores are located in the muscles, bones, and liver. Under conditions of reduced nutritional  $Mg^{2+}$  supplementation (or impaired  $Mg^{2+}$  resorption), these stores can maintain normal levels of plasma  $Mg^{2+}$  for longer periods without indications of  $[Mg^{2+}]_i$  deficit. In MKs and platelets, the  $[Mg^{2+}]_i$  stores have not yet been identified, but the dense tubular system (DTS), mitochondria, and the Mg-ATP complex have been proposed as potential  $Mg^{2+}$  stores in mammalian cells [74]. The cytosolic concentration of  $[Mg^{2+}]_i$  is the result of a balance of  $Mg^{2+}$  influx through the plasma membrane, intracellular free  $Mg^{2+}$   $[Mg^{2+}]_i$  storage, and  $Mg^{2+}$  efflux. Our group investigated the mRNA expression profiles of more than twenty  $Mg^{2+}$  transporters and channels in mouse platelets. Among them, only TRPM7, MAGT1, and tumor suppressor candidate 3 (TUSC3) were found to be predominantly expressed, while other known transporters were not detectable [75]. This suggests that only a limited number of  $Mg^{2+}$  channels and transporters may regulate  $Mg^{2+}$  homeostasis in (mouse) platelets.

The TRPM7 channel is constitutively active, thereby allowing slow permeation of  $Mg^{2+}$  into the cytoplasm of resting cells [76]. Reducing the levels of  $Mg^{2+}$  or ATP in the cytosol results in activation of TRPM7, thus suggesting that both  $[Mg^{2+}]_i$  and  $[ATP]_i$  are important regulators of its activity [77]. TRPM7 consists of six trans-membrane segments, cytoplasmic N- and C-termini. The C-terminus is linked to an atypical  $\alpha$ -kinase domain (**Figure 4**). Auto-phosphorylation of the kinase domain of TRPM7 enhances kinase-substrate interactions leading to serine/threonine phosphorylation of different proteins. However, only a limited number of endogenous substrates of TRPM7 kinase have been identified so far, including PLC, calpain and myosin IIa [78, 79].

Global deletion of *Trpm7* in mice resulted in embryonic lethality. Tissue-specific deletion of the *Trpm7* floxed gene in the T cell lineage was compatible with life, but caused defective thymopoiesis [80]. An abolished TRPM7 function *in vitro* was accompanied by growth arrest [81]. Selective deletion of the kinase domain of TRPM7 in knock-in mice resulted in altered  $Mg^{2+}$  homeostasis [82]. In this case, lower  $Mg^{2+}$  concentrations were measured in the blood, urine and bones, in comparison to control mice. When the mutant mice received a  $Mg^{2+}$

deficient diet, increased mortality was observed, suggestive for an accelerated development of hypomagnesemia. Our group showed that reduced channel activity of TRPM7 can cause thrombocytopenia in humans and mice [75]. This reduced the  $Mg^{2+}$  content in platelets, thereby increasing the activity of myosin IIa, which in turn resulted in cytoskeletal abnormalities. A  $Mg^{2+}$  supplementation could normalize the proplatelet formation defect of mutant MKs, highlighting the regulatory role of TRPM7-mediated  $Mg^{2+}$  influx in megakaryopoiesis and platelet function [75].

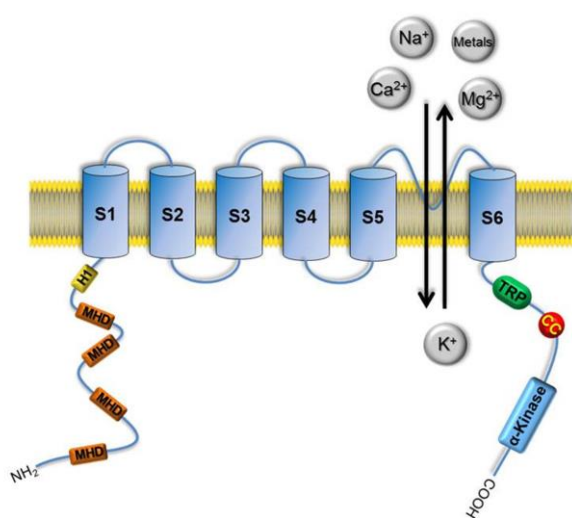


**Figure 4. TRPM7 channel and kinase domain:** Graphic showing the different domains, N and C termini of TRPM7 channel. Every single subunit of TRPM7 consists of six transmembrane segments (S1-S6), pore-forming loop (arrows indicated), a cytoplasmic N-terminus, containing a hydrophobic region (H1) and four homology regions (MHD), and a cytoplasmic C-terminus linked to an atypical serine/threonine protein kinase domain. Since TRPM7 is a non-selective cation channel, the graphic depicts various monovalent and divalent cation fluxes across the pore of the channel (Graphic is taken from [83]).

The MAGT1 transporter contains five TM domains, a short N-terminus with a signal peptide and a longer cytoplasmic tail with putative phosphorylation sites. The crystal structure of MAGT1 is not yet described. However, using hydropathy profile analysis, it was found that the five TM domains in MAGT1 consist of  $\alpha$ -helical structures. The first extracellular loop of MAGT1 contains an N-glycosylation site, four putative cyclic adenosine monophosphate (cAMP) and PKC-dependent phosphorylation sites, whilst the C-terminus lacks similar phosphorylation sites [84].

A low  $Mg^{2+}$  diet in mice was found to enhance MAGT1 expression in different tissues, such in comparison to animals fed with a diet containing normal level of  $Mg^{2+}$ . In addition, knockdown of MAGT1 in mammalian cells resulted in a low level of  $[Mg^{2+}]_i$ , implying a role of this transporter in cellular  $Mg^{2+}$  homeostasis [85]. Interestingly, the gene expression of *Magt1* is upregulated in *Trpm7*<sup>-/-</sup> cells, enabling these cells to increase the uptake of extracellular  $Mg^{2+}$ . Over-expression of human *Magt1* in *Trpm7*<sup>-/-</sup> cells could also rescue a severe growth impairment [86]. This indicates a partial functional redundancy between *Magt1* and *TRPM7*.

Ionic  $Mg^{2+}$  can exert several regulatory functions in immune cells, *e.g.* affecting proliferation, cell cycle progression and differentiation [87, 88]. Recently, new  $Mg^{2+}$  transporters and channels have been identified that regulate  $Mg^{2+}$  homeostasis in T lymphocytes [89]. Among these, MAGT1 may play a pivotal role in the XMEN syndrome, *i.e.* X-linked immunodeficiency with magnesium defect, Epstein-Barr virus infection, and neoplasia syndrome [18]. MAGT1 deficiency in such patients leads to a lowering in the  $[Mg^{2+}]_i$  in resting T cells, and to an impaired signaling after activation of the TCR, which could be reverted by  $Mg^{2+}$  supplementation. Interestingly, ionomycin or phorbol-12-myristate-13-acetate (PMA) mediated T cell activation was normal in patients with XMEN syndrome, indicating a proximal defect in TCR signaling. However, PLC $\gamma$ 1 activity was reduced in MAGT1-deficient human T cells [18].

Although MAGT1-related diseases are frequently characterized by dysgammaglobulinemia and an increased number of circulating CD19<sup>+</sup> cells, patients do not present with obvious activation defects in B cells upon IgM stimulation [89], which suggested that dysregulated T cell effector functions are major drivers of the associated disorders. The MAGT1-deficient patients are frequently infected with Epstein-Barr virus, which induces lymphoproliferative diseases such as Hodgkin's, Burkitt's and non-Hodkin's B cell lymphomas. Decreased levels of the receptor NKG2D on natural killer (NK) cells may account for the defective NK cell-mediated recognition of infected B cells [89], thereby reducing the immune responses against viral infections. To date, MAGT1-deficient animal models mimicking the human XMEN syndrome have not been established.

### 1.5.3 Zinc

$Zn^{2+}$  circulates in blood plasma at a concentration of 10-20  $\mu$ M, but only a small fraction of it exists in free ionic form (0.1-0.5  $\mu$ M), which can be taken up by blood cells [90]. Ionic  $Zn^{2+}$  modulates the function of several enzymes, *e.g.* regulates the structure of zinc finger domains, induces diverse signaling events as a second messenger, and acts as a cofactor in metabolic pathways. The  $Zn^{2+}$  concentration in serum was found to be higher than in blood plasma, suggesting that activated platelets release a significant amount of  $Zn^{2+}$  during blood clotting [91]. However, the authors of this paper were unable to identify the  $Zn^{2+}$  store in platelets and detected only  $Mg^{2+}$  and  $Ca^{2+}$  in the dense granules [92]. It was therefore postulated that during the clotting process  $Zn^{2+}$  slowly leaks through the plasma membrane. Later, a study showed that extracellular  $Zn^{2+}$  increases the cytosolic and  $\alpha$ -granule  $Zn^{2+}$  concentrations in platelets [6]. Based on the results, both  $\alpha$ -granules (40%) and the cytoplasm (60%) were postulated as  $Zn^{2+}$  stores in platelets [6]. In addition,  $Zn^{2+}$  binds to fibrinogen, albumin, histidine-rich glycoprotein and factor (F)XIII, present in the  $\alpha$ -granules of platelets [93]. While there is

evidence that  $Zn^{2+}$  modulates the coagulation cascade and the contact activation system [94], the precise platelet  $Zn^{2+}$  store and its function in the regulation of hemostasis still awaits experimental evaluation.

In mammals, zinc transporters are encoded by 24 different solute-linked carrier genes (*Slc30a/Slc39a*) and are grouped into two protein families, called Zrt-/Irt-like protein (ZIP) and Zn transporter (ZnT) [95]. ZIP family members mediate  $Zn^{2+}$  influx, thereby increasing the cytoplasmic  $Zn^{2+}$  concentrations [96]. The ZnT isoforms regulate  $Zn^{2+}$  efflux from the cytosol to the extracellular space or into intracellular organelles, thus reducing the cytoplasmic  $Zn^{2+}$  concentration [97]. Up to date, the molecular composite of  $Zn^{2+}$  transporters and their role in MKs and platelets have not been investigated at the molecular level.

### 1.6 Roles of cations in clinical thrombosis and hemostasis

Interfering with platelet function can severely alter the hemostatic function, leading to life-threatening bleeding complications. So far, GPVI [98], P2X<sub>1</sub> [99] and FXII [100] have been proposed as safe anti-thrombotic targets, since blocking these molecules results in a protection from *in vivo* thrombosis, but induces no more than mild bleeding in animal models. In humans, Revacept, a soluble dimeric GPVI-Fc fusion protein, it was shown that this drug could inhibit platelet GPVI-specific responses without altering the hemostatic function. Revacept also did not affect platelet GPCR-induced responses [101].

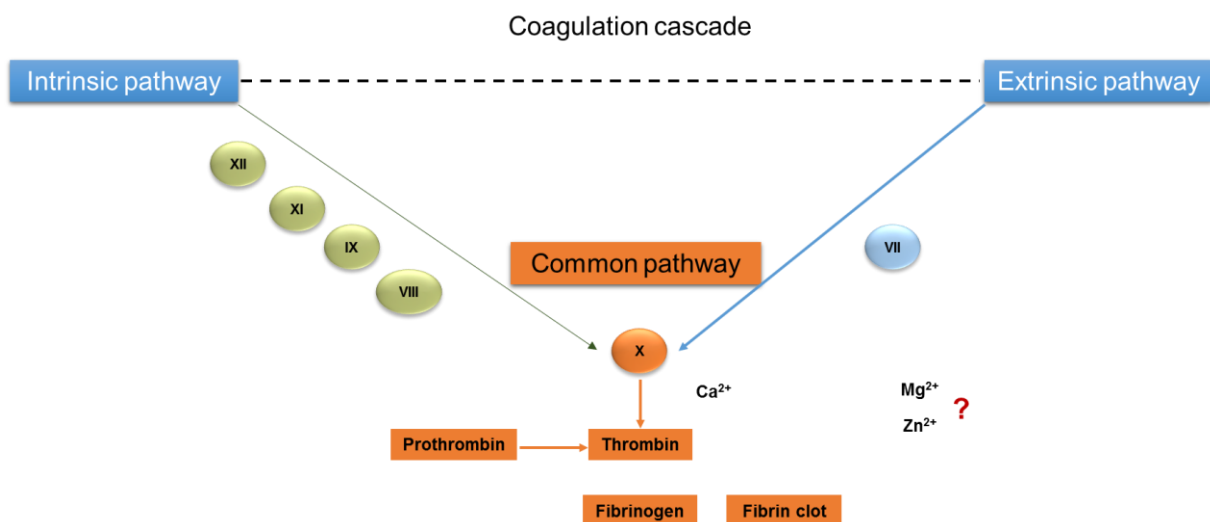


**Figure 5. Coagulation cascade:** Graphic depicting the involvement of various factors and  $Ca^{2+}$  in the coagulation cascade. Roman numbers refer to coagulation factors that are activated in cascade. See also text. (Graphic is modified from [102-105]).

The coagulation cascade is divided into extrinsic and intrinsic pathways, both of which converge in the activation of FX. The extrinsic pathway is triggered by the interaction of tissue factor and activated factor VII (FVIIa) [102]. Few studies showed that FVIIa can bind platelets during FX activation [103]. The intrinsic pathway encompasses activatory steps of coagulation factors XII, XI, IX and VIII. In brief, FXI is activated by FXII, prekallikrein and high molecular weight kininogen. FXIa activates FIX to FIXa, which along with FVIII activates FX [104] (**Figure 5**).

Previous studies applying knockout mouse models for proteins involved in  $\text{Ca}^{2+}$  transport such as ORAI1, STIM1, TRPC6 and  $\text{P2X}_1$  revealed the *in vivo* relevance of  $\text{Ca}^{2+}$  for thrombosis and hemostasis [13, 42, 44, 99]. In this thesis, the roles of  $\text{Ca}^{2+}$ ,  $\text{Mg}^{2+}$ , and  $\text{Zn}^{2+}$  in thrombosis and hemostasis are described in the following sections.

### 1.6.1 Calcium

Platelet reactivity in thrombus formation requires the activation of various pathways. Initially, via hem(ITAM) involving GPVI and CLEC-2 receptor stimulation [106, 107], and in later stages, via GPCR activation, involving stimulation via the protease-activated receptors (PARs), ADP receptors and thromboxane receptors [108]. Signal transduction due to the activation of these pathways culminates in an increase in  $[\text{Ca}^{2+}]_i$ . Various  $\text{Ca}^{2+}$  influx channels have been identified to be involved in the regulation of thrombus growth. *In vivo* imaging of  $\text{Ca}^{2+}$  signaling during thrombus formation, using adoptive transfer of Fura-2 labeled platelets, revealed a marked increase specifically in platelets that were recruited at the injured vessel wall. This observation underlines the importance of elevated  $[\text{Ca}^{2+}]_i$  in the propagation of thrombus growth, specifically upon high shear stresses *in vivo* [109].

Thrombus growth *in vivo* depends on integrin  $\alpha_{IIb}\beta_3$ - and  $\text{P2Y}_{12}$ -dependent signaling for the recruitment of platelets by already activated platelets [26]. Similarly, ORAI1-mediated SOCE appears to be one of the driving forces for thrombus formation via the (hem)ITAM-PLC $\gamma$ 2 signaling axis [110]. Accordingly, *Orai1*<sup>-/-</sup> mice were protected in a model of mechanical injury of the abdominal aorta, in which thrombosis is mainly triggered by exposed collagen. In contrast, upon  $\text{FeCl}_3$ -induced injury of mesenteric arteries, where thrombus growth is mainly driven by thrombin, the thrombosis time appeared to be normal. On the other hand, *Stim1*<sup>-/-</sup> mice were protected in both models of *in vivo* thrombosis. The differences between *Orai1*<sup>-/-</sup> and *Stim1*<sup>-/-</sup> mice in thrombus formation highlights the importance of the  $\text{Ca}^{2+}$  store content, which

is reduced only in *Stim1*<sup>-/-</sup> platelets, but not in *Orai1*<sup>-/-</sup> platelets. Emptying of the Ca<sup>2+</sup> stores seems to be crucial for *in vivo* thrombosis, perhaps by enhancing the procoagulant activity of activated platelets within the growing thrombus. Considering hemostasis, *Orai1*<sup>-/-</sup> mice showed no obvious change in bleeding times, whereas *Stim1*<sup>-/-</sup> mice showed prolonged bleeding times to a variable extent [44].

The *in vivo* relevance of a second major route of Ca<sup>2+</sup> influx in platelets, *i.e.* DAG-mediated ROCE, for arterial thrombosis is differently discussed in the literature. It has been reported that TRPC6 knockout mice (*Trpc6*<sup>-/-</sup>) show normal arterial thrombosis and bleeding time compared to control mice [42]. In contrast, others have shown that either pharmacological inhibition or genetic deletion of TRPC6 (*Trpc6*<sup>-/-</sup>) in mice resulted in a protection in models of arterial thrombosis and a significantly altered hemostatic function. In this case, the protection from arterial thrombosis was attributed to an impaired platelet reactivity downstream of the TXA<sub>2</sub> receptor [49, 50]. Nevertheless, further investigation is necessary to understand the underlying molecular mechanisms.

A further route of platelet Ca<sup>2+</sup> influx relevant for *in vivo* thrombosis is mediated by the P2X<sub>1</sub> receptor. Platelets isolated from P2X<sub>1</sub> knockout mice (*P2x1*<sup>-/-</sup>) showed a reduced aggregation response upon stimulation with collagen, were protected in a laser injury induced model of *in vivo* thrombosis (high shear), and displayed improved survival upon collagen/epinephrine-induced thromboembolism. Of note, bleeding time was normal in these mice [99]. Mice overexpressing P2X<sub>1</sub> showed enhanced aggregation responses upon stimulation with low doses of collagen or to the stable TXA<sub>2</sub> analog U46619. Furthermore, an increased surface coverage under flow on collagen *ex vivo*, and a rapid thromboembolism were observed after collagen/epinephrine injection *in vivo*. However, these mice also displayed a normal bleeding time [111]. These results clearly demonstrated the contribution of P2X<sub>1</sub> to collagen-dependent thrombus formation, but a redundant function in hemostasis.

### 1.6.2 Magnesium

To date, only a few studies reveal the importance of dysregulated Mg<sup>2+</sup> homeostasis in the development of cardiovascular diseases, thrombosis, stroke or atherosclerosis [112]. Increased platelet reactivity is observed in the development of cardiovascular diseases. In a clinical setting, Mg<sup>2+</sup> supplementation was found to have a beneficial effect on coronary artery disease, suggesting that combined Mg<sup>2+</sup> supplementation can be a novel treatment strategy for this disease condition [113]. A study using an *ex vivo* perfusion system (Badimon chamber) showed the beneficial effects of Mg<sup>2+</sup> supplementation in blood from cardiovascular patients [114]. Similarly, in rats undergoing transverse arteriotomy, it was shown that topical application

or intravenous injection of  $Mg^{2+}$  could reduce thrombus size *in vivo* [115]. Supplemented  $Mg^{2+}$  can also modulate endothelial cells to release nitric oxide and prostaglandins, which induce vasodilation and inhibit thrombus growth [116]. In swine, using an *ex vivo* arteriovenous shunt model, it was found that  $Mg^{2+}$  supplementation reduced the thrombus weight, when blood is perfused at a high shear on the exposed shunts [117]. In rats, using a model of *in vivo* thrombosis (arteriotomy), it was demonstrated that  $Mg^{2+}$  injection prior to surgery resulted in thrombo-protective effects. Rats receiving  $Mg^{2+}$  showed a reduced time to full vessel occlusion and had fewer events of thromboembolism, compared to control animals. This study, however, provided only limited mechanistic information [118]. So far,  $Mg^{2+}$  supplementation seems to be a safe antithrombotic therapeutic approach without adverse effects, thus highlighting the necessity to identify the molecular composition of the  $Mg^{2+}$  transport mechanism in platelets, endothelial and vascular smooth muscle cells.

### 1.6.3 Zinc

Gordon *et al.* previously identified that a low  $Zn^{2+}$  level in the blood from patients is associated with an increased bleeding tendency and a prolonged clotting time [119]. In the plasma  $Zn^{2+}$  levels are tightly regulated by dietary zinc intake and are considered to play a crucial role in blood clotting. Reduced  $Zn^{2+}$  uptake in the body may alter platelet aggregation responses and hemostatic function, suggestive for a role of systemic  $Zn^{2+}$  in platelet physiology [120]. Ionic zinc is known to regulate several steps of the coagulation cascade to activate plasma factors and the contact system. It directly interact with FXII, which leads to a conformational change in this coagulation factor, improving its susceptibility for enzymatic activation [121, 122]. In addition, platelet-derived  $Zn^{2+}$  can mediate FXI binding to glyocalicin (*i.e.* the ectodomain of GPIb) [123] and potentiate platelet tyrosine phosphorylation [10, 124]. Electron microscopic studies showed a two-fold increase in fibrin fiber diameter in the presence of  $Zn^{2+}$  [125]. Additionally,  $Zn^{2+}$  aids in the binding of FXI to activated platelets, thereby affecting the thrombin generation pathway. Extracellular  $Zn^{2+}$  can thereby accelerate the clotting process. Ionic  $Zn^{2+}$  also binds the plasma protein histidine-rich glycoprotein, thereby regulating processes such as apoptosis, antimicrobial activity and adhesion of immune cells [126]. Although these studies revealed the involvement of  $Zn^{2+}$  in different steps of the coagulation and platelet activation pathways, this topic has so far obtained no more than little attention.

Platelets incubated with a high concentration of  $ZnCl_2$  can increase their  $\alpha$ -granule  $Zn^{2+}$  content, likely along with fibrinogen uptake through the integrin  $\alpha_{IIb}\beta_3$  receptors [6]. Besides this, there are indications that extracellular  $Zn^{2+}$  can potentiate platelet reactivity, independently of  $TXA_2$  and serotonin release [127]. Whereas these studies underline the importance of  $Zn^{2+}$



for platelet reactivity and coagulation, mouse models and human platelets with hypo- or hyper-zincemia have not been investigated to date. An incidental paper indicates that the chelation of  $[Zn^{2+}]_i$  reduces thrombin- and CRP-induced platelet aggregation [10], suggesting that  $Zn^{2+}$  transporters can regulate platelet activation. However, the expression pattern of the transporters and the exact molecular mechanisms, by which  $Zn^{2+}$ -dependent aggregation responses are regulated are still unknown.

### **1.7 Thrombo-inflammation in stroke brain damage**

To study stroke, various experimental models of ischemic infarction in animals has been in practice [128]. Nevertheless, most widely used model of stroke in animals is the transient middle cerebral artery occlusion (tMCAO). Here, a small filament is advanced to the origin of the middle cerebral artery (MCA) via the internal carotid artery from 30 min to 1 h (depending on the required severity of the injury). Occlusion of the vessel with the filament simulates vessel closure caused by an embolized thrombus in humans. Later, the filament is removed to allow reflow of the blood. This still results in a full infarct build up in the MCA within 24 h post reflow of the blood. The observed infarct is due to 'reperfusion injury' which can be visualized by tetrazolium chloride (TTC) staining, where the live tissue stains red and the dead tissue remains unstained [129]. For many years pathological thrombus formation was considered to be the major cause of infarct progression during stroke. Nevertheless, pharmacological intervention (thrombolysis) to resolve the thrombus resulted in intracranial bleeding and no clinical improvement [130, 131]. Additionally, two independent research groups demonstrated that GPIIb/IIIa receptor blockade in humans or mice caused either a lethal intracerebral hemorrhage or no benefit in stroke outcome in the surviving animals [132, 133]. This gave the first report that targeting early platelet adhesion and activation, rather a complete inhibition of platelet aggregation, could be a better therapeutic option. It was also understood that platelet aggregation mediated by GPIIb/IIIa is not mandatory for infarct progression [133]. Although these studies gave a compelling evidence that platelet GPIIb-IIIa binding to be crucial during stroke, a question still remained if this weak interaction could lead to a profound infarct progression. The use of a GPVI blocking antibody (JAQ1) significantly protecting the animals from stroke progression with no intracranial bleeding, highlighted the importance of GPIIb-VWF-GPVI signaling nexus in the pathology of stroke [133]. Apart from this, platelet GPIIb also interacts with coagulation factor FXII, HMWK, thrombin, Mac-1 (expressed on lymphocytes and neutrophils) and P-selectin [134], underlining the importance of platelets in mediating the complex interactions with both the coagulation cascade and the immune system during stroke progression. It is also well known that T cells are involved in the inflammatory responses

caused by stroke. Recombination activating gene 1-deficient (*Rag1*<sup>-/-</sup>) mice lacking lymphocytes when transplanted with *WT* CD4<sup>+</sup> or CD8<sup>+</sup> T cells could develop infarct volumes normally in tMCAO. On the other hand, *Rag1*<sup>-/-</sup> mice transplanted with *WT* B cells still showed defective infarct volume in stroke, indicating that B cells might not be important for stroke progression [135, 136]. Considering these findings, the study of stroke progression emerged into a more inflammatory setting rather just as an ischemic insult, and the term ‘thrombo-inflammatory’ disease best applies to stroke. Several studies also highlighted T cell-derived cytokines like tumor necrosis factor alpha (TNF)- $\alpha$  [137], interferon (IFN)- $\gamma$  [138] and interleukin (IL)-17 [139] to be promoting thrombo-inflammation.

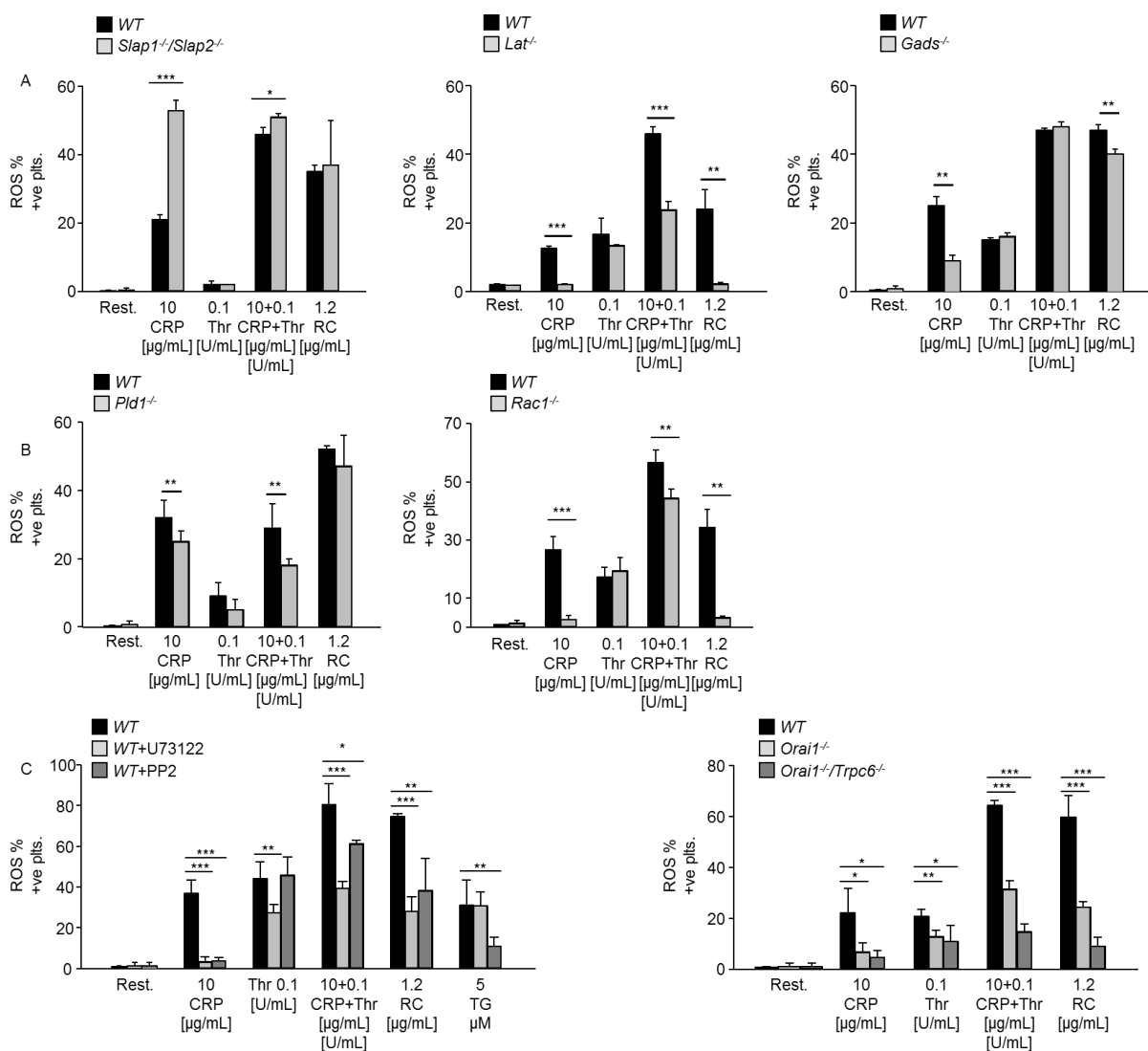


**Figure 6. ROS levels in platelets:** (A-C) ROS measured upon indicated stimulations using flow cytometry in H2DCFDA stained platelets. Results from three independent experiments are presented (n = 4). ROS: reactive oxygen species; Rest.: resting; Thr: thrombin; CRP: collagen-related peptide; RC: Rhodocytin; TG: Thapsigargin. Student's t-test was used as a test of significance. \*P < 0.05, \*\*P < 0.01, \*\*\*P < 0.001. (S.K. Gotru unpublished observation).

Stroke progression after re-perfusion injury is first mediated by resident microglial cells which release reactive oxygen species (ROS) [140], cytokines [141] and matrix metalloprotease-9 (MMP-9) [142]. The released mediators further lead to the recruitment of circulating leukocytes, increase the permeability of the blood-brain barrier (BBB) and induce neuronal death [143]. Additionally, glutathione peroxidase-3 (GPx-3) a plasma protein that scavenges reactive oxygen species (ROS) deletion in mice (*GPx-3<sup>-/-</sup>*) resulted in an increased infarct volume in the stroke which correlated to an increased occurrence of platelet-dependent thrombosis in an *in vivo* model of thromboembolism [144]. However, the exact role of the platelet signaling machinery in ROS production needs a detailed investigation. In a pilot experiment, using the fluorescent dye H2DCFDA (specific for ROS) in flow cytometry, we studied the levels of ROS in various knockout mice. Results indicate that the adaptor proteins SLAPs, as negative regulators, while molecules associated with the GPVI signalosome (LAT and GADS) and cytoplasmic enzyme PLD as positive regulators for ROS production. Platelets from *Rac1<sup>-/-</sup>* mice also showed a defective ROS release upon activation. Use of PLC or PP2 inhibitors also showed a reduced ROS release in activated platelets, indicating a prominent role of PLC enzyme and Src-family kinases to platelet released ROS (**Figure 6**). Calcium channel proteins ORAI1 and TRPC6 are also crucial for ROS production in activated platelets. Nevertheless, the exact role of other cation channel transport proteins and the physiological role of platelet ROS still needs to be investigated during a stroke. All these experiments were performed in suspension, again indicating that platelet aggregation is not mandatory for ROS release during a stroke.

### 1.7.1 Calcium

In the stroke, a dysregulated  $\text{Ca}^{2+}$  homeostasis induces cell death, strongly influences vascular integrity and endothelial cell function. Blood-brain barrier is disrupted in this process causing intracranial bleeding [145]. A tMCAO model of stroke has been established in mice and rats to mimic reperfusion-induced ischemic infarction [146]. This experimental stroke model resembles in several aspects the pathological process of ischemic brain infarction in humans. In the ischemic brain, pronounced activation of glutamate receptors accounts for tissue necrosis which further enhances PLC- and  $\text{IP}_3$ -dependent  $\text{Ca}^{2+}$  mobilization and consequently accelerates SOCE [147]. In line with this, a local accumulation of  $\text{Ca}^{2+}$  in the ipsilateral/ipsilesional region of the brain tissue was detected after 24 h in rats subjected to tMCAO [148].

In humans, a randomized double-blinded placebo clinical trial in 186 stroke patients showed a protective effect for the  $\text{Ca}^{2+}$  channel blocker nimodipine. This study followed the positive

effects of nimodipine for 6 months and only a few patients died during this period, while survivors showed a significantly improved neurological outcome as compared to patients receiving placebo. Surprisingly, the protective effects of nimodipine were restricted to male patients [149]. In mice, genetic ablation of SOCE through ORAI1 or STIM1 specifically in the hematopoietic system, using BM chimeric mice, also protected from experimentally induced stroke without intracranial bleeding [13, 44].

It is important to note that neurons lacking ORAI1 or STIM1 were not protected from apoptosis under *in vitro* hypoxic conditions suggesting the existence of a compensatory mechanism between the corresponding isoforms of both ORAI and STIM, respectively. In sharp contrast, constitutive STIM2 deletion resulted in protection of neurons in the tMCAO model of stroke, suggesting that STIM2 is a key player of neuronal SOCE during a stroke. Regarding ORAI isoforms, it was found that ORAI2 is predominantly expressed compared to ORAI1 in brain tissue, suggesting an important role in SOCE in the brain [150]. Altogether, these results point out that SOCE and the  $Ca^{2+}$  signaling machinery are actively involved in the progression of experimental ischemic stroke [149].

### **1.7.2 Magnesium**

Ionic  $Mg^{2+}$  is known to antagonize  $Ca^{2+}$  entry, lower blood pressure and cause vasodilation [151]. Supplementation of  $Mg^{2+}$  in a model of forebrain ischemia significantly reduced cell death in various lobes of the rat brain [152]. In a model of temporary focal ischemia, infarct volume was strongly reduced (60%) after  $MgSO_4$  administration at 24 h prior to ischemia. It was also demonstrated that the survival rate of ischemia-induced rats improved, if the  $Mg^{2+}$  was supplemented up to a maximum of 6 h post vessel occlusion and reperfusion [153]. On the contrary, in rats subjected to permanent middle cerebral artery occlusion (pMCAO) showed different results. Here,  $MgSO_4$  supplementation only in the presence of mild hypothermia resulted in a significant neuroprotection and a reduced infarct size until a maximum of 4 h after stroke. This study underlined the beneficial effects of mild hypothermia in enhancing the time window of  $Mg^{2+}$  therapy [154]. In rats, using the tMCAO model of stroke,  $Mg^{2+}$  was found to inhibit nitric oxide synthase which diminished the NOS positive cortical neurons, thereby protecting rats from ischemia [155]. These different studies using various models of brain ischemia provide evidence for a certain beneficial effect of  $Mg^{2+}$  in reducing infarct size, while the underlying mechanisms still have remained elusive.

In a clinical trial,  $MgSO_4$  was infused at 2 h after stroke occurrence, which resulted in protective effects (assessed by Rankin scores) in >60% of the total patients receiving  $MgSO_4$  [156]. On

the other hand, prehospital use of  $Mg^{2+}$  did not appear to have an additional benefit in improving the neurological function of stroke patients [157].

The current literature is controversial concerning a role of TRPM7 in the regulation of cellular divalent cation homeostasis. In mice, some studies state that TRPM7 is important for cell survival without a major role in  $Mg^{2+}$  homeostasis [80], while other papers using *in vitro* cell culture systems point to a role for TRPM7 in  $Mg^{2+}$  homeostasis [81]. Few other studies describe that during stroke TRPM7 can conduct  $Ca^{2+}$  influx pathways and mediate the generation of reactive oxygen species [158, 159]. It has also been shown that TRPM7 protein expression is upregulated in ischemic neurons [160], whereas the inhibition of TRPM7 under hypoxia increases cell viability [158]. In line with this, it was concluded that upregulation of the TRPM7 channel activity may induce an aberrant  $Ca^{2+}$  influx in neurons, thereby accelerating cell death in stroke [161]. This study suggested that TRPM7 is important for both  $Ca^{2+}$  and  $Mg^{2+}$  homeostasis, because TRPM7-mediated  $Mg^{2+}$  entry can support cell survival under physiological conditions, whereas a TRPM7-induced  $Ca^{2+}$  influx under hypoxia was deleterious. In mice that were subjected to a model of tMCAO, the use of a non-selective TRPM7 inhibitor carvacrol reduced infarct volume, inhibited apoptosis in neurons and improved neurological function in hypoxic ischemia. This study underlined the potential of carvacrol as a potential drug to prevent stroke in patients [162]. Up to date, no other mouse models with defects in  $Mg^{2+}$  channels or transporters have been investigated to assess their importance in platelet function as well as stroke development and progression.

Although the above-stated studies point to a potential beneficial effect of  $Mg^{2+}$  supplementation in prevention or treatment of ischemic stroke, a clear understanding of the  $Mg^{2+}$  entry routes, the underlying molecular mechanisms and associated signaling pathways still need to be obtained.

### 1.7.3 Zinc

One of the most abundant mineral elements in brain tissue is  $Zn^{2+}$ .  $[Zn^{2+}]_i$  is frequently released together with glutamate into the synaptic cleft serving as neuromodulator [163, 164]. Dysregulation of  $Zn^{2+}$  homeostasis causes  $Zn^{2+}$  accumulation either in the cytoplasm or in the extracellular space. Aberrant  $Zn^{2+}$  accumulation was observed in various neurological disorders including traumatic brain injury, stroke, and seizure. Administration of the  $Zn^{2+}$  chelator, N,N,N',N'-tetrakis 2-pyridinylmethyl-1,2-ethanediamine (TPEN) in rats subjected to experimental ischemia led to a neuroprotective effect. TPEN inhibited neuronal damage by reducing brain infarct size, improved neurological function and prevented apoptosis in ischemic neurons [165]. Mice lacking ZnT3 ( $ZnT3^{-/-}$ ) showed an increased sensitivity to seizure and

inhibited postsynaptic potential in neurons, thus underlining the importance of ZnT3 in maintaining optimal levels of Zn<sup>2+</sup> in the synaptic cleft [166].

In rats, using a Zn<sup>2+</sup> specific fluorescent dye *N*-(6-methoxy-8-quinolyl)-*p*-toluene sulfonamide (TSQ), it was observed that, upon transient forebrain ischemia, Zn<sup>2+</sup> accumulation increased in parts of the brain including hippocampus and stratum regions during the first minutes. After a time period of 24 h, the Zn<sup>2+</sup> staining moved to hilar neurons, which started to degenerate. This suggested that Zn<sup>2+</sup> accumulation can selectively damage specific neurons upon ischemia. Using the Zn<sup>2+</sup> chelator dithizone, this effect appeared to be preventable [167]. Interestingly, induction of hypoxia with subsequent re-oxygenation in astrocytes did not change the expression level of ZIP-1, whilst that of ZnT-1 was reduced. In addition, Zn<sup>2+</sup> supplementation under these conditions could not normalize the expression level of ZnT-1, which together with insufficient Zn<sup>2+</sup> efflux systems, accounts for the intracellular accumulation of Zn<sup>2+</sup> and consequently increased cell death during stroke [168].

The importance of ZIP isoforms in brain-related diseases has received less attention, when compared to the ZnT isoforms. Out of a total of 14 ZIP isoforms, only ZIP-1 and ZIP-3 are predominantly expressed in brain tissue. Limited *in vitro* findings have been reported which describe their role during ischemia in the brain. For example, in a study using an *in vitro* system, patch clamp recordings in pyramidal neurons from brain slices showed that *Zip1/Zip3*<sup>-/-</sup> double-deficient cells demonstrate almost 50% less Zn<sup>2+</sup> uptake, when compared to control cells. These results were obtained using fluorescence intensity ratio measurements of FluoZin-3 (specific to [Zn<sup>2+</sup>]<sub>i</sub>) and fluorescent tracer Alexa-568 as counterstaining. *In vivo*, using kainic acid injections to induce seizures in mice, it appeared that *Zip-1/Zip-3*<sup>-/-</sup> double-deficient animals survived well compared to control mice, compatible with the importance of Zn<sup>2+</sup> homeostasis in brain-related diseases. Due to the limited research detailing the role of Zn<sup>2+</sup> transporters in stroke, further studies are necessary to identify the storage pools of Zn<sup>2+</sup> release/uptake mechanism in ischemic neurons and decipher the underlying signaling mechanisms of ZIP/ZnT isoforms in this pathological setting.

### **1.8 Aims of the thesis**

Cytosolic Ca<sup>2+</sup> is one of the crucial and well described second messengers in platelets. Ca<sup>2+</sup> release from intracellular stores, as well as entry from the extracellular space through SOCE and ROCE, have been well described. Other divalent cations including Mg<sup>2+</sup> and Zn<sup>2+</sup> although known to be involved in various steps of platelet activation and coagulation received less attention.

TRPM7 is a ubiquitously expressed bifunctional protein comprising a transient receptor potential channel segment that is linked to a cytosolic  $\alpha$ -type serine/threonine protein kinase domain. TRPM7 forms a constitutively active  $Mg^{2+}$  and  $Ca^{2+}$  permeable channel, which regulates diverse cellular processes in both healthy and diseased conditions. Although  $Mg^{2+}$  holds an antithrombotic potential, the physiological role of TRPM7 kinase and the channel itself in platelet signaling, thrombosis and stroke remain largely unknown. Addressing these questions, we analyzed the importance of TRPM7 kinase using *Trpm7<sup>R/R</sup>* and TRPM7 channel functions using *Trpm7<sup>fl/fl-Pf4Cre</sup>* mice under various *in vitro* and *in vivo* settings of platelet reactivity and stroke.

In coronary artery disease, diabetes and stroke pathogenic and experimental settings, beneficial effects of  $Mg^{2+}$  supplementation have been described. Underlying molecular mechanisms, signaling pathways and  $Mg^{2+}$  interference with the function of other cations have not been investigated. Addressing these questions, we studied the *in vitro* and *in vivo* relevance of the MAGT1-mediated  $Mg^{2+}$  transport utilizing the *Magt1<sup>-/-</sup>* mouse model. A function of MAGT1 has recently been elucidated in virus-infected patients with combined immune deficiency. In the described XMEN syndrome, which primarily is initiated by infecting B cells, an altered T cell cellularity,  $Ca^{2+}$  responses, and PLC activity were described. Surprisingly, in the described infectious conditions, B cell  $Mg^{2+}$  homeostasis and B cell receptor signaling were not investigated. Utilizing the *Magt1<sup>-/-</sup>* mouse model, we studied the primary function of MAGT1 in T and B cells, the underlying signaling pathways and the physiological function of MAGT1 using various assays.

Blood coagulation is a complex process involving extrinsic and intrinsic pathways. Extrinsic and intrinsic pathways coordinate fibrin formation and fibrinolysis which regulates the stability/fluidity of the blood clot. Impaired coagulation results in bleeding diathesis. The role of  $Zn^{2+}$  was described in the activation of various coagulation factors, reducing fibrin fiber stiffness, and thereby accelerating clotting. However, the consequence of dysregulated platelet  $Zn^{2+}$  uptake, storage and release still needed to be investigated.

## 2. Materials and Methods

### 2.1 Materials

#### 2.1.1 Chemicals

Reagent	Company (Country)
Acetic acid	Roth (Karlsruhe, Germany)
Adenosine diphosphate (ADP)	Sigma-Aldrich (Schnelldorf, Germany)
Agarose	Roth (Karlsruhe, Germany)
Alexa Fluor 488	Invitrogen (Karlsruhe, Germany)
Amersham Hyperfilm ECL	GE Healthcare (Little Chalfont, UK)
Ammonium peroxodisulfate (APS)	Roth (Karlsruhe, Germany)
Apyrase (grade III)	Sigma-Aldrich (Schnelldorf, Germany)
Atipamezole	Pfizer (Karlsruhe, Germany)
$\beta$ -mercaptoethanol	Roth (Karlsruhe, Germany)
Bovine serum albumin (BSA)	AppliChem (Darmstadt, Germany)
Bromophenol blue	Sigma-Aldrich (Schnelldorf, Germany)
Cacodylate	AppliChem (Darmstadt, Germany)
Calcium chloride	Roth (Karlsruhe, Germany)
Chrono-Lume luciferase reagent	Chrono-log (Havertown, PA, USA)
Chloroform	AppliChem (Darmstadt, Germany)
Collagen Horm suspension & SFK solution	Takeda (Linz, Austria)
Complete mini protease inhibitors	Roche Diagnostics (Mannheim, Germany)
Convulxin (CVX)	Enzo Lifesciences (Lorrach, Germany)
Cryo-Gel	Leica Microsystems (Wetzlar, Germany)
4',6-diamidino-2-phenylindole (DAPI)	Invitrogen (Karlsruhe, Germany)
Dimethyl sulfoxide (DMSO)	Sigma-Aldrich (Steinheim, Germany)
Deoxynucleotide triphosphates (dNTP) mix	Fermentas (St. Leon-Rot, Germany)
Eosin	Roth (Karlsruhe, Germany)
Ethanol	Roth (Karlsruhe, Germany)
Ethylenediaminetetraacetic acid (EDTA)	AppliChem (Darmstadt, Germany)
Ethylene glycol tetraacetic acid (EGTA)	Sigma-Aldrich (Steinheim, Germany)
Ethidium bromide	Roth (Karlsruhe, Germany)
Fat-free dry milk	AppliChem (Darmstadt, Germany)
Fentanyl	Janssen-Cilag GmbH (Neuss, Germany)
Fibrillar type I collagen (Horm)	AppliChem (Darmstadt, Germany)
Fibrinogen from human plasma (F3879)	Sigma-Aldrich (Steinheim, Germany)



Fibrinogen from human plasma (F4883)	Sigma-Aldrich (Steinheim, Germany)
Fluorescein-isothiocyanate (FITC)	Molecular Probes (Oregon, USA)
Fluoroshield	Sigma-Aldrich (Steinheim, Germany)
Fluorshield with DAPI	Sigma-Aldrich (Steinheim, Germany)
Flumazenil	Delta Select GmbH (Dreieich, Germany)
Fura-2/AM	Molecular Probes/Invitrogen (Germany)
GeneRuler 1kbp DNA Ladder	Fermentas (St. Leon-Rot, Germany)
GeneRuler 100bp DNA Ladder	Fermentas (St. Leon-Rot, Germany)
Glucose	Roth (Karlsruhe, Germany)
Glutaraldehyde	EMS (Hatfield, USA)
Glycerol	Roth (Karlsruhe, Germany)
Hematoxylin	Sigma-Aldrich (Steinheim, Germany)
Heparin sodium	Fermentas (St. Leon-Rot, Germany)
High molecular weight heparin	Ratiopharm (Ulm, Germany)
Human fibrinogen	Roth (Karlsruhe, Germany)
IGEPAL CA-630	Sigma-Aldrich (Steinheim, Germany)
Immobilon-P transfer membrane, PVDF	Merck Millipore (Darmstadt Germany)
Integrilin (Eptifibatide)	Millennium Pharmaceuticals Inc. (Cambridge, USA)
Iron-III-chloride hexahydrate (FeCl <sub>3</sub> .6H <sub>2</sub> O)	Roth (Karlsruhe, Germany)
Indomethacin	Cisbio (Paris, France)
Isofluran CP	cp-pharma (Burgdorf, Germany)
Isopropanol	Roth (Karlsruhe, Germany)
Loading Dye solution, 6x	Fermentas (St. Leon-Rot, Germany)
Magnesium chloride	Roth (Karlsruhe, Germany)
Mag-Fluo4	Molecular Probes/Invitrogen (Germany)
Medetomidine (Dormitor)	Pfizer (Karlsruhe, Germany)
Midazolam (Dormicum)	Roche (Grenzach-Wyhlen, Germany)
Midori Green DNA stain	Pfizer (Karlsruhe, Germany)
N-2-Hydroxyethylpiperazine-	Roth (Karlsruhe, Germany)
N'-2-ethanesulfonic acid (HEPES)	
3-(N-morpholino) propanesulfonic acid (MOPS)	AppliChem (Darmstadt, Germany)
Naloxon	Delta Select GmbH (Dreieich, Germany)
N-ethylmaleimide (NEM)	Roche (Grenzach-Wyhlen, Germany)
Nonidet P-40 (NP-40)	Roche Diagnostics (Mannheim, Germany)

Oleoyl-2-acetyl-sn-glycerol (OAG)	Sigma (Deisenhofen, Germany)
PageRuler prestained protein ladder	Fermentas (St. Leon-Rot, Germany)
Paraformaldehyde (PFA)	Roth (Karlsruhe, Germany)
Phalloidin atto647N	Sigma (Deisenhofen, Germany)
Phenol/chloroform/isoamyl alcohol	AppliChem (Darmstadt, Germany)
Phorbol 12-myristate 13-acetate (PMA)	Sigma (Deisenhofen, Germany)
Pluronic F-127	Roth (Karlsruhe, Germany)
Prostacyclin (PGI <sub>2</sub> )	Calbiochem (Bad Soden, Germany)
Poly-L-lysine	Sigma-Aldrich (Steinheim, Germany)
Potassium acetate	Roth (Karlsruhe, Germany)
Potassium chloride	Roth (Karlsruhe, Germany)
Propidium iodide (PI)	Invitrogen (Karlsruhe, Germany)
Protease inhibitor cocktail (100x)	Sigma (Schnelldorf, Germany)
Proteinase K	Fermentas (St. Leon-Rot, Germany)
Protein G Sepharose	GE Healthcare (Uppsala, Sweden)
RNase A	Fermentas (St. Leon-Rot, Germany)
Recombinant human IL-2 (Proleukin)	Novartis (Germany)
Sodium azide	Sigma-Aldrich (Steinheim, Germany)
Sodium dodecyl sulfate (SDS)	Sigma-Aldrich (Steinheim, Germany)
Sodium orthovanadate	Sigma-Aldrich (Steinheim, Germany)
Sucrose	Sigma-Aldrich (Steinheim, Germany)
Tetramethylethylenediamine (TEMED)	Roth (Karlsruhe, Germany)
Thapsigargin	Molecular Probes (Eugene, Oregon, USA)
Thrombin from human plasma	Roche Diagnostics (Mannheim, Germany)
Tissue Freezing Medium	Jung Leica (Wetzlar, Germany)
Tris(hydroxymethyl)aminomethane (TRIS)	Roth (Karlsruhe, Germany)
Triton X-100	Sigma-Aldrich (Steinheim, Germany)
TRIzol	Invitrogen (Karlsruhe, Germany)
TRPC6 inhibitor	MedChem Express, (Germany)
Tween 20	Roth (Karlsruhe, Germany)
U46619	Alexis Biochemicals (San Diego, USA)
Vectashield hardset mounting medium	Vector Laboratories (Burlingame, USA)
Water, nuclease-free	Roth (Karlsruhe, Germany)

### 2.1.2 Cell culture materials

70 µm nylon cell strainer	BD Falcon (Heidelberg, Germany)
β-mercaptoethanol	Roth (Karlsruhe, Germany)
Fetal calf serum (FCS)	Gibco (Karlsruhe, Germany)
L-glutamine	Gibco (Karlsruhe, Germany)
Non-essential amino acids	Gibco (Karlsruhe, Germany)
Phosphate buffered saline (PBS)	Gibco (Karlsruhe, Germany)
Penicillin/streptomycin	Gibco (Karlsruhe, Germany)
RPMI medium	Gibco (Karlsruhe, Germany)
Sodium pyruvate	Gibco (Karlsruhe, Germany)
Well plates (6-well, 12-well, 24-well or 96-well)	Greiner (Frickenhausen, Germany)

RMA, RMA-H60, or RMArae1b cell lines were kindly provided by Prof. Dr. Andreas Diefenbach (Charité – Universitätsmedizin Berlin) and described previously [169].

### 2.1.3 Kits

<b>Kit (catalog)</b>	<b>Company (Country)</b>
IP1 ELISA kit (72LP1PEA)	Cisbio Bioassays (Parc Marcel Boiteux, France)
Thromboxane B <sub>2</sub> ELISA kit (4684)	DRG (Marburg, Germany)
Serotonin ELISA kit (BAE5900)	LDN (Nordhorn, Germany)
Chrono-Lume reagent	Chrono-Log (Philadelphia, PA, USA)
CD43 (Ly-48) MicroBeads, Mouse	Miltenyi Biotec (Bergisch Gladbach, Germany)
MagniSort Mouse CD4 T cell Enrichment Kit	eBioscience (Darmstadt, Germany)
MagniSort™ Mouse NK cell Enrichment Kit	Affymetrix/ThermoFisher Scientific (Germany)

### 2.1.4 Commercially purchased antibodies

#### 2.1.4.1 Unconjugated

<b>Antibody (catalog)</b>	<b>Host</b>	<b>Company (Country)</b>
---------------------------	-------------	--------------------------

Anti phospho-Syk (Y525/526) (#2711)	Rabbit	Cell Signaling (Denver, USA)
Anti phospho-LAT (Y191) (#3584)	Rabbit	Cell Signaling (Denver, USA)
Anti phospho-PLC $\gamma$ 2 (Y759) (#3874)	Rabbit	Cell Signaling (Denver, USA)
Anti phospho-PKC $\epsilon$ (ser729) (#C2013)	Goat	Santa Cruz Biotech (Heidelberg, Germany)
Anti phospho-PKC Antibody Sampler Kit (#9921)	Rabbit	Cell Signaling (Denver, USA)
Anti-PKC $\epsilon$ (#1681)	Mouse	Santa Cruz Biotech (Heidelberg, Germany)
Anti-Syk (#2712)	Rabbit	Cell Signaling (Denver, USA)
Anti-LAT (06-807)	Rabbit	Millipore (Darmstadt, Germany)
Anti-PLC $\gamma$ 2 (#5283)	Mouse	Santa Cruz Biotech (Heidelberg, Germany)
Anti- $\beta$ -actin (A2066)	Rabbit	Sigma-Aldrich (Steinheim, Germany)

#### 2.1.4.2 Conjugated

Antibody (clone/catalog)	Host	Company (Country)
Anti-goat HRP-linked (P0449)	Rabbit	DAKO (Hamburg, German)
Anti-rabbit IgG, HRP-linked (#7074)	Goat	Cell Signaling (Denver, USA)
Anti-mouse IgG, HPR-linked (#P0260)	Rat	DAKO (Hamburg, Germany)

#### 2.1.4.3 Antibodies for immune cell analysis

IgD, clone 11-26c.2a	BD Biosciences (1:100) (Heidelberg, Germany)
IgM, clone R6-60.2	BD Biosciences (1:100) (Heidelberg, Germany)

CD21/CD35, clone 7G6	BD Biosciences (1:100) (Heidelberg, Germany)
CD5, clone L17F12	BD Biosciences (1:100) (Heidelberg, Germany)
CD23, clone B3B4	BD Biosciences (1:200) (Heidelberg, Germany)
CD45R, clone RA3-6B2	BD Biosciences (1:250) (Heidelberg, Germany)
CD45, clone 30-F11	BD Biosciences (1:300) (Heidelberg, Germany)
CD3, clone 500A2	BD Biosciences (1:300) (Heidelberg, Germany)
CD8a, clone 53-6.7	BD Biosciences (1:300) (Heidelberg, Germany)
CD138, clone 281-2	BD Biosciences (1:800) (Heidelberg, Germany)
CD4, clone GK1.5	eBioscience (1:300) (Frankfurt, Germany)
CFDA-SE-labeled	Life Technologies (Paisley, UK)

#### 2.1.4.4 Home made monoclonal antibodies

Antibody	Clone	Isotype	Antigen	Described
JAQ1	98A3	IgG2a	GPVI	[98]
DOM2	89H11	IgG2a	GPV	[170]
INU1	11E9	IgG1	CLEC-2	[171]
p0p4	15E2	IgG2b	GPIIb $\alpha$	[170]
p0p6	56F8	IgG2b	GPIX	[170]
ULF1	97H1	IgG2a	CD9	[170]
WUG1.9	5C8	IgG1	P-selectin	unpublished
LEN1	12C6	IgG2b	$\alpha_2$ integrin	[172]
JON/A	4H5	IgG2b	GPIIb/IIIa	[172, 173]
EDL1	57B10	IgG2a	GPIIb/IIIa	[172, 173]
JON6	14A3	IgG1	$\alpha_{IIb}\beta_3$	unpublished
MWREG30	5D7	IgG1	$\alpha_{IIb}$	[172, 174]
HB.197™	2.4G2	IgG2b	FC $\gamma$ R	[175]

Collagen-related peptide (CRP) was kindly provided by Prof. Dr. S. P. Watson (University of Birmingham, UK) and was previously described [176]. Rhodocytin (RC) was a generous gift from Prof. Dr. J. Eble (University Hospital Frankfurt, Germany). All other non-listed chemicals were obtained from AppliChem (Darmstadt, Germany), Sigma (Schnelldorf, Germany) or Roth (Karlsruhe, Germany).

## 2.2 Methods

### 2.2.1 Generation and genotyping of mice.

#### 2.2.1.1 *Trpm7<sup>R/R</sup>* mice

The *Trpm7<sup>R/R</sup>* mouse line was received from the RIKEN BRC Center through the National Bio-Resource Project of the MEXT, Japan (RBRC03318, [www.brc.riken.jp](http://www.brc.riken.jp)) and has been described previously [177]. 129SV.B6 *Trpm7<sup>R/R</sup>* mice were backcrossed several times with C57B6J mice. PCR genotyping was performed using *Trpm7* specific primers to amplify the mutated exonic region:

TRPM7<sup>K1646R</sup>forward: 5`-ATGGGAGGT GGTTCACGA-3`

TRPM7<sup>K1646R</sup>reverse: 5`-GGGAAGGGCCTTATCAATATG-3`

PCR fragment was digested with *Mes I* enzyme and DNA fragments were separated using a 2.5% agarose gel. *WT* DNA fragment was digested into 128bp and 86 bp whereas *Trpm7<sup>R/R</sup>* fragment was not digested by *Mes I* into a 214 bp fragment.

#### 2.2.1.2 *Magt1<sup>-/-</sup>* mice

*Magt1<sup>-/-</sup>* mice (TIGM, Texas, USA) were bred on a C57BL/6 background and housed under specific pathogen-free conditions on a standard light-dark cycle. Functional consequences of X-linked *Magt1* gene deletion were investigated in age-matched *WT* and *Magt1<sup>-/-</sup>* male mice (12-16 weeks old) from an inbred mouse colony. The genotyping protocol was provided by Texas A&M Institute for Genomic Medicine (TX, USA). *Magt1* specific forward and reverse primers were used to amplify the gene-trap cassette insertion in intron 1.

Forward: 5`-CCAATCCTGGACTTTGTGCA-3`

Reverse-1: 5`-CCTCTTCTGACCTCCAAAAG-3`

Reverse-2: 5`-CCAATAAACCTCTTGCAGTTGC-3`

PCR DNA fragments were separated using a 2% agarose gel (*WT* allele: 644 bp and knockout allele: 377 bp).

For quantitative RT-PCR, two sets of MAGT1 primers were used.

Forward1: 5`-AGAAATTACTIONCAGTTGTCGTCATGTT-3`;

Reverse-1: 5`-CTTCATCAGCTTGCTTGCAAAC-3` ,

Forward-2: 5`-ACCATGGCTATCCATACAGCTTTC-3`;

Reverse-2: 5`-GTGAGTTGCATTCTTCAAACACC-3`.

Experiments were performed according to the manufacturer's protocol (Qiagen, Hilden, Germany).

### 2.2.1.3 *Trpm7<sup>fl/fl</sup>-Pf4Cre* mice

MK and platelet-specific conditional knockout mice of *Trpm7* were generated as described earlier [75]. Briefly, mice were used possessing loxP sites flanking exon 17 of the *Trpm7* gene. Homozygous floxed mice (*Trpm7<sup>fl/fl</sup>*) were intercrossed with PF4Cre mice to obtain a MK- and platelet-specific deletion of *Trpm7* (*Trpm7<sup>fl/fl</sup>-Pf4Cre*) *in vivo*.

*Trpm7* specific forward and reverse primers were used which flanked the deleted exonic region.

Forward-1: 5`-GCTATTGAAAAAGTCCGTGAGG-3`;

Reverse-1: 5`-AACCATACTTTAATCTTCTGGCTGAT-3`;

Forward2: 5`-TTCACCTCGGTG CAAGCAG AA-3`;

Reverse-2: 5`-ACCAATCCGGTAACAAAGCTG-3`.

### 2.2.1.4 *Nbeal2<sup>-/-</sup>*, *Unc13d<sup>-/-</sup>* mice

*Nbeal2<sup>-/-</sup>* and *Unc13d<sup>-/-</sup>* mice were generated as described earlier [21, 178].

### 2.2.1.5 RNA preparation from tissues using RNeasy Kit

Anesthetized mice were sacrificed by cervical dislocation and organs were collected immediately. Later, organs were washed in sterile PBS and cut into small pieces of approximately 30 mg. Cut tissue samples were homogenized in 600 µL of RLT buffer and centrifuged at 14,000 rpm (Eppendorf 5417R) for 3 min. The supernatant was collected and mixed with equal volume of 70% ethanol and added onto an RNeasy spin column. The columns were centrifuged at 14,000 rpm for 15 sec and the procedure was repeated. Later, columns

were washed once with 700  $\mu\text{L}$  RW1 buffer (15 sec, 14,000 rpm), twice with 500  $\mu\text{L}$  RPE buffer (15 sec, 14,000 rpm), and the RNA was eluted by adding 40  $\mu\text{L}$  of RNase free water. After incubated for 1 min, the samples were centrifuged at 14,000 rpm for 1 min. Using NanoDrop, RNA concentration was quantified.

## **2.2.2 *In vitro* analysis of platelet function**

### **2.2.2.1 Platelet preparation and washing**

Mice were bled under isoflurane anesthesia from the retro-orbital plexus. 700  $\mu\text{L}$  blood was collected in a reaction tube containing 300  $\mu\text{L}$  heparin in TBS (20 U/mL, pH 7.3). The blood was centrifuged at 1,500 rpm for 6 min at room temperature (RT). The supernatant was transferred to a new reaction tube (red cell contamination was allowed) and centrifuged at 800 rpm for 6 min at RT to obtain platelet-rich plasma (PRP). The obtained PRP was centrifuged at 2,500 rpm for 6 min at RT, and the pellet was re-suspended into 1 mL  $\text{Ca}^{2+}$ -free Tyrode's HEPES buffer containing apyrase (0.02 U/mL) and  $\text{PGI}_2$  (0.1  $\mu\text{g}/\text{mL}$ ). The sample was further centrifuged at 2,500 rpm for 5 min. A second washing step was performed using the same centrifugation procedure. The final platelet pellet was resuspended in an appropriate volume of Tyrode's HEPES buffer to the required platelet concentration.

Whole blood platelet count and size were determined by collecting 50  $\mu\text{L}$  blood from anesthetized mice to 300  $\mu\text{L}$  heparin in TBS (20 U/mL, pH 7.3), using a Sysmex KX-21N automated hematology analyzer (Sysmex Corp, Kobe, Japan).

Human platelets were washed by centrifuging citrated whole blood at 900 rpm for 15 min with deceleration break 3 at RT. Straw-colored PRP was collected (only 80% of the total) avoiding red blood cell contamination into new tubes. Later, PRP was supplemented with apyrase and  $\text{PGI}_2$  (as above) and centrifuged break-free for 5-8 min at 2,800 rpm. If required, the plasma was stored at  $-80\text{ }^\circ\text{C}$  for further use. Platelet pellets were re-suspended into Tyrode's HEPES buffer without  $\text{CaCl}_2$ , and used for indicated assays.

### **2.2.2.2 Aggregometry**

Washed platelets at  $5 \times 10^5/\mu\text{L}$  in Tyrode's HEPES buffer containing apyrase (0.02 U/mL) but without  $\text{CaCl}_2$  were prepared. To determine platelet aggregation, 50  $\mu\text{L}$  of the prepared platelet suspension was added to 110  $\mu\text{L}$  of Tyrode's HEPES buffer containing 70  $\mu\text{g}/\text{mL}$  fibrinogen and light transmission was recorded on a Fibrinometer 4 channel aggregometer (Apect 4-channel optical aggregation system, AFACT, Hamburg, Germany). For activation with thrombin, washed platelets were diluted into Tyrode's HEPES buffer containing 2 mM  $\text{CaCl}_2$ ,



but without fibrinogen. Activation was performed with different concentrations of agonists specific for GPVI- (CRP, collagen) or GPCR-induced signaling (thrombin) or stable analog of thromboxane, U46619. To stimulate CLEC-2, rhodocytin was used. Each measurement was carried out until 10 min. Platelet aggregation was expressed in arbitrary units, setting the transmission of Tyrode's HEPES buffer with  $\text{Ca}^{2+}$  and fibrinogen at 100%.

### 2.2.2.3 Measurement of $[\text{Mg}^{2+}]_i$ or $[\text{Zn}^{2+}]_i$ on FACS Canto II

Washed platelets ( $5 \times 10^5$  cells/ $\mu\text{L}$ ) were loaded with Mag-Fluo-4 ( $[\text{Mg}^{2+}]_i$ ) or FluoZin-3 ( $[\text{Zn}^{2+}]_i$ ) (5  $\mu\text{g}/\text{mL}$  of dye in DMSO mixed 1:1 with 37 °C pre-heated pluronic acid), left shaking at 300 rpm for 30 min at 37 °C in the dark. Loaded platelets were left idle for an additional 20 min at 37 °C in the dark. 25  $\mu\text{L}$  of the loaded platelets were diluted to 1 mL with HBSS with 1 mM  $\text{MgCl}_2$  (for Mag-Fluo-4) or with Tyrode's HEPES buffer without calcium (for FluoZin-3), and fluorescence intensity was recorded for an initial 50 sec to establish basal  $\text{Mg}^{2+}$  or  $\text{Zn}^{2+}$  levels. Subsequently, 2 mM  $\text{CaCl}_2$  and agonist were added to 500  $\mu\text{L}$  of the platelet suspension, and changes of fluorescence intensity were recorded for an additional 300 s. Measurements are shown as a complete kinetic curve by appending the first 50 sec to the following 300 sec. To perform the measurements, a BD FACS Canto II was used, and the results were analyzed by FlowJo 10.0 Software (TreeStar, USA) . Approximately, the initial 10% and final 10% of the geometric mean fluorescence intensity (Geo-MFI) from each dot plot were used to calculate the percentage of loss and residual fluorescence signal for Mag-Fluo-4 or FluoZin-3. Data are reported as Mag-Fluo-4 Geo MFI% or FluoZin-3 Geo-MFI  $\pm$  SD.

### 2.2.2.4 Measurement of $[\text{Ca}^{2+}]_i$ using fluorimeter

100  $\mu\text{L}$  of washed platelets ( $2.5 \times 10^5$  cells/ $\mu\text{L}$ ) were loaded with Fura2 (5  $\mu\text{g}/\text{mL}$  of dye in DMSO mixed 1:1 with 37°C pre-heated pluronic acid), left 20 min at 37°C in the dark. Thereafter, cells were centrifuged at 2,500 rpm for 2 min (washing step) and the pellet re-suspended with 500  $\mu\text{L}$  of measuring buffer (HBSS with 1 mM  $\text{MgCl}_2$ ) and transferred to a cuvette (provided by Perkin Elmer, Boston, USA) with a magnetic stirrer. Fluorescence measurements were carried out on a PerkinElmer LS 55 fluorimeter (alternate excitation at 340 and 380 nm, and emission at 509 nm), equipped with FLWinlab software. After 50 sec of recording time the agonist was added and the measurement was continued until 300 sec, without extracellular  $\text{CaCl}_2$  for store release; or with 1 mM  $\text{Ca}^{2+}$  for calcium entry studies. In case of measurements with thapsigargin, store release was recorded until 300 sec in the absence of  $\text{CaCl}_2$ , later 1 mM  $\text{CaCl}_2$  was added and  $\text{Ca}^{2+}$  entry was recorded until 500 sec. Each measurement was stopped by adding 100  $\mu\text{L}$  of 1% Triton-X100 to lyse the platelets to

get a maximal  $\text{Ca}^{2+}$  level and subsequently 100  $\mu\text{L}$  EDTA (0.5 M) was added to get a minimal  $\text{Ca}^{2+}$  level. Using FLWinlab software each measurement curve was calibrated to report nanomolar changes in the  $[\text{Ca}^{2+}]_i$  levels.

#### **2.2.2.5 Flow Cytometry using FACS Calibur**

To assess the activation of  $\alpha_{\text{IIb}}\beta_3$  integrin and P-selectin exposure (a marker for  $\alpha$ -granule release), platelets were washed as described above and diluted to a concentration of  $2 \times 10^4$  platelets/ $\mu\text{L}$  in Tyrode's HEPES buffer with 1 mM  $\text{CaCl}_2$ . Tubes were prepared in advance, containing a 1:1 mixture of fluorophore-conjugated antibodies against activated  $\alpha_{\text{IIb}}\beta_3$  integrin (PE-coupled 4H5) and P-selectin (FITC-coupled 5C8). Agonist dilutions were prepared and maintained on ice. CRP was used as a GPVI-specific agonist, whereas thrombin, ADP, and the  $\text{TXA}_2$  stable analog U46619 were used as GPCR-specific agonists. Seven  $\mu\text{L}$  of each agonist dilution was added to the specific reaction tubes containing the antibodies and maintained at 4 °C until use. Fifty  $\mu\text{L}$  of the prepared platelets were then added to the reaction tubes and incubated for 6 min at 37 °C, followed by 6 min at RT. Reactions were stopped by the addition of 500  $\mu\text{L}$  PBS, and measurements were carried out immediately using a FACS Calibur (BD Biosciences) flow cytometer. For determination of basal glycoprotein expression levels, washed platelets were stained for 10 min at RT in the dark with saturating amounts of fluorophore-conjugated antibodies. Reactions were stopped by the addition of 500  $\mu\text{L}$  PBS, and samples were immediately analyzed on the FACS Calibur instrument.

#### **2.2.2.6 Platelet life span**

Platelets were labeled *in vivo* by intravenous injection of 5  $\mu\text{g}$  of DyLight 488-conjugated anti-GPIX antibody derivative diluted in sterile phosphate saline buffer (PBS). At indicated time points, samples of 50  $\mu\text{L}$  blood were collected and incubated with a PE-conjugated anti-GPIb antibody for 10 min at RT. The percentage of double positive platelets was determined by flow cytometry.

#### **2.2.2.7 Measurements of second wave mediators**

ATP secretion was determined using CHRONO-LUME reagent on a Chronolog aggregometer (Chrono-Log, Philadelphia, PA, USA), serotonin release was measured using a commercially available ELISA kit (5-HT ELISA<sup>Fast Track</sup>, LDN, Nordhorn, Germany), and thromboxane release was measured using an ELISA kit (DRG, Marburg, Germany). Briefly,  $5 \times 10^5$  platelets/ $\mu\text{L}$  isolated platelets were stimulated with the indicated agonists for 5 min, and the reaction was

stopped by adding 100  $\mu$ L of the activated platelet suspension to 5 mM EDTA and 1 mM aspirin containing reaction tubes. Samples were then pelleted by centrifugation (2,800 rpm; 5 min) and 50  $\mu$ L of supernatant was added to 950  $\mu$ L of Tyrode's HEPES buffer without  $\text{CaCl}_2$ , and the  $\text{TXB}_2$  concentration was measured following the manufacturer's protocols. To determine phospholipase C activity, washed platelets were prepared in phosphate-free Tyrode's HEPES buffer containing 50 mM LiCl, with or without 1 mM  $\text{CaCl}_2$ . An ELISA for IP1 was performed according to the manufacturer's protocol (Cisbio Bioassays, Codolet, France).

#### **2.2.2.8 Mepacrine uptake and release**

Mepacrine uptake and release (kinetic/end-point) measurements were performed by loading whole blood samples with mepacrine dihydrochloride (Sigma-Aldrich, St. Louis, MO, USA) for 30 min at 37 °C (5  $\mu$ M final concentration) in the dark. After loading, baseline fluorescence of unlabeled platelets was recorded, excited at 488 nm for 60 sec. Subsequently, the fluorescence signal after mepacrine addition was recorded for an additional 60 sec to determine mepacrine uptake. Finally, following the indicated activation, the fluorescence signal was recorded for an additional 600 sec to assess mepacrine release. Healthy controls subjects, whose blood was drawn on the same day as of the patients, were used as controls for comparative analysis. In case of mepacrine measurement in mouse platelets, littermate age/sex matched controls were used.

#### **2.2.2.9 Adhesion under flow conditions**

Rectangular coverslips (24 x 60 mm) were coated with 0.2 mg/mL fibrillar type I collagen (Horm, Nycomed) overnight at 37°C and blocked for 30 min with 1% BSA in PBS. Blood (700  $\mu$ L) was collected to reaction tubes containing 300  $\mu$ L heparin (20 U/mL in TBS, pH 7.3) across the retro-orbital plexus. The collected blood was supplemented with Dylight-488 conjugated anti-GPIX Ig derivative (0.2  $\mu$ g/mL) and incubated at 37 °C for 5 min. Subsequently, the blood was diluted 2:1 in Tyrode's HEPES buffer containing  $\text{CaCl}_2$  and filled into a 1 mL syringe. Transparent flow chambers with a slit depth of 50  $\mu$ m was equipped with the coated coverslips and connected to the syringe filled with diluted whole blood. Blood was perfused using a pulse-free pump at the mentioned shear rates for 4 min. Thereafter, coverslips were perfused with Tyrode's HEPES buffer at the same shear rate for 2 min, and later phase-contrast and fluorescent images were taken from different microscopic fields (40x objective) using a Zeiss Axiovert 200 inverted microscope equipped with a CoolSNAP-EZ camera (Visitron, Puchheim, Germany)). Image analysis was done using offline version of Metavue software (Visitron,

Puchheim, Germany). Surface coverage area and integrated fluorescence intensity were reported.

#### **2.2.2.10 Determination of phosphatidylserine exposure in platelets**

Washed platelets ( $2 \times 10^4/\mu\text{L}$ ), re-suspended in Tyrode's HEPES buffer with 1 mM  $\text{CaCl}_2$ , were incubated with 10  $\mu\text{L}$  of Dylight 488-labeled annexin A5 together with the agonist for 15 min at 37°C. Subsequently, the reaction was stopped by adding 500  $\mu\text{L}$  of Tyrode's HEPES buffer with 1 mM  $\text{CaCl}_2$ , and the percentage of fluorescently labeled platelets was analyzed by flow cytometry. To determine phosphatidylserine (PS) exposure under flow, heparinized whole blood containing 20 U/mL of heparin was perfused over a collagen-coated surface at mentioned shear rate for 4 min. Subsequently, washing was performed with Tyrode's HEPES buffer with 2 mM  $\text{CaCl}_2$ , 5 U/mL heparin and 0.25 mg/ml DyLight488 annexin A5 antibody for an additional 4 min. Phase-contrast and fluorescent images were acquired during this time and analyzed using offline version of Metavue software (Visitron, Munich, Germany). Surface coverage area and procoagulant index were reported.

#### **2.2.2.11 Spreading assay**

Glass coverslips (24 x 60 mm) were coated with 100  $\mu\text{g}$  of human fibrinogen under humid conditions at 4°C o/n and blocked for at least 1 h at RT with 1% BSA in sterile PBS. The coverslips were rinsed with Tyrode's-HEPES buffer containing 1 mM  $\text{CaCl}_2$  and left to air dry before being used for spreading. 30 - 60  $\mu\text{L}$  washed platelets ( $3 \times 10^5$  cells/ $\mu\text{L}$ ) were diluted to  $5 \times 10^4$  cells/ $\mu\text{L}$  for 5 min timepoint and  $2 \times 10^4$  cells/ $\mu\text{L}$  for 15 and 30 min timepoint spreading with Tyrode's-HEPES containing 1 mM  $\text{CaCl}_2$  and added immediately to fibrinogen coated coverslips to spread. Samples for 15 min and 30 min spreading were stimulated with thrombin (0.01 U/mL). Platelet spreading was stopped by the addition of 300  $\mu\text{L}$  4% PFA/PBS. Excessive fixative was removed, and platelets were visualized by differential interference contrast (DIC) microscopy on a Zeiss Axiovert 200 inverted microscope (100 x, 1.4 N.A. oil objective). Representative images were taken using a CoolSNAP EZ camera (Visitron, Munich, Germany), and evaluated for the different stages of platelet spreading with ImageJ (National Institutes of Health, Bethesda, MD, USA). Spreading stages were defined as: 1) round, no filopodia and lamellipodia; 2) only filopodia; 3) filopodia and lamellipodia; 4) fully spread.

### 2.2.2.12 Tyrosine phosphorylation

Platelets were washed as described above, and suspended at a concentration of  $1 \times 10^6$  cells/mL into BSA-free Tyrode's HEPES buffer with or without  $\text{CaCl}_2$  as stated. Furthermore,  $50 \mu\text{g/mL}$  integrilin was added to prevent integrin activation and aggregation of platelets. To study tyrosine phosphorylation patterns during the initial steps of activation, platelets were resuspended in Tyrode's HEPES buffer without  $\text{Ca}^{2+}$  but supplemented with  $2 \text{ U/mL}$  apyrase,  $10 \mu\text{M}$  indomethacin (I7378-5G, Sigma Aldrich) and  $1 \text{ mM}$  EDTA (Roth). Stated agonist was added, while the platelet suspension was constantly stirred ( $300 \text{ rpm}$ , thermocycler) at  $37 \text{ }^\circ\text{C}$ . At specific time points,  $50 \mu\text{L}$  of the suspension was lysed into an equal volume of ice-cold 2x lysis buffer ( $300 \text{ mM NaCl}$ ,  $20 \text{ mM TRIS}$ ,  $2 \text{ mM EGTA}$ ,  $2 \text{ mM EDTA}$ ,  $10 \text{ mM NaF}$ ,  $\text{pH } 7.5$ ), supplemented with protease inhibitor cocktail ( $1:100$ , Sigma) and PhosSTOP ( $1 \text{ tablet}/10 \text{ mL}$ , Roche). Lysates were maintained on ice for  $10 \text{ min}$ , denatured with 4x reducing sample buffer and boiled at  $96 \text{ }^\circ\text{C}$  for  $10 \text{ min}$ . The prepared protein lysates were frozen at  $-80 \text{ }^\circ\text{C}$  for future use up to a maximum of two weeks. Sodium dodecyl sulfate (SDS) polyacrylamide gel electrophoresis (PAGE) was performed and using a semi-dry transfer method, the proteins were transferred onto a polyvinylidene difluoride (PVDF) membrane. After blocking with  $5\%$  BSA or  $5\%$  non-fat dry milk in TBST-T (as required), membranes were immunoblotted for the indicated phosphorylated residues. After developing the signals, respective membranes were stripped for  $45 \text{ min}$  at RT and re-blotted for total proteins. Again after developing the signals, the membrane was stripped again and re-blotted using an anti- $\beta$ -actin antibody which served as a loading control. Bands were visualized via horseradish-peroxidase coupled secondary antibodies and enhanced chemiluminescence solution. Films were developed using an X-ray film processor (GE Healthcare or Cawo Solutions, Schrobenhausen, Germany).

### 2.2.2.13 Confocal microscopy of platelets

For confocal microscopy, isolated platelets ( $5 \times 10^5/\mu\text{L}$ ) supplemented with apyrase ( $0.02 \text{ U/mL}$ ) and  $\text{PGI}_2$  ( $0.1 \mu\text{g/mL}$ ) were loaded with the indicated AM fluorescent dye ( $5 \mu\text{g/mL}$  of dye in DMSO mixed 1:1 with  $37 \text{ }^\circ\text{C}$  pre-heated pluronic acid) and left shaking at  $300 \text{ rpm}$  for  $30 \text{ min}$  at  $37 \text{ }^\circ\text{C}$  in the dark. After an additional  $20 \text{ min}$  incubation, the loaded platelets ( $7 \times 10^4/\mu\text{L}$ ) were fixed with an equal volume of  $2\%$  PFA/PHEM and allowed to adhere immediately to poly-L-lysine for  $20 \text{ min}$  at RT (served as resting samples). For activated platelet samples,  $5 \times 10^4$  of loaded platelets/ $\mu\text{L}$  were diluted with equal volume of Tyrode's HEPES buffer (supplemented with  $2$  or  $0.2 \text{ mM CaCl}_2$ ), activated with indicated agonist, and placed directly on fibrinogen ( $100 \mu\text{g/mL}$ ) coated coverslips for  $30 \text{ min}$  at  $37 \text{ }^\circ\text{C}$  in the dark. Spread platelets were fixed with  $2\%$  PFA/PHEM for  $20 \text{ min}$ . Subsequently, coverslips were washed with D-PBS,

and platelets were counterstained with phalloidin-Atto 647N (1:300 in PBS) for 90 min at RT in the dark. After the counterstaining, coverslips were washed with D-PBS shortly, and mounted onto glass slides using Fluoro shield mounting medium (Dako). 2D images or Z-stacks were obtained on Leica TCS SP5 confocal microscope (Leica Microsystems, Wetzlar, Germany) and analyzed with using Fiji, Leica LAS AF Lite and Imaris softwares as required.

### **2.2.3 *In vivo* analysis of platelet function**

All experiments with mice were performed in accordance with the governmental authorities of lower franconia (Regierung von Unterfranken) and the recently published ARRIVE guidelines (<http://www.nc3rs.org/ARRIVE>).

#### **2.2.3.1 Tail bleeding and tMCAO model of stroke**

Tail bleeding was performed by resecting 1 mm tail tip and collecting blood every 20 sec until the wound cessation up to a maximum of 20 min. 60 min or 30 min transient middle cerebral artery occlusion (tMCAO) model of stroke was performed and compared between the respective test and control groups. Experiments were performed as previously described [133]. Briefly, a filament was advanced through the right carotid artery into the MCA to induce an ischemic stroke. After the stated time of occlusion, the filament was removed and reperfusion was allowed. Functional tests were performed and the extent of infarction was assessed 24 h after reperfusion on 2,3,5-triphenyltetrazolium chloride (TTC)-stained brain sections from sacrificed mice and reported.

#### **2.2.3.2 Generation of BM chimera mice**

BMchimera mice were generated by lethally irradiated 5 to 6 weeks old *WT* or indicated recipient mice at a single dose of 10 Gray; subsequently  $4 \times 10^6$  BM cells from the indicated donor mice were retro-orbitally injected. All recipient animals received acidified water containing 2 g/L neomycin sulfate for 2 weeks after BM transplantation. All experiments with mice were performed in accordance with the governmental authorities of lower Franconia (Regierung von Unterfranken) and the recently published ARRIVE guidelines (<http://www.nc3rs.org/ARRIVE>).

#### **2.2.4 Determination of Mg<sup>2+</sup> level in serum and platelets**

Blood from 8-weeks old male mice was collected and mice were sacrificed. Serum was isolated

by centrifugation (1,400 rpm; 10 minutes at 4°C) of coagulated blood. Mg<sup>2+</sup> levels in the obtained serum and in bone samples were determined by inductively coupled plasma mass spectrometry (ICP-MS) (ALS laboratories, Luleå, Sweden). The Mg<sup>2+</sup> content of platelet and plasma samples was analyzed by taking a total of 10<sup>8</sup> pelleted platelets or 300 µL of plasma (collected while washing platelets) and analysed again by ICP-MS (Izotoptech Zrt, Debrecen, Hungary).

### **2.2.5 Histology**

Stated organs were obtained from sacrificed mice, washed in sterile PBS and fixed overnight at 4 °C in 4% PFA/PBS. The following day, all organs except femura were washed in sterile PBS, dehydrated and embedded in paraffin. Femura were decalcified for 3 days in 10% EDTA/PBS, which was exchanged each day. Later, the femura were also embedded in paraffin. Using a Cool Cut Microtome (Thermo Scientific, Braunschweig, Germany), embedded organs were cut to 3 µm thick sections and left to dry at 37 °C overnight. Prepared sections were deparaffinized by xylene, rehydrated using decreasing EtOH concentrations (100%, 90%, 80% and 70%), followed by a final incubation in milli-Q water for 2 min. Later, sections were stained in hematoxylin solution for 30 sec, and washed for 10 min in running water. Next, sections were stained for 2 min with 0.05% Eosin G and after a short wash in Millipore water, dehydration steps were repeated as above but in reverse order. Finally, sections were mounted using Eukitt medium and analyzed using a Leica DMI 4000B inverse microscope.

### **2.2.6 Immune cell analysis**

#### **2.2.6.1 Flow cytometry with immune cells on FACS Canto II**

For FACS analysis, tissues were disrupted and passed through a 70 µm cell strainer (BD Biosciences, USA) to obtain single-cell suspensions in PBS with 2 mM EDTA, 1% fetal calf serum (FCS). Blood leukocytes were obtained by withdrawing 100 µL of blood from the retro-orbital plexus into EDTA-coated tubes (Sarstedt, Nümbrecht, Germany). Red blood cells were lysed by adding red blood cell lysis buffer (155 mM NH<sub>4</sub>Cl, 10 mM KHCO<sub>3</sub> and 0.1 mM EDTA) for 5 min at RT, and samples centrifuged at 1,500 rpm at 4 °C. Pellets were resuspended in antibody cocktails, and the cells were stained for 30 min at 4 °C in the dark. The following combinations were used with specific antibodies from BD: diluted 1:100: IgD, clone 11-26c.2a; IgM, clone R6-60.2; CD21/CD35, clone 7G6 and CD5, clone L17F12; diluted 1:200: CD23, clone B3B4; diluted 1:250: CD45R, clone RA3-6B2; diluted 1:300: CD45, clone 30-F11; CD3, clone 500A2 and CD8α, clone 53-6.7; diluted 1.800: CD138, clone 281-2; and eBioscience:

diluted 1:300: CD4, clone GK1.5. Probes were analyzed using FACSCanto II (BD Biosciences, Heidelberg, Germany) and FlowJo 10.0 Software (TreeStar, USA).

### 2.2.6.2 B cell proliferation

B cell proliferation was performed by staining naïve B cells with carboxyfluorescein succinimidyl ester (CFSE), as previously described [179]. Briefly, pure uncaptured naïve B cells from the spleen were isolated using CD43-coupled (Ly-48) MicroBeads (Miltenyi, Germany) following the manufacturer's instructions. The percentage of CD19<sup>+</sup> cells after enrichment was determined by flow cytometry (90-99%). Pure B cells ( $5 \times 10^6$ /mL) were incubated with 5 mM CFSE at 37 °C for 10 min, and after an extensive washing  $2 \times 10^5$  cells were cultured in round-bottom 96-well plates. Cells were left untreated or were stimulated with 10 µg/ml lipopolysaccharide (LPS) (Sigma Aldrich, Saint Louis, USA), 5 µg/mL anti-IgM antibody (Jackson Immunology, USA), 50 ng/mL phorbol 12-myristate 13-acetate (PMA) (Sigma Aldrich) plus 500 ng/mL ionomycin (Sigma Aldrich) for 48 h. Thereafter, the percentage of proliferating cells was determined, using unstained B cells as controls.

### 2.2.6.3 Immunoblotting with immune cell lysates

A certain number of  $10^5$  purified B or CD4<sup>+</sup> cells/µL, derived from *WT* or *Magt1<sup>-/-</sup>* mouse spleens, was suspended in Hank's balanced salt solution (HBSS), supplemented with 1 mM MgCl<sub>2</sub> and 2 mM CaCl<sub>2</sub>. The cells were activated with anti-IgM antibody under constant stirring (300 rpm) at 37 °C. Samples of 50 µL of the cell suspension were lysed with equal volume of ice-cold lysis buffer (300 mM NaCl, 20 mM TRIS, 2 mM EDTA, 2 mM EDTA, 10 mM NaF, pH 7.5), supplemented with protease inhibitor cocktail (1:100, Sigma) and phosphatase inhibitors (PhosSTOP; (1 tablet/10 mL, Roche) at the indicated time points and maintained on ice for 10 min. Cell debris was removed by centrifuging the samples at 14,000 rpm for 10 min at 4 °C. The supernatants were collected and denatured by boiling at 96 °C for 10 min in 4x reducing sample buffer, upon constant stirring at 300 rpm. Lysates were stored at -80 °C until immunoblotting was performed, for a maximum period of 4 weeks. Denatured protein lysate was loaded onto an 8% acrylamide gels and run at 15-20 mA/gel. Subsequently, a semi-dry transfer was performed for 1 h at 50 mA/gel, and proteins transferred to a polyvinylidene difluoride (PVDF) membrane (#10600023, VEF, Germany). Membranes were blocked with 5% BSA TBS-T for 1 h at RT, washed shortly and probed with primary antibodies [rabbit anti phospho-PLC $\gamma$ 2 (Tyr759) (#3874), phospho-Syk (Y525/526) (#2711), phospho-PKC (pan) ( $\beta$ II Ser660) (#9371), phospho-PKC $\delta$  (Tyr311) (#2055), phospho-PKC $\zeta/\lambda$  (Thr410/403) (#9378),



anti-PLC $\gamma$ 2 (#3872), anti-Syk (#2712) all from Cell Signaling, USA]. Mouse anti-PKC  $\beta$ II (sc-13149) mAb was from Santa Cruz Biotech, Germany. Rabbit anti-PKC $\delta$  (D10E2) (#9616) and PKC $\zeta$  (#9372) antibodies were from Cell Signaling, USA). Probing was overnight at 4 °C, followed by a 3-4 times wash (5 min each), signal development in TBS-T. After stripping for 1 h at RT, membranes were re-probed for the respective total proteins and signals developed as above. Membranes containing cellular  $\beta$ -actin were stripped again for 1 h at RT, and signals developed as above. Relevant secondary antibodies [anti-rabbit IgG HRP-linked (#7074) or rabbit anti-goat HRP-linked (#P0449) or anti-mouse (#P0260) antibodies from DAKO, Hamburg, Germany] were used for 1 h at RT, and using an enhanced chemiluminescence detection kit (GE Healthcare) signals were obtained. Antibody for  $\beta$ -actin (A2066, Sigma-Aldrich, Germany) was used as a loading control.

#### 2.2.6.4 Measurement of [ $\text{Ca}^{2+}$ ]<sub>i</sub> in immune cells

Purified B or CD4<sup>+</sup> cells ( $2 \times 10^6$ ) were loaded with Fura-2 AM (F1221, Invitrogen) in pluronic acid for 20 min at 37 °C in the dark. After loading, cells were spun in an eppendorf centrifuge at 1,500 rpm for 2 min and the pellet was resuspended in 500  $\mu$ L HBSS containing 1 mM MgCl<sub>2</sub>. The Ca<sup>2+</sup> store release induced by anti-IgM or thapsigargin was recorded during 300 sec, after which 1 mM CaCl<sub>2</sub> was added to follow Ca<sup>2+</sup> influx until 500 sec. A Perkin Elmer LS-55 fluorimeter was used for the measurements. Triton-X-100 (for maximum Ca<sup>2+</sup>) and EDTA (for minimum Ca<sup>2+</sup>) were used to calibrate each measurement in order to quantify the final reported Ca<sup>2+</sup> levels as described before [13].

#### 2.2.6.5 Measurement of [ $\text{Mg}^{2+}$ ]<sub>i</sub> in immune cells

Mature B or CD4<sup>+</sup> cells were purified using the respective cell isolation kits following manufacturer's protocols.  $5 \times 10^5$  cells/ $\mu$ L were loaded with 1 mg/mL MagFluo-4 AM (#M14206, Invitrogen) in DMSO, mixed 1:1 with pluronic acid. Cells were left at 37 °C in the dark for approximately 1 h. Samples of 25  $\mu$ L of the loaded cells were diluted to 1 mL with HBSS containing 1 mM MgCl<sub>2</sub>, and fluorescent events were recorded for 50 s (for a basal Mg<sup>2+</sup> level). Subsequently, 2 mM CaCl<sub>2</sub> and agonist were added to 500  $\mu$ L aliquotes of the cell suspension, and fluorescent events were recorded for an additional 300 sec. Data are shown as Mag-Fluo-4-geometric mean fluorescence intensity (Geo-MFI)  $\pm$  SD from approximately 10% of each dot plot before (resting) and after (activation) agonist addition for each data point. FACSCanto II (BD Biosciences) was used and results were analyzed using FlowJo 10.0 software (TreeStar).

### 2.2.6.6 Natural killer cell isolation and killing assay

Natural killer (NK) cells were isolated from red blood cell-lysed spleen cell suspension using magnetic beads according to the manufacturer's protocol (Affymetrix/ThermoFisher Scientific). Seeding was at  $1 \times 10^6$  cells/well (48-well plate, Greiner) in a total volume of 1 mL RPMI 1640 medium, supplemented with 1 mM sodium pyruvate, non-essential amino acids MEM (0.05-2 mM), 100 U/mL penicillin and 100  $\mu$ g/mL streptomycin, 30  $\mu$ M mercaptoethanol, 2 mM L-glutamine (all Gibco) and 10% (v/v) heat-inactivated fetal calf serum per well. Recombinant human IL-2 (Proleukin, Novartis) was added at 10  $\mu$ M and the cells were cultured for three days (37° C; 5% CO<sub>2</sub>) in order to activate NK cells (average purity: 70% CD3<sup>-</sup> NK1.1<sup>high</sup> cells). NK cell killing assays were performed using  $1 \times 10^4$  CFDA-SE-labeled (5  $\mu$ M, Life Technologies) RMA, RMA-H60 or RMA-Rae1 $\beta$  cells [169] per well (96-well V-bottom plate) together with decreasing amounts of activated NK cells from *WT* or *Magt1*<sup>-/-</sup> mice. After 4 h of incubation at 37 ° C and 5% CO<sub>2</sub>, annexin A5 (Becton Dickinson) and propidium iodide (Sigma) were added to the cultures to assess the survival of the CFDA-SE positive cells. In similar cultures, mAb C7 (BioLegend) was added at 10  $\mu$ g/mL to block NKG2D-mediated killing. Protocols were as previously described [180].

### 2.2.7 Data analysis

Results are presented as means  $\pm$  standard deviation (SD) from at least three independent experiments per group. Differences between the controls and the respective test groups were statistically analyzed using the unpaired Student's t-test. For the Bederson score and grip test, Mann-Whitney U test was used. *P*-values <0.05 were considered as statistically significant (\**P*<0.05; \*\**P*<0.01; \*\*\**P*<0.001).

### 3. Results

#### 3.1 Analysis of kinase-dead TRPM7 knockin (*Trpm7<sup>R/R</sup>*) mice

##### 3.1.1 Platelet aggregation response upon activation

Recently, in MKs, TRPM7 was identified as a critical regulator of  $Mg^{2+}$  homeostasis, which is essential for thrombopoiesis in the BM [66]. A kinase-dead knockin mouse strain (*Trpm7<sup>R/R</sup>*) carrying a point mutation (Lys1646 to Arg) in the  $Mg^{2+}$ -ATP binding site of the kinase domain, was generated to detect an *in vivo* functional role of TRPM7 kinase and channel. It was demonstrated using electrophysiological studies that inactivation of kinase activity does not influence the channel activity of TRPM7 [159]. Additionally, the mice did not show any alterations in  $Mg^{2+}$  levels of platelets, bones, or other vital organs [160].

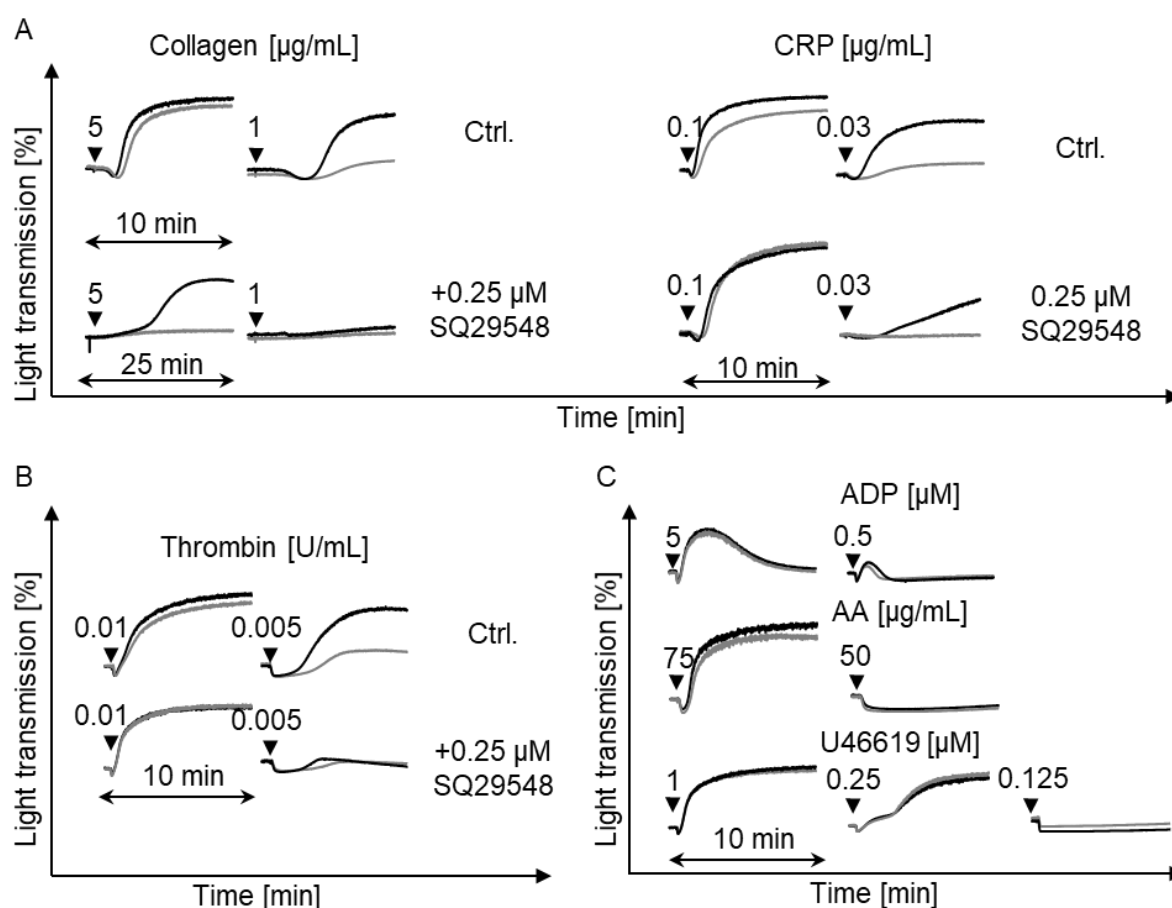


**Figure 7. Defective platelet aggregation responses in *Trpm7<sup>R/R</sup>* mice:** (A-C) Aggregation traces of *WT* (black) and *Trpm7<sup>R/R</sup>* (grey) platelets in response to the indicated agonists with or without the stated treatments. Washed platelets were stirred for the indicated time in the presence of the indicated agonists and light transmission was recorded with an Fibrinmeter 4-channel aggregometer over time. ADP activation measurements were performed with PRP. Representative traces from three independent experiments are presented ( $n = 4$ ). Thr: thrombin; CRP: collagen-related peptide; Coll: Horm collagen. SQ29548: TP receptor blocker; AA: arachidonic acid; PRP: platelet-rich plasma.

Interestingly, agonist-induced inside-out activation of integrin  $\alpha_{IIb}\beta_3$  and P-selectin surface exposure, as a marker of  $\alpha$ -granule release, were significantly reduced in response to stimulation of GPVI and stimulation with thrombin. *Trpm7<sup>R/R</sup>* platelets also showed defective ATP and serotonin release in response to lower doses of CRP or thrombin. Additionally, under flow *Trpm7<sup>R/R</sup>* whole blood produced thrombi with reduced surface coverage area. These results have been described earlier by Dr. Wenchun Chen in his Ph.D. thesis. In the present study, using various inhibitors, a better understanding of the signaling mechanisms behind the observed aggregation defects was demonstrated. Amplification of the GPVI signaling requires activation of the LAT complex through Syk, as well as the release of TXA<sub>2</sub>, ADP and serotonin. The thromboxane receptor blocker SQ29548, inhibited the aggregation response of *Trpm7<sup>R/R</sup>* platelets to high dose collagen, mimicking the defect observed to low dose collagen stimulation in control samples (**Figure 7A**). In contrast, low dose thrombin-induced aggregation in *WT* platelets was inhibited to *Trpm7<sup>R/R</sup>* level in the presence of SQ29548 (**Figure 7B**). Next, platelets were stimulated with arachidonic acid, resulting in normal aggregation responses (**Figure 7C**). This indicates that the arachidonic acid metabolism (generation of TXA<sub>2</sub> by cyclooxygenase) is unchanged during the activation of *Trpm7<sup>R/R</sup>* platelets.

### 3.1.2 Calcium responses in *Trpm7<sup>R/R</sup>* platelets

An activation-dependent increase in  $[Ca^{2+}]_i$  through the release of  $Ca^{2+}$  from intracellular stores and subsequent SOCE and receptor-operated  $Ca^{2+}$  entry (ROCE) are prerequisite events for platelet integrin  $\alpha_{IIb}\beta_3$  activation, as well as for degranulation [181, 182]. To investigate whether altered  $Ca^{2+}$  responses accounted for the impaired  $\alpha$ - and  $\delta$ -granule secretion in *Trpm7<sup>R/R</sup>* platelets, GPVI-ITAM and GPCR signaling pathways were analyzed by fluorimetric determination of agonist-induced changes in  $[Ca^{2+}]_i$ . In line with a reduced integrin activation and degranulation,  $Ca^{2+}$  store release was significantly reduced in *Trpm7<sup>R/R</sup>* platelets in response to CRP or thrombin, indicating a combined GPVI and PAR receptor signaling defect. As a consequence of the abnormal  $Ca^{2+}$  store release, the GPVI-Syk-LAT-PLC $\gamma$ 2 and thrombin-Gq-PLC $\beta$  induced  $Ca^{2+}$  influx was also reduced in *Trpm7<sup>R/R</sup>* platelets (**Figure 8A & B**). To study whether TRPM7 kinase could directly contribute to the regulation of SOCE, thapsigargin was used to bypass the GPVI and PAR receptor-induced  $Ca^{2+}$  mobilization defect and to directly modulate SOCE. Despite the normal basal cytoplasmic  $Ca^{2+}$  level and the unchanged thapsigargin-induced  $Ca^{2+}$  store release, SOCE was strongly reduced in *Trpm7<sup>R/R</sup>* platelets, suggesting a direct role of the TRPM7 kinase in the regulation of STIM1/Orai1 complex (**Figure 8C**).

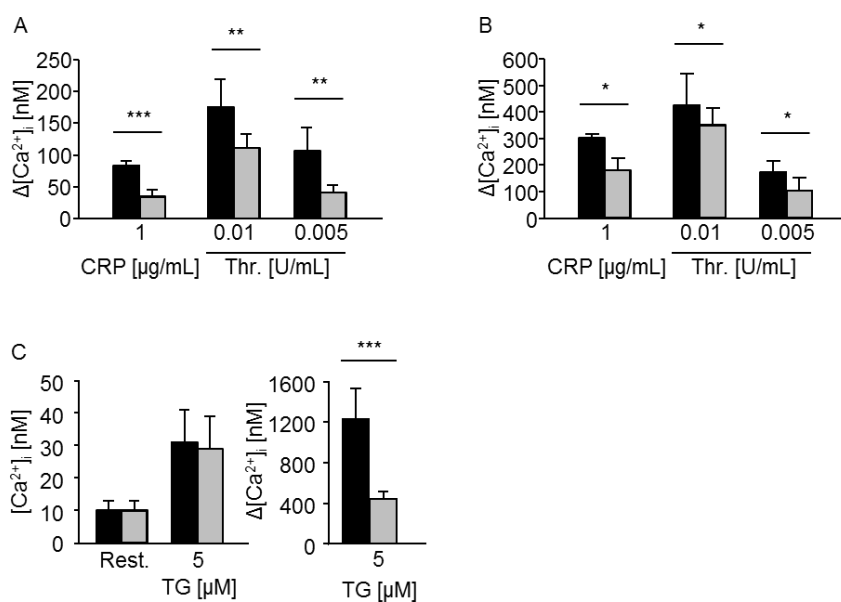


**Figure 8. Reduced  $Ca^{2+}$  responses in *Trpm7<sup>R/R</sup>* platelets:** Platelets were activated with the indicated agonists and (A)  $Ca^{2+}$  store release in the absence of extracellular  $Ca^{2+}$ , and (B)  $Ca^{2+}$  entry in the presence of extracellular  $Ca^{2+}$ , were measured in Fura-2-loaded platelets. (C)  $Ca^{2+}$  store release (left), and SOCE (right) were measured in response to thapsigargin (TG). Mean increase in  $[Ca^{2+}]_i$  was quantified by subtracting the baseline levels before the stimulus from the peak value.  $\Delta[Ca^{2+}]_i \pm$  SD is reported. Triton-X-100 was used for maximal and EDTA for minimal  $Ca^{2+}$  levels to calibrate each measurement. Results from

three independent experiments are presented ( $n = 8$ ). WT (black bars) and *Trpm7<sup>R/R</sup>* (grey bars). Thr: thrombin; CRP: collagen-related peptide. An unpaired Student's t-test was used to test significance. \* $P < 0.05$ , \*\* $P < 0.01$ , \*\*\* $P < 0.001$ .

### 3.1.3 Tyrosine phosphorylation in *Trpm7<sup>R/R</sup>* platelets

The GPVI signalosome is regulated by the Src family kinase member Lyn and the tyrosine kinase Syk, which modulates the enzymatic activity of PLC $\gamma$ 2 and other signaling molecules [183]. In agreement with the previously presented results (**Figure 7 & Figure 8**), tyrosine phosphorylation of Syk<sup>Y525/526</sup>, LAT<sup>Y132/Y191</sup> and PLC $\gamma$ 2<sup>Y759</sup> was delayed in *Trpm7<sup>R/R</sup>* platelets in response to stimulation with a low dose of CRP (**Figure 9A**), whereas the phosphorylation was normal when a high dose of CRP was used (**Figure 9B**). Furthermore, phosphorylation of serine residue 729 on PKC $\epsilon$ , a downstream effector of PLC $\gamma$ 2, was also diminished suggesting a strongly impaired PLC activity under this condition. In sharp contrast, phosphorylation of Lyn<sup>Y507</sup> within the inhibitory loop of the enzyme was unaltered. In addition, PLC $\beta$ 3 phosphorylation was reduced upon stimulation with thrombin (**Figure 9C**). To further address the potential role of Syk in TRPM7 kinase signaling, the (hem)ITAM receptor CLEC-2 was stimulated using rhodocytin. Similarly to the GPVI signaling pathway, a reduced phosphorylation of Syk<sup>Y525/526</sup>, LAT<sup>Y132/Y191</sup> and PLC $\gamma$ 2<sup>Y759</sup> was observed upon the stimulation of *Trpm7<sup>R/R</sup>* platelets with rhodocytin (**Figure 9D**). Altogether, these results suggest that altered activation of Syk and PLC isoforms can account for the general signaling defects of *Trpm7<sup>R/R</sup>* platelets.

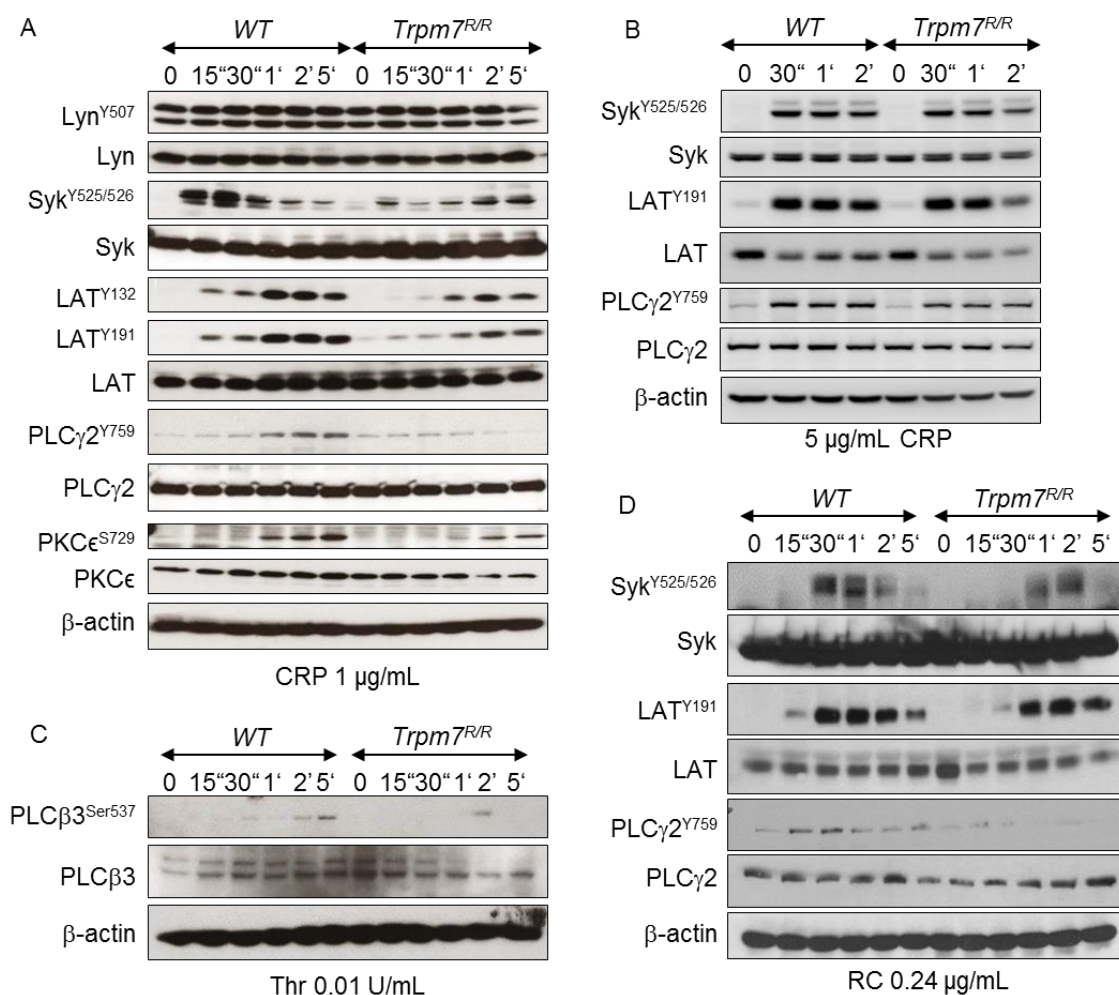


**Figure 9. TRPM7 kinase regulates GPVI, PAR, and CLEC-2-mediated signaling pathways:** (A & B) Western blot showing the time-dependent tyrosine phosphorylation pattern of *Trpm7<sup>R/R</sup>* platelets upon CRP, (C) thrombin or (D) rhodocytin stimulation. Representative blots from three independent experiments are presented. Thr: thrombin; CRP: collagen-related peptide; RC: rhodocytin.

### 3.2 Analysis of *Trpm7<sup>f/f-Pf4Cre</sup>* mice

#### 3.2.1 Count, size, glycoprotein expression and $[Mg^{2+}]_i$ in platelets

In an earlier study, *Trpm7<sup>f/f-Pf4Cre</sup>* mice were reported to have macrothrombocytopenia with an abnormal spleen and BM structure and an increased number of MKs in these organs. We found that major glycoproteins expressed on the surface of platelets were not altered between *WT* and *Trpm7<sup>f/f-Pf4Cre</sup>* mice (**Figure 10A & B**). Using Mag-Fluo-4, the concentration of  $[Mg^{2+}]_i$  in whole blood was found to be lower in mutant mice [75]. Washed mutant platelets, loaded with Mag-Fluo-4, also showed a defective  $[Mg^{2+}]_i$ , irrespective of the condition of hypomagnesemia (0 mM  $MgCl_2$ ) or physiological magnesia (1 mM  $MgCl_2$ ) (**Figure 10C & D**).

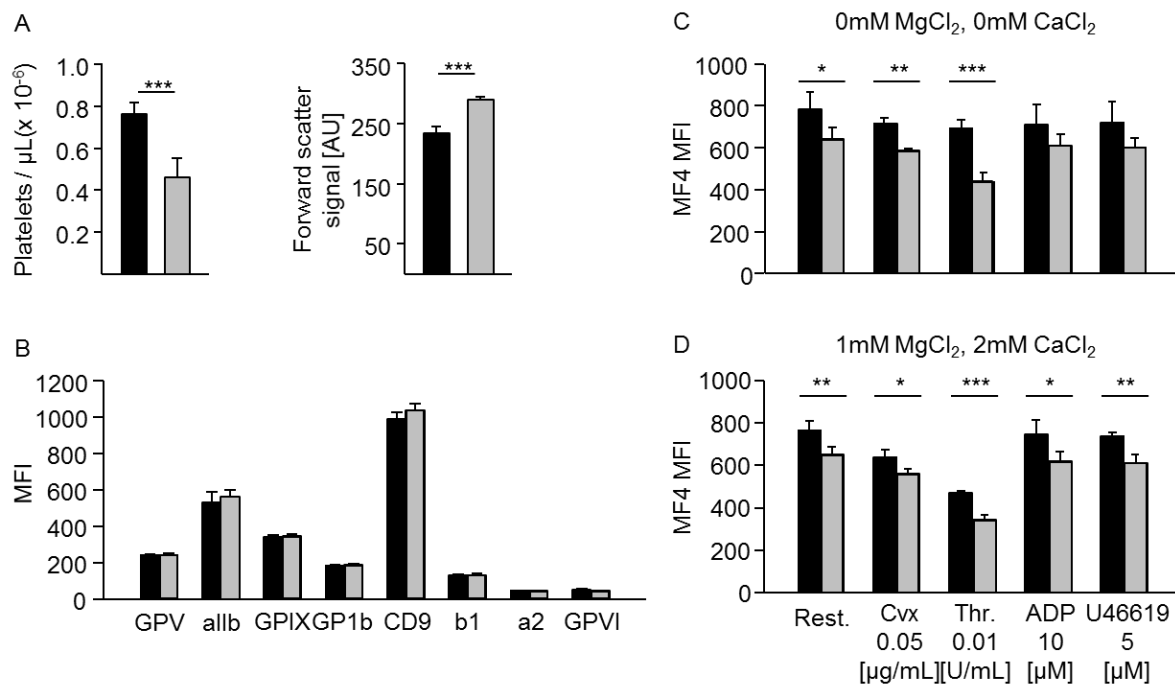


**Figure 10.  $[\text{Mg}^{2+}]_i$  deficit in *Trpm7<sup>fl/fl-Pf4Cre</sup>* platelets:** (A) Platelet count (left) and mean platelet volume (right) measured in heparinized whole blood by flow cytometry. A representative of three independent experiments is presented ( $n = 4$ ). (B) Surface expression of major platelet glycoproteins, as assessed by flow cytometry. A representative of three independent experiments is shown ( $n = 5$ ). MFI: mean fluorescence intensity. (C & D)  $[\text{Mg}^{2+}]_i$  concentration was measured in platelets incubated with HBSS buffer containing (C) 0 mM  $\text{MgCl}_2$  and 0 mM  $\text{CaCl}_2$  or (D) 1 mM  $\text{MgCl}_2$  and 2 mM  $\text{CaCl}_2$  using Mag-Fluo-4, as explained in the methods. Results from three independent experiments are shown as mean fluorescence intensity  $\pm$  SD ( $n = 3$ ). *WT* mice are represented by black bars and *Magt1<sup>-/-</sup>* mice are represented by gray bars. Rest.: resting, Cvx.: convulxin, MF4: Mag-Fluo-4, Thr: thrombin, HBSS: Hank's balanced salt solution. An unpaired Student's t-test was used to test significance. \* $P < 0.05$ , \*\* $P < 0.01$ , \*\*\* $P < 0.001$ . (Data in Figure 10A & B kindly provided by Dr. Simon Stritt).

### 3.2.2 Platelet reactivity in *Trpm7<sup>fl/fl-Pf4Cre</sup>* mice

#### 3.2.2.1 $\text{Ca}^{2+}$ responses

To investigate the physiological relevance of TRPM7 channel for platelet reactivity, we analyzed the  $\text{Ca}^{2+}$  responses in *Trpm7<sup>fl/fl-Pf4Cre</sup>* platelets. It has been shown that TRPM7 is localized on the plasma membrane and on intracellular vesicle membranes [184]. When *Trpm7<sup>fl/fl-Pf4Cre</sup>* platelets were activated in the absence of extracellular  $\text{Ca}^{2+}$ , a profound increase of  $\text{Ca}^{2+}$  store release was observed in response to thrombin, CRP, rhodocytin or U46619 stimulation, in comparison to *WT* platelets (**Figure 11A**). To study whether TRPM7 could directly contribute to the regulation of SOCE, *Trpm7<sup>fl/fl-Pf4Cre</sup>* platelets were stimulated with thapsigargin. Interestingly, thapsigargin-triggered SOCE was significantly reduced in the *Trpm7<sup>fl/fl-Pf4Cre</sup>* platelets compared to *WT* platelets, although the store release was normal in response to thapsigargin (**Figure 11B & C**). In the presence of 1 mM extracellular  $\text{CaCl}_2$ , a defective agonist-induced  $\text{Ca}^{2+}$  influx was detected, indicating that the enhanced  $\text{Ca}^{2+}$  store release could not amplify SOCE in the mutant platelets (**Figure 11D**).

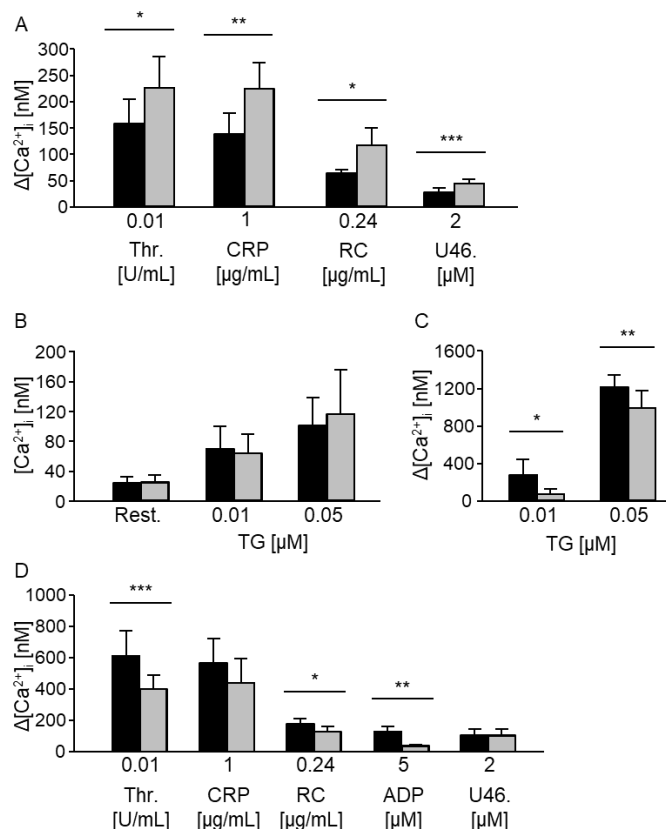


**Figure 11. Abnormal  $Ca^{2+}$  mobilization in *Trpm7*<sup>fl/fl-Pf4Cre</sup> platelets:** Platelets were activated with the indicated agonists and (A)  $Ca^{2+}$  store release and (B & C) thapsigargin (TG) induced (B)  $Ca^{2+}$  store release and (C) store-operated  $Ca^{2+}$  entry (SOCE) were measured. (D)  $Ca^{2+}$  entry was measured in Fura-2-loaded platelets in the presence of extracellular  $CaCl_2$ . Mean increase in  $[Ca^{2+}]_i$  was quantified by subtracting baseline levels before the stimulus from peak values.  $\Delta[Ca^{2+}]_i \pm SD$  is reported. Triton-X-100 was used for maximal and EDTA for minimal  $Ca^{2+}$  levels to calibrate each measurement. WT platelets (black bars) and *Trpm7*<sup>fl/fl-Pf4Cre</sup> platelets (grey bars). Results from three independent experiments are presented (n=8). Thr.: thrombin; CRP: collagen-related peptide; RC: rhodocytin; U46.: U46619. An unpaired Student's t-test was used to test significance. \*P<0.05, \*\*P<0.01, \*\*\*P<0.001.

### 3.2.2.2 Agonist-induced platelet activation in *Trpm7*<sup>fl/fl-Pf4Cre</sup> mice

Integrin activation and degranulation have been assessed by flow cytometry to assess the functional implications of the altered  $Ca^{2+}$  signaling in *Trpm7*<sup>fl/fl-Pf4Cre</sup> platelets. Washed platelets from either WT or *Trpm7*<sup>fl/fl-Pf4Cre</sup> mice were stimulated with ITAM or GPCR specific agonists, and  $\alpha_{IIb}\beta_3$  integrin activation and granule release (P-selectin exposure) were assessed by flow cytometry using the JON/A-PE and anti-P-selectin antibodies, respectively [173]. Depending on the type of agonist used, the TRPM7-deficient platelets displayed variable activation responses. This ranged from increased integrin  $\alpha_{IIb}\beta_3$  activation with GPCR agonists (ADP, ADP + U46619, thrombin), to a slightly reduced integrin activation in response to low doses of CRP (**Figure 12A**). On the other hand, a consistent and significant decrease in P-selectin exposure was observed in *Trpm7*<sup>fl/fl-Pf4Cre</sup> platelets, when triggered with high doses of thrombin or any dose of (hem)ITAM agonists (**Figure 12B**).



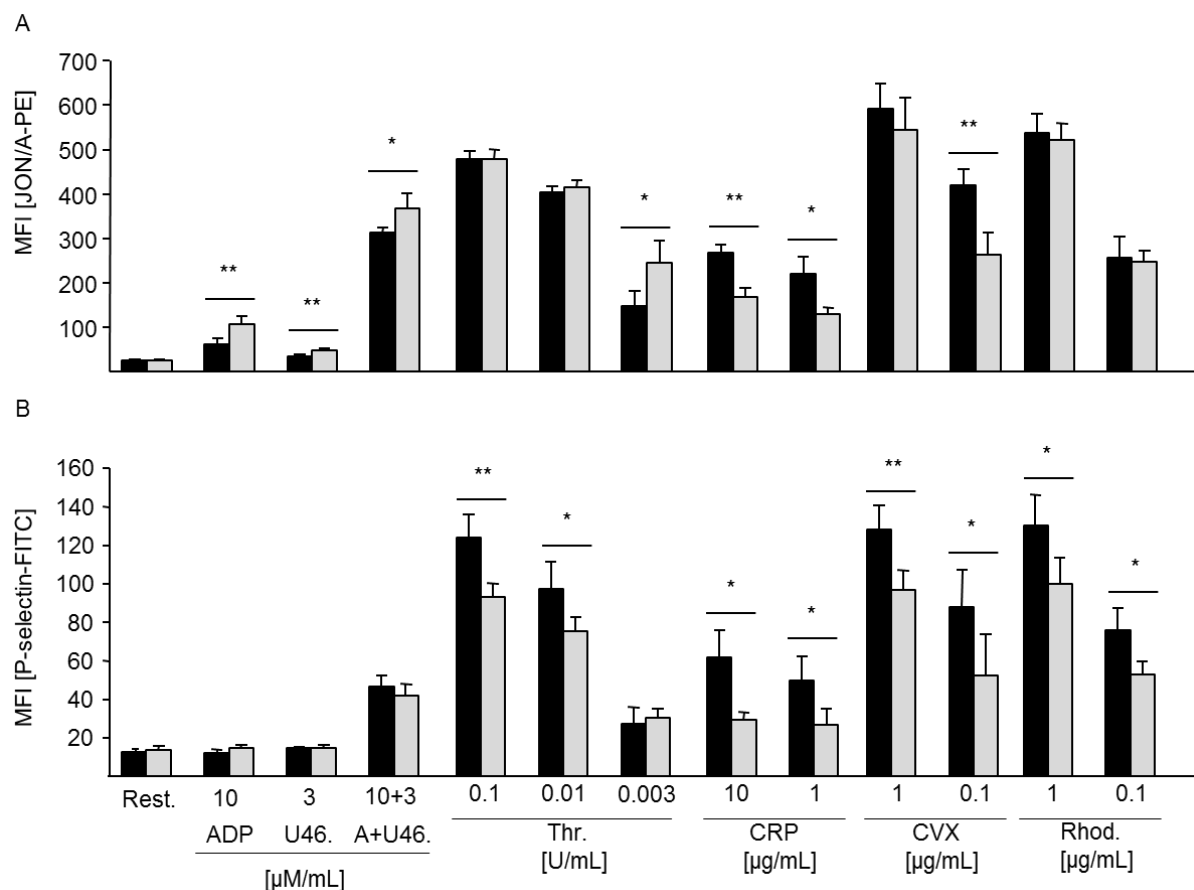


**Figure 12. Abnormal integrin activation and degranulation in *Trpm7*<sup>fl/fl-Pf4Cre</sup> mice:** (A) Flow cytometric analysis of integrin  $\alpha_{IIb}\beta_3$  activation (upper panel) and (B) degranulation-dependent P-selectin exposure (lower panel) measured upon activation with the indicated agonists in *WT* (black bar) and *Trpm7*<sup>fl/fl-Pf4Cre</sup> (grey bar) platelets. Results are expressed as mean fluorescence intensity (MFI)  $\pm$  SD. A representative from three independent experiments is presented (n = 6). Thr: thrombin; U46., U46619; CRP: collagen-related peptide; CVX: convulxin; Rhod: rhodocytin. An unpaired Student's t-test was used to test significance. \*P<0.05, \*\*P<0.01, \*\*\*P<0.001.

### 3.2.2.3 PS exposure in *Trpm7*<sup>fl/fl-Pf4Cre</sup> platelets

Besides platelet integrin activation and degranulation,  $Ca^{2+}$  mobilization is an important step for PS exposure, which enhances the procoagulant activity of stimulated platelets [185]. Therefore, this functional consequence of a dysregulated  $Ca^{2+}$  homeostasis in *Trpm7*<sup>fl/fl-Pf4Cre</sup> platelets was studied by measuring the binding of annexin A5. A significant reduction of PS exposure was detected in *Trpm7*<sup>fl/fl-Pf4Cre</sup> platelets upon stimulation with high and intermediate doses of CRP, rhodocytin, or upon a co-stimulation of CRP and thrombin. Stimulation with the calcium ionophore, A23187 served as a positive control to measure the maximal PS exposure in platelets (**Figure 13**).

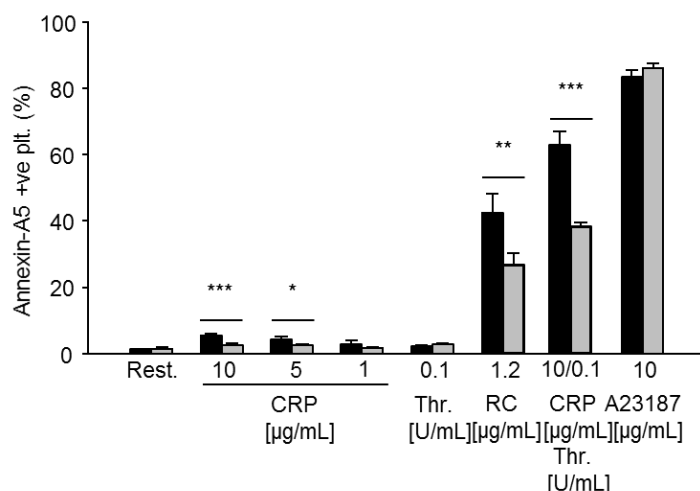


**Figure 13. Abnormal PS exposure in *Trpm7<sup>fl/fl-Pf4Cre</sup>* platelets:** Flow cytometric analysis of phosphatidylserine exposure tested by measuring annexin-A5 binding to platelets. *WT* (black bar) and *Trpm7<sup>fl/fl-Pf4Cre</sup>* (grey bar). Results are expressed as mean  $\pm$  SD. A representative from three independent experiments is presented ( $n = 4$ ). Rest.: Resting; Thr.: thrombin; CRP: collagen-related peptide; RC: rhodocytin; A23187: calcium ionophore; plt.: platelets. An unpaired Student's t-test was used to test significance. \* $P < 0.05$ , \*\* $P < 0.01$ , \*\*\* $P < 0.001$ .

### 3.2.2.4 Aggregation in *Trpm7<sup>fl/fl-Pf4Cre</sup>* platelets

Similar to the flow cytometric assessment of platelet integrin activation and degranulation, also the aggregation responses of *Trpm7<sup>fl/fl-Pf4Cre</sup>* platelets were variable. Mutant platelets were hyper-aggregated in response to thrombin and U46619 (**Figure 14A**), while upon CRP or collagen stimulation *Trpm7<sup>fl/fl-Pf4Cre</sup>* platelets showed defective aggregation. Stimulation with RC did not show any difference in aggregation between *WT* and *Trpm7<sup>fl/fl-Pf4Cre</sup>* platelets (**Figure 14B**).

To investigate the reason for the hyper-aggregability of *Trpm7<sup>fl/fl-Pf4Cre</sup>* platelets to thrombin or U46619 stimulations, both *WT* and *Trpm7<sup>fl/fl-Pf4Cre</sup>* platelets were treated with various inhibitors or extracellular  $MgCl_2$ . Here, pre-incubation with 5 mM  $MgCl_2$ , blebbistatin or a TP receptor blocker normalized the hyper-aggregation of *Trpm7<sup>fl/fl-Pf4Cre</sup>* platelets to the level seen in *WT* platelets, upon thrombin stimulation (**Figure 14A left**). However, upon stimulation with U46619, the *Trpm7<sup>fl/fl-Pf4Cre</sup>* platelets still showed hyper-aggregation in all the treatments, except when using a  $P2Y_{12}$  inhibitor, 2MeSAMP (**Figure 14A right**). On the other hand, a  $P2Y_1$  inhibitor MRS 2179 could not normalize the hyper-aggregation of *Trpm7<sup>fl/fl-Pf4Cre</sup>* platelets.

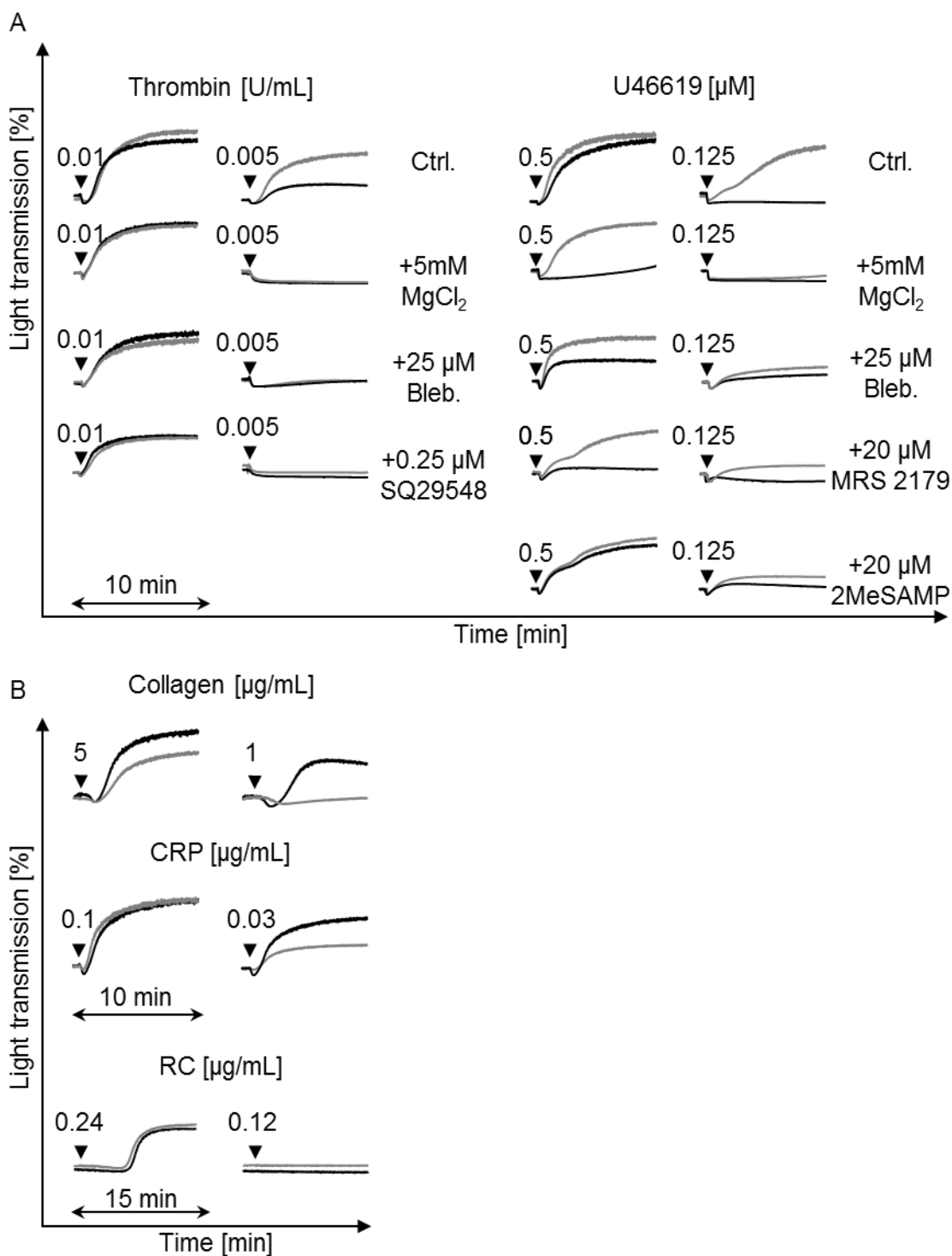


**Figure 14. Variable aggregation responses of *Trpm7<sup>fl/fl-Pf4Cre</sup>* platelets towards GPCR and GPVI specific agonists:** (A & B) Washed platelets from either *WT* (black traces) or *Trpm7<sup>fl/fl-Pf4Cre</sup>* (grey traces) mice were stimulated with the indicated agonists in the presence or absence of the stated treatments and light transmission was recorded on a Fibrinometer 4-channel aggregometer. Representative traces from three independent experiments are presented (n = 4). Thr: thrombin; U46619: stable thromboxane A<sub>2</sub> analog; CRP: collagen-related peptide; Collagen: Horn collagen; Ctrl.: Control; Bleb.: blebbistatin; MRS 2179: P2Y<sub>1</sub> inhibitor; 2MeSAMP: P2Y<sub>12</sub> inhibitor; SQ29548: TP receptor inhibitor.

### 3.2.2.5 Defective aggregate formation of *Trpm7<sup>fl/fl-Pf4Cre</sup>* platelets under flow

To find the significance of *Trpm7* for thrombus formation *ex vivo* and to follow-up on the observation that *Trpm7<sup>fl/fl-Pf4Cre</sup>* platelets showed a defective collagen induced aggregation, flow chamber experiments were carried out. Here, significantly decreased surface coverage and relative thrombus volume were observed when heparinized whole blood of *Trpm7<sup>fl/fl-Pf4Cre</sup>* mice was perfused over collagen coated surface at a shear rate of  $1000 \text{ sec}^{-1}$  (**Figure 15A & B**).

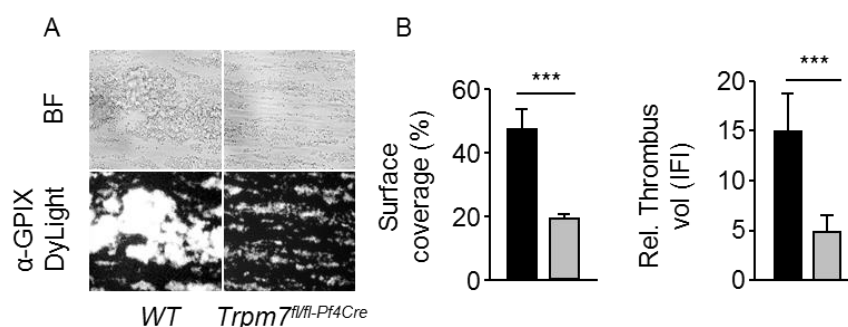


**Figure 15. Abnormal *ex vivo* thrombus formation of *Trpm7<sup>fl/fl-Pf4Cre</sup>* platelets under flow:** (A) Heparinized whole blood (anti-GPIX-DyLight-488 labeled) of either *WT* (black bar) or *Trpm7<sup>fl/fl-Pf4Cre</sup>* (grey bar) mice was perfused at  $1000 \text{ s}^{-1}$  over collagen-coated coverslips ( $0.2 \text{ mg/mL}$ ). Representative phase contrast (upper panel), fluorescence microscopy (lower panel)

images are shown. (B) Mean surface coverage and relative thrombus volume were quantified and are presented as mean  $\pm$  SD. Results from three independent experiments are presented ( $n = 5$ ). An unpaired Student's t-test was used to test significance. \* $P < 0.05$ , \*\* $P < 0.01$ , \*\*\* $P < 0.001$ .

### 3.2.3 TRPM7 deficiency does not affect the stroke outcome

The role of TRPM7 in  $\text{Ca}^{2+}$  entry under conditions of hypoxia or ischemic brain infarction has been highlighted [186]. In collaboration with the Department of Neurology, University Hospital of Würzburg, *Trpm7<sup>fl/fl-Pf4Cre</sup>* mice were challenged with a 60 min tMCAO model of stroke. In *WT* and *Trpm7<sup>fl/fl-Pf4Cre</sup>* mice equal infarct volumes were detected, and no differences were observed in the Bederson score and Grip tests (**Figure 16**).

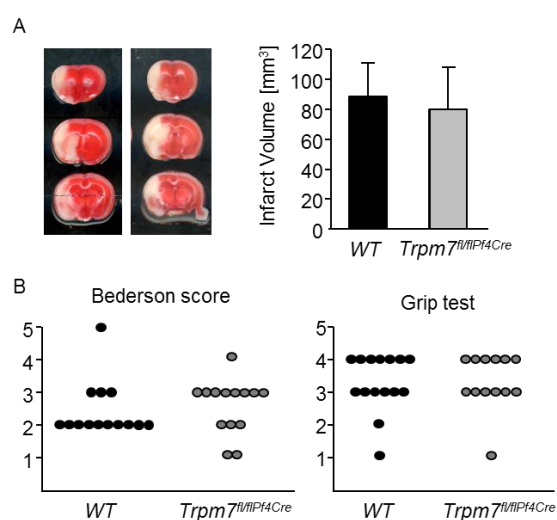


**Figure 16. Platelet TRPM7 is dispensable for stroke development:** (A) 2,3,5-triphenyltetrazolium chloride (TTC) staining of coronal brain sections (left) of mice sacrificed 24 h post subsection to 60 min of tMCAO, Infarct volume quantified by planimetry (right) in brains of *WT* and *Trpm7<sup>fl/fl-Pf4Cre</sup>* mice. Planimetric quantification represents mean infarct volume [ $\text{mm}^3$ ]  $\pm$  S.D. (B) Bederson score (left) and grip test (right) are shown for the same group of mice 24 h post tMCAO. Each symbol represents one animal. Representative images and results from two independent experiments are shown. Unpaired Student's t-test for infarct volume or Mann-Whitney U test for Bederson score and Grip test were used and \* $P < 0.05$ , \*\* $P < 0.01$ , \*\*\* $P < 0.001$ . (Experiments were performed by Dr. Michael Schuhmann).

### 3.3 Analysis of *Magt1*<sup>-y</sup> mice

#### 3.3.1 Normal organogenesis and thrombopoiesis in *Magt1*<sup>-y</sup> mice

MAGT1 expression was abrogated by inserting a gene trap cassette into intron 1 of the *Magt1* gene (**Figure 17A left**). An alternative 3'UTR containing a polyadenylation signal (pA) of the inserted GEO gene terminated mRNA expression of *Magt1*, deleting MAGT1 which was confirmed by immunoblotting (**Figure 17A right**). Since *Magt1* is located on the X chromosome, all studies were performed in hemizygous male mice (further referred to as *Magt1*<sup>-y</sup>). *Magt1*<sup>-y</sup> mice were healthy, bred normally and histological analysis of major organs revealed no apparent alterations. (**Figure 17B**).

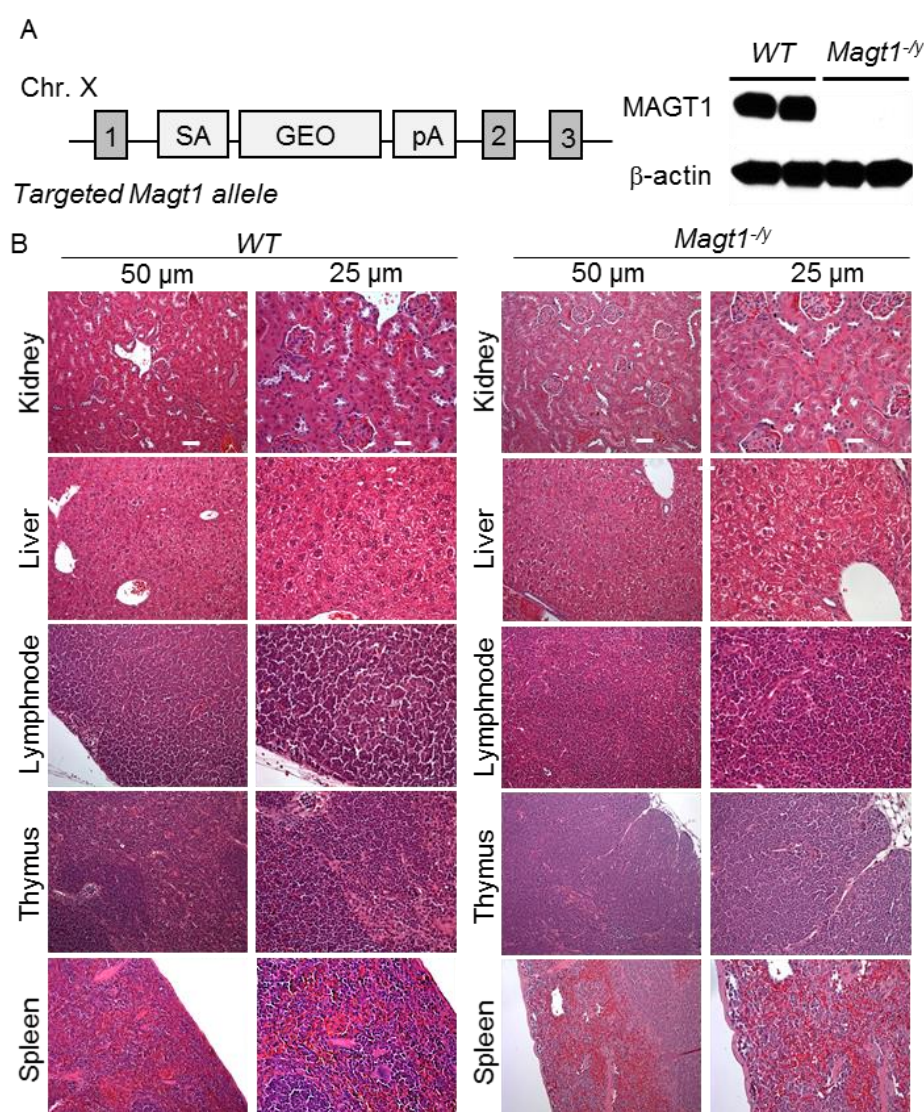


**Figure 17. Generation and primary characterization of MAGT1 knockout mice:** (A) Targeting strategy of the used *Magt1*<sup>-y</sup> mouse model (left) and western blot showing MAGT1 expression at 38 kDa in *WT* but not in *Magt1*<sup>-y</sup> samples (right). Anti  $\beta$ -actin Ab was used as loading control. (B) Hematoxylin and eosin (H & E) staining of different organs from *WT* and *Magt1*<sup>-y</sup> mice.

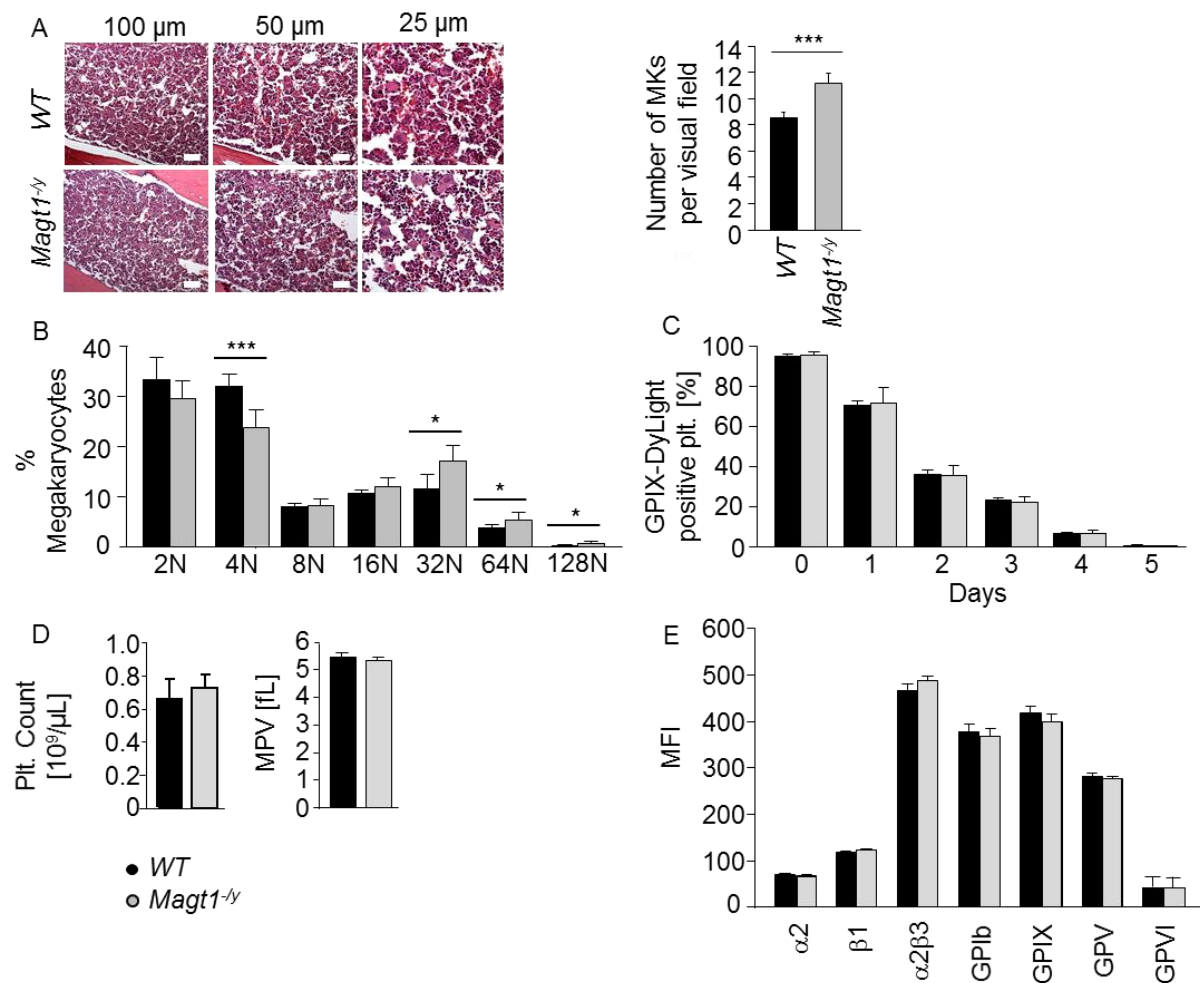


**Figure 18. Altered MK number but normal platelet count and size in *Magt1*<sup>-/-</sup> mice:** (A) (Haematoxylin and Eosin staining of BM (left) and MK numbers quantification (right). (B) Ploidy of BM MKs was determined by propidium iodide staining and flow cytometry. A representative from three independent experiments is shown (n=5) [174]. (C) Platelet lifespan was assessed by flow cytometry. A representative from three independent experiments is shown (n = 6). (D) Platelet count (left) and mean platelet volume (right) assessed in whole blood using an automated Sysmex blood analyzer. (E) Surface expression of the stated glycoproteins assessed by flow cytometry. A representative of three independent experiments is shown (n = 5). *WT* (black bars) and *Magt1*<sup>-/-</sup> (gray bars) mice. MK: megakaryocyte; Plt.: platelet; MPV: mean platelet volume; MFI: mean fluorescence intensity. An unpaired Student's t-test was used to test significance. \*P<0.05, \*\*P<0.01, \*\*\*P<0.001.

BM MKs number and ploidy was slightly increased in *Magt1*<sup>-/-</sup> compared to *WT* mice (**Figure 18A & B**). Nevertheless, platelet lifespan, count, and size were unaltered in *Magt1*<sup>-/-</sup> mice compared to *WT* controls (**Figure 18C & D**).

Similarly, the expression of major glycoproteins on the platelet surface, as analyzed by flow cytometry in washed platelets, was indistinguishable between *WT* and *Magt1*<sup>-/-</sup> mice (**Figure 18E**).

### 3.3.2 Platelet reactivity in *Magt1*<sup>-/-</sup> mice

#### 3.3.2.1 Increased Mg<sup>2+</sup> efflux in *Magt1*<sup>-/-</sup> platelets in response to GPVI stimulation

To study the changes in [Mg<sup>2+</sup>]<sub>i</sub>, washed platelets from *WT* and *Magt1*<sup>-/-</sup> mice were labeled with Mag-Fluo-4, and fluorescence intensity was recorded for 5 min. Upon stimulation with a low dose of CRP, the *Magt1*<sup>-/-</sup> platelets showed an increased loss of [Mg<sup>2+</sup>]<sub>i</sub> in comparison to *WT* platelets.

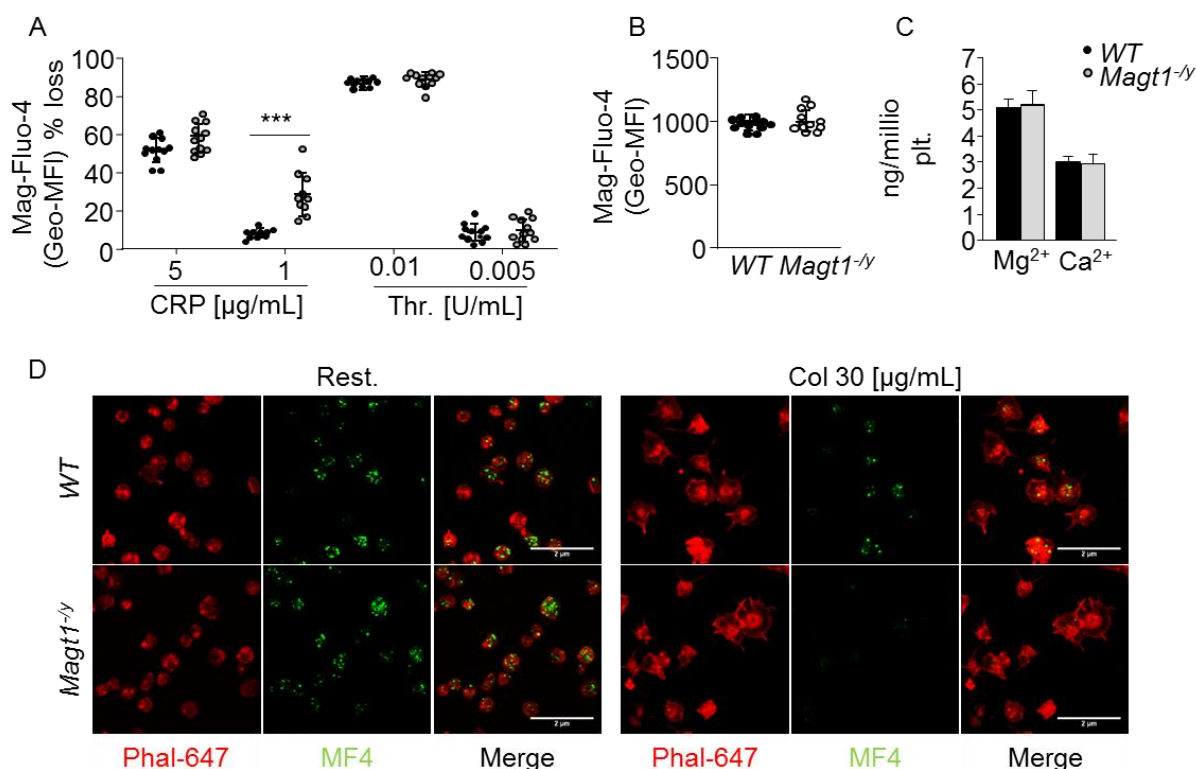


**Figure 19. Altered GPVI induced [Mg<sup>2+</sup>]<sub>i</sub> efflux in *Magt1*<sup>-/-</sup> platelets.** (A) Mag-Fluo-4 loaded *WT* or *Magt1*<sup>-/-</sup> platelets were stimulated with the indicated agonists. The relative decrease (%) in fluorescence intensity of [Mg<sup>2+</sup>]<sub>i</sub> was determined in the presence of 2 mM extracellular CaCl<sub>2</sub> and 1 mM extracellular MgCl<sub>2</sub>. Results from three independent experiments (n = 5) presented. Each symbol represents one animal. (B) Mag-Fluo-4 loaded *WT* or *Magt1*<sup>-/-</sup> platelets basal [Mg<sup>2+</sup>]<sub>i</sub> in resting platelets was determined by flow cytometry. Results from three independent experiments (n = 5) presented. Each symbol represents one animal. (C) Determination of the total Mg<sup>2+</sup> and Ca<sup>2+</sup> content in resting platelets using ICP-MS. Results result from three independent experiments (n = 5) are presented. *WT* represent black dot/bar and *Magt1*<sup>-/-</sup> represent grey dot/bar. (D) Mag-Fluo-4 loaded *WT* or *Magt1*<sup>-/-</sup> platelets were allowed to adhere to poly-L-lysine coated coverslips either in resting (left) or in collagen-activated (30 μg/mL) (right) condition for 30 min. Samples were counterstained with phalloidin-647 and images were taken using a confocal microscope (TCS-SP5). Scalebar is 2 μm. Representative images from three independent experiments are presented (n = 6). MFI: mean fluorescence intensity; MF4: Mag-Fluo-4; Geo-MFI: geometric mean fluorescence intensity; CRP: Collagen related peptide; Thr.: thrombin; Rest.: resting; Col: collagen. An unpaired Student's t-test was used to test significance. \*P<0.05, \*\*P<0.01, \*\*\*P<0.001.

However, upon stimulation with a high dose of CRP or thrombin, the decrease in [Mg<sup>2+</sup>]<sub>i</sub> was comparable between *WT* and *Magt1*<sup>-/-</sup> platelets (**Figure 19A**). The resting level of [Mg<sup>2+</sup>]<sub>i</sub> was indistinguishable between *WT* and *Magt1*<sup>-/-</sup> platelets (**Figure 19B**). Also, platelet total

magnesium content showed no differences between *WT* and *Magt1<sup>-/-</sup>* mice (**Figure 19C**). *WT* and *Magt1<sup>-/-</sup>* platelets loaded with Mag-Fluo-4 were analyzed using a confocal microscope to confirm the findings from flow cytometry. Here, resting platelets showed puncta structures in both *WT* and *Magt1<sup>-/-</sup>* samples. However, upon activation with collagen (30  $\mu\text{g}/\text{mL}$ ), the spread platelets from *Magt1<sup>-/-</sup>* mice showed almost no signal for Mag-Fluo-4 and spread platelets from *WT* still showed some Mag-Fluo-4 puncta (**Figure 19D**). These results suggested that the function of MAGT1 is selectively regulated by the GPVI signalosome, whilst its role is dispensable in resting platelets.

### 3.3.2.2 Increased $\text{Ca}^{2+}$ influx in *Magt1<sup>-/-</sup>* platelets upon activation

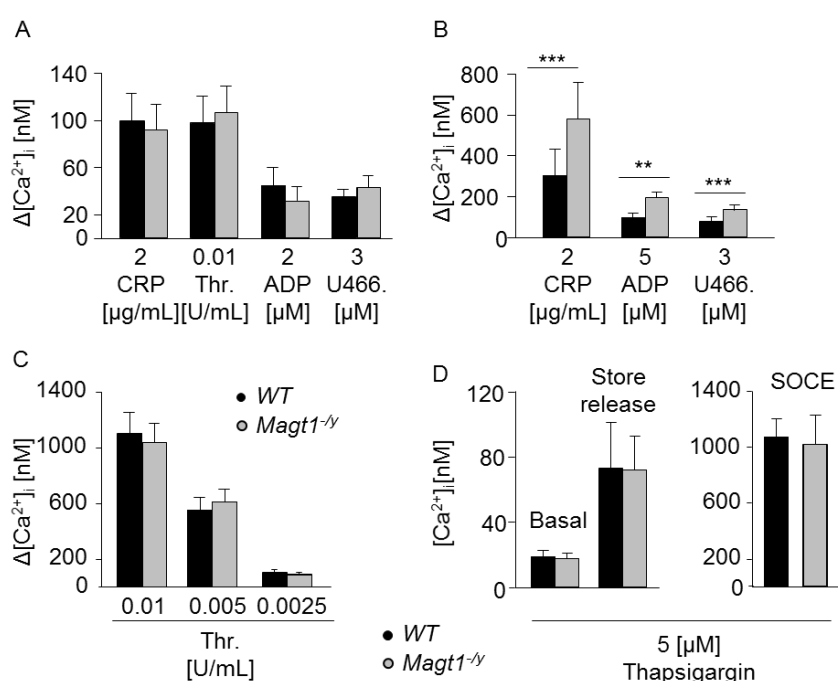


**Figure 20. An abnormal  $\text{Ca}^{2+}$  influx in *Magt1<sup>-/-</sup>* platelets:** Fura-2 loaded *WT* or *Magt1<sup>-/-</sup>* platelets were stimulated with the indicated agonists (A) in the absence of calcium for  $\text{Ca}^{2+}$  store release or (B & C) in the presence of 1 mM extracellular  $\text{CaCl}_2$  for  $\text{Ca}^{2+}$  entry. (D) Thapsigargin-induced  $\text{Ca}^{2+}$  store release (left) and store-operated  $\text{Ca}^{2+}$  entry (SOCE) (right). Results are shown as  $\Delta[\text{Ca}^{2+}]_i \pm \text{SD}$  obtained by subtracting the baseline  $[\text{Ca}^{2+}]_i$  from the peak  $[\text{Ca}^{2+}]_i$  after stimulation. Results from three independent experiments are shown (n = 6). Triton-X was used for maximal and EDTA for minimal  $\text{Ca}^{2+}$  levels to calibrate each measurement. CRP: Collagen related peptide; Thr.: Thrombin;

U466.: U46619 a stable analog of thromboxane  $\text{A}_2$ . An unpaired Student's t-test was used to test significance. \* $P < 0.05$ , \*\* $P < 0.01$ , \*\*\* $P < 0.001$ .

Agonist-induced platelet activation requires an increase in  $\text{Ca}^{2+}$  that occurs through the release of  $\text{Ca}^{2+}$  from the intracellular stores and entry through  $\text{Ca}^{2+}$  channels in the plasma membrane [46]. To investigate whether MAGT1 deficiency leads to abnormal  $\text{Ca}^{2+}$  responses, resting and activated *Magt1<sup>-/-</sup>* platelets were subjected to a detailed analysis of  $\text{Ca}^{2+}$  homeostasis. In line with an unaltered  $[\text{Mg}^{2+}]_i$  in resting platelets, the basal  $[\text{Ca}^{2+}]_i$  was normal as well. Similarly, agonist-induced  $\text{Ca}^{2+}$  store release was also normal in *Magt1<sup>-/-</sup>* platelets (**Figure 20A**). Strikingly,  $\text{Ca}^{2+}$  influx was significantly elevated in response to stimulation with the receptor



agonists CRP, ADP or the TXA<sub>2</sub> analog U46619 (**Figure 20B**). However, upon thrombin stimulation, no difference of Ca<sup>2+</sup> influx was observed between *WT* and *Magt1*<sup>-/-</sup> platelets (**Figure 20C**). To directly test whether store-operated Ca<sup>2+</sup> entry was dysregulated in *Magt1*<sup>-/-</sup> platelets, thapsigargin was used to bypass platelet receptor-induced Ca<sup>2+</sup> store depletion, thereby directly activating STIM1-dependent ORAI1 activation in platelets. Surprisingly, normal SOCE was detected in *Magt1*<sup>-/-</sup> platelets (**Figure 20D**) upon thapsigargin stimulation, indicating that MAGT1 regulates an alternative Ca<sup>2+</sup> entry mechanism that is independent of STIM1/ORAI1 mediated SOCE.

### 3.3.2.3 Abnormal Mg<sup>2+</sup> and Ca<sup>2+</sup> responses in *Magt1*<sup>-/-</sup> platelets can be normalized by Mg<sup>2+</sup> supplementation *in vitro*

In DT40 B cells it has been shown that loss of TRPM7 mediated Mg<sup>2+</sup> influx can be compensated by overexpression of MAGT1 [86]. Therefore loss of MAGT1 function could also be partially compensated by upregulation of TRPM7. However, mRNA expression of TRPM7 was not changed in *Magt1*<sup>-/-</sup> platelets (**Figure 21A**), excluding a role of overexpression of TRPM7 in the MAGT1 pathology.

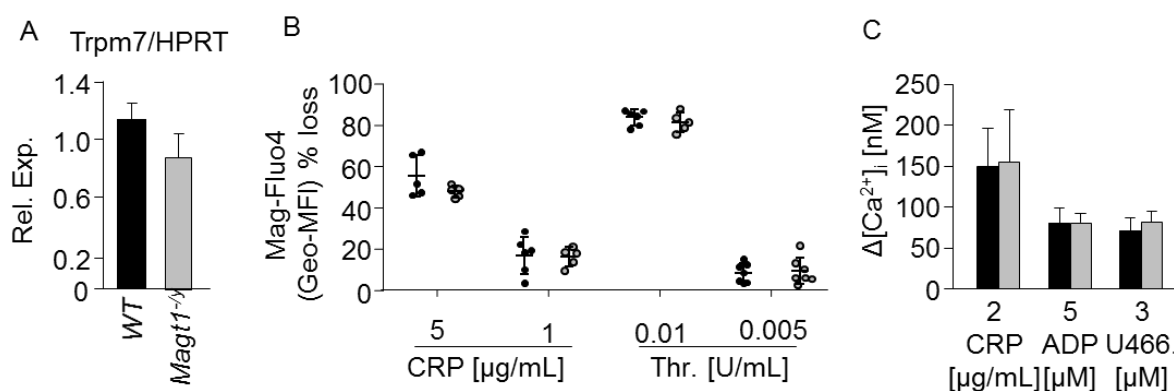


**Figure 21. Abnormal Mg<sup>2+</sup> and Ca<sup>2+</sup> homeostasis in *Magt1*<sup>-/-</sup> platelets can be normalized by extracellular MgCl<sub>2</sub> supplementation:** (A) Relative *Trpm7* mRNA expression level quantified relative to housekeeping gene *Hprt*. A representative result from three independent experiments (n = 4) presented. (B) Mag-Fluo-4 loaded *WT* or *Magt1*<sup>-/-</sup> platelets were stimulated with the indicated agonists in the presence of 1 mM extracellular CaCl<sub>2</sub> and 5 mM extracellular MgCl<sub>2</sub>. Each symbol represents one animal. Results from three independent experiments presented (n = 4). (C) Fura-2 loaded *WT* or *Magt1*<sup>-/-</sup> platelets were stimulated with the indicated agonists in the presence of 1 mM extracellular CaCl<sub>2</sub> and 5 mM extracellular MgCl<sub>2</sub> and changes in [Ca<sup>2+</sup>]<sub>i</sub> were monitored using a fluorimeter. Results are shown as Δ[Ca<sup>2+</sup>]<sub>i</sub> ± SD obtained by subtracting the baseline [Ca<sup>2+</sup>]<sub>i</sub> from a peak [Ca<sup>2+</sup>]<sub>i</sub> after stimulation. Results from three independent experiments are shown (n = 3). Triton-X was used for maximal and EDTA for minimal Ca<sup>2+</sup> levels to calibrate each measurement. CRP: Collagen related peptide; Thr.: Thrombin; ADP: Adenosine diphosphate; U46619: a stable analog of thromboxane A<sub>2</sub>. An unpaired Student's t-test was used to test significance. \*P<0.05, \*\*P<0.01, \*\*\*P<0.001.

Next, platelets were incubated with 5 mM MgCl<sub>2</sub>, and Mg<sup>2+</sup> efflux and Ca<sup>2+</sup> influx were measured using the Mag-Fluo4 and Fura-2 dyes, respectively. Interestingly, MgCl<sub>2</sub> supplementation could normalize Mg<sup>2+</sup> efflux and the aberrant Ca<sup>2+</sup> influx in *Magt1*<sup>-/-</sup> platelets upon CRP stimulation but had no additive effects in thrombin-stimulated platelets (**Figure 21B & C**).

### 3.3.2.4 Normal integrin activation and P-selectin exposure in *Magt1*<sup>-/-</sup> platelets

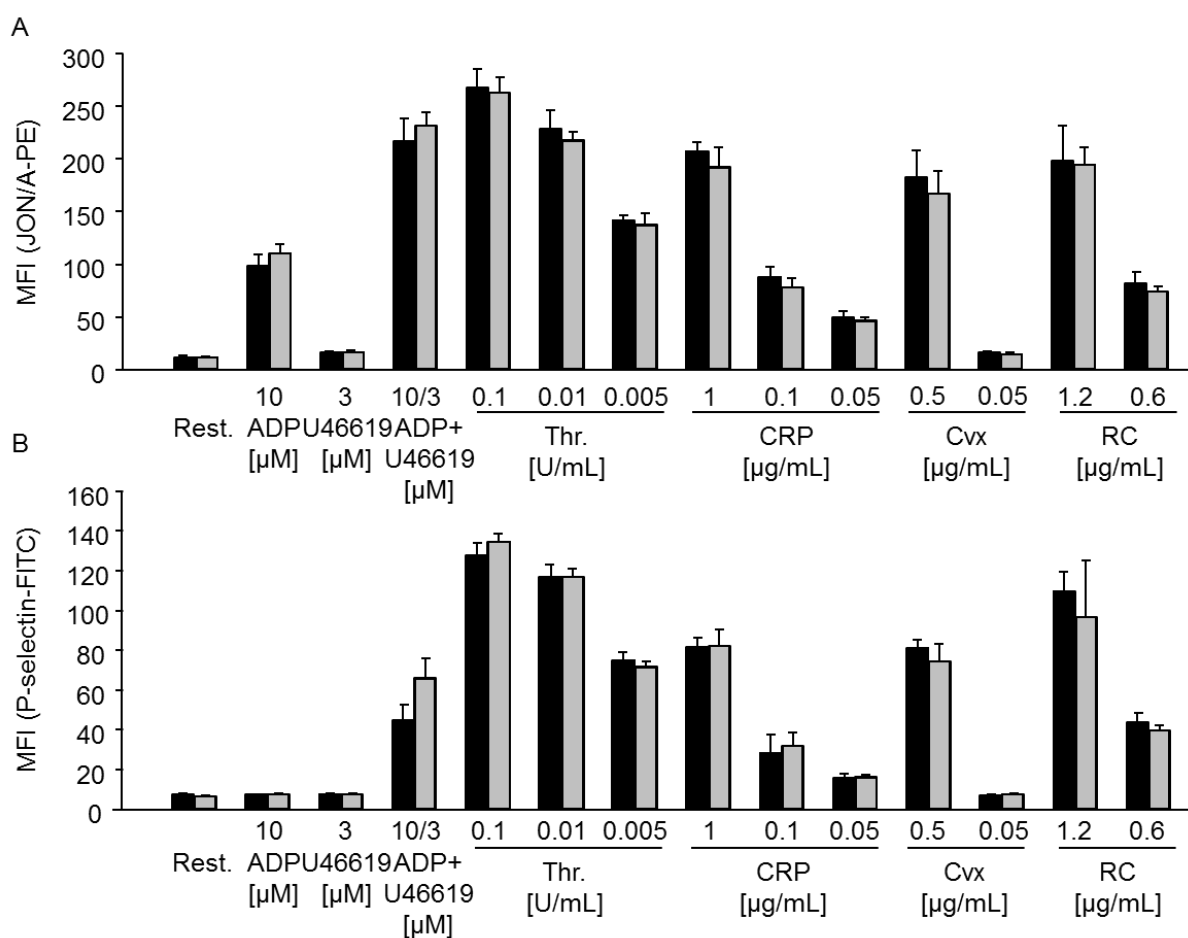


**Figure 22. Normal  $\alpha_{IIb}\beta_3$  integrin activation and degranulation of *Magt1*<sup>-/-</sup> platelets:** (A) Flow cytometric analysis of integrin  $\alpha_{IIb}\beta_3$  activation (upper panel) and (B) degranulation-dependent P-selectin exposure (lower panel) measured upon activation with the indicated agonists in *WT* (black bars) and *Magt1*<sup>-/-</sup> (grey bars) platelets. Results are expressed as mean fluorescence intensities (MFI)  $\pm$  SD (n = 8). A representative from three independent experiments is presented. Thr: thrombin; U46619: stable thromboxane A<sub>2</sub> analog; CRP: collagen-related peptide; CVX: convulxin; RC: rhodocytin. Unpaired Student's t-test was used as a test of significance. \*P<0.05, \*\*P<0.01, \*\*\*P<0.001.

To determine the functional consequences of the activation-dependent enhanced Mg<sup>2+</sup> depletion in *Magt1*<sup>-/-</sup> platelets, washed platelets of either *WT* or *Magt1*<sup>-/-</sup> mice were stimulated with ITAM and GPCR specific agonists, and  $\alpha_{IIb}\beta_3$  integrin activation and granule release (P-

selectin exposure) were assessed by flow cytometry using the JON/A-PE and anti-P-selectin antibodies [173]. Surprisingly, *Magt1*<sup>-/-</sup> platelets displayed normal integrin activation and degranulation in response to all tested agonists (**Figure 22**).

### 3.3.2.5 Partially impaired integrin outside-in activation in *Magt1*<sup>-/-</sup> platelets

Despite the described role for Mg<sup>2+</sup> in binding to and activating integrins, integrin inside-out activation was normal in *Magt1*<sup>-/-</sup> platelets under static conditions, where the role of second wave mediators is negligible (**Figure 22**). To test a possible role of Mg<sup>2+</sup> in platelet integrin outside-in activation, spreading assay was carried out. The *WT* and *Magt1*<sup>-/-</sup> platelets activated with a low dose of thrombin, spread normally on a fibrinogen-coated surface, thus excluding a role of MAGT1 in this process (**Figure 23A**).

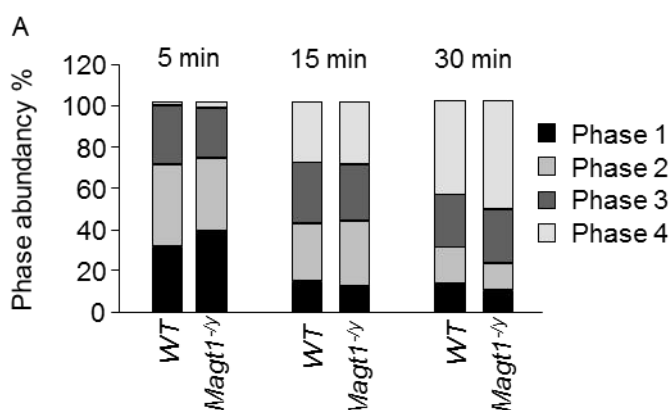
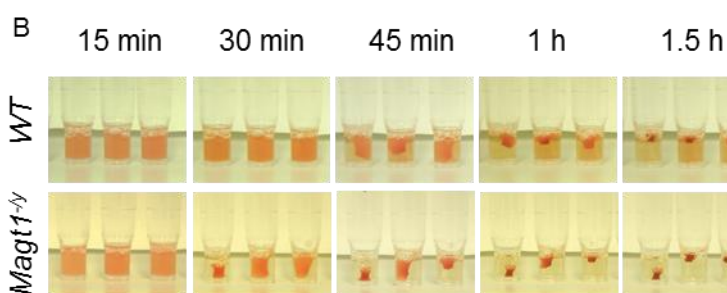


**Figure 23. *Magt1*<sup>-/-</sup> platelets spread normally but show an accelerated clot retraction:** (A) Washed platelets of either *WT* or *Magt1*<sup>-/-</sup> mice were allowed to spread on 100 µg/mL fibrinogen-coated coverslips upon stimulation with 0.01 U/mL thrombin. Phase abundance of different platelet spreading stages (1: no filopodia, 2: only filopodia, 3: filopodia and lamellipodia, 4: fully spread) was manually quantified using Fiji software. (B) Platelet clot retraction was followed over time after activation with 2.5 U/mL thrombin in the presence of 20 mM CaCl<sub>2</sub>. Images were acquired at the indicated time points. A representative of three independent experiments is shown (n = 3).



However, platelet clot retraction, which also strongly depends on integrin outside-in activation and the cytoskeleton, but also on second wave mediators, was significantly accelerated in samples of *Magt1*<sup>-/-</sup> mice. In *WT* samples, retraction of the clot started 45 min after stimulation, while in *Magt1*<sup>-/-</sup> samples clot retraction started as early as 30 min after stimulation. Although, after 1.5 h both *Magt1*<sup>-/-</sup> and *WT* clots retracted to a similar extent (**Figure 23B**).

### 3.3.2.6 Increased TXA<sub>2</sub> and ATP release in *Magt1*<sup>-/-</sup> platelets

The accelerated clot retraction suggested an increased release or production of second wave mediators. During platelet activation, TXA<sub>2</sub> is released into the extracellular space where it binds to and activates TXA<sub>2</sub> (TP) receptors on the platelet surface, thus amplifying platelet activation and promoting thrombus growth [45].

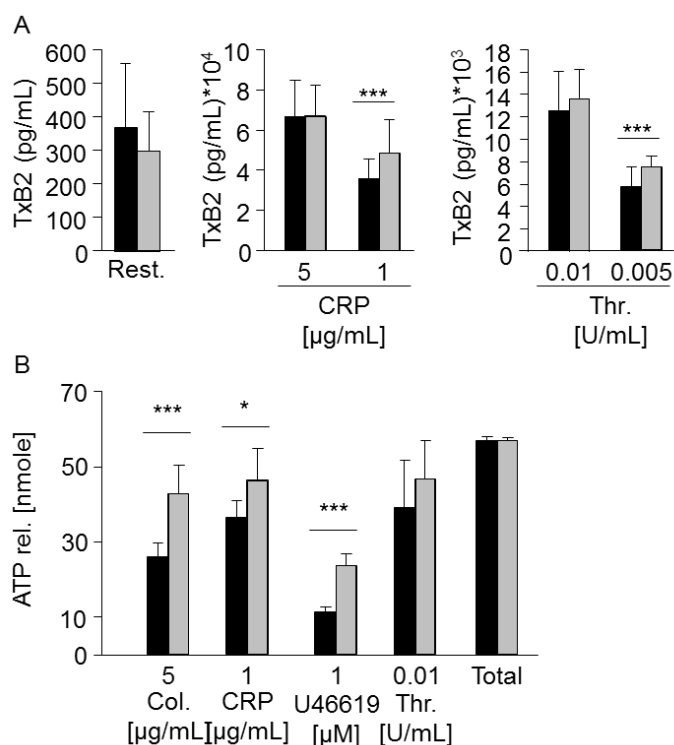


**Figure 24. Enhanced TXA<sub>2</sub> production and ATP release by *Magt1*<sup>-/-</sup> platelets:** (A) Platelet released TXA<sub>2</sub> was measured by ELISA quantifying the stable thromboxane B<sub>2</sub> (TXB<sub>2</sub>) metabolite. Results are presented as mean TXA<sub>2</sub> (pg/mL) ± S.D. Data from three independent experiments are shown (n = 10 in total). *WT* (black bar/line) and *Magt1*<sup>-/-</sup> (grey bar/line). (B) Washed *WT* or *Magt1*<sup>-/-</sup> platelets were incubated with luciferase-luciferin reagent followed by the addition of the indicated agonists. ATP release was measured by lumi-aggregometry. Mean ATP release ± SD is reported. Data from 4 independent experiments are shown (n = 12 in total). Thr: thrombin; U46619: stable thromboxane A<sub>2</sub> analog; CRP: collagen-related peptide; Col: Horm collagen. Rest.: resting. An unpaired Student's t-test was used to test significance. \*P<0.05, \*\*P<0.01, \*\*\*P<0.001.

To investigate whether TXA<sub>2</sub> production is altered in *Magt1*<sup>-/-</sup> mice, platelets were activated with low and high doses of CRP or thrombin. Subsequently, TXB<sub>2</sub>, as a stable metabolite of TXA<sub>2</sub>, was quantified by an ELISA. *Magt1*<sup>-/-</sup> platelets showed increased TXB<sub>2</sub> levels upon stimulation with a low dose of CRP or thrombin (**Figure 24A**). Besides TXA<sub>2</sub>, ATP is also an essential second wave mediator released from  $\delta$ -granules upon platelet activation and reinforces platelet activation through P2X<sub>1</sub> receptor-mediated Ca<sup>2+</sup> entry. Furthermore, the Mg<sup>2+</sup>-ATP complex represents a major Mg<sup>2+</sup> store in mammalian cells, which can also directly modulate enzymatic activities. In response to stimulation with collagen, CRP or U46619, *Magt1*<sup>-/-</sup> platelets showed an increased ATP release as compared to *WT* platelets. However, upon activation with thrombin, ATP release was normal. Additionally, the total ATP content was normal in MAGT1-deficient platelets indicating that their energy metabolism is not altered (**Figure 24B**).

### 3.3.2.7 TRPC6 inhibition or Mg<sup>2+</sup> supplementation normalizes aggregation in *Magt1*<sup>-/-</sup> platelets

Previous studies with human platelets showed that pre-incubation of platelets in the presence of high concentrations of extracellular Mg<sup>2+</sup> inhibits platelet aggregation [187]. To study whether MAGT1 might be involved in this process, the effect of extracellular magnesium on aggregation was tested in *WT* and *Magt1*<sup>-/-</sup> platelets.

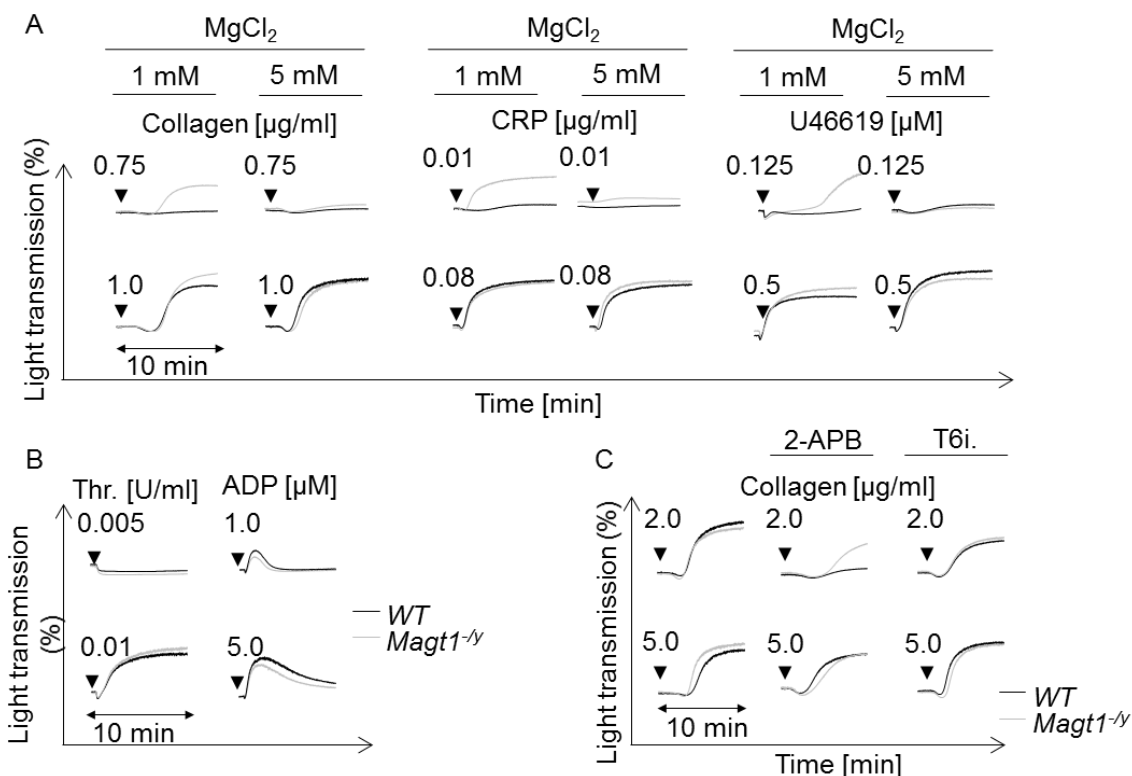


**Figure 25. Enhanced aggregation of *Magt1*<sup>-/-</sup> platelets:** (A, B) Washed platelets from either *WT* or *Magt1*<sup>-/-</sup> mice were stimulated with the indicated agonists in the presence of stated extracellular MgCl<sub>2</sub>, and light transmission was recorded on a Fibrinometer 4-channel aggregometer. ADP measurements were performed using PRP. (C) Washed platelets from *WT* and *Magt1*<sup>-/-</sup> mice were pre-treated with the indicated inhibitors and stimulated with collagen. Light transmission was recorded on a Fibrinometer 4-channel aggregometer. Representative traces from three independent experiments are presented (n = 4). Thr: thrombin; U46619: stable thromboxane A<sub>2</sub> analog; CRP: collagen-related peptide; Col: Horm collagen; T6i.: TRPC6 inhibitor aminoindane derivative; 2-APB: aminoethoxydiphenyl borate; PRP: platelet-rich plasma.

At a physiological concentration of MgCl<sub>2</sub> (1 mM) *Magt1*<sup>-/-</sup> platelets showed markedly enhanced aggregation responses upon threshold concentrations of collagen, CRP or U46619 stimulation, while upon ADP or thrombin stimulation, a comparable aggregation response was observed between *WT* and *Magt1*<sup>-/-</sup> platelets. In the presence of high extracellular MgCl<sub>2</sub> (5 mM), the enhanced aggregation response in *Magt1*<sup>-/-</sup> platelets were normalized (**Figure 25A & B**). Next, the contribution of a dysregulated Ca<sup>2+</sup> entry to the altered aggregation responses was

assessed in *Magt1*<sup>-/-</sup> platelets by performing aggregation studies in the presence of 2-aminoethoxydiphenyl borate (2-APB), a non-selective SOCE blocker, or in the presence of a TRPC6 inhibitor (T6i). At an intermediate dose of collagen, *WT* and *Magt1*<sup>-/-</sup> platelets aggregated to a similar degree. Under these conditions, pretreatment with T6i efficiently blocked aggregation in both groups to a similar extent. However, 2-APB did not affect the hyper-aggregation of *Magt1*<sup>-/-</sup> platelets. Of note, aggregation of *WT* samples was significantly inhibited in 2-APB treated groups when compared to untreated samples. Together, these results indicate that the dysregulated TRPC6 mediated Ca<sup>2+</sup> entry contributed to the abnormal phenotype observed in *Magt1*<sup>-/-</sup> platelets (**Figure 25C**).

### 3.3.2.8 Increased thrombus formation of *Magt1*<sup>-/-</sup> platelets on collagen *ex vivo* can be rescued by Mg<sup>2+</sup> supplementation or by TRPC6 inhibition

At sites of vascular injury, platelets adhere to components of the exposed extracellular matrix. Besides GPIb-vWF, the platelet-vessel wall interactions are known to be regulated by the collagen binding receptors GPVI,  $\alpha_2\beta_1$  integrin, as well as by GPV, and the fibrinogen receptor integrin  $\alpha_{IIb}\beta_3$ . Ligation of these receptors to their respective ligands further enhances platelet reactivity, also by promoting the secretion of second wave mediators. Firm adhesion of platelets at the site of vessel wall injury is mediated by both GPVI and integrin  $\alpha_2\beta_1$  [23, 24, 188]. To determine whether MAGT1-mediated Mg<sup>2+</sup> transport is involved in this process, anticoagulated whole blood from either *WT* or *Magt1*<sup>-/-</sup> mice was perfused over collagen- or vWF-coated surfaces at defined wall shear conditions, mimicking the arterial blood flow, and compared for the extent of thrombus formation. At a wall-shear rate of 1000 sec<sup>-1</sup>, no significant differences in surface coverage and relative thrombus volume were observed between *WT* and *Magt1*<sup>-/-</sup> mice on collagen (**Figure 26A & B**). In addition, no differences were found regarding shear-dependent platelet adhesion to vWF at the higher shear rate of 1700 sec<sup>-1</sup> (**Figure 26C**). In sharp contrast on collagen, at the higher shear rate of 1700 sec<sup>-1</sup>, *Magt1*<sup>-/-</sup> platelets showed significantly enhanced surface coverage and relative thrombus volume compared to *WT* controls (**Figure 27**).

To study the effects of extracellular Mg<sup>2+</sup> on thrombus formation, we supplemented heparinized blood of *WT* and *Magt1*<sup>-/-</sup> mice with 2.5 mM or 5 mM MgCl<sub>2</sub> for 5 min and subsequently perfused on collagen-coated coverslips at a shear rate of 1700 sec<sup>-1</sup>. In the presence of 2.5 mM MgCl<sub>2</sub>, both *WT* and *Magt1*<sup>-/-</sup> samples showed a reduced surface coverage and relative thrombus volume, although *Magt1*<sup>-/-</sup> samples still showed much larger aggregates compared to *WT* samples. At a higher dose of MgCl<sub>2</sub> (5 mM), *WT* and *Magt1*<sup>-/-</sup> blood samples showed no differences under flow. It is important to note that the surface coverage and relative thrombus

volume in samples treated with 5 mM  $MgCl_2$ , were strongly decreased compared to untreated samples (**Figure 27A, C & D**). Altogether, these experiments suggested that the MAGT1 function is tightly regulated by shear stress, being suppressive on collagen-dependent thrombus formation at high arterial shear rates.

To test if dysregulated cation channel activity caused the enhanced thrombus formation in *Magt1*<sup>-/-</sup> samples via ROCE or SOCE, and to follow up on the findings from the aggregation studies, blood samples were pretreated with SOCE or ROCE inhibitors and subjected to the flow chamber assay.

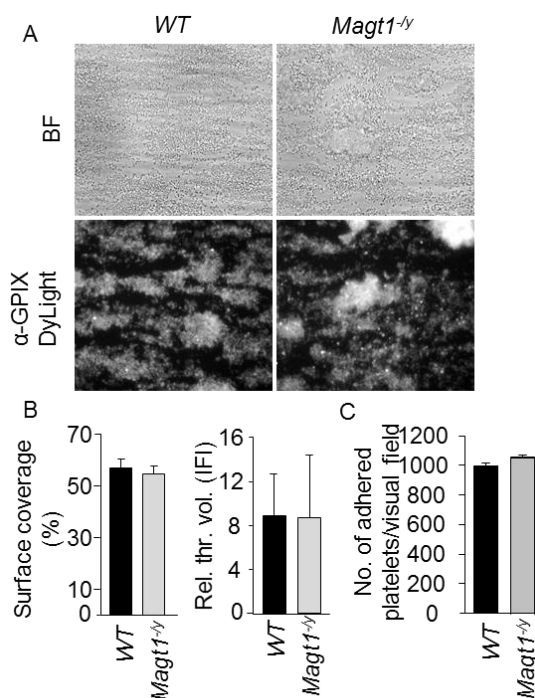


**Figure 26. Normal thrombus formation by *Magt1*<sup>-/-</sup> platelets at a shear rate of 1000 sec<sup>-1</sup>:** (A) Heparinized whole blood (anti-GPIX-DyLight-488 labeled) of either *WT* (black bar) or *Magt1*<sup>-/-</sup> (grey bar) mice was perfused at 1000 sec<sup>-1</sup> over collagen-coated coverslips (0.2 mg/mL). Representative phase contrast (upper panel) and fluorescence microscopy (lower panel) images are shown. (B) Mean surface coverage (left) and relative thrombus volume (right) were quantified and are presented as mean  $\pm$  SD from three independent experiments ( $n = 4$ ). (C) Washed platelets were perfused over vWF coated coverslips, and the average number of adhered platelets per visual field  $\pm$  SD ( $n = 3$ ) were quantified using CellProfiler software and shown. Presented data are from two independent experiments ( $n = 4$ ). An unpaired Student's t-test was used to test significance.

To inhibit SOCE whole blood was incubated with 10  $\mu$ M 2APB for 5 min along with platelet labeling antibody, and then perfused at 1700 sec<sup>-1</sup> over a collagen-coated surface. Platelet aggregate formation was inhibited in *WT* samples while *Magt1*<sup>-/-</sup> whole blood still showed hyper-aggregate formation, although to a lesser extent than the untreated *Magt1*<sup>-/-</sup> samples.

Using another SOCE blocker, 3,5-bis(trifluoromethyl)pyrazole (BTP2), these results were validated. Whole blood from either *WT* or *Magt1*<sup>-/-</sup> mice was incubated with 1 mM BTP2 for 5 min, and perfused at 1700 sec<sup>-1</sup> over collagen. In this case, also *WT* samples showed impaired adhesion and aggregate formation, while *Magt1*<sup>-/-</sup> whole blood still showed hyper-aggregate formation (**Figure 27B, C & D**).

To inhibit ROCE, the TRPC6 blocker T6i was used, which could normalize the aggregation response of *Magt1*<sup>-/-</sup> platelets to a level observed in *WT* platelets (**Figure 27B, C & D**). These results suggest that a dysregulated TRPC6 activity contributes to the aberrant thrombus formation under flow, whereas ORAI1-mediated SOCE does not directly add to this process.

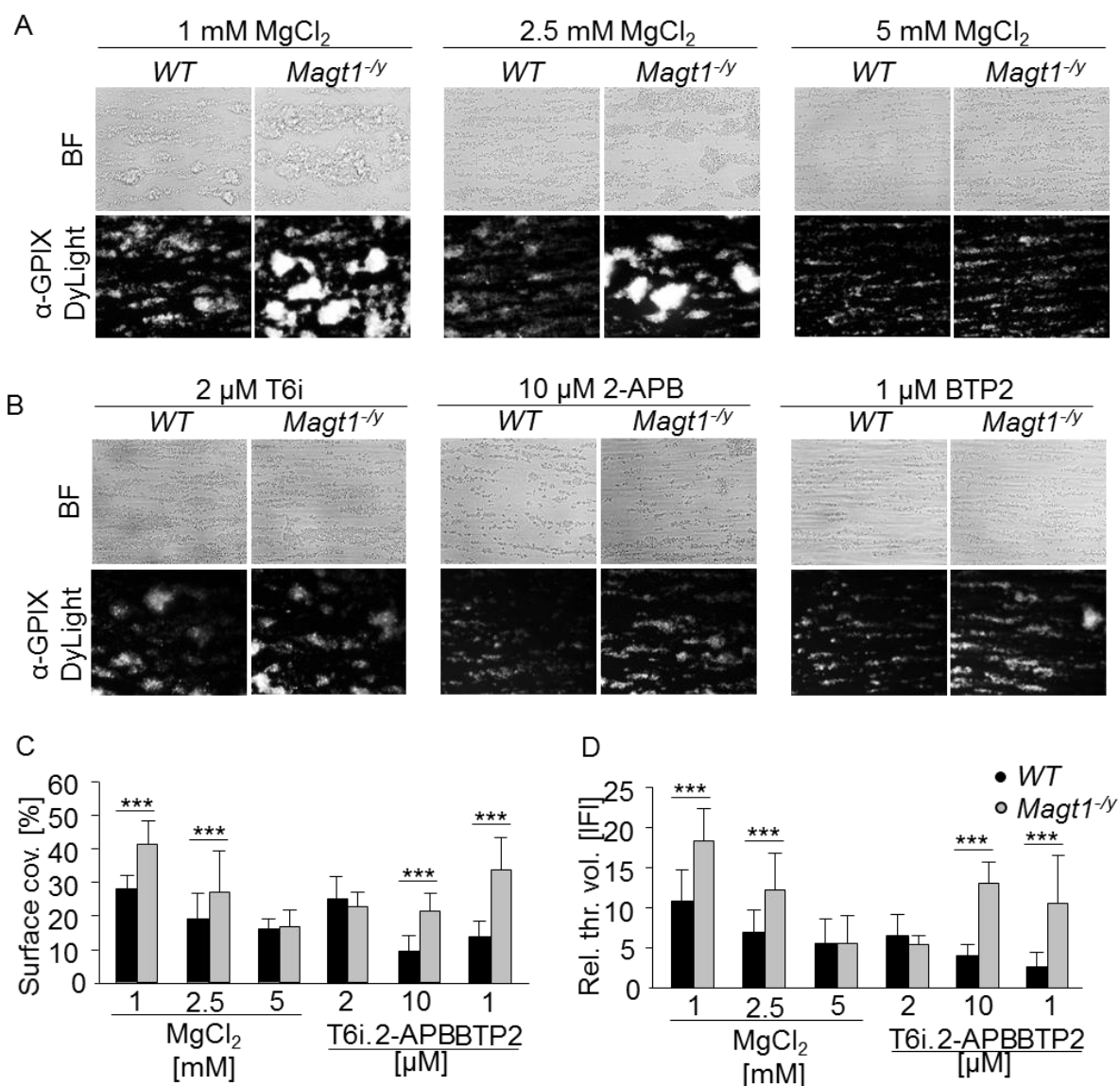


**Figure 27. Magnesium supplementation or TRPC6 inhibition rescues enhanced *ex vivo* thrombus formation in *Magt1*<sup>-/-</sup> platelets:** (A) Heparinized whole blood (anti-GPIX-DyLight-488 labeled) from either *WT* or *Magt1*<sup>-/-</sup> was perfused at 1700 sec<sup>-1</sup> over collagen-coated (0.2 mg/mL) cover glasses after pretreatment with the indicated MgCl<sub>2</sub> concentrations, or (B) the indicated inhibitors. Representative phase contrast (upper panel) and fluorescence microscopy (lower panel) images are shown (n=5). (C-D) Mean surface coverage (left) and relative thrombus volume (right) were quantified using MetaVue software and are presented as mean ± SD (n=5) from three independent experiments. T6i.: TRPC6 inhibitor aminoindane derivative; 2APB: 2-aminoethoxydiphenyl borate; 3,5-BTP2: bis(trifluoromethyl)pyrazole (BTP). An unpaired Student's t-test was used to test significance. \*P<0.05, \*\*P<0.01, \*\*\*P<0.001.



### 3.3.2.9 Functional crosstalk between MAGT1, PKC and TRPC6

Earlier, our group identified TRPC6 as a major DAG-induced ROCE channel in platelets. To exclude a non-specific effect of the TRPC6 inhibitor, the *Trpc6* mutant mouse model (*Trpc6*<sup>-/-</sup>) was used to confirm the direct consequence of reduced TRPC6 channel activity in *Magt1*<sup>-/-</sup> platelets. Therefore, *Magt1*<sup>-/-</sup> mice were intercrossed with *Trpc6*<sup>-/-</sup> mice to obtain *Magt1*<sup>-/-</sup>/*Trpc6*<sup>+/-</sup> platelets, which were tested in different *in vitro* and *ex vivo* assays.

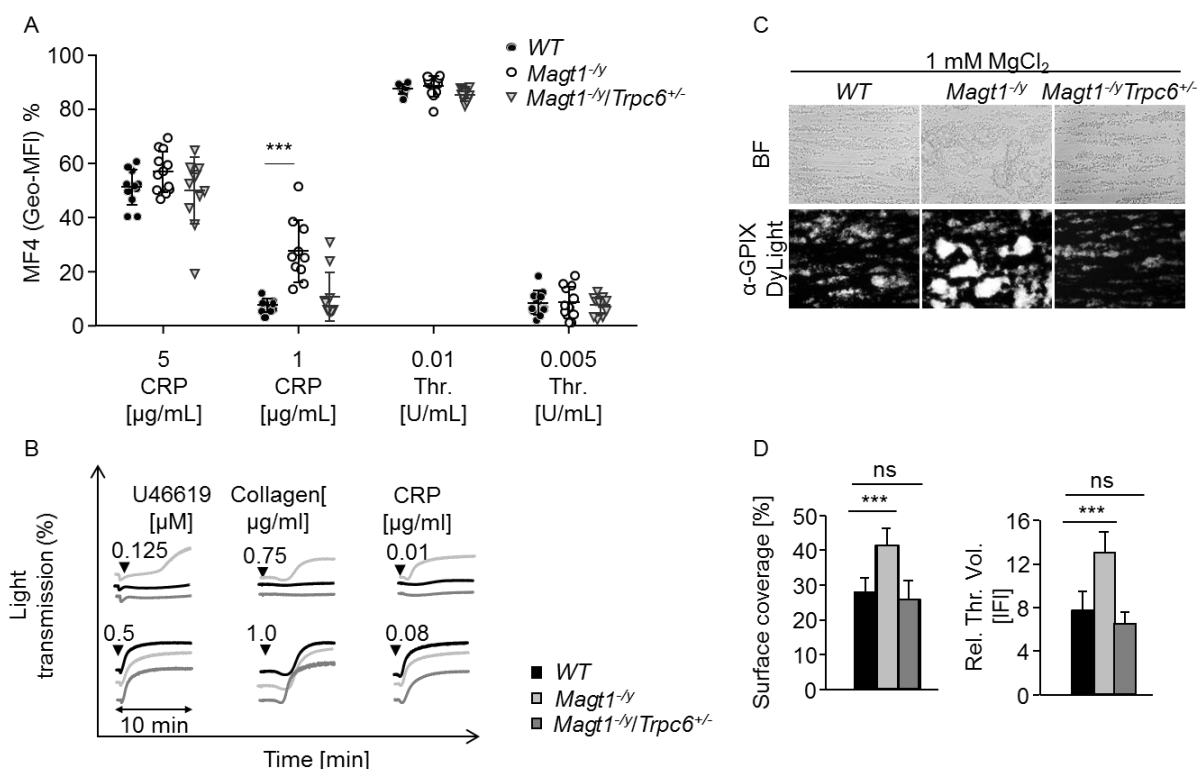


**Figure 28. TRPC6 heterozygosity rescues the hyperreactive *Magt1*<sup>-/-</sup> phenotype:** (A) Mag-Fluo-4 loaded *WT* (closed dots), *Magt1*<sup>-/-</sup> (open dots), or *Magt1*<sup>-/-</sup>/*Trpc6*<sup>+/-</sup> (inverted triangle) platelets were stimulated with the indicated agonists in the presence of 2 mM CaCl<sub>2</sub> and 1 mM MgCl<sub>2</sub>. Percentage loss of fluorescence intensity upon activation is shown. Each symbol represents one mouse. (B) Washed platelets from either *WT*, *Magt1*<sup>-/-</sup> or *Magt1*<sup>-/-</sup>/*Trpc6*<sup>+/-</sup> mice were stimulated with the indicated agonists in presence of 1 mM MgCl<sub>2</sub>, and light transmission was recorded on a Fibrinmeter 4 channel aggregometer. Aggregation traces were recorded during 10 min. (C) Whole blood of the indicated groups was perfused over collagen at 1700 sec<sup>-1</sup>. Representative phase contrast (upper panel) and fluorescence microscopy (lower panel) images are shown. (D) Mean surface coverage (left), and relative thrombus volume (right) were quantified using MetaVue software and are presented as mean ± SD. (n = 5). A representative of three independent experiments is shown. Thr: thrombin; CRP: collagen-related peptide; Col: Horm collagen. An unpaired Student's t-test was used to test significance. \*P<0.05, \*\*P<0.01, \*\*\*P<0.001.

Initially, Mg<sup>2+</sup> efflux was measured using the probe Mag-Fluo-4. In this assay, *Magt1*<sup>-/-</sup>/*Trpc6*<sup>+/-</sup> platelets showed comparable kinetics to those of *WT* platelets (**Figure 28A**). Yet, the *Magt1*<sup>-/-</sup> platelets showed an accelerated depletion of Mg<sup>2+</sup>, as we observed before. Likely, as a consequence of this, aggregation responses under stasis and flow of *Magt1*<sup>-/-</sup>/*Trpc6*<sup>+/-</sup> platelets were normalized to the level of *WT* controls (**Figure 28 B-D**). Altogether, we concluded that an

abnormal regulation of the TRPC6 channel activity can contribute to the accelerated thrombus growth seen in *Magt1<sup>-y</sup>* mice.

To further investigate the effects of abnormal TRPC6 function at the molecular level, *WT*, *Magt1<sup>-y</sup>* and *Magt1<sup>-y</sup>/Trpc6<sup>+/-</sup>* platelets were stimulated with CRP in the presence or absence of extracellular  $\text{CaCl}_2$ , and tyrosine phosphorylation of the GPVI/LAT signalosome was analyzed. In the *Magt1<sup>-y</sup>* platelets, we observed a hyperphosphorylation of Syk, LAT and PLC $\gamma$ 2, which was normalized to that of the *WT* levels in *Magt1<sup>-y</sup>/Trpc6<sup>+/-</sup>* platelets, whilst the phosphorylation status was normal in the absence of extracellular  $\text{CaCl}_2$  (**Figure 29A & B**). It has been shown that after PLC $\gamma$ 2 activation, PKC isoforms are activated, which transduce the signal from PLC $\gamma$ 2 to other diverse effector molecules, including TRPC6 channels

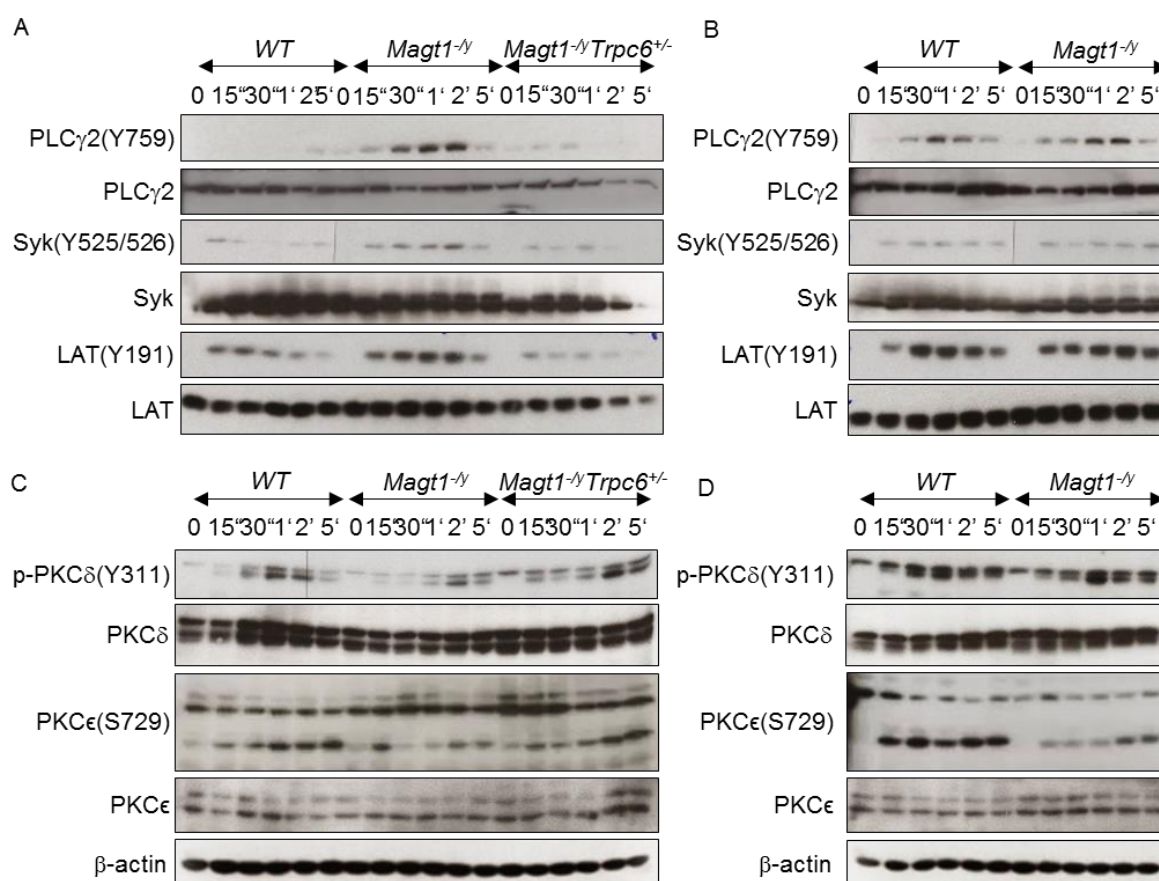


**Figure 29. TRPC6 heterozygosity normalized the enhanced GPVI induced tyrosine phosphorylation and attenuated PKC regulation in *Magt1<sup>-y</sup>* platelets.** (A & B) Western blot showing the tyrosine phosphorylation pattern of the components of the GPVI signalosome after CRP stimulation in the (A) presence or (B) absence of 2 mM extracellular  $\text{CaCl}_2$ . (C & D) Phosphorylation pattern of PKC isoforms after CRP stimulation in the (C) presence or (D) absence of 2 mM extracellular  $\text{CaCl}_2$ . Representative blots of three independent experiments are presented.

To investigate this, the phosphorylation status of two DAG-dependent PKC isoforms was analyzed in CRP-stimulated platelets, in the presence of 2 mM extracellular  $\text{CaCl}_2$ . Strikingly,

phosphorylation of PKC $\delta$ <sup>Y311</sup> and PKC $\epsilon$ <sup>S729</sup> was strongly reduced in *Magt1*<sup>-/-</sup> platelets, but not in *Magt1*<sup>-/-</sup>/*Trpc6*<sup>+/-</sup> platelets. The phosphorylation status of PKC $\delta$  was normal in the absence of CaCl<sub>2</sub>, but PKC $\epsilon$  showed defective phosphorylation both in the presence or absence of extracellular CaCl<sub>2</sub> (**Figure 29C & D**).

### 3.3.3 Altered hemostasis in *Magt1*<sup>-/-</sup> mice

The observed enhanced thrombus formation suggested that MAGT1 can also regulate hemostatic functions in mice. Therefore, the bleeding time was assessed by resecting 1 mm of the tail tip, and determination of the time to blood cessation from the wound. Both *WT* and *Magt1*<sup>-/-</sup> mice, as well as BM chimeric *WT* mice that had been transplanted either with *WT* or *Magt1*<sup>-/-</sup> BM cells, were analyzed. As expected, a significantly shorter stop of bleeding was found in *Magt1*<sup>-/-</sup> mice or in irradiated *WT* mice that had received *Magt1*<sup>-/-</sup> BM cells (**Figure 30**).

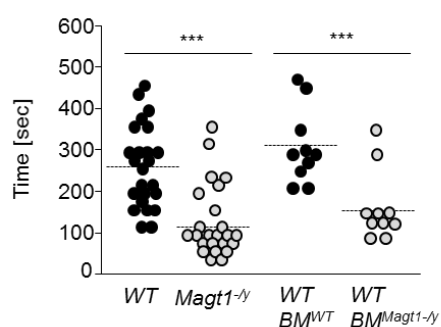


**Figure 30. *Magt1*<sup>-/-</sup> mice have a shortened bleeding time:** (A) Hemostatic function was assessed by resecting 1 mm of the tail tip and collecting blood every 20 sec on filter paper until a maximum of 20 min. Each dot represents one animal with black dots for (*WT* or *WT*<sup>BM<sup>WT</sup>) and grey dots for (*Magt1*<sup>-/-</sup> or *WT*<sup>BM<sup>Magt1</sup>-/-</sup>). Results are expressed as mean time to wound cessation  $\pm$  SD from two independent experiments. BM: bone marrow. An unpaired Student's t-test was used to compare mean wound closure times. \**P*<0.05, \*\**P*<0.01, \*\*\**P*<0.001.</sup>

### 3.3.4 Enhanced susceptibility of *Magt1*<sup>-/-</sup> mice towards ischemic brain infarction

Besides thrombosis, ischemic brain infarction is also one of the leading causes of death. Although Mg<sup>2+</sup> supplementation has been in practice in patients with ischemic brain infarction for a long time [189], the underlying molecular mechanisms of how the supplemented Mg<sup>2+</sup> may protect the brain from stroke are still not well understood. On the other hand, increased Ca<sup>2+</sup> influx, through glutamate receptor-mediated SOCE, is known to be one of the deleterious factors in stroke leading to tissue necrosis. In this process, Mg<sup>2+</sup> influx can have an antagonistic effect on Ca<sup>2+</sup> signaling mechanisms by blocking Ca<sup>2+</sup> channels or by interfering with enzymatic or receptor activities [189-192]. To understand the importance of *Magt1* in stroke, *Magt1*<sup>-/-</sup> mice were subjected to the tMCAO model of stroke and compared to *WT* mice. Due to an enhanced thrombus formation in *Magt1*<sup>-/-</sup> mice, the severity of the injury was reduced by inserting the filament only inserted for 30 min only. In this case, *WT* mice showed only a minor infarct volume, whereas *Magt1*<sup>-/-</sup> mice had a fully grown infarct size (**Figure 31A**). To study the

contribution of platelets, brain sections were stained using a platelet-specific (anti-GPIX) antibody. This revealed an increased platelet accumulation in the occluded vessels of *Magt1*<sup>-/-</sup> mice (**Figure 31B**). To decipher the role of hematopoietic MAGT1 in this process, BM chimeric mice were generated, and animals from all three groups were challenged with 30 min tMCAO.

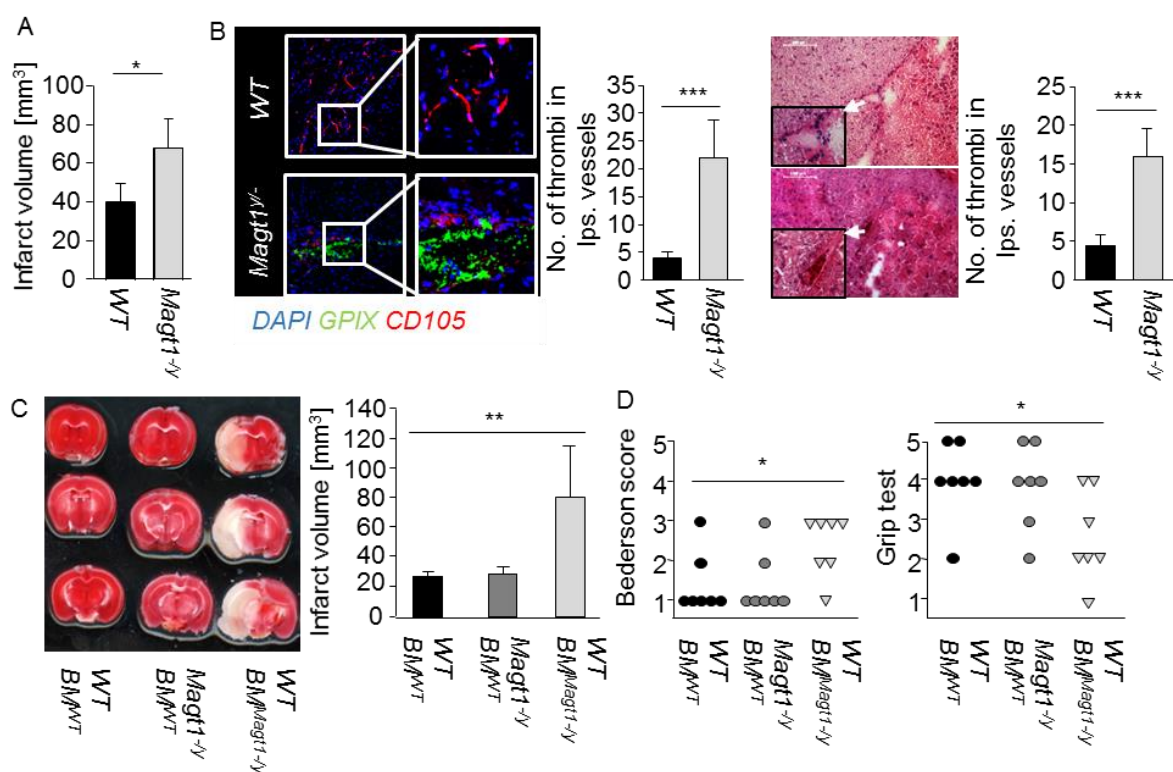


**Figure 31. *Magt1*<sup>-/-</sup> hematopoietic cells cause increased damage to brain tissue during focal cerebral ischemia:** (A) Infarct volume quantified by planimetry in *WT* and *Magt1*<sup>-/-</sup> brains after tMCAO. (B) Representative confocal pictures of (tMCAO induced) brain cryosections stained for nuclei (DAPI-blue), platelets (GPIX-green) and endothelium (CD105-red) (left) and quantification of the number of thrombi in the ipsilateral hemisphere (right) are presented. Results are presented as mean  $\pm$  SD. (C) Representative pictures of H&E stained sections (tMCAO induced) brain cryosections (left) and quantification of the number of thrombi in the ipsilateral hemisphere (right) are presented. Results are presented as mean  $\pm$  SD. (D) 2,3,5-triphenyltetrazolium chloride (TTC) staining of coronal brain sections of BM chimeric mice sacrificed 24 h post 30 min tMCAO and (E) planimetric quantifications for *WT*BM<sup>WT</sup> (black bar), *Magt1*<sup>-/-</sup>BM<sup>WT</sup> (dark grey bar), *WT*BM<sup>*Magt1*<sup>-/-</sup></sup> (light grey bar) for infarct volume (right) presented. Results are presented as infarct volume [mm<sup>3</sup>]  $\pm$  S.D. (F) Bederson score (left), and grip test (right) are shown for the same group of mice at 24 h post tMCAO. Each symbol represents one animal. Results from at least two independent experiments is shown. Unpaired Student's t-test or Mann-Whitney U test was used to assess statistical significance. \*P<0.05, \*\*P<0.01, \*\*\*P<0.001. (Experiments performed by Dr. Michael Schuhmann and Dr. Peter Kraft).

At 24 h after tMCAO, the mice were sacrificed and the infarct volume was quantified. Strikingly, only *WT* mice which received *Magt1*<sup>-/-</sup> BM cells showed increased infarct sizes, whereas infarct volumes in *WT* and *Magt1*<sup>-/-</sup> mice transplanted with *WT* BM cells were indistinguishable (**Figure 31C**). This observation also translated into a worsened functional outcome in *WT*-

$BM^{Magt1^{-/y}}$  chimeras with an increased Bederson and a decreased Grip test score (**Figure 31D**). All presented *in vivo* experiments of stroke (surgery) were performed and materials kindly provided for further analysis by Dr. Michael Schuhmann and Dr. Peter Kraft (Department of Neurology, University Hospital of Würzburg, Germany).

### 3.3.5 Dispensable role of $Magt1^{-/y}$ CD4<sup>+</sup> T cells in stroke development

CD4<sup>+</sup> T cells play a prominent role in promoting infarct progression in the tMCAO model. In line with this,  $Rag1^{-/-}$  mice which *per se* do not have B and T cells, are protected in the model of tMCAO. Adoptive transfer of CD4<sup>+</sup>/CD8<sup>+</sup> cells to  $Rag1^{-/-}$  mice resulted in normal infarct progression similar to *WT* mice [138, 193]. To identify whether  $Magt1^{-/y}$  CD4<sup>+</sup> cells contribute to the enhanced stroke development,  $Rag1^{-/-}$  mice were transplanted with either *WT* CD4<sup>+</sup> or  $Magt1^{-/y}$  CD4<sup>+</sup> cells, and tMCAO was performed for 30 min as described earlier. Both mouse groups showed similar infarct volumes (**Figure 32**), thus proving that  $Magt1^{-/y}$  CD4<sup>+</sup> cells alone do not contribute to the increased infarct development in  $Magt1^{-/y}$  mice.

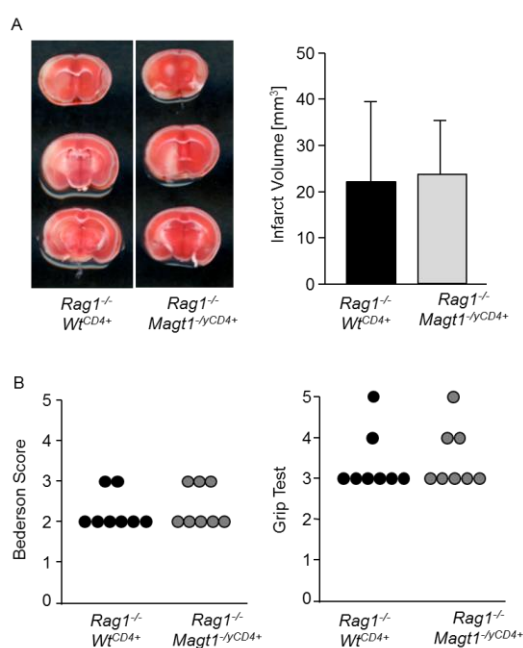


**Figure 32. Adoptive transfer of  $Magt1^{-/y}$  CD4<sup>+</sup> cells does not recapitulate increased stroke in  $Rag1^{-/-}$  mice:** (A) 2,3,5-triphenyltetrazolium chloride (TTC) staining of coronal brain sections (left) of mice sacrificed 24 h post 30 min tMCAO and quantification of infarct volumes by planimetry (right) in  $Rag1^{-/-}$  mice adoptively transferred with CD4<sup>+</sup> cells from either *WT* ( $Rag1^{-/-}WT^{CD4+}$ , black bar) or  $Magt1^{-/y}$  mice ( $Rag1^{-/-}Magt1^{-/y}CD4+$ , grey bar). Data are presented as infarct volume [mm<sup>3</sup>] ± S.D. (B) Bederson score (left), and grip test (right) are shown for the indicated groups. Each dot represents one animal. Results from two independent experiments are shown. Unpaired Student's t-test or Mann-Whitney U test was used to assess statistical significance. \*P<0.05, \*\*P<0.01, \*\*\*P<0.001. (Experiments performed by Dr. Michael Schuhmann).

### 3.4 Investigation of T and B cells in $Magt1^{-/y}$ mice

It has been shown that *MAGT1* variants with XMEN syndrome suffer from CD4 lymphopenia, chronic viral infections (EBV), and from defective T-lymphocyte activation downstream of the TCR. Patients were shown to have an inverted CD4: CD8 ratio in their peripheral blood and T cells contain less Mg<sup>2+</sup> [18, 89]. Another study presented a case history of a 58-year-old XMEN

patient. The patient presented with normal serum immunoglobulins secretion, regular T, B and NK cell numbers but with a slightly inverted CD4: CD8 ratio. He was diagnosed with specific polysaccharide antibody deficiency and known to have bronchiectasis. When the patient aged, he developed thrombocytopenia, a severely reduced CD4<sup>+</sup> cell count and B-cell lymphopenia [194]. These and few other recent studies highlighted MAGT1 function in lymphocyte development and function. However, to date, no study has taken advantage of a *Magt1*<sup>-/-</sup> mouse model to study further the primary cause of above mentioned abnormal immunological phenotypes. To this end, immune cell numbers and function were assessed in different lymphoid organs and peripheral blood of *Magt1*<sup>-/-</sup> mice.

### 3.4.1 T cell subsets in various lymphoid organs and peripheral blood of *Magt1*<sup>-/-</sup> mice

To dissect the primary role of MAGT1 in immune cells, we analyzed B and T lymphocytes under non-infected conditions in *Magt1*<sup>-/-</sup> mice. Similar to human XMEN syndrome [195], a slight but significant decrease in T cell frequencies, as well as a slight but significant reduction in the CD4<sup>+</sup>/CD8<sup>+</sup> ratio was observed in the spleen and lymph nodes but not in the blood of *Magt1*<sup>-/-</sup> mice (**Figure 33**).

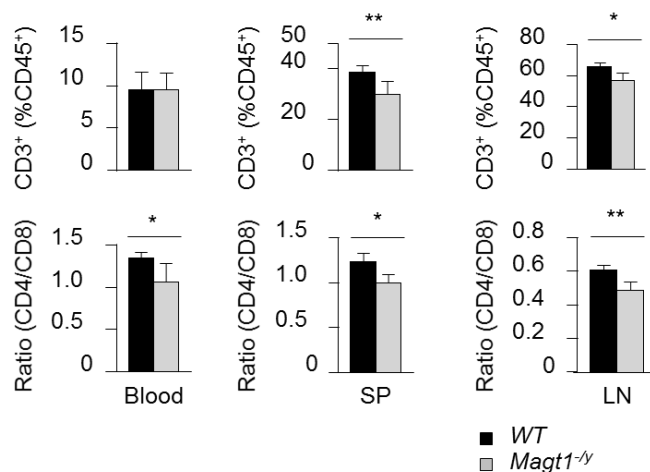


**Figure 33. Altered CD4/CD8 ratio in *Magt1*<sup>-/-</sup> mice:** Percentage of CD3<sup>+</sup> T cells (upper panel) and CD4<sup>+</sup>/CD8<sup>+</sup> ratio of CD3<sup>+</sup> T cells (lower panel) in the indicated organs is presented (n = 10). Cells are expressed in percentages of pre-gated CD45<sup>+</sup> cells. Data are shown as mean ± SD. Unpaired Student's t-test was used as a test of significance. \*P<0.05, \*\*P<0.01, \*\*\*P<0.001.

### 3.4.2 Magnesium and calcium responses in *Magt1*<sup>-/-</sup> CD4<sup>+</sup> cells

To investigate the levels of [Mg<sup>2+</sup>]<sub>i</sub> and [Ca<sup>2+</sup>]<sub>i</sub> in resting and activated CD4<sup>+</sup> cells (in response to TCR stimulation), purified CD4<sup>+</sup> cells were activated with an anti-CD3 antibody, or with thapsigargin, as a non-competitive inhibitor of SERCA that directly stimulates SOCE. [Mg<sup>2+</sup>]<sub>i</sub> and [Ca<sup>2+</sup>]<sub>i</sub> showed no differences under these conditions between WT and *Magt1*<sup>-/-</sup> CD4<sup>+</sup> cells (**Figure 34**).

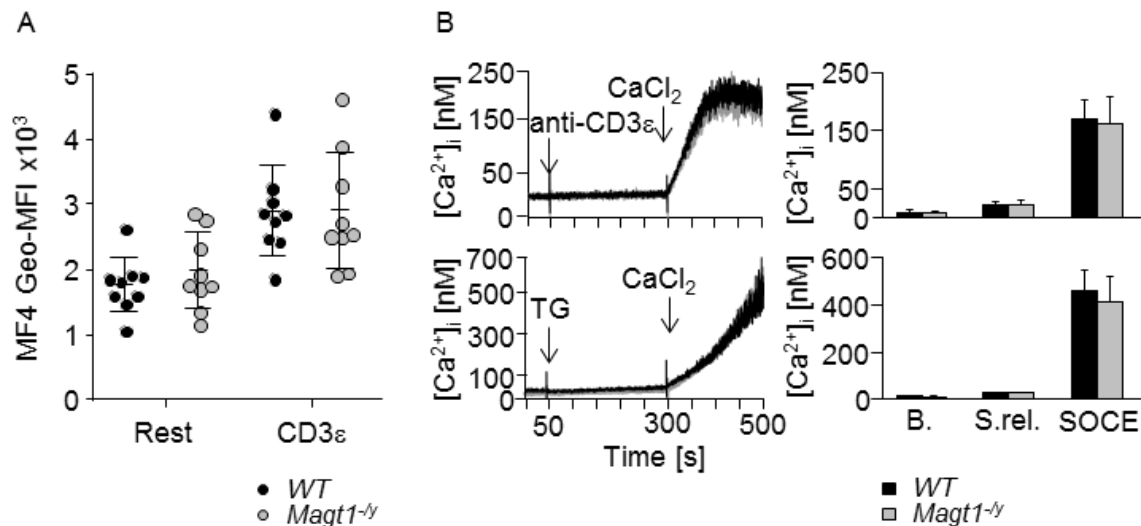


**Figure 34. Normal [Mg<sup>2+</sup>]<sub>i</sub> and [Ca<sup>2+</sup>]<sub>i</sub> levels in CD4<sup>+</sup> cells of *Magt1*<sup>-/-</sup> mice:** (A) Purified mature resting and an anti-CD3 activated (5  $\mu$ g/mL) CD4<sup>+</sup> T cells isolated from spleens of the indicated genotypes were loaded with Mag-Fluo-4 and [Mg<sup>2+</sup>]<sub>i</sub> levels were quantified from kinetic measurements. Data represents Geo-MFI  $\pm$  SD. Each symbol represents one animal. (B) Untouched CD4<sup>+</sup> cells from spleens were loaded with Fura-2, and representative traces of [Ca<sup>2+</sup>]<sub>i</sub> levels (left) and quantification (right) upon an anti-CD3 antibody (5  $\mu$ g/mL; upper panel) or thapsigargin (TG) (5  $\mu$ M; lower panel) stimulation are presented. Data represent mean  $\pm$  SD of calcium influx (n = 10). Data are shown as mean  $\pm$  SD. Black bars/traces correspond to *WT* and grey bars/traces to *Magt1*<sup>-/-</sup> samples. An unpaired Student's t-test was used to test significance. Geo-MFI: geometric mean fluorescence intensity; Rest.: resting; MFI: mean fluorescence intensity. B.: basal [Ca<sup>2+</sup>]<sub>i</sub>; S. rel.: store release; SOCE: store-operated Ca<sup>2+</sup> entry.

### 3.4.3 Effector function of NK cells in *Magt1*<sup>-/-</sup> mice

In patients with XMEN syndrome, the cytotoxic NKG2D receptor (a C-type lectin surface receptor of the NKG2 family) showed reduced expression on natural killer (NK) cells. This study also showed that normal cytotoxic T cells (CTLs) when cultured in magnesium deprived medium display a reduced [Mg<sup>2+</sup>]<sub>i</sub> level and NKG2D expression. It has also been proposed that the reduced NKG2D level contributes to the poor killing efficiency of CTLs in XMEN patients [89]. To test if this is also true for the *Magt1*<sup>-/-</sup> mouse model, NK cells from spleens were isolated and NKG2D receptor expression was quantified by flow cytometry. To address the effector function, NK cells were cultivated together with cells expressing NKG2D ligands and were pre-activated with IL-2 to enhance their killing potential. The percentage of CTL specific lysis was plotted to assess the killing potential and compared between *WT* and *Magt1*<sup>-/-</sup> NK cells. Surprisingly, similar kinetics of the E:T (effector to target ratio) were observed between the two groups. NK cells from either *Magt1*<sup>-/-</sup> or *WT* mice were cultured with cells expressing *WT* ligands for NKG2D as a control, H60 or Rae1b (specific ligands for NKG2D) to test NK cell-specific lysis. In all cases, the killing ability of *Magt1*<sup>-/-</sup> and *WT* NK cells was indistinguishable (**Figure 35**).

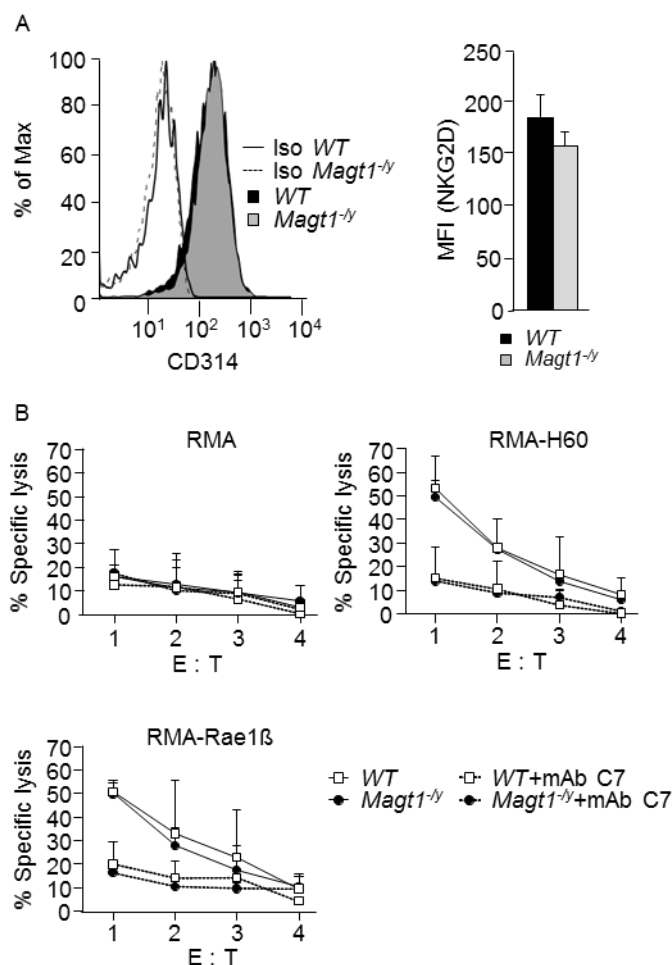


**Figure 35. Normal NKG2D expression and cytolytic activity of spleen-derived NK cells in *Magt1*<sup>-/-</sup> mice:** (A) Representative histograms of purified (spleen) NK cells stained for NKG2D (left) and quantification of the NKG2D expression levels (right). Open histograms represent isotype controls and filled histograms represent NKG2D staining of the indicated genotypes. Data are presented as MFI  $\pm$  SD (n = 9). (B) NK killing activity shown by % specific lysis vs. E:T ratio in NK cells co-cultured with the indicated cell lines. Recombinant human IL-2 was added to trigger NK cell activation. NK cell killing assays were performed using  $1 \times 10^4$  CFDA-SE-labeled RMA, RMA-H60 or RMA-Rae1 $\beta$  cells per well together with decreasing amounts of activated NK cells from WT or *Magt1*<sup>-/-</sup> mice. Annexin A5 and propidium iodide was added to cell cultures to assess survival of CFDA-SE<sup>+</sup> cells. In similar cultures, mAb C7 was added at 10  $\mu$ g/mL to block NKG2D-mediated killing. Black bars correspond to WT and grey bars to *Magt1*<sup>-/-</sup>. Data are shown as mean  $\pm$  SD or as individual data points. An unpaired Student's t-test was used to test significance. MFI: mean fluorescence intensity; E:T: effector to target ratio.

### 3.4.4 B cell subsets in various lymphoid organs and peripheral blood of *Magt1*<sup>-/-</sup> mice

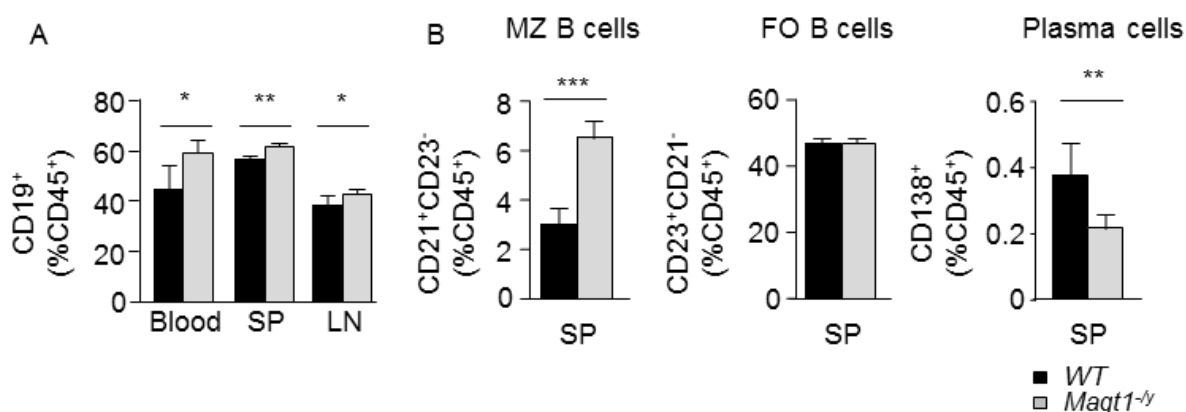


**Figure 36. Abnormal plasma cell numbers and marginal zone B cell development in *Magt1*<sup>-/-</sup> mice:** Single cell suspensions from WT and *Magt1*<sup>-/-</sup> mice (n = 6) were generated and the frequency of (A) CD19<sup>+</sup> B cells in the specified organs, (B) marginal zone (MZ) B cells, as well as follicular (FO) and B220-CD138<sup>+</sup> plasma cells from spleens were quantified among the CD45<sup>+</sup> population. Data are shown as mean  $\pm$  SD. An unpaired Student's t-test was used to test significance. \*P < 0.05, \*\*P < 0.01, \*\*\*P < 0.001. SP: spleen; LN: lymph node(s).



A cell suspension of the stated organs stained for mature B cells (gating on either CD19<sup>+</sup> or B220<sup>+</sup> cells) pointed to a higher abundance in the spleen and blood from *Magt1*<sup>-/-</sup> mice, when compared to their *WT* littermates. Further investigation of splenic B cell subsets revealed a reduced number of plasma B220<sup>+</sup>CD138<sup>+</sup> cells, which was considerable in *Magt1*<sup>-/-</sup> mice compared to their *WT* controls. Naïve B cells can be divided into B1 cells, follicular B cells, and marginal zone B cells. In the *Magt1*<sup>-/-</sup> spleens, no differences in follicular B cell number were observed, but a significant and almost two-fold increased number of marginal zone B cells was seen as compared to the *WT* spleens, when expressed as percent of total CD45<sup>+</sup> cells (**Figure 36**).

### 3.4.5 Magnesium and calcium responses in *Magt1*<sup>-/-</sup> B cells

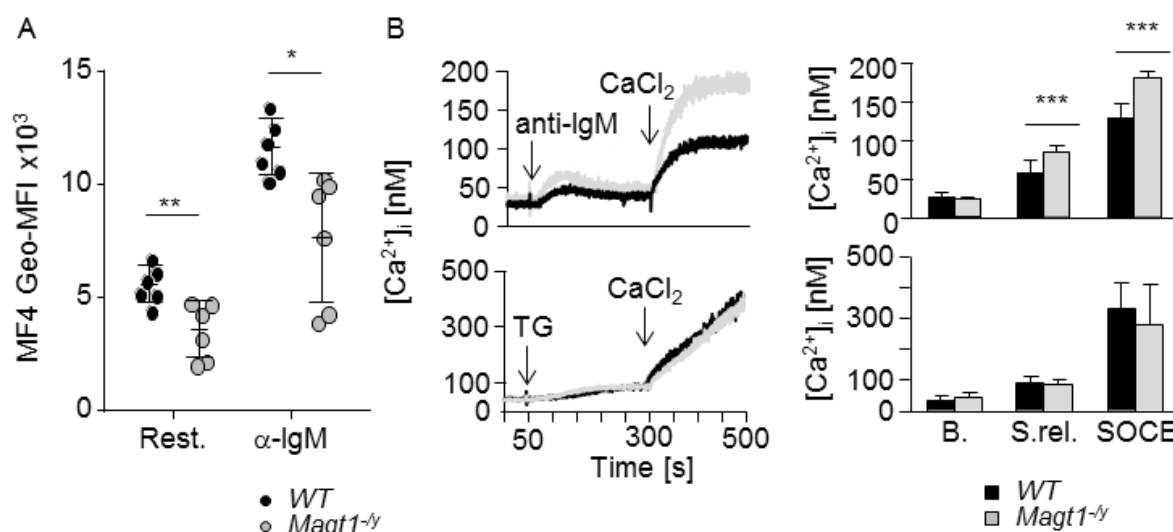


**Figure 37. Abnormal [Mg<sup>2+</sup>]<sub>i</sub> and [Ca<sup>2+</sup>]<sub>i</sub> levels in B cells of *Magt1*<sup>-/-</sup> mice:** (A) [Mg<sup>2+</sup>]<sub>i</sub> was quantified in kinetic measurements of resting and anti-IgM (5 µg/mL) activated B cells. Data represent Mag-Fluo-4 Geo-MFI ± SD. Each symbol represents one animal. (B) Untouched mature B cells from spleens were loaded with Fura-2, and representative traces of [Ca<sup>2+</sup>]<sub>i</sub> levels (left) as well as the respective quantifications (right) upon anti-IgM (5 µg/mL) or thapsigargin (TG) (5 µM) stimulation are presented. Data represent mean ± SD of Ca<sup>2+</sup> influx (n = 10). Black bars/curve correspond to *WT* and grey bars/traces to *Magt1*<sup>-/-</sup> samples. An unpaired Student's t-test was used to test significance. \*P<0.05, \*\*P<0.01, \*\*\*P<0.001. Geo-MFI: geometric mean fluorescence intensity; B.: basal [Ca<sup>2+</sup>]<sub>i</sub>; S.rel: store release; SOCE: store-operated Ca<sup>2+</sup> entry; anti-IgM: anti-immunoglobulin M antibody.

To test whether an imbalanced Mg<sup>2+</sup> and Ca<sup>2+</sup> homeostasis can account for the observed developmental defect in *Magt1*<sup>-/-</sup> B cells, cation levels were determined in resting cells and after stimulation with anti-IgM antibody or thapsigargin. Strikingly, the [Mg<sup>2+</sup>]<sub>i</sub> levels in both resting and activated *Magt1*<sup>-/-</sup> B cells were significantly reduced, when compared with *WT* cells. In contrast, the IgM-induced Ca<sup>2+</sup> store release was elevated, and also an increased Ca<sup>2+</sup> influx was observed in *Magt1*<sup>-/-</sup> B cells, compared with *WT* controls. Direct involvement of

STIM/ORAI1 mediated SOCE in this process could be excluded, as  $\text{Ca}^{2+}$  store release and  $\text{Ca}^{2+}$  influx were normal in *Magt1*<sup>-/-</sup> B cells upon thapsigargin stimulation (**Figure 37**).

### 3.4.6 Tyrosine phosphorylation in *Magt1*<sup>-/-</sup> B cells

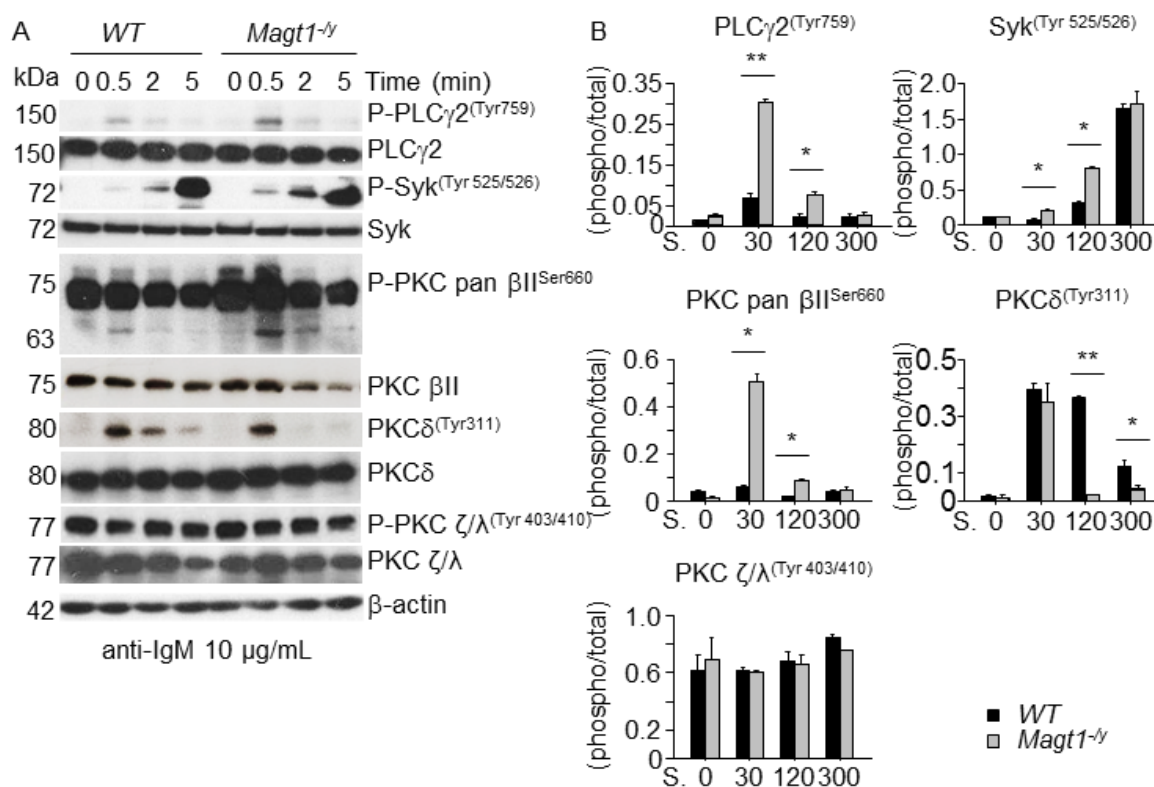


**Figure 38. Abnormal PKC phosphorylation in *Magt1*<sup>-/-</sup> B cells:** (A) Phosphorylation of the indicated proteins in B cell receptor signaling cascade and PKC isoforms assessed by immunoblotting in *WT* and *Magt1*<sup>-/-</sup> B cells upon IgM stimulation. (B) Quantification of phosphorylated protein relative to total protein intensity shown using Fiji software. Staining for  $\beta$ -actin was used as loading control. A representative of three independent experiments is presented. (A) and quantification (B) from all experiments is shown. Anti-IgM: anti-immunoglobulin M antibody. An unpaired Student's t-test was used to test significance. \* $P < 0.05$ , \*\* $P < 0.01$ , \*\*\* $P < 0.001$ .

To investigate the biochemical consequences of the dysregulated cation homeostasis in B cells, the proteins tyrosine phosphorylation downstream of BCR signaling was investigated. After BCR engagement with an anti-IgM antibody, we found increased phosphorylation of Syk, PLC $\gamma$ 2 and PKC $\beta$ II ( $\text{Ca}^{2+}$ -dependent and DAG-independent). Also, we found that although the initial activation of DAG-dependent PKC $\delta$  was normal at 30 s, the subsequent dephosphorylation was enhanced at later steps in *Magt1*<sup>-/-</sup> B cells compared to *WT* cells. In contrast, the regulation of PKC $\zeta/\lambda$  was not altered in *Magt1*<sup>-/-</sup> or *WT* B cells (**Figure 38**).

### 3.4.7 Proliferation of B cells in *Magt1*<sup>-/-</sup> mice

Magnesium is essential for cell survival and proliferation. Recent reports showed that vertebrate B cells lacking the Mg<sup>2+</sup> channel TRPM7, display normal Mg<sup>2+</sup> homeostasis and proliferation due to the compensatory upregulation of the magnesium transporter MAGT1 [196]. Using DT40 B cells, it has been demonstrated that a TRPM7 deficiency can be functionally compensated for by transport activity across MAGT1 channels [196]. To evaluate the physiological consequences of MAGT1 loss in murine B cells, a proliferation experiment was carried out using purified mature B cells. Herein, *Magt1*<sup>-/-</sup> B cells stimulated with IgM/IL-4 or PMA/ionomycin showed enhanced proliferation rates compared to the *WT* control cells. However, LPS-induced proliferation responses showed no differences between *WT* and *Magt1*<sup>-/-</sup> B cells (**Figure 39**).

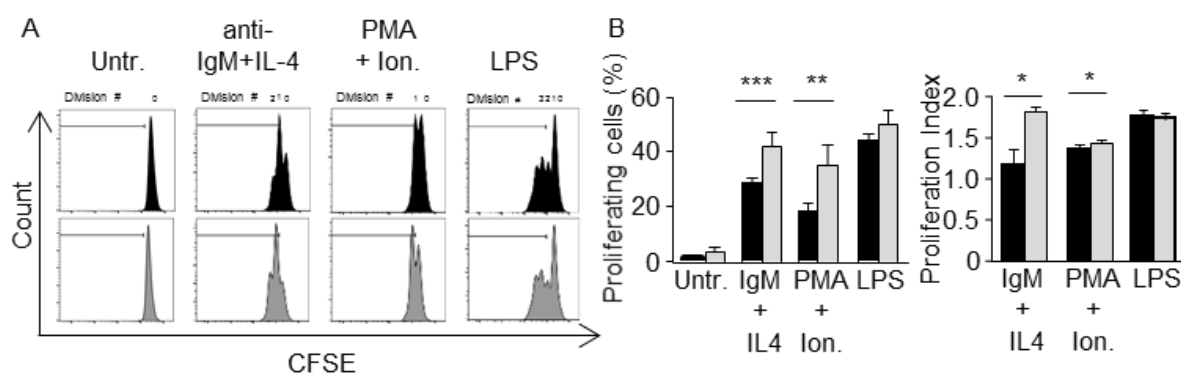


**Figure 39. Enhanced proliferation of *Magt1*<sup>-/-</sup> B cells:** B cells were either left untreated or stimulated with 5 µg/mL anti-IgM antibody in combination with IL-4 (10 ng/mL), 50 ng/mL PMA together with 500 ng/mL ionomycin or with 10 µg/mL LPS for 48 h. (A) Representative histograms for proliferation, (B) proliferated cells% (left) and proliferation index (right) shown in *WT* and *Magt1*<sup>-/-</sup> cells. A representative of three independent experiments is presented. Data represents mean ± SD (n = 4). Black bars/histograms correspond to *WT* and grey bars/histograms to *Magt1*<sup>-/-</sup> samples. Unpaired Student's t-test was used as a test of significance. \*P<0.05, \*\*P<0.01, \*\*\*P<0.001. Untr.: untreated; IL-4: interleukin 4; PMA: phorbol 12-myristate 13-acetate; Ion.: ionomycin; LPS: lipopolysaccharide; CFSE: carboxyfluorescein succinimidyl.

## 3.5 Identification of the Zn<sup>2+</sup> store in human and murine platelets

### 3.5.1 [Zn<sup>2+</sup>]<sub>i</sub> quantification

Given the controversy on the storage of [Zn<sup>2+</sup>]<sub>i</sub> in platelets, human and mouse platelets with abnormalities in their granules have been analyzed to identify their contribution to zinc storage. Human and murine platelets were loaded with the [Zn<sup>2+</sup>]<sub>i</sub> specific fluorescence dye FluoZin-3 and analyzed by confocal microscopy.

Resting platelets showed several FluoZin-3 positive foci, which were markedly less abundant in fibrinogen spread platelets (**Figure 40A**). This suggested that a substantial part of platelet

$[Zn^{2+}]_i$  is concentrated in secretory granules and released upon activation. To understand the dynamics of  $Zn^{2+}$  homeostasis, FluoZin-3-stained platelets were activated in suspension with thrombin and the changes in Geo-MFI were recorded over time by flow cytometry. Stimulation with thrombin caused a rapid decrease of approximately 60-70% in  $[Zn^{2+}]_i$  in control human and *WT* mouse platelets (**Figure 40A**).

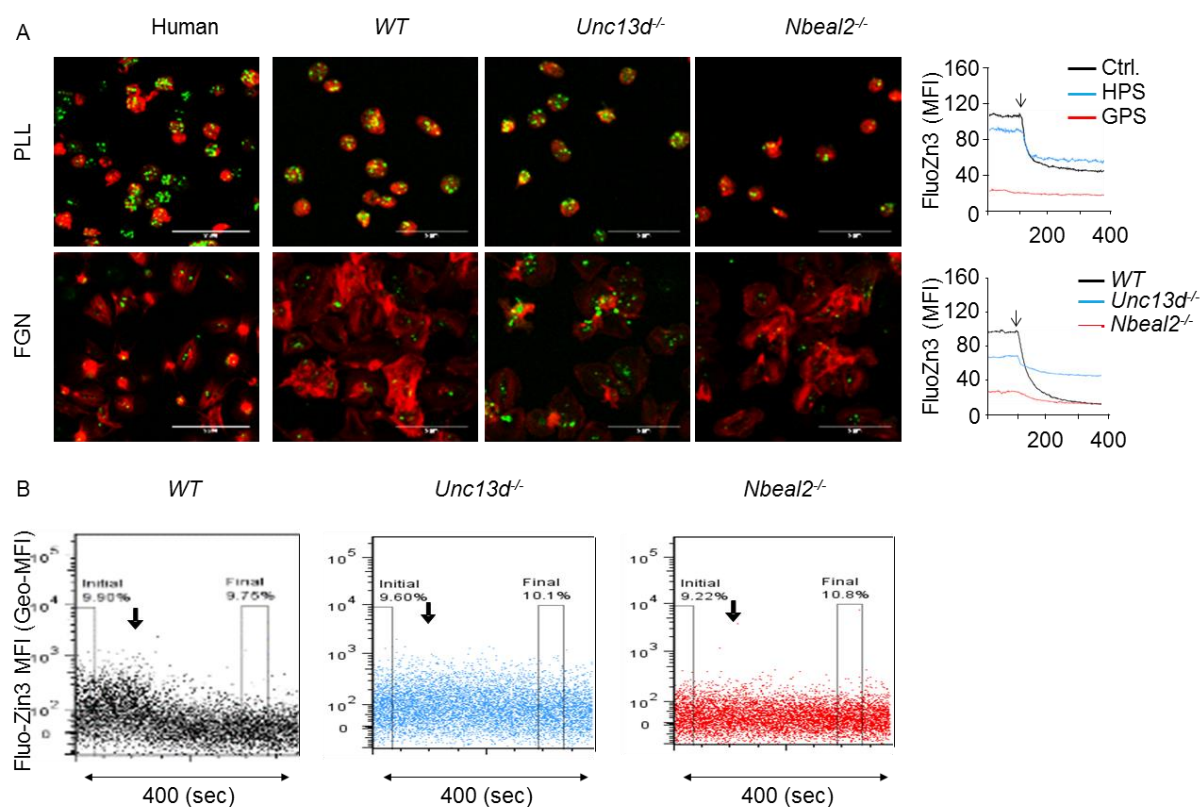


**Figure 40.  $[Zn^{2+}]_i$  levels in human and murine platelets:** (A) Confocal images of resting (PLL) and fibrinogen spread (FGN) FluoZin-3 loaded human (Ctrl.) (n = 3) and murine (*WT*, *Unc13d*<sup>-/-</sup>, *Nbeal2*<sup>-/-</sup>) (n = 3) platelets. Samples were counterstained with phalloidin-647 (left). Representative images from three independent experiments shown.  $[Zn^{2+}]_i$  kinetic measurements of the stated human (center) and mouse platelets (right) shown. (B) Representative dot plots of a kinetic  $[Zn^{2+}]_i$  efflux measurement for the indicated mice. Boxed areas were considered for FluoZin-3 fluorescence quantification. Arrows in panel A and B indicate agonist addition. PLL: poly-L-lysine; FGN: fibrinogen; HPS: Hermansky-Pudlak syndrome; GPS: Gray platelet syndrome; Geo-MFI: geometric mean fluorescence intensity.

Platelets from a Hermansky-Pudlak syndrome (HPS) patient characterized by routine diagnostics (**Table I & Figure 40 right**) displayed a slightly reduced basal  $[Zn^{2+}]_i$  level, but had a nearly normal  $Zn^{2+}$  release. On the other hand, platelets from *Unc13d*<sup>-/-</sup> mice showed FluoZin-3 positive foci both in resting and activated states (**Figure 40A**), slightly reduced basal  $[Zn^{2+}]_i$  level and a severely impaired  $Zn^{2+}$  release upon thrombin stimulation (**Figure 40A right**). Platelets from a patient with Gray-platelet syndrome, carrying a mutation in the *Nbeal2* gene,

or from *Nbeal2*<sup>-/-</sup> mice showed severely reduced  $[Zn^{2+}]_i$  levels in both resting and activated conditions (**Figure 40A**).

ID	Age	Sex (1=M,2=F)	Bleeding score (ISTH-BAT)	Platelet count ( $\times 10^9/L$ )			MPV (fL)
				Reference: 150-450			Reference: 8.1-9.9
GF1	28	2	3	194			11.1
ID	PFA-100 Col/EPI (sec)	PFA-100 Col/ADP (sec)	Agg-Col (AU) [1 $\mu$ g/mL]	Agg-TRAP (AU) [20 $\mu$ mol/L]	Agg-ADP (AU) [10 $\mu$ mol/L]	ATP release ( $\mu$ M/ $10^{12}$ platelets)	ADP amount ( $\mu$ M/ $10^{12}$ platelets)
	Reference: 84-160	Reference: 68-121	Reference: 76-95%	Reference: 68-97%	Reference: 59-95%	Reference: >10.1	Reference: >49.1
GF1	>296	99	6	35	58	n.d.	n.d.

**Table I. Diagnostic test results of Hermansky-Pudlak syndrome (HPS) patient platelets:** Values in grey box are in pathological range. ISTHG-BAT score, International Society on Thrombosis and Haemostasis Bleeding Assessment Tool, MPV: mean platelet volume, PFA: platelet function analyzer, Col: collagen, Agg: aggregation, TRAP: thrombin receptor-activating peptide. (Data obtained from routine diagnostic tests from University Clinic, Giessen, Germany).

### 3.5.2 Defective $Zn^{2+}$ homeostasis in storage pool deficient human platelets

To further analyze  $Zn^{2+}$  homeostasis in platelets,  $[Zn^{2+}]_i$  levels was analyzed in resting and thrombin-activated human platelets from phenotypically characterized storage pool disease (SPD) patients. These patients were diagnosed with a bleeding diathesis, defective ADP/ATP release, impaired aggregation responses to various agonists and a reduced mepacrine uptake or release upon TRAP-6 stimulation (**Table II-IV**). In platelets from patients with SPD, a reduced basal  $[Zn^{2+}]_i$  was detected, indicating a dysregulated platelet  $Zn^{2+}$  homeostasis. However, the remaining  $Zn^{2+}$  content of SPD platelets appeared to be released with similar kinetics as in healthy control platelets, whereas a difference between control and SPD platelets persisted (**Figure 41**).

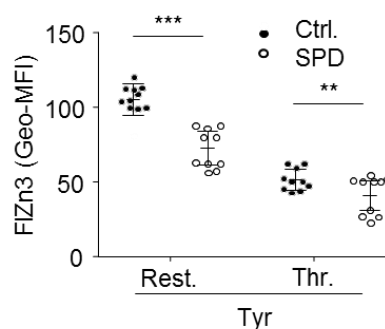


**Figure 41.  $[Zn^{2+}]_i$  quantification in SPD patients:**  $[Zn^{2+}]_i$  of human platelets was determined by flow cytometry using FluoZin-3 dye. An unpaired Student's t-test was used to test significance. \* $P < 0.05$ , \*\* $P < 0.01$ , \*\*\* $P < 0.001$ . Ctrl.: control, SPD: storage pool disease.

ID	Age	Sex (1=M,2=F)	Bleeding score (ISTH-BAT)	Platelet count (x10 <sup>9</sup> /L) Reference: 150-450	MPV (fL) Reference: 8.1-9.9
418	6	1	2	274	10.6
419	7	1	4	300	10.6
420	8	1	3	472	10.2
426	7	1	2	427	9.9
428	9	1	3	281	10.1
456	7	1	3	223	10.2
457	9	1	3	382	9.7
458	14	2	3	281	11.7
466	8	2	1	257	10.8
467	12	2	3	284	10.6

**Table II. Age, sex, bleeding score, platelet count and size of storage pool disease (SPD) patient platelets:** ISTHG-BAT score, International Society on Thrombosis and Haemostasis Bleeding Assessment Tools; MPV, mean platelet volume. (Data obtained from routine diagnostic tests from University Clinic, Munich, Germany).

ID	PFA-100 Col/EPI (sec) Reference: 84-160	PFA-100 Col/ADP (sec) Reference: 68-121	Agg-Col (AU) Reference: 45-95	Agg- TRAP (AU) Reference: 66-127	Agg-ADP (AU) Reference: 51-203	ATP release ( $\mu\text{M}/10^{12}$ platelets) Reference: >10.1	ADP amount ( $\mu\text{M}/10^{12}$ platelets)Refe rence: >49.1
418	162	108	38	58	46	n.d.	n.d.
419	115	n.d.	35	61	48	0.8	56.4
420	194	146	66	88	61	2.8	127.1
426	118	n.d.	7	62	23	4.1	80.1
428	120	n.d.	23	53	52	4.8	236.5
456	164	151	10	27	16	3.4	85.6
457	115	n.d.	37	63	35	n.d.	n.d.
458	n.d.	n.d.	n.d.	n.d.	n.d.	n.d.	n.d.
466	175	113	n.d.	n.d.	n.d.	n.d.	n.d.
467	146	n.d.	n.d.	n.d.	n.d.	n.d.	n.d.

**Table III. Platelet function test, aggregation, ATP release and ADP content of platelets from storage pool disease (SPD) patients:** Values in grey box are in pathological range. PFA, platelet function analyzer; Agg, aggregation; Col, collagen; TRAP, thrombin receptor-activating peptide. (Data obtained from routine diagnostic tests from University Clinic, Munich, Germany).

ID	Mepacrine loading (MFI)	Mepacrine release (MFI)	Mepacrine release (delta-MFI)
418	724	597	127
419	708	539	169
420	730	669	61
426	563	259	303
428	530	337	193
456	687	353	334
457	710	374	336
458	n.d.	n.d.	n.d.
466	650	450	200
467	700	525	175

**Table IV. Mepacrine loading and release of platelets from storage pool disease (SPD) patients analyzed by flow cytometry.** Values in grey box are in pathological range. MFI, mean fluorescence intensity. (Data obtained from routine diagnostic tests from University Clinic, München, Germany).

### 3.5.3 Effects of Zn<sup>2+</sup> supplementation and TPEN pretreatment on FluoZin-3 loaded murine platelets

$\alpha$ - and  $\delta$ -granule release from activated platelets affects several processes in the blood including coagulation and additionally contributes to wound healing and inflammation. It has been shown that *Unc13d* deficiency abolishes  $\delta$ -granule and also approximately 70 % of  $\alpha$ -granule secretion thereby leading to severe bleeding upon injury [197]. On the other hand, in patients with Gray-platelet syndrome characterized by a *Nbeal2* mutation and  $\alpha$ -granule deficit [21, 198], severe bleeding complications were observed. To further describe [Zn<sup>2+</sup>]<sub>i</sub> levels in platelets with these granule abnormalities, kinetic [Zn<sup>2+</sup>]<sub>i</sub> efflux measurements of platelets from *Unc13d*<sup>-/-</sup> and *Nbeal2*<sup>-/-</sup> mice were performed by flow cytometry. Under resting conditions, *Unc13d*<sup>-/-</sup> platelets showed a slightly reduced basal [Zn<sup>2+</sup>]<sub>i</sub> level, while *Nbeal2*<sup>-/-</sup> platelets showed an almost diminished basal [Zn<sup>2+</sup>]<sub>i</sub> level. Upon stimulation with thrombin, *Unc13d*<sup>-/-</sup> platelets displayed a severely impaired Zn<sup>2+</sup> efflux, while *Nbeal2*<sup>-/-</sup> platelets did not show any changes, reflecting the low basal [Zn<sup>2+</sup>]<sub>i</sub> level (**Figure 42A**).

To further investigate whether a defective Zn<sup>2+</sup> influx or altered Zn<sup>2+</sup> storage accounted for the reduced [Zn<sup>2+</sup>]<sub>i</sub> in mutant platelets, *WT*, *Unc13d*<sup>-/-</sup> and *Nbeal2*<sup>-/-</sup> platelets were either incubated with 100  $\mu$ M ZnCl<sub>2</sub> for 5 min, or with the Zn<sup>2+</sup> chelator N,N,N',-tetrakis(2-pyridylmethyl) ethylenediamine (TPEN). Subsequently, [Zn<sup>2+</sup>]<sub>i</sub> concentration was measured by flow cytometry

using the FluoZin-3 dye. Although basal  $[Zn^{2+}]_i$  levels of resting platelets increased for all genotypes in the presence of 100  $\mu M$  extracellular  $ZnCl_2$ , the differences between the groups persisted as in the untreated samples (**Figure 42B**). TPEN treatment, on the other hand, reduced the  $[Zn^{2+}]_i$  levels in a similar manner in *WT* and *Unc13d<sup>-/-</sup>* platelets to levels reaching those of *Nbeal2<sup>-/-</sup>* platelets  $[Zn^{2+}]_i$ , reflecting efficient  $Zn^{2+}$  chelation.  $[Zn^{2+}]_i$  levels in *Nbeal2<sup>-/-</sup>* platelets remained unaltered upon TPEN treatment, suggesting that the  $[Zn^{2+}]_i$  store in *Nbeal2<sup>-/-</sup>* platelets is nearly absent (**Figure 42C**).

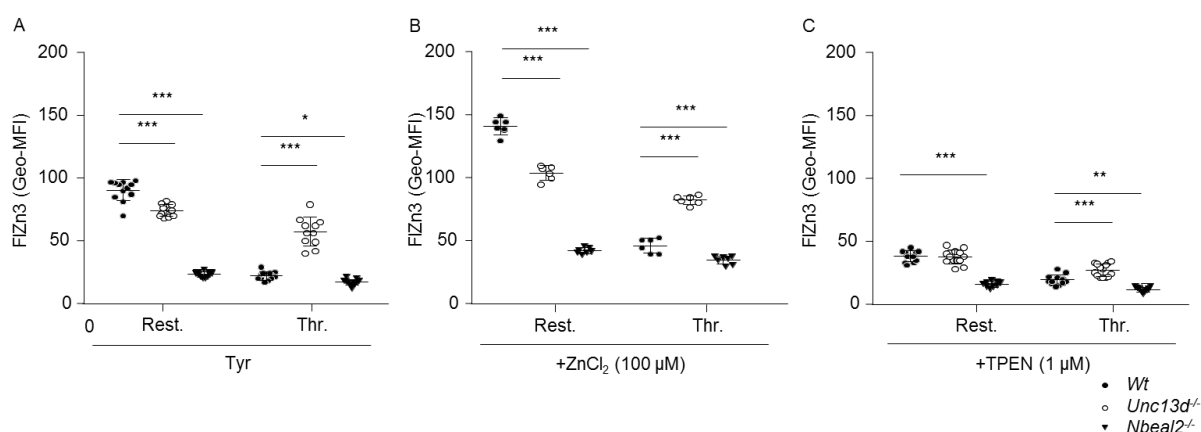


**Figure 42. Dysregulated  $[Zn^{2+}]_i$  homeostasis in *Unc13d<sup>-/-</sup>* and *Nbeal2<sup>-/-</sup>* platelets:** Washed mouse platelets from indicated strains were loaded with FluoZin-3, stimulated with thrombin and fluorescence changes observed by quantitative flow cytometry. (A-C) Quantification of  $[Zn^{2+}]_i$  in resting mouse platelets and after 0.01 U/mL thrombin stimulation in Tyrode's HEPES buffer (A). Similarly, after pre-incubation with 100  $\mu M$   $ZnCl_2$  (B) or 1  $\mu M$  TPEN (C). Each symbol represents one mouse. \* $P < 0.05$ ; \*\* $P < 0.01$ ; \*\*\* $P < 0.001$ . An unpaired Student's t-test was used to test significance. \* $P < 0.05$ , \*\* $P < 0.01$ , \*\*\* $P < 0.001$ . Tyr.: Tyrode's HEPES buffer; Rest.: resting; Thr.: thrombin; Geo-MFI: geographic mean of fluorescence intensity; TPEN: N,N,N',-tetrakis(2-pyridylmethyl)ethylenediamine.

### 3.5.4 Platelet zinc is essential for fibrin formation under flow

It has been proposed that platelet released  $Zn^{2+}$  can modulate local hemostatic reactions, including contact activation and fibrin clotting [29, 124, 199]. It is hypothesized that defective granule biogenesis or granule release alter platelet  $Zn^{2+}$  homeostasis or  $Zn^{2+}$  release, respectively, and thereby affects fibrin clot formation during hemostasis and thrombosis. The recording of fibrin formation in platelet thrombi formed in whole blood, perfused over collagen microspots, provides an adequate way to evaluate hemostatic activity *ex vivo*. Parallel-plate flow chamber studies at a wall shear rate of 1000  $sec^{-1}$  were performed, and the kinetics of fibrin clot formation was assessed using the accumulation of AF647-labeled fibrin as readout. In comparison to blood samples from healthy controls, platelet-dependent fibrin clot formation was prolonged in the blood of five different SPD patients. Upon *in vitro* addition of  $Zn^{2+}$ , this prolongation could be rescued (**Figure 43A & B**). On the other hand, similar to SPD patients, whole blood from *Unc13d<sup>-/-</sup>* mice showed delayed time to fibrin formation which could be



normalized by  $Zn^{2+}$  supplementation *ex vivo* (**Figure 43C & D**). Furthermore, a severely impaired thrombus and fibrin formation was observed with the blood from a GPS patient, which defect could not be restored by  $Zn^{2+}$  addition, thus indicating an essential role of  $\alpha$ -granular components in this process (**Figure 43A & B**). This suggests that other  $\alpha$ -granular factors besides  $Zn^{2+}$  are required for platelet-dependent fibrin formation. Also, whole blood from *Nbeal2<sup>-/-</sup>* mice either with or without  $Zn^{2+}$  supplementation did not show any observable alterations in time to fibrin formation (**Figure 43C & D**).

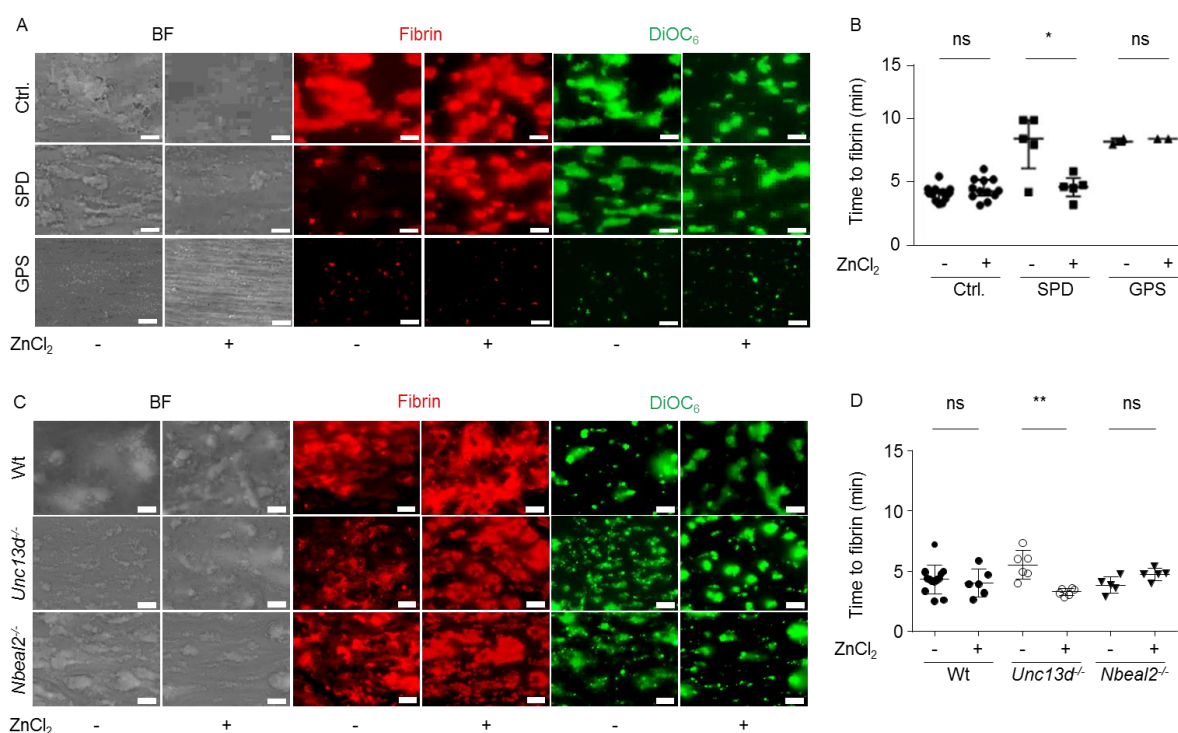


**Figure 43. Delayed time to fibrin formation in blood from storage pool deficient human patients and *Unc13d* deficient mice:** (A, C) Representative images and (B, D) time to appearance of first fibrin fibers in the indicated human and murine blood samples. BF: bright field, DiOC<sub>6</sub>: 3,3-dihexyloxycarbocyanine iodide, SPD: storage pool disease. An unpaired Student's t-test was used to assess statistical significance. \* $P < 0.05$ , \*\* $P < 0.01$ , \*\*\* $P < 0.001$ . (Experiments performed by Johanna P. van Geffen).

### 3.5.5 Higher total zinc content in *Nbeal2<sup>-/-</sup>* platelets

Quantification of the total amount of  $Zn^{2+}$  in platelets and plasma of *WT* and mutant mice by inductively coupled plasma mass spectrometry (ICP-MS) revealed an increased  $Zn^{2+}$  concentration in *Nbeal2<sup>-/-</sup>* platelets, but normal levels in *Unc13d<sup>-/-</sup>* platelets. However, the plasma  $Zn^{2+}$  concentrations were normal in both mouse models, when compared to *WT* mice (**Figure 44**). These results suggest that the abolished granular  $Zn^{2+}$  store in *Nbeal2<sup>-/-</sup>* platelets is compensated for by other so far unknown sources of compounded zinc, which could be a sequestering protein, like metallothionein. It seems that the protein-bound forms of  $Zn^{2+}$  in the

cytoplasm support a  $Zn^{2+}$ -dependent metabolism in *Nbeal2*<sup>-/-</sup> platelets and the platelet-dependent fibrin clot formation.

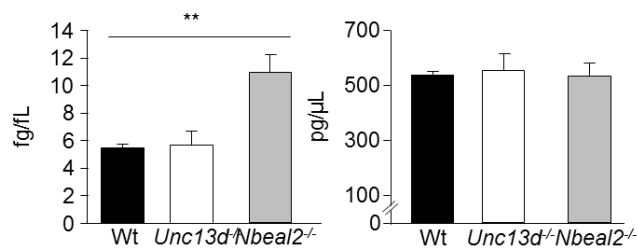


**Figure 44. Elevated platelet zinc content in *Nbeal2*<sup>-/-</sup>:** Total zinc content of platelets (left) and plasma (right) of *WT*, *Unc13d*<sup>-/-</sup> and *Nbeal2*<sup>-/-</sup> mice was determined by inductively coupled plasma mass spectrometry (ICP-MS). Results from two independent experiments presented (n = 6). An unpaired Student's t-test was used to test significance. \*P<0.05, \*\*P<0.01, \*\*\*P<0.001.

## 4. Discussion

Divalent cations exist in different forms in mammalian cells, either bound to proteins, stored in intracellular organelles, or in their free ionic form. Ion gradients existing between the extracellular milieu and cytoplasm on the one hand, and between the intracellular store and cytoplasm on the other side, permanently stimulate ATP-dependent ion transport mechanisms. Some ion channels transiently conduct cations both into and out of the cells, whereas other types of ion channels need to be stimulated to open and close their channel pore. In the present thesis, the transport/conduction mechanisms of  $\text{Ca}^{2+}$ ,  $\text{Mg}^{2+}$  and  $\text{Zn}^{2+}$  and their implications in platelet and immune cell signaling and function were investigated using different knockout mouse models. In case of  $\text{Zn}^{2+}$ , we also could use blood samples from patients with alterations in platelet granule content or release.

### 4.1 TRPM7 kinase controls calcium responses in arterial thrombosis and stroke in mice

The  $\alpha$ -kinase TRPM protein family comprises various members including TRPM6 [200], TRPM7 [201] and eEF2 serine/threonine kinases [202]. To date, only a few substrates of TRPM7 kinase have been identified *in vitro*, namely myosin IIa [203], PLC $\gamma$ 2 [204] and annexin-1 [205]. Whereas in platelets the protein tyrosine kinase-dependent signaling has been extensively studied [206], the physiological importance of serine/threonine phosphorylation for ITAM receptor signaling triggered by a TRPM7 kinase or other  $\alpha$ -kinases is unknown.

The GPVI signalosome is regulated by SFK isoforms, which bind the cytoplasmic tail of GPVI [207], and are critical in the initial steps of GPVI signalosome activation. However, these isoforms can also inhibit platelet activation through phosphorylation of immunoreceptor tyrosine-based inhibition motifs (ITIMs) on platelet endothelial cell adhesion molecule-(PECAM)1 [208, 209]. The tyrosine kinase Syk transduces the signal from the GPVI/FcR $\gamma$ -chain to LAT, which in turn induces the recruitment of different adaptors and PLC $\gamma$ 2 from the cytosol. It has been shown that several PLC isoforms can bind to the kinase domain of TRPM7, and that TRPM7 kinase phosphorylates PLC $\gamma$ 2, although the physiological relevance of these interactions remained elusive [204, 210, 211].

In the present thesis, we could demonstrate that ablation of TRPM7 kinase activity strongly inhibited the tyrosine phosphorylation cascade downstream of GPVI and CLEC-2, via a mechanism involving the Syk-LAT-PLC $\gamma$ 2 signaling axis. In addition, also the thrombin receptor PAR-PLC $\beta$ 3 signaling axis was regulated by the TRPM7 kinase, as deduced from a reduced serine phosphorylation of PLC $\beta$ 3 in *Trpm7<sup>R/R</sup>* platelets after thrombin stimulation. Altogether,

these results suggest an essential role of TRPM7 kinase activity in PLC-mediated  $\text{Ca}^{2+}$  store depletion during platelet activation.

It is understood that several phosphorylation events on serine residues of STIM1 are involved in the modulation of SOCE [212]. However, the underlying mechanisms and the responsible kinases regulating STIM1 had not been investigated in platelets. Using heterologous expression in DT40 cells, it could be established that TRPM7 governs SOCE [213]. In line with this, in this thesis it is shown for the first time *in vivo*, that TRPM7 kinase activity indeed regulates SOCE in mouse platelets. The obtained results suggest that a combined signaling defect via GPVI, CLEC-2 and PAR receptors can result in a reduced SOCE. This translated to an impaired aggregation response of *Trpm7<sup>R/R</sup>* platelets. Further investigation is required to decipher the exact molecular mechanism and identify the phosphorylation sites on STIM1, by which TRPM7 kinase may regulate SOCE.

TRPM7 is expressed in the human vascular system, where it modulates  $\text{Mg}^{2+}$  homeostasis, cell growth and proliferation in vascular smooth muscle and endothelial cells [214]. Abnormal expression of this channel has been linked to the development of cardiovascular diseases [215]. The present study demonstrated for the first time that the kinase activity of TRPM7 regulates platelet activation in arterial thrombosis and brain stroke. This establishes the TRPM7 kinase as a potential target in the modulation of platelet reactivity in thrombo-inflammatory settings.

Ionic  $\text{Mg}^{2+}$  was found to be a potent  $\text{Ca}^{2+}$  antagonist thereby protecting ischemic neurons from  $\text{Ca}^{2+}$  overload [216]. Supporting this concept, a reduced  $[\text{Mg}^{2+}]_i$  concentration was detected in the ischemic rat and human brain. Additionally, in experimental hypomagnesemia, increased infarct volumes after photo-thrombosis were observed [217-219]. Using BM chimeras and adoptive platelet transfer, the function of TRPM7 kinase in hematopoietic and non-hematopoietic cells could be distinguished. The evidence for improved motor functions and reduced infarct volumes in *Trpm7<sup>R/R</sup>/BM<sup>WT</sup>* mice clearly showed that TRPM7 kinase activity in the brain (most likely in neurons) can also be a critical factor for the progression of ischemic brain infarction [158].

Interestingly, in the cortex of *WT* mice subjected to tMCAO, a 2-3 fold increase in TRPM7 expression was observed after reperfusion [220, 221], which likely contributed in the  $\text{Ca}^{2+}$  overload and neuronal cell death as well as to the infarct progression [222]. In line with this, knockdown of TRPM7 could prevent neuronal cell death [223]. Based on this work, inhibition of TRPM7 channel activity was proposed as a promising potential therapeutic strategy [224]. Surprisingly, the results obtained in the course of this thesis showed that disruption of TRPM7

kinase activity either in platelets or in neurons is sufficient to protect the brain from the thrombo-inflammatory cerebral ischemic reperfusion injury.

These results suggest that, under pathological conditions, an increased TRPM7 channel activity cannot overcome the protective effect of an abolished TRPM7 kinase function in *Trpm7<sup>R/R</sup>* mice. This leads to the concept that TRPM7 kinase accelerates the PLC-mediated  $\text{Ca}^{2+}$  mobilization and SOCE, rather than the TRPM7 channel activity.

The finding that selective disruption of TRPM7 kinase function did not cause bleeding in an ischemic brain, but only moderately influenced hemostasis, highlights the TRPM7 kinase as a promising potential therapeutic target to develop safe anti-thrombo-inflammatory agents. Nevertheless, further investigation is required to establish the exact molecular mechanism, by which TRPM7 kinase can regulate the integrity of the blood-brain barrier or neuronal cell death upon ischemic stroke.

#### 4.2 Multiple roles of TRPM7 in the regulation of $\text{Mg}^{2+}$ and $\text{Ca}^{2+}$ homeostasis

Numerous studies have described the two-step process of  $\text{Ca}^{2+}$  entry in platelets, and it has been shown that defective  $\text{Ca}^{2+}$  store release consequently causes a reduction in  $\text{Ca}^{2+}$  entry [13, 46]. In line with this, one could expect a significantly enhanced  $\text{Ca}^{2+}$  entry in *Trpm7<sup>fl/fl-Pf4Cre</sup>* platelets due to the increased  $\text{Ca}^{2+}$  store release. Surprisingly, activation-dependent  $\text{Ca}^{2+}$  entry in *Trpm7<sup>fl/fl-Pf4Cre</sup>* platelets was decreased. Conversely, in *Serca3<sup>-/-</sup>* platelets a reduced store release preceded an increased  $\text{Ca}^{2+}$  entry upon thrombin stimulation. The authors concluded that the enhanced  $\text{Ca}^{2+}$  entry compensates for a reduced  $\text{Ca}^{2+}$  store release [60]. Based on these findings, we can speculate that in *Trpm7<sup>fl/fl-Pf4Cre</sup>* platelets the increased  $\text{Ca}^{2+}$  store release can compensate for the reduced  $\text{Ca}^{2+}$  entry. Previous studies have implicated a role of the TRPM7 channel in the regulation of SOCE [213], and the present results point to such a role in regulating both  $\text{Ca}^{2+}$  store release and SOCE. Unfortunately, due to the low expression levels and the unavailability of a functional antibody detecting low amounts of protein, TRPM7 expression and localization could not be assessed in murine platelets.

A consistent defective P-selectin exposure was observed in *Trpm7<sup>fl/fl-Pf4Cre</sup>* platelets, indicating a possible role of TRPM7 in  $\text{Ca}^{2+}$ -dependent platelet granule release. Explanations for this change are an enlarged size and altered cytoskeletal dynamics of *Trpm7<sup>fl/fl-Pf4Cre</sup>* platelets [75]. In support of a decreased  $\text{Ca}^{2+}$  entry, the *Trpm7<sup>fl/fl-Pf4Cre</sup>* platelets were decreased in PS exposure upon activation. Yet the *Trpm7<sup>fl/fl-Pf4Cre</sup>* platelets hyper-aggregated in response to GPCR stimulation, but dysresponded upon GPVI stimulation. We can only speculate that *Trpm7<sup>fl/fl-Pf4Cre</sup>* platelets show these ambiguous responses due to some unknown compensatory

mechanisms. Nevertheless, *in vivo*, in models of neither thrombosis nor stroke, the *Trpm7<sup>fl/fl-Pf4Cre</sup>* mice showed differences compared to *WT* mice.

Comparing the results obtained with the *TRPM7<sup>R/R</sup>* and *Trpm7<sup>fl/fl-Pf4Cre</sup>* mouse strains, it became clear that a constitutive deletion of the kinase activity is a promising anti-thrombotic strategy rather than deleting TRPM7 specifically in MKs and platelets. Our group identified a patient family carrying a *TRPM7* variant resulting in a strongly inhibited channel activity. Similar to *Trpm7<sup>fl/fl-Pf4Cre</sup>* mice, these patients also developed macrothrombocytopenia with a complex MK and platelet dysfunction [75]. In summary, these findings highlight the selective inhibition of TRPM7 kinase as a promising therapeutic approach in thrombo-inflammatory diseases, whereas blockade of the TRPM7 channel activity is disadvantageous, since it results in thrombocytopenia with multiple platelet defects [75].

#### **4.3 Defective Mg<sup>2+</sup> transport enhances receptor-operated Ca<sup>2+</sup> entry in murine platelets and thereby results in accelerated thrombosis and stroke**

In mammalian cells,  $[Mg^{2+}]_i$  is regulated by Mg<sup>2+</sup> influx and efflux through plasma membrane and intracellular stores. In MKs and platelets, the  $[Mg^{2+}]_i$  stores have not yet been identified, but in mammalian cells the endoplasmic reticulum, mitochondria, secretory granules and the Mg<sup>2+</sup>-ATP complex have been proposed as potential Mg<sup>2+</sup> stores [74]. Interestingly, an elevated  $[Ca^{2+}]_i$  has been observed in cardiomyocytes under conditions of hypomagnesemia, which indicates a regulatory role of Mg<sup>2+</sup> in Ca<sup>2+</sup> homeostasis [72].

We identified TRPM7 as a key regulator of Mg<sup>2+</sup> homeostasis in platelets and MKs, and found that dysregulated  $[Mg^{2+}]_i$  can cause macrothrombocytopenia. Earlier, we also observed an increased expression of MAGT1 in TRPM7-deficient MKs [75], indicating a possible compensatory role of MAGT1 in Mg<sup>2+</sup> homeostasis in this pathological condition. The results presented in this thesis further suggest that basal  $[Mg^{2+}]_i$  and Mg<sup>2+</sup> efflux are normal in resting *Magt1<sup>-/-</sup>* platelets as well as upon stimulation of PAR receptors. However, in response to CRP, a more pronounced  $[Mg^{2+}]_i$  depletion was detected in *Magt1<sup>-/-</sup>* mice, indicating that MAGT1 activity is selectively regulated by downstream effectors of GPVI.

In *Drosophila* cells, PKC was shown to bind and phosphorylate MAGT1 at serine residues, thereby enhancing its Mg<sup>2+</sup> transport activity [225]. The identified PKC phosphorylation sites on MAGT1 appeared to be highly conserved between different species, suggesting an evolutionarily conserved function of PKC in the regulation of MAGT1 activity.

Mammalian platelet activation is a balance between positive [68, 226] and negative [69, 227] signaling pathways, which are mainly regulated by different PKC isoforms. PKC $\delta$  negatively

regulates collagen-induced platelet activation, and this feedback loop is mediated by the complex interplay between Lyn, SHIP-1, and PKC $\delta$ , which control downstream effectors of GPVI [209]. Our present results showed for the first time that MAGT1 deficiency reduces PKC $\delta$  phosphorylation on Y311 residue downstream of GPVI thereby losing an inhibitory signaling component. Consequently, this signaling defect accelerates phosphorylation of Syk, LAT and PLC $\gamma$ 2. Others have shown that PKC $\delta$  exerts a negative feedback on the TRPC6 channel through phosphorylation of serine residue 448 [228]. Based on this, we speculate that a reduced PKC $\delta$  activity can no longer inhibit TRPC6 channel activity and thus leads to an increased Ca<sup>2+</sup> influx in *Magt1*<sup>-/-</sup> platelets. In support of this idea, we found normal PKC $\delta$  phosphorylation in *Magt1*<sup>-/-</sup>/*Trpc6*<sup>+/-</sup> platelets in response to GPVI activation. Accordingly, in the double knockouts platelet aggregation responses were normalized *in vitro* and *ex vivo* under flow.

Along the same line is the evidence that PKC $\delta$  deficiency can enhance collagen-dependent aggregation responses and that this effect is accelerated by increased TXA<sub>2</sub> release [69, 229]. We similarly detected an increased TXA<sub>2</sub> release upon collagen or CRP stimulation in *Magt1*<sup>-/-</sup> platelets. However, *in vivo* thrombus formation in the carotid artery was unaltered in *Pkc $\delta$* <sup>-/-</sup> mice, whereas the *Magt1*<sup>-/-</sup> mice showed a pro-thrombotic phenotype. This discrepancy may be due to the usage of a rather high dose of FeCl<sub>3</sub> (10%) in *Pkc $\delta$* <sup>-/-</sup> mice, which induces a fast vessel occlusion already in *WT* mice, thus limiting the detection of small dynamic changes in thrombus formation [69]. We found that application of 6% FeCl<sub>3</sub> was efficient to detect a significantly prolonged occlusion time in the carotid artery of *WT* mice, whereas an accelerated occlusion was observed in *Magt1*<sup>-/-</sup> mice.

Translocation of PKC $\epsilon$  to the plasma membrane in hepatocytes is known to trigger Mg<sup>2+</sup> accumulation in the cytoplasm [230]. Strikingly, in our hands an increased expression of MAGT1 in the plasma membrane was found at 24 h after constitutive activation of PKC in hepatocytes by phorbol 12-myristate 13-acetate (PMA) treatment [231], thus supporting a functional crosstalk between PKC and MAGT1. The phosphorylation of PKC $\epsilon$  on serine 729, which correlates with its enzymatic activity, was reduced in *Magt1*<sup>-/-</sup> platelets in response to CRP. This alteration was normalized in *Magt1*<sup>-/-</sup> *Trpc6*<sup>+/-</sup> platelets, thus supporting a functional crosstalk between MAGT1, PKC $\epsilon$  and TRPC6. Interestingly, reduced PKC $\epsilon$  phosphorylation was also detected in the absence of extracellular Ca<sup>2+</sup>, pointing to a redundant role of TRPC6-mediated Ca<sup>2+</sup> influx in the regulation of PKC $\epsilon$  activity. Upon platelet activation, PKC $\epsilon$  was found to translocate from the cytoplasm to the GPVI complex and then phosphorylate serine residues at the FcR $\gamma$  chain, thereby increasing Syk binding [70]. The physiological consequence of this biochemical interaction is difficult to interpret because conflicting results

have been obtained by using a non-selective PKC $\epsilon$  inhibitor or PKC $\epsilon$  knockout mice, which revealed either a positive or an adverse effect of PKC $\epsilon$  on GPVI signaling [227, 232]. Nevertheless, there is a consensus that PKC $\epsilon$  negatively regulates collagen-induced platelet activation through inhibition of cyclooxygenase activity [227]. In addition, also Mg<sup>2+</sup> inhibits cyclooxygenase activity in platelets [73]. Taken these results together, we conclude that the reduced PKC $\epsilon$  activity and the enhanced [Mg<sup>2+</sup>]<sub>i</sub> depletion in *Magt1*<sup>-/-</sup> platelets can account for an increased cyclooxygenase activity and TXA<sub>2</sub> production, which further amplifies the collagen-induced aggregation response. These changes can translate into a shortened time to vessel occlusion in a model *in vivo* thrombosis and hemostasis in both *Pkcε*<sup>-/-</sup> mice [227] and *Magt1*<sup>-/-</sup> mice. Our results thus point to a critical role of the MAGT1/PKC $\epsilon$  signaling route in the regulation of thrombosis and hemostasis. The recapitulation of the pro-thrombotic phenotype in *WT-BM*<sup>*Magt1*<sup>-/-</sup></sup> mice revealed that a defective Mg<sup>2+</sup> transport in the hematopoietic system can contribute to an accelerated thrombus growth.

Using the tMCAO model of ischemic stroke in combination with pre- or post-surgical administration of Mg<sup>2+</sup> supplements, several *in vivo* studies showed inhibitory effects of Mg<sup>2+</sup> on brain infarct progression in rats [233, 234]. Although the clinical benefit of Mg<sup>2+</sup> supplementation is apparent, the molecular mechanism of Mg<sup>2+</sup> uptake and release in ischemic stroke remains elusive. In the study presented in this thesis, we demonstrated that MAGT1 deficiency in platelets strongly enhances the formation of platelet aggregates in ipsilesional vessels of the ischemic brain, and thereby accelerates brain infarct progression. The *in vitro* and *ex vivo* platelet function analysis revealed that Mg<sup>2+</sup> supplementation or partial inhibition of TRPC6 channel activity might be a promising therapeutic intervention in MAGT1-related pathology to limit platelet reactivity and possibly infarct progression.

In summary, we conclude that abolished MAGT1 function strongly enhances the activity of the GPVI signalosome through an aberrant activation of TRPC6 and moderately increases TP receptor and purinergic receptor signaling. Also, the PKC $\delta$ - and PKC $\epsilon$ -mediated inhibition of GPVI signaling are dependent on MAGT1 activity and are partially regulated by TRPC6. A loss of this negative feedback loop on GPVI signaling appeared to lead to a pro-thrombotic phenotype in *Magt1*<sup>-/-</sup> mice *in vivo*. In this context, a decreased [Mg<sup>2+</sup>]<sub>i</sub> in platelets, due to a defective or suppressed MAGT1 function, can be a risk factor for the development of arterial thrombosis and stroke triggered by hyperactive platelets. Supplementation of Mg<sup>2+</sup> can be a promising therapeutic strategy in such pathology to limit platelet reactivity.



#### 4.4 Imbalanced cation homeostasis dysregulates B cell development and signaling of MAGT1-deficient B cells

To date, our understanding of the mechanisms governing EBV infection in MAGT1-deficient patients is limited. In particular, the mechanisms are unknown, which initiate the interplay between viruses and host B cells, thereby leading to further alterations of T-cell responses. Under infectious conditions, it is difficult to decipher the relative contribution of MAGT1 to the reported defects in T or B cells, since inflammation caused by the EBV infection could modify cation homeostasis and the immunogenic function in lymphocytes.

To dissect the primary role of MAGT1 in immune cells, we used a MAGT1-deficient mouse line (*Magt1*<sup>-/-</sup>). Similarly to the XMEN syndrome in humans, we found a slight but significant reduction in both T cell numbers and the CD4<sup>+</sup>/CD8<sup>+</sup> ratio in the spleen, lymph nodes and blood from *Magt1*<sup>-/-</sup> mice. However, levels of [Mg<sup>2+</sup>]<sub>i</sub> and [Ca<sup>2+</sup>]<sub>i</sub> in resting and activated CD4<sup>+</sup> cells (TCR or thapsigargin stimulation) were unaltered between *WT* and *Magt1*<sup>-/-</sup> mice. In the NK cells from MAGT1-deficient patients, it has been shown that the expression and function of the activating receptor NKG2D is reduced [89]. In our evaluation for NKG2D expression and NKG2D-induced killing by NK cells, we did not observe differences between *WT* and *Magt1*<sup>-/-</sup> NK cells. This distinction between mouse and human could indicate that the dysregulation of Mg<sup>2+</sup> and Ca<sup>2+</sup> homeostasis in human MAGT1-deficient T cells is due to secondary defects that are triggered by EBV infection or other lymphocyte subtypes.

Therefore, we next assessed the primary function of MAGT1 in B lymphocytes. We found an increased fraction of CD19<sup>+</sup> B cells among the CD45<sup>+</sup> cell population, in the blood and lymphoid organs from *Magt1*<sup>-/-</sup> mice, which is in accordance with the findings in XMEN patients [195]. Additionally, we found that levels of plasma cells were decreased, but that follicular B cell levels were unaltered. A profound increase in the frequencies of the marginal zone B cells was observed in the spleen from *Magt1*<sup>-/-</sup> mice, indicative for a selective defect in B cell development. Of note, total numbers of B cells were increased in the peripheral blood, splenic tissue or lymph nodes, but not in the BM from *Magt1*<sup>-/-</sup> mice. In contrast, T cell numbers in blood and the hematopoietic organs were indistinguishable between *Magt1*<sup>-/-</sup> and *WT* mice. To test whether imbalanced Mg<sup>2+</sup> and Ca<sup>2+</sup> homeostasis accounts for the developmental defect of *Magt1*<sup>-/-</sup> B cells, we determined the levels of these cations in resting cells and after stimulation with anti-IgM antibody or thapsigargin. Strikingly, [Mg<sup>2+</sup>]<sub>i</sub> levels in both resting and activated *Magt1*<sup>-/-</sup> B cells was significantly reduced compared with *WT* cells. In contrast, IgM-induced Ca<sup>2+</sup> store release was elevated and consequently, an increase in Ca<sup>2+</sup> influx was also observed in *Magt1*<sup>-/-</sup> B cells compared to *WT* controls. We could exclude a direct involvement of STIM/ORAI1-mediated SOCE in this process, as Ca<sup>2+</sup> store release and Ca<sup>2+</sup> influx was found to be normal in *Magt1*<sup>-/-</sup> B cells upon thapsigargin stimulation.

Binding of IgM to the B cell surface induces two synergistic activating signals, catalyzing the hydrolysis of phosphatidylinositol 4,5-bisphosphate (PIP<sub>2</sub>) through the BCR-Syk-PLC $\gamma$ 2 and CD19-PI3K-Btk-PLC $\gamma$ 2 pathways [235]. The metabolic product of PIP<sub>2</sub>, IP<sub>3</sub>, further triggers Ca<sup>2+</sup> store depletion through the IP<sub>3</sub> receptors. The second hydrolysis product of PIP<sub>2</sub>, diacylglycerol (DAG) in turn, activates PKC- and DAG- dependent transient receptor potential cation (TRPC) channel activity in B cells [236]. In addition, PKC has been reported to phosphorylate MAGT1 on serine 100/106 residues, thereby enhancing Mg<sup>2+</sup> transport activity [237], likely to limit excessive Ca<sup>2+</sup> signaling. After BCR engagement with an anti-IgM antibody, we found increased phosphorylation of Syk, PLC $\gamma$ 2 and Ca<sup>2+</sup>-dependent (but DAG-independent) PKC $\beta$ II. In addition, we found that although the initial activation of DAG-dependent PKC $\delta$  was normal 30 s after IgM ligation, its de-phosphorylation was enhanced at later time points in *Magt1*<sup>-/-</sup> B cells compared to *WT* cells. In contrast, regulation of PKC $\zeta/\lambda$  was not altered in both *Magt1*<sup>-/-</sup> and *WT* B cells. Based on these findings, we propose that PKC function is regulated by a dynamic change in Mg<sup>2+</sup> and Ca<sup>2+</sup> homeostasis upon B cell activation, which is controlled by the MAGT1-mediated Mg<sup>2+</sup> influx and Ca<sup>2+</sup> release from Ca<sup>2+</sup> stores. It has previously been shown that phosphorylation of PKC $\beta$ II<sup>S660</sup> is strongly dependent on Ca<sup>2+</sup> release from intracellular Ca<sup>2+</sup> stores, which in turn regulates the subcellular localization of the enzyme [238, 239]. Interestingly, dephosphorylation of PKC $\beta$ II<sup>S660</sup> is a PP2A phosphatase-dependent, and inhibition of PP2A enzymatic activity strongly accelerates PKC $\beta$ II<sup>S660</sup> phosphorylation [238]. The increase in Ca<sup>2+</sup> store depletion and enhanced PKC $\beta$ II<sup>S660</sup> phosphorylation in *Magt1*<sup>-/-</sup> B cells may similarly dysregulate the subcellular localization of the enzyme, and abnormally phosphorylate downstream effectors of the BCR signalosome. PKC $\delta$  is phosphorylated on several tyrosine residues, which regulate Ca<sup>2+</sup> mobilization and Ca<sup>2+</sup>-dependent degranulation through Lyn inactivation and PKC $\delta$ -SHIP protein complex formation in mast cells and platelets [209, 240, 241]. We speculate that reduced phosphorylation of PKC $\delta$ <sup>Y311</sup> in *Magt1*<sup>-/-</sup> B cells may inhibit this negative feedback loop to Lyn, thereby enhancing BCR-Syk-PLC $\gamma$ 2 mediated IP<sub>3</sub> and DAG production, and in turn accelerating Ca<sup>2+</sup> responses in B cells deficient in MAGT1.

To evaluate the physiological consequence of abnormal cation homeostasis and PKC functions, we investigated Ca<sup>2+</sup> and PKC dependent B cell proliferation *in vitro*. In line with the increased Ca<sup>2+</sup> influx, IgM/IL-4 or PMA/ionomycin-stimulated *Magt1*<sup>-/-</sup> B cells showed enhanced proliferation rates compared to *WT* controls, whereas Ca<sup>2+</sup>-independent B cell activation with LPS induced a strong but unaltered proliferative response.

In conclusion, our study reveals an essential contribution of MAGT1 to the regulation of Mg<sup>2+</sup> homeostasis in resting and activated B cells. Genetic ablation of MAGT1 in mice leads to an

enhanced BCR-induced  $\text{Ca}^{2+}$  store release and abnormal PKC activation, which likely disturbs the development of marginal zone B cells and plasma cells. These changes in cation homeostasis may also contribute to disorders in humans suffering from XMEN syndrome, and should stimulate future research addressing the role of MAGT1 signaling in B cell-mediated diseases.

#### **4.5 Defective $\text{Zn}^{2+}$ homeostasis of human and mouse platelets with $\alpha$ - and $\delta$ -storage pool disorders**

Given the ambiguity of the cellular location of ionic  $\text{Zn}^{2+}$  and the role of platelet  $\text{Zn}^{2+}$  release in clot formation, we re-evaluated these topics in human and mouse platelets with granular abnormalities. Loading of control human and *WT* mouse platelets with the  $\text{Zn}^{2+}$ -specific fluorescence dye, FluoZin-3, indicated that the cells at resting state contained several stained foci, which markedly reduced upon platelet spreading on a fibrinogen-coated surface. This observation suggests that a substantial part of the  $[\text{Zn}^{2+}]_i$  is concentrated in the secretory granules, which is released upon platelet activation. Using flow cytometry experiments in thrombin-stimulated FluoZin-3 loaded platelets, these results were confirmed. Taken together, this points to the platelet granules as major  $\text{Zn}^{2+}$  stores. Nevertheless, the remaining part of  $\text{Zn}^{2+}$  can be available for sequestering proteins such as metallothionein, which was previously reported in MKs and platelets [242, 243].

The release of the  $\alpha$ - and  $\delta$ -granule content from activated platelets affects several processes in the blood including coagulation, wound repair or inflammation [244]. Platelets from *Unc13d*<sup>-/-</sup> mice show abolished  $\delta$ -granule release and reduced  $\alpha$ -granule secretion [197]. To study whether  $\text{Zn}^{2+}$  efflux accompanies granule release, we loaded platelets from both *WT* and *Unc13d*<sup>-/-</sup> mice with FluoZin-3. In comparison to *WT*, the knockout platelets showed a slightly reduced basal  $[\text{Zn}^{2+}]_i$ , but a severely impaired  $\text{Zn}^{2+}$  efflux after thrombin stimulation. Similarly, we used *Nbeal2*<sup>-/-</sup> platelets with an  $\alpha$ -granule defect, which displayed a severely reduced  $\text{Zn}^{2+}$  level in both the resting and activated conditions. Furthermore,  $\text{Zn}^{2+}$  levels were analyzed in platelets derived from phenotypically characterized SPD patients with defective platelet ADP/ATP release and aggregation responses; impaired platelet mepacrine release and a bleeding diathesis. In platelets from 4 out of 5 SPD patients, a low basal  $\text{Zn}^{2+}$  level was detected, suggestive for a dysregulated  $\text{Zn}^{2+}$  homeostasis. However, the remaining  $\text{Zn}^{2+}$  content of SPD platelets could be released with similar kinetics as in control platelets.

To investigate whether defective  $\text{Zn}^{2+}$  influx or altered  $\text{Zn}^{2+}$  storage could account for the reduced  $[\text{Zn}^{2+}]_i$  in mutant platelets, we utilized mouse models and incubated *WT*, *Unc13d*<sup>-/-</sup> and *Nbeal2*<sup>-/-</sup> platelets with either  $\text{ZnCl}_2$  or  $\text{Zn}^{2+}$  chelator TPEN; and  $[\text{Zn}^{2+}]_i$  concentration was

measured again with FluoZin-3. While the addition of  $\text{ZnCl}_2$  increased the basal  $[\text{Zn}^{2+}]_i$  in all mutant platelets, the level did not reach that in *WT* platelets. This observation is compatible with a regular  $\text{Zn}^{2+}$  uptake, but defective storage in the mutant platelets. Markedly, TPEN treatment correspondingly reduced the  $[\text{Zn}^{2+}]_i$  level in *WT* and *Unc13d*<sup>-/-</sup> platelets, but not in *Nbeal2*<sup>-/-</sup> platelets suggesting that  $[\text{Zn}^{2+}]_i$  store in *Nbeal2*<sup>-/-</sup> platelets is very limited. In mammals, protein members of the ZIP protein family mediate  $\text{Zn}^{2+}$  influx, thereby increasing  $[\text{Zn}^{2+}]_i$  concentrations. On the other hand, ZnT isoforms regulate  $\text{Zn}^{2+}$  efflux from the cytosol to the extracellular space or into intracellular organelles lowering the  $[\text{Zn}^{2+}]_i$  concentration [245]. Whether the expression profiles of ZIP/ZnT isoforms are also altered in mutant or SPD platelets with secretion defects is unknown.

Several authors have indicated that platelet-released  $\text{Zn}^{2+}$  can modulate local hemostatic reactions, including contact activation and fibrin clotting [29, 124, 199]. We considered that defective granule biogenesis or granule secretion alters platelet  $\text{Zn}^{2+}$  release, thereby affecting fibrin clot formation. Recording of the fibrin formation on platelet thrombi during whole blood flow over collagen microspots provides an adequate way to evaluate hemostatic activity *ex vivo* [246]. Using microfluidics and a high wall-shear rate, we assessed the kinetics of fibrin clot formation from the accumulation of AF647-labeled fibrin on platelet thrombi. In blood samples from healthy controls,  $\text{Zn}^{2+}$  addition did not change the times to fibrin formation, thus indicating that  $\text{Zn}^{2+}$  was not a limiting factor in this process. With blood from four out of five SPD patients, platelet-dependent fibrin clot formation was prolonged but became normalized upon *in vitro* addition of  $\text{Zn}^{2+}$ .

Similar flow experiments were performed with blood from mice carrying platelet secretion defects. Dysregulation of platelet-dependent fibrin clot formation under flow was observed with blood from *Unc13d*<sup>-/-</sup> mice, which was normalized by  $\text{Zn}^{2+}$  supplementation. No significant alteration in fibrin clot formation was found with  $\text{Zn}^{2+}$  in whole blood from *Nbeal2*<sup>-/-</sup> mice. We speculate an alternative  $\text{Zn}^{2+}$  sequestering mechanism could compensate the lack of  $[\text{Zn}^{2+}]_i$  store in these platelets. We found that the total amount of  $\text{Zn}^{2+}$  strongly increased in *Nbeal2*<sup>-/-</sup> platelets. FluoZin-3 cannot detect this protein bound  $\text{Zn}^{2+}$  pool in the cytoplasm. Further investigation is necessary to study whether metallothionein expression is increased in *Nbeal2*<sup>-/-</sup> platelets, which may compensate the lack of granular  $\text{Zn}^{2+}$  store upon platelet-dependent fibrin formation.

Altogether, our data significantly extend the earlier observations from 1985 [199], that extracellular  $\text{Zn}^{2+}$ , as well as platelet  $\text{Zn}^{2+}$  release, have a procoagulant effect. Also, our data indicate that several platelet degranulation defects impair  $\text{Zn}^{2+}$  release, which especially in SPD patients and *Unc13d*<sup>-/-</sup> mice is a limiting factor for platelet-dependent fibrin formation. These results together suggest that determination of the platelet  $\text{Zn}^{2+}$  content, while staining

with FluoZin-3 could act as a novel prognostic biomarker for SPD and related bleeding disorders.

## 5. Concluding remarks and future plans

In the present thesis, two crucial  $Mg^{2+}$  entry routes were identified in platelets and characterized using *Trpm7<sup>R/R</sup>*, *Trpm7<sup>fl/fl-Pf4Cre</sup>*, and *Magt1<sup>-y</sup>* mice. Although we could show that TRPM7 kinase regulates platelet SOCE, Syk and PLC isoforms, thereby controlling platelet reactivity, it is essential to better understand how the TRPM7 kinase regulates other molecules. Since TRPM7 kinase is a serine/threonine kinase, the described tyrosine phosphorylation abnormalities in this thesis may help to show how this indirect crosstalk is regulated during platelet activation. Previously were described cytoskeletal abnormalities in MKs from *Trpm7<sup>fl/fl-Pf4Cre</sup>* mice and *TRPM7* variants [75]. In this thesis, we elucidated the functional responses of mutant platelets in both *in vitro* and *in vivo* conditions. It would be imperative to compare TRPM7 variants in human platelets with mutant TRPM7 mouse platelets. Nevertheless, comparing functional tests of platelets from *TRPM7<sup>R/R</sup>* and *Trpm7<sup>fl/fl-Pf4Cre</sup>* mice, inhibition of TRPM7 kinase activity could be a novel strategy to prevent thrombosis and stroke instead of TRPM7 channel blockage.

Global deletion of *Magt1* in mice does not influence postnatal development, but resulted in a pro-thrombotic phenotype, thus highlighting the crucial role of MAGT1 in platelet physiology. Our mouse model has limitations, since we could not fully recapitulate the situation found in XMEN patients, likely due to the fact that the mice could not be infected with EBV *in vivo*. Nevertheless, *Magt1<sup>-y</sup>* mice showed a significantly altered B cell development, which was partially described in some XMEN patients. In further studies, it would be essential to test *Magt1<sup>-y</sup>* mice in different *in vivo* models of sepsis or related disorders. Using different kinds of immunizations in *Magt1<sup>-y</sup>* mice, it will be relevant to correlate the effector functions of lymphocytes to human MAGT1 variants.

In this thesis, various classes of PKC isoforms were found to be differentially regulated in *Magt1<sup>-y</sup>* platelets and B cells. In *Magt1<sup>-y</sup>* mice, using disease models like immune thrombocytopenia, ischemic brain infarction, and atherosclerosis. It would be interesting to further deepen the understanding of  $Mg^{2+}$  homeostasis between the different hematopoietic cells. Using co-culture systems and conditional deletion strategies in *Magt1<sup>-y</sup>* mice, the specific role of this interesting transporter in different cell systems need to be characterized in the future. Further, it will be of interest to obtain *Magt1/Trpm7* double-deficient mice, where a severe [ $Mg^{2+}$ ] deficiency is expected, if these mice would develop normally.

Besides MAGT1 and TRPM7, also TUSC3, another  $Mg^{2+}$  transporter, was found to be expressed in murine platelets. Hence, it would also be interesting to study the (patho)physiological significance of this transporter as well as its interplay with MAGT1 and TRPM7 in platelet function.

In the final part of this thesis, we made progress in identifying the location and function of the  $[Zn^{2+}]_i$  stores in platelets. This study may help to better understand the mechanism of zinc storage in platelets, particularly concerning aberrant biogenesis and release of granules. Due to the limitations of the existing technical tools, we could however not precisely define the localization of platelet  $[Zn^{2+}]_i$ . This work should hence be taken further. Moreover, studying the expression of ZIP and ZnT isoforms in platelets with various granule abnormalities or SPD would be an important step to improve the understanding of the role of  $Zn^{2+}$  in granule biogenesis and hemostasis. These studies open the possibility to develop mouse models, which will further underline the importance of zinc homeostasis to thrombosis and stroke at the molecular level.

## 6. References

1. Italiano, J.E., Jr., S. Patel-Hett, and J.H. Hartwig, Mechanics of proplatelet elaboration. *J Thromb Haemost*, 2007. **5 Suppl 1**: p. 18-23.
2. Varga-Szabo, D., I. Pleines, and B. Nieswandt, Cell adhesion mechanisms in platelets. *Arterioscler Thromb Vasc Biol*, 2008. **28**(3): p. 403-12.
3. Jackson, S.P., Arterial thrombosis--insidious, unpredictable and deadly. *Nat Med*, 2011. **17**(11): p. 1423-36.
4. Murray, C.J. and A.D. Lopez, Mortality by cause for eight regions of the world: Global Burden of Disease Study. *Lancet*, 1997. **349**(9061): p. 1269-76.
5. Chesney, C.M., D. Pifer, and R.W. Colman, Subcellular localization and secretion of factor V from human platelets. *Proc Natl Acad Sci U S A*, 1981. **78**(8): p. 5180-4.
6. Marx, G., et al., Packaging zinc, fibrinogen, and factor XIII in platelet alpha-granules. *J Cell Physiol*, 1993. **156**(3): p. 437-42.
7. Wolf, K., et al., Partially Defective Store Operated Calcium Entry and Hem(ITAM) Signaling in Platelets of Serotonin Transporter Deficient Mice. *PLoS One*, 2016. **11**(1): p. e0147664.
8. Chen, W., et al., Orai1-induced store-operated Ca(2+) entry enhances phospholipase activity and modulates canonical transient receptor potential channel 6 function in murine platelets. *J Thromb Haemost*, 2014. **12**(4): p. 528-39.
9. Varga-Szabo, D., A. Braun, and B. Nieswandt, Calcium signaling in platelets. *J Thromb Haemost*, 2009. **7**(7): p. 1057-66.
10. Watson, B.R., et al., Zinc is a transmembrane agonist that induces platelet activation in a tyrosine phosphorylation-dependent manner. *Metallomics*, 2016. **8**(1): p. 91-100.
11. Polasek, J., Lysosomal concept of platelet secretion--revisited. *Eur J Haematol Suppl*, 1989. **50**: p. 3-24.
12. Braun, A., et al., STIM1 is essential for Fcγ receptor activation and autoimmune inflammation. *Blood*, 2009. **113**(5): p. 1097-104.
13. Braun, A., et al., Orai1 (CRACM1) is the platelet SOC channel and essential for pathological thrombus formation. *Blood*, 2009. **113**(9): p. 2056-63.
14. Muir, K.W., Magnesium in stroke treatment. *Postgrad Med J*, 2002. **78**(925): p. 641-5.
15. Sensi, S.L. and J.M. Jeng, Rethinking the excitotoxic ionic milieu: the emerging role of Zn(2+) in ischemic neuronal injury. *Curr Mol Med*, 2004. **4**(2): p. 87-111.
16. Rabbani, L.E. and E.M. Antman, The role of magnesium therapy in acute myocardial infarction. *Clin Cardiol*, 1996. **19**(11): p. 841-4.
17. Low, W.I. and H. Ikram, Plasma zinc in acute myocardial infarction. Diagnostic and prognostic implications. *Br Heart J*, 1976. **38**(12): p. 1339-42.
18. Li, F.Y., et al., Second messenger role for Mg<sup>2+</sup> revealed by human T-cell immunodeficiency. *Nature*, 2011. **475**(7357): p. 471-6.
19. Haase, H. and L. Rink, Zinc signals and immune function. *Biofactors*, 2014. **40**(1): p. 27-40.
20. Ren, Q., et al., Munc13-4 is a limiting factor in the pathway required for platelet granule release and hemostasis. *Blood*, 2010. **116**(6): p. 869-77.
21. Deppermann, C., et al., Gray platelet syndrome and defective thrombo-inflammation in Nbeal2-deficient mice. *J Clin Invest*, 2013.

22. Nesbitt, W.S., et al., A shear gradient-dependent platelet aggregation mechanism drives thrombus formation. *Nat Med*, 2009. **15**(6): p. 665-73.
23. Savage, B., E. Saldivar, and Z.M. Ruggeri, Initiation of platelet adhesion by arrest onto fibrinogen or translocation on von Willebrand factor. *Cell*, 1996. **84**(2): p. 289-97.
24. Nieswandt, B. and S.P. Watson, Platelet-collagen interaction: is GPVI the central receptor? *Blood*, 2003. **102**(2): p. 449-61.
25. Furie, B. and B.C. Furie, Thrombus formation in vivo. *J Clin Invest*, 2005. **115**(12): p. 3355-62.
26. Nesbitt, W.S., et al., Intercellular calcium communication regulates platelet aggregation and thrombus growth. *J Cell Biol*, 2003. **160**(7): p. 1151-61.
27. Tozer, E.C., P.E. Hughes, and J.C. Loftus, Ligand binding and affinity modulation of integrins. *Biochem Cell Biol*, 1996. **74**(6): p. 785-98.
28. Whiss, P.A. and R.G. Andersson, Divalent cations and the protein surface co-ordinate the intensity of human platelet adhesion and P-selectin surface expression. *Blood Coagul Fibrinolysis*, 2002. **13**(5): p. 407-16.
29. Henderson, S.J., et al., Zinc delays clot lysis by attenuating plasminogen activation and plasmin-mediated fibrin degradation. *Thromb Haemost*, 2015. **113**(6): p. 1278-88.
30. Cruz, M.A., et al., Interaction of the von Willebrand factor (vWF) with collagen. Localization of the primary collagen-binding site by analysis of recombinant vWF A domain polypeptides. *J Biol Chem*, 1995. **270**(33): p. 19668.
31. Dong, J.F., et al., Magnesium maintains endothelial integrity, up-regulates proteolysis of ultra-large von Willebrand factor, and reduces platelet aggregation under flow conditions. *Thromb Haemost*, 2008. **99**(3): p. 586-93.
32. Asselin, J., et al., Monomeric (glycine-proline-hydroxyproline)<sub>10</sub> repeat sequence is a partial agonist of the platelet collagen receptor glycoprotein VI. *Biochem J*, 1999. **339** (Pt 2): p. 413-8.
33. Kanaji, S., et al., Convulxin binds to native, human glycoprotein Ib alpha. *J Biol Chem*, 2003. **278**(41): p. 39452-60.
34. Clemetson, J.M., et al., The platelet collagen receptor glycoprotein VI is a member of the immunoglobulin superfamily closely related to FcalphaR and the natural killer receptors. *J Biol Chem*, 1999. **274**(41): p. 29019-24.
35. Suzuki-Inoue, K., et al., Association of Fyn and Lyn with the proline-rich domain of glycoprotein VI regulates intracellular signaling. *J Biol Chem*, 2002. **277**(24): p. 21561-6.
36. Gibbins, J., et al., Tyrosine phosphorylation of the Fc receptor gamma-chain in collagen-stimulated platelets. *J Biol Chem*, 1996. **271**(30): p. 18095-9.
37. Watson, S.P., et al., GPVI and integrin alphaIIb beta3 signaling in platelets. *J Thromb Haemost*, 2005. **3**(8): p. 1752-62.
38. Smith-Garvin, J.E., G.A. Koretzky, and M.S. Jordan, T cell activation. *Annu Rev Immunol*, 2009. **27**: p. 591-619.
39. Suzuki-Inoue, K., et al., Murine GPVI stimulates weak integrin activation in PLCgamma2<sup>-/-</sup> platelets: involvement of PLCgamma1 and PI3-kinase. *Blood*, 2003. **102**(4): p. 1367-73.
40. Elvers, M., et al., Platelet hyperreactivity and a prothrombotic phenotype in mice with a gain-of-function mutation in phospholipase Cgamma2. *J Thromb Haemost*, 2010. **8**(6): p. 1353-63.



41. Rink, T.J. and S.O. Sage, Calcium signaling in human platelets. *Annu Rev Physiol*, 1990. **52**: p. 431-49.
42. Ramanathan, G., et al., Defective diacylglycerol-induced Ca<sup>2+</sup> entry but normal agonist-induced activation responses in TRPC6-deficient mouse platelets. *J Thromb Haemost*, 2012. **10**(3): p. 419-29.
43. Feske, S., et al., A mutation in Orai1 causes immune deficiency by abrogating CRAC channel function. *Nature*, 2006. **441**(7090): p. 179-85.
44. Varga-Szabo, D., et al., The calcium sensor STIM1 is an essential mediator of arterial thrombosis and ischemic brain infarction. *J Exp Med*, 2008. **205**(7): p. 1583-91.
45. Grosse, J., et al., An EF hand mutation in Stim1 causes premature platelet activation and bleeding in mice. *J Clin Invest*, 2007. **117**(11): p. 3540-50.
46. Braun, A., et al., STIM and Orai in hemostasis and thrombosis. *Front Biosci (Landmark Ed)*, 2011. **16**: p. 2144-60.
47. Hofmann, T., et al., Direct activation of human TRPC6 and TRPC3 channels by diacylglycerol. *Nature*, 1999. **397**(6716): p. 259-63.
48. Ramanathan, G. and C. Mannhalter, Increased expression of transient receptor potential canonical 6 (TRPC6) in differentiating human megakaryocytes. *Cell Biol Int*, 2016. **40**(2): p. 223-31.
49. Paez Espinosa, E.V., et al., Mouse transient receptor potential channel 6: role in hemostasis and thrombogenesis. *Biochem Biophys Res Commun*, 2012. **417**(2): p. 853-6.
50. Vemana, H.P., et al., A critical role for the transient receptor potential channel type 6 in human platelet activation. *PLoS One*, 2015. **10**(4): p. e0125764.
51. North, R.A., Molecular physiology of P2X receptors. *Physiol Rev*, 2002. **82**(4): p. 1013-67.
52. Rolf, M.G., C.A. Brearley, and M.P. Mahaut-Smith, Platelet shape change evoked by selective activation of P2X1 purinoceptors with alpha,beta-methylene ATP. *Thromb Haemost*, 2001. **85**(2): p. 303-8.
53. Jones, S., R.J. Evans, and M.P. Mahaut-Smith, Ca<sup>2+</sup> influx through P2X1 receptors amplifies P2Y1 receptor-evoked Ca<sup>2+</sup> signaling and ADP-evoked platelet aggregation. *Mol Pharmacol*, 2014. **86**(3): p. 243-51.
54. Tolhurst, G., et al., Interplay between P2Y(1), P2Y(12), and P2X(1) receptors in the activation of megakaryocyte cation influx currents by ADP: evidence that the primary megakaryocyte represents a fully functional model of platelet P2 receptor signaling. *Blood*, 2005. **106**(5): p. 1644-51.
55. Strehler, E.E. and D.A. Zacharias, Role of alternative splicing in generating isoform diversity among plasma membrane calcium pumps. *Physiol Rev*, 2001. **81**(1): p. 21-50.
56. Enouf, J., et al., Human platelets express the SERCA2-b isoform of Ca(2+)-transport ATPase. *Biochem J*, 1992. **286** ( Pt 1): p. 135-40.
57. Brune, B. and V. Ullrich, Different calcium pools in human platelets and their role in thromboxane A2 formation. *J Biol Chem*, 1991. **266**(29): p. 19232-7.
58. Cavallini, L., M. Coassin, and A. Alexandre, Two classes of agonist-sensitive Ca<sup>2+</sup> stores in platelets, as identified by their differential sensitivity to 2,5-di-(tert-butyl)-1,4-benzohydroquinone and thapsigargin. *Biochem J*, 1995. **310** ( Pt 2): p. 449-52.

59. Papp, B., et al., Demonstration of two forms of calcium pumps by thapsigargin inhibition and radioimmunoblotting in platelet membrane vesicles. *J Biol Chem*, 1991. **266**(22): p. 14593-6.
60. Elaib, Z., et al., Full activation of mouse platelets requires ADP secretion regulated by SERCA3 ATPase-dependent calcium stores. *Blood*, 2016. **128**(8): p. 1129-38.
61. Lian, L., et al., The relative role of PLCbeta and PI3Kgamma in platelet activation. *Blood*, 2005. **106**(1): p. 110-7.
62. Williams, R.L., Mammalian phosphoinositide-specific phospholipase C. *Biochim Biophys Acta*, 1999. **1441**(2-3): p. 255-67.
63. Suzuki-Inoue, K., et al., A novel Syk-dependent mechanism of platelet activation by the C-type lectin receptor CLEC-2. *Blood*, 2006. **107**(2): p. 542-9.
64. Crittenden, J.R., et al., CalDAG-GEFI integrates signaling for platelet aggregation and thrombus formation. *Nat Med*, 2004. **10**(9): p. 982-6.
65. Bergmeier, W. and L. Stefanini, Novel molecules in calcium signaling in platelets. *J Thromb Haemost*, 2009. **7 Suppl 1**: p. 187-90.
66. Murugappan, S., et al., Differential role of protein kinase C delta isoform in agonist-induced dense granule secretion in human platelets. *J Biol Chem*, 2004. **279**(4): p. 2360-7.
67. Konopatskaya, O., et al., PKCalpha regulates platelet granule secretion and thrombus formation in mice. *J Clin Invest*, 2009. **119**(2): p. 399-407.
68. Nagy, B., Jr., et al., Impaired activation of platelets lacking protein kinase C-theta isoform. *Blood*, 2009. **113**(11): p. 2557-67.
69. Chari, R., et al., Protein kinase C[delta] differentially regulates platelet functional responses. *Arterioscler Thromb Vasc Biol*, 2009. **29**(5): p. 699-705.
70. Pears, C.J., et al., Differential roles of the PKC novel isoforms, PKCdelta and PKCepsilon, in mouse and human platelets. *PLoS One*, 2008. **3**(11): p. e3793.
71. Crosby, D. and A.W. Poole, Physical and functional interaction between protein kinase C delta and Fyn tyrosine kinase in human platelets. *J Biol Chem*, 2003. **278**(27): p. 24533-41.
72. Borkowski, B.J., et al., Cation dyshomeostasis and cardiomyocyte necrosis: the Fleckenstein hypothesis revisited. *Eur Heart J*, 2011. **32**(15): p. 1846-53.
73. Hwang, D.L., C.F. Yen, and J.L. Nadler, Effect of extracellular magnesium on platelet activation and intracellular calcium mobilization. *Am J Hypertens*, 1992. **5**(10): p. 700-6.
74. Kubota, T., et al., Mitochondria are intracellular magnesium stores: investigation by simultaneous fluorescent imagings in PC12 cells. *Biochim Biophys Acta*, 2005. **1744**(1): p. 19-28.
75. Stritt, S., et al., Defects in TRPM7 channel function deregulate thrombopoiesis through altered cellular Mg(2+) homeostasis and cytoskeletal architecture. *Nat Commun*, 2016. **7**: p. 11097.
76. Paravicini, T.M., V. Chubanov, and T. Gudermann, TRPM7: a unique channel involved in magnesium homeostasis. *Int J Biochem Cell Biol*, 2012. **44**(8): p. 1381-4.
77. Penner, R. and A. Fleig, The Mg<sup>2+</sup> and Mg(2+)-nucleotide-regulated channel-kinase TRPM7. *Handb Exp Pharmacol*, 2007(179): p. 313-28.

78. Clark, K., et al., Massive autophosphorylation of the Ser/Thr-rich domain controls protein kinase activity of TRPM6 and TRPM7. *PLoS One*, 2008. **3**(3): p. e1876.
79. Dorovkov, M.V. and A.G. Ryazanov, Phosphorylation of annexin I by TRPM7 channel-kinase. *J Biol Chem*, 2004. **279**(49): p. 50643-6.
80. Jin, J., et al., Deletion of *Trpm7* disrupts embryonic development and thymopoiesis without altering Mg<sup>2+</sup> homeostasis. *Science*, 2008. **322**(5902): p. 756-60.
81. Nadler, M.J., et al., LTRPC7 is a Mg.ATP-regulated divalent cation channel required for cell viability. *Nature*, 2001. **411**(6837): p. 590-5.
82. Ryazanova, L.V., et al., TRPM7 is essential for Mg(2+) homeostasis in mammals. *Nat Commun*, 2010. **1**: p. 109.
83. Park, H.S., et al., The Pathophysiologic Roles of TRPM7 Channel. *Korean J Physiol Pharmacol*, 2014. **18**(1): p. 15-23.
84. Goytain, A. and G.A. Quamme, Identification and characterization of a novel mammalian Mg<sup>2+</sup> transporter with channel-like properties. *BMC Genomics*, 2005. **6**: p. 48.
85. Zhou, H. and D.E. Clapham, Mammalian MagT1 and TUSC3 are required for cellular magnesium uptake and vertebrate embryonic development. *Proc Natl Acad Sci U S A*, 2009. **106**(37): p. 15750-5.
86. Deason-Towne, F., A.L. Perraud, and C. Schmitz, The Mg<sup>2+</sup> transporter MagT1 partially rescues cell growth and Mg<sup>2+</sup> uptake in cells lacking the channel-kinase TRPM7. *FEBS Lett*, 2011. **585**(14): p. 2275-8.
87. Hartwig, A., Role of magnesium in genomic stability. *Mutation research*, 2001. **475**(1-2): p. 113-21.
88. Wu, N. and A. Veillette, Immunology: Magnesium in a signalling role. *Nature*, 2011. **475**(7357): p. 462-3.
89. Chaigne-Delalande, B., et al., Mg<sup>2+</sup> regulates cytotoxic functions of NK and CD8 T cells in chronic EBV infection through NKG2D. *Science*, 2013. **341**(6142): p. 186-91.
90. Sprenger, K.B. and H.E. Franz, Viscosity adaption for an automated micromethod of flame atomic absorption spectrometry, and intracellular trace-element analysis after pressure decomposition: zinc determination in plasma and erythrocytes. *Clin Chem*, 1983. **29**(8): p. 1522-6.
91. Tubek, S., Selected zinc metabolism parameters in premenopausal and postmenopausal women with moderate and severe primary arterial hypertension. *Biol Trace Elem Res*, 2007. **116**(3): p. 249-56.
92. Meyers, K.M., H. Holmsen, and C.L. Seachord, Comparative study of platelet dense granule constituents. *Am J Physiol*, 1982. **243**(3): p. R454-61.
93. Lu, J., et al., Albumin as a zinc carrier: properties of its high-affinity zinc-binding site. *Biochem Soc Trans*, 2008. **36**(Pt 6): p. 1317-21.
94. Tubek, S., P. Grzanka, and I. Tubek, Role of zinc in hemostasis: a review. *Biol Trace Elem Res*, 2008. **121**(1): p. 1-8.
95. Kambe, T., et al., The Physiological, Biochemical, and Molecular Roles of Zinc Transporters in Zinc Homeostasis and Metabolism. *Physiological Reviews*, 2015. **95**(3): p. 749-784.
96. Eide, D.J., The SLC39 family of metal ion transporters. *Pflugers Arch*, 2004. **447**(5): p. 796-800.

97. Fukada, T., et al., Zinc homeostasis and signaling in health and diseases: Zinc signaling. *J Biol Inorg Chem*, 2011. **16**(7): p. 1123-34.
98. Nieswandt, B., et al., Long-term antithrombotic protection by in vivo depletion of platelet glycoprotein VI in mice. *J Exp Med*, 2001. **193**(4): p. 459-69.
99. Hechler, B., et al., A role of the fast ATP-gated P2X1 cation channel in thrombosis of small arteries in vivo. *J Exp Med*, 2003. **198**(4): p. 661-7.
100. Kleinschnitz, C., et al., Targeting coagulation factor XII provides protection from pathological thrombosis in cerebral ischemia without interfering with hemostasis. *J Exp Med*, 2006. **203**(3): p. 513-8.
101. Ungerer, M., et al., Novel antiplatelet drug revacept (Dimeric Glycoprotein VI-Fc) specifically and efficiently inhibited collagen-induced platelet aggregation without affecting general hemostasis in humans. *Circulation*, 2011. **123**(17): p. 1891-9.
102. Lasne, D., B. Jude, and S. Susen, From normal to pathological hemostasis. *Can J Anaesth*, 2006. **53**(6 Suppl): p. S2-11.
103. Hoffman, M., D.M. Monroe, 3rd, and H.R. Roberts, Activated factor VII activates factors IX and X on the surface of activated platelets: thoughts on the mechanism of action of high-dose activated factor VII. *Blood Coagul Fibrinolysis*, 1998. **9 Suppl 1**: p. S61-5.
104. Macfarlane, R.G., An Enzyme Cascade in the Blood Clotting Mechanism, and Its Function as a Biochemical Amplifier. *Nature*, 1964. **202**: p. 498-9.
105. Hall, A.C.G.a.J.E., Guyton and Hall Textbook of Medical Physiology, in *Guyton and Hall Textbook of Medical Physiology*, R. Grulow, Editor. 2006, Saunders, an imprint of Elsevier Inc.: United States of America. p. 457-9.
106. Bender, M., I. Hagedorn, and B. Nieswandt, Genetic and antibody-induced glycoprotein VI deficiency equally protects mice from mechanically and FeCl(3) -induced thrombosis. *J Thromb Haemost*, 2011. **9**(7): p. 1423-6.
107. Suzuki-Inoue, K., et al., Essential in vivo roles of the C-type lectin receptor CLEC-2: embryonic/neonatal lethality of CLEC-2-deficient mice by blood/lymphatic misconnections and impaired thrombus formation of CLEC-2-deficient platelets. *J Biol Chem*, 2010. **285**(32): p. 24494-507.
108. Offermanns, S., Activation of platelet function through G protein-coupled receptors. *Circ Res*, 2006. **99**(12): p. 1293-304.
109. Dubois, C., et al., Thrombin-initiated platelet activation in vivo is vWF independent during thrombus formation in a laser injury model. *J Clin Invest*, 2007. **117**(4): p. 953-60.
110. Gruner, S., et al., Relative antithrombotic effect of soluble GPVI dimer compared with anti-GPVI antibodies in mice. *Blood*, 2005. **105**(4): p. 1492-9.
111. Oury, C., et al., Overexpression of the platelet P2X1 ion channel in transgenic mice generates a novel prothrombotic phenotype. *Blood*, 2003. **101**(10): p. 3969-76.
112. Maier, J.A., Endothelial cells and magnesium: implications in atherosclerosis. *Clin Sci (Lond)*, 2012. **122**(9): p. 397-407.
113. Sheehan, J., Importance of magnesium chloride repletion after myocardial infarction. *Am J Cardiol*, 1989. **63**(14): p. 35G-38G.
114. Shechter, M., et al., Oral magnesium supplementation inhibits platelet-dependent thrombosis in patients with coronary artery disease. *Am J Cardiol*, 1999. **84**(2): p. 152-6.

115. Toft, G., H.B. Ravn, and V.E. Hjortdal, Intravenously and topically applied magnesium in the prevention of arterial thrombosis. *Thromb Res*, 2000. **99**(1): p. 61-9.
116. Avdonin, P., U.S. Ryan, and B. Hayes, Receptor-dependent regulation of  $[Ca^{2+}]_i$  and phospholipase C in vascular endothelial cells. *J Recept Signal Transduct Res*, 2000. **20**(4): p. 235-54.
117. Rukshin, V., et al., Intravenous magnesium in experimental stent thrombosis in swine. *Arterioscler Thromb Vasc Biol*, 2001. **21**(9): p. 1544-9.
118. Ravn, H.B., et al., Early administration of intravenous magnesium inhibits arterial thrombus formation. *Arterioscler Thromb Vasc Biol*, 1997. **17**(12): p. 3620-5.
119. Gordon, P.R., et al., Effect of acute zinc deprivation on plasma zinc and platelet aggregation in adult males. *Am J Clin Nutr*, 1982. **35**(1): p. 113-9.
120. Importance of zinc for hormone binding and signal transduction: limiting mechanisms in zinc deficiency? *Nutr Rev*, 1991. **49**(12): p. 369-70.
121. Bernardo, M.M., et al., Surface-independent acceleration of factor XII activation by zinc ions. I. Kinetic characterization of the metal ion rate enhancement. *J Biol Chem*, 1993. **268**(17): p. 12468-76.
122. Rojkaer, R. and I. Schousboe, Partial identification of the  $Zn^{2+}$ -binding sites in factor XII and its activation derivatives. *Eur J Biochem*, 1997. **247**(2): p. 491-6.
123. Baglia, F.A., et al., Factor XI binding to the platelet glycoprotein Ib-IX-V complex promotes factor XI activation by thrombin. *J Biol Chem*, 2002. **277**(3): p. 1662-8.
124. Vu, T.T., J.C. Fredenburgh, and J.I. Weitz, Zinc: an important cofactor in haemostasis and thrombosis. *Thromb Haemost*, 2013. **109**(3): p. 421-30.
125. Henderson, S.J., et al., Zinc promotes clot stability by accelerating clot formation and modifying fibrin structure. *Thromb Haemost*, 2016. **115**(3): p. 533-42.
126. Priebatsch, K.M., et al., Functional Regulation of the Plasma Protein Histidine-Rich Glycoprotein by  $Zn^{2+}$  in Settings of Tissue Injury. *Biomolecules*, 2017. **7**(1).
127. Heyns Adu, P., et al., Zinc-induced platelet aggregation is mediated by the fibrinogen receptor and is not accompanied by release or by thromboxane synthesis. *Blood*, 1985. **66**(1): p. 213-9.
128. Durukan, A., D. Strbian, and T. Tatlisumak, Rodent models of ischemic stroke: a useful tool for stroke drug development. *Curr Pharm Des*, 2008. **14**(4): p. 359-70.
129. Braeuninger, S., et al., Focal cerebral ischemia. *Methods Mol Biol*, 2012. **788**: p. 29-42.
130. Sussman, B.J. and T.S. Fitch, Thrombolysis with fibrinolytic in cerebral arterial occlusion. *J Am Med Assoc*, 1958. **167**(14): p. 1705-9.
131. Fletcher, A.P., et al., A pilot study of urokinase therapy in cerebral infarction. *Stroke*, 1976. **7**(2): p. 135-42.
132. Choudhri, T.F., et al., Reduced microvascular thrombosis and improved outcome in acute murine stroke by inhibiting GP IIb/IIIa receptor-mediated platelet aggregation. *J Clin Invest*, 1998. **102**(7): p. 1301-10.
133. Kleinschnitz, C., et al., Targeting platelets in acute experimental stroke: impact of glycoprotein Ib, VI, and IIb/IIIa blockade on infarct size, functional outcome, and intracranial bleeding. *Circulation*, 2007. **115**(17): p. 2323-30.
134. Berndt, M.C., et al., The vascular biology of the glycoprotein Ib-IX-V complex. *Thromb Haemost*, 2001. **86**(1): p. 178-88.

135. Kleinschnitz, C., et al., Early detrimental T-cell effects in experimental cerebral ischemia are neither related to adaptive immunity nor thrombus formation. *Blood*, 2010. **115**(18): p. 3835-42.
136. Schuhmann, M.K., et al., B cells do not have a major pathophysiologic role in acute ischemic stroke in mice. *J Neuroinflammation*, 2017. **14**(1): p. 112.
137. Barone, F.C., et al., Tumor necrosis factor- $\alpha$ . A mediator of focal ischemic brain injury. *Stroke*, 1997. **28**(6): p. 1233-44.
138. Yilmaz, G., et al., Role of T lymphocytes and interferon- $\gamma$  in ischemic stroke. *Circulation*, 2006. **113**(17): p. 2105-12.
139. Gelderblom, M., et al., Neutralization of the IL-17 axis diminishes neutrophil invasion and protects from ischemic stroke. *Blood*, 2012. **120**(18): p. 3793-802.
140. Pun, P.B., J. Lu, and S. Mochhala, Involvement of ROS in BBB dysfunction. *Free Radic Res*, 2009. **43**(4): p. 348-64.
141. Nakajima, K. and S. Kohsaka, Microglia: activation and their significance in the central nervous system. *J Biochem*, 2001. **130**(2): p. 169-75.
142. del Zoppo, G.J., et al., Microglial activation and matrix protease generation during focal cerebral ischemia. *Stroke*, 2007. **38**(2 Suppl): p. 646-51.
143. Amantea, D., et al., Post-ischemic brain damage: pathophysiology and role of inflammatory mediators. *FEBS J*, 2009. **276**(1): p. 13-26.
144. Jin, R.C., et al., Glutathione peroxidase-3 deficiency promotes platelet-dependent thrombosis in vivo. *Circulation*, 2011. **123**(18): p. 1963-73.
145. Siesjo, B.K., Pathophysiology and treatment of focal cerebral ischemia. Part II: Mechanisms of damage and treatment. *J Neurosurg*, 1992. **77**(3): p. 337-54.
146. Clark, W.M., et al., Monofilament intraluminal middle cerebral artery occlusion in the mouse. *Neurol Res*, 1997. **19**(6): p. 641-8.
147. Giorgi, C., et al., Mitochondrial Ca(2+) and apoptosis. *Cell Calcium*, 2012. **52**(1): p. 36-43.
148. Rappaport, Z.H., W. Young, and E.S. Flamm, Regional brain calcium changes in the rat middle cerebral artery occlusion model of ischemia. *Stroke*, 1987. **18**(4): p. 760-4.
149. Gelmers, H.J., et al., A controlled trial of nimodipine in acute ischemic stroke. *N Engl J Med*, 1988. **318**(4): p. 203-7.
150. Berna-Erro, A., et al., STIM2 regulates capacitive Ca<sup>2+</sup> entry in neurons and plays a key role in hypoxic neuronal cell death. *Sci Signal*, 2009. **2**(93): p. ra67.
151. Altura, B.M., et al., Mg<sup>2+</sup>-Ca<sup>2+</sup> interaction in contractility of vascular smooth muscle: Mg<sup>2+</sup> versus organic calcium channel blockers on myogenic tone and agonist-induced responsiveness of blood vessels. *Can J Physiol Pharmacol*, 1987. **65**(4): p. 729-45.
152. Sirin, B.H., et al., Neuroprotective effects of preischemia subcutaneous magnesium sulfate in transient cerebral ischemia. *Eur J Cardiothorac Surg*, 1998. **14**(1): p. 82-8.
153. Yang, Y., et al., Survival and histological evaluation of therapeutic window of post-ischemia treatment with magnesium sulfate in embolic stroke model of rat. *Neurosci Lett*, 2000. **285**(2): p. 119-22.
154. Campbell, K., B.P. Meloni, and N.W. Knuckey, Combined magnesium and mild hypothermia (35 degrees C) treatment reduces infarct volumes after permanent middle cerebral artery occlusion in the rat at 2 and 4, but not 6 h. *Brain Res*, 2008. **1230**: p. 258-64.

155. Sun, X., Y. Mei, and E. Tong, Effect of magnesium on nitric oxide synthase of neurons in cortex during early period of cerebral ischemia. *J Tongji Med Univ*, 2000. **20**(1): p. 13-5, 42.
156. Saver, J.L., et al., Prehospital neuroprotective therapy for acute stroke: results of the Field Administration of Stroke Therapy-Magnesium (FAST-MAG) pilot trial. *Stroke*, 2004. **35**(5): p. e106-8.
157. Saver, J.L., et al., Prehospital use of magnesium sulfate as neuroprotection in acute stroke. *N Engl J Med*, 2015. **372**(6): p. 528-36.
158. Aarts, M., et al., A key role for TRPM7 channels in anoxic neuronal death. *Cell*, 2003. **115**(7): p. 863-77.
159. Aarts, M.M. and M. Tymianski, TRPM7 and ischemic CNS injury. *Neuroscientist*, 2005. **11**(2): p. 116-23.
160. Jiang, H., et al., TrkA pathway(s) is involved in regulation of TRPM7 expression in hippocampal neurons subjected to ischemic-reperfusion and oxygen-glucose deprivation. *Brain Res Bull*, 2008. **76**(1-2): p. 124-30.
161. Aarts, M.M. and M. Tymianski, TRPMs and neuronal cell death. *Pflugers Arch*, 2005. **451**(1): p. 243-9.
162. Chen, W., et al., TRPM7 inhibitor carvacrol protects brain from neonatal hypoxic-ischemic injury. *Mol Brain*, 2015. **8**: p. 11.
163. Takeda, A., Significance of Zn(2+) signaling in cognition: insight from synaptic Zn(2+) dyshomeostasis. *J Trace Elem Med Biol*, 2014. **28**(4): p. 393-6.
164. Torres-Vega, A., et al., Limbic system pathologies associated with deficiencies and excesses of the trace elements iron, zinc, copper, and selenium. *Nutr Rev*, 2012. **70**(12): p. 679-92.
165. Zhao, Y., et al., Chelating intracellularly accumulated zinc decreased ischemic brain injury through reducing neuronal apoptotic death. *Stroke*, 2014. **45**(4): p. 1139-47.
166. Lee, J.Y., et al., Accumulation of zinc in degenerating hippocampal neurons of ZnT3-null mice after seizures: evidence against synaptic vesicle origin. *J Neurosci*, 2000. **20**(11): p. RC79.
167. Koh, J.Y., et al., The role of zinc in selective neuronal death after transient global cerebral ischemia. *Science*, 1996. **272**(5264): p. 1013-6.
168. Pan, R. and K.J. Liu, ZNT-1 Expression Reduction Enhances Free Zinc Accumulation in Astrocytes After Ischemic Stroke. *Acta Neurochir Suppl*, 2016. **121**: p. 257-61.
169. Diefenbach, A., et al., Rae1 and H60 ligands of the NKG2D receptor stimulate tumour immunity. *Nature*, 2001. **413**(6852): p. 165-71.
170. Nieswandt, B., et al., Identification of critical antigen-specific mechanisms in the development of immune thrombocytopenic purpura in mice. *Blood*, 2000. **96**(7): p. 2520-7.
171. May, F., et al., CLEC-2 is an essential platelet-activating receptor in hemostasis and thrombosis. *Blood*, 2009. **114**(16): p. 3464-72.
172. Stritt, S., et al., Rap1-GTP-interacting adaptor molecule (RIAM) is dispensable for platelet integrin activation and function in mice. *Blood*, 2015. **125**(2): p. 219-22.
173. Bergmeier, W., et al., Flow cytometric detection of activated mouse integrin alphaIIb beta3 with a novel monoclonal antibody. *Cytometry*, 2002. **48**(2): p. 80-6.

174. Nieswandt, B., et al., Acute systemic reaction and lung alterations induced by an antiplatelet integrin gpIIb/IIIa antibody in mice. *Blood*, 1999. **94**(2): p. 684-93.
175. Unkeless, J.C., Characterization of a monoclonal antibody directed against mouse macrophage and lymphocyte Fc receptors. *J Exp Med*, 1979. **150**(3): p. 580-96.
176. Knight, C.G., et al., Collagen-platelet interaction: Gly-Pro-Hyp is uniquely specific for platelet Gp VI and mediates platelet activation by collagen. *Cardiovasc Res*, 1999. **41**(2): p. 450-7.
177. Matsushita, M., et al., Channel function is dissociated from the intrinsic kinase activity and autophosphorylation of TRPM7/ChaK1. *Journal of Biological Chemistry*, 2005. **280**(21): p. 20793-20803.
178. Stegner, D., et al., Munc13-4-mediated secretion is essential for infarct progression but not intracranial hemostasis in acute stroke. *J Thromb Haemost*, 2013. **11**(7): p. 1430-3.
179. Quah, B.J., H.S. Warren, and C.R. Parish, Monitoring lymphocyte proliferation in vitro and in vivo with the intracellular fluorescent dye carboxyfluorescein diacetate succinimidyl ester. *Nature protocols*, 2007. **2**(9): p. 2049-56.
180. Ho, E.L., et al., Costimulation of multiple NK cell activation receptors by NKG2D. *Journal of immunology*, 2002. **169**(7): p. 3667-75.
181. Braun, A., et al., STIM and Orai in hemostasis and thrombosis. *Frontiers in bioscience*, 2011. **16**: p. 2144-60.
182. Varga-Szabo, D., A. Braun, and B. Nieswandt, Calcium signaling in platelets. *J Thromb Haemost*, 2009. **7**(7): p. 1057-66.
183. Watson, S.P., et al., GPVI and integrin alphaIIb beta3 signaling in platelets. *J Thromb Haemost*, 2005. **3**(8): p. 1752-62.
184. Abiria, S.A., et al., TRPM7 senses oxidative stress to release Zn<sup>2+</sup> from unique intracellular vesicles. *Proc Natl Acad Sci U S A*, 2017. **114**(30): p. E6079-E6088.
185. Strehl, A., et al., Dual role of platelet protein kinase C in thrombus formation: stimulation of pro-aggregatory and suppression of procoagulant activity in platelets. *J Biol Chem*, 2007. **282**(10): p. 7046-55.
186. Xu, H.L., et al., Suppression of cortical TRPM7 protein attenuates oxidative damage after traumatic brain injury via Akt/endothelial nitric oxide synthase pathway. *Neurochem Int*, 2017.
187. Ravn, H.B., et al., Magnesium inhibits human platelets. *Blood Coagul Fibrinolysis*, 1996. **7**(2): p. 241-4.
188. Fredrickson, B.J., et al., Shear-dependent rolling on von Willebrand factor of mammalian cells expressing the platelet glycoprotein Ib-IX-V complex. *Blood*, 1998. **92**(10): p. 3684-93.
189. Westermaier, T., et al., Magnesium treatment for neuroprotection in ischemic diseases of the brain. *Exp Transl Stroke Med*, 2013. **5**(1): p. 6.
190. Schmid-Elsaesser, R., et al., Combination drug therapy and mild hypothermia: a promising treatment strategy for reversible, focal cerebral ischemia. *Stroke*, 1999. **30**(9): p. 1891-9.
191. Muir, K.W., New experimental and clinical data on the efficacy of pharmacological magnesium infusions in cerebral infarcts. *Magnes Res*, 1998. **11**(1): p. 43-56.
192. Iseri, L.T. and J.H. French, Magnesium: nature's physiologic calcium blocker. *Am Heart J*, 1984. **108**(1): p. 188-93.



193. Kraft, P., et al., Characterization of Peripheral Immune Cell Subsets in Patients with Acute and Chronic Cerebrovascular Disease: A Case-Control Study. *Int J Mol Sci*, 2015. **16**(10): p. 25433-49.
194. Dhalla, F., et al., Identification of a novel mutation in MAGT1 and progressive multifocal leucoencephalopathy in a 58-year-old man with XMEN disease. *J Clin Immunol*, 2015. **35**(2): p. 112-8.
195. Li, F.Y., et al., XMEN disease: a new primary immunodeficiency affecting Mg<sup>2+</sup> regulation of immunity against Epstein-Barr virus. *Blood*, 2014. **123**(14): p. 2148-52.
196. Sahni, J., Y. Song, and A.M. Scharenberg, The B. subtilis MgtE magnesium transporter can functionally compensate TRPM7-deficiency in vertebrate B-cells. *PLoS One*, 2012. **7**(9): p. e44452.
197. Harper, M.T., et al., Platelet dense granule secretion defects may obscure alpha-granule secretion mechanisms: evidence from Munc13-4-deficient platelets. *Blood*, 2015. **125**(19): p. 3034-6.
198. Gunay-Aygun, M., et al., NBEAL2 is mutated in gray platelet syndrome and is required for biogenesis of platelet alpha-granules. *Nat Genet*, 2011. **43**(8): p. 732-4.
199. Marx, G. and A. Eldor, The procoagulant effect of zinc on fibrin clot formation. *Am J Hematol*, 1985. **19**(2): p. 151-9.
200. Chubanov, V. and T. Gudermann, Trpm6. *Handbook of experimental pharmacology*, 2014. **222**: p. 503-20.
201. Fleig, A. and V. Chubanov, Trpm7. *Handbook of experimental pharmacology*, 2014. **222**: p. 521-46.
202. Middelbeek, J., et al., The alpha-kinase family: an exceptional branch on the protein kinase tree. *Cellular and molecular life sciences : CMLS*, 2010. **67**(6): p. 875-90.
203. Clark, K., et al., TRPM7 regulates myosin IIA filament stability and protein localization by heavy chain phosphorylation. *Journal of molecular biology*, 2008. **378**(4): p. 790-803.
204. Deason-Towne, F., A.L. Perraud, and C. Schmitz, Identification of Ser/Thr phosphorylation sites in the C2-domain of phospholipase C gamma 2 (PLC gamma 2) using TRPM7-kinase. *Cellular Signalling*, 2012. **24**(11): p. 2070-2075.
205. Dorovkov, M.V. and A.G. Ryazanov, Phosphorylation of annexin I by TRPM7 channel-kinase. *The Journal of biological chemistry*, 2004. **279**(49): p. 50643-6.
206. Asselin, J., et al., A collagen-like peptide stimulates tyrosine phosphorylation of syk and phospholipase C gamma2 in platelets independent of the integrin alpha2beta1. *Blood*, 1997. **89**(4): p. 1235-42.
207. Ezumi, Y., et al., Physical and functional association of the Src family kinases Fyn and Lyn with the collagen receptor glycoprotein VI-Fc receptor gamma chain complex on human platelets. *J Exp Med*, 1998. **188**(2): p. 267-76.
208. Ming, Z., et al., Lyn and PECAM-1 function as interdependent inhibitors of platelet aggregation. *Blood*, 2011. **117**(14): p. 3903-6.
209. Chari, R., et al., Lyn, PKC-delta, SHIP-1 interactions regulate GPVI-mediated platelet-dense granule secretion. *Blood*, 2009. **114**(14): p. 3056-63.
210. Runnels, L.W., L. Yue, and D.E. Clapham, TRP-PLIK, a bifunctional protein with kinase and ion channel activities. *Science*, 2001. **291**(5506): p. 1043-7.
211. Runnels, L.W., L. Yue, and D.E. Clapham, The TRPM7 channel is inactivated by PIP(2) hydrolysis. *Nature cell biology*, 2002. **4**(5): p. 329-36.

- 
212. Pozo-Guisado, E., et al., Phosphorylation of STIM1 at ERK1/2 target sites modulates store-operated calcium entry. *Journal of cell science*, 2010. **123**(Pt 18): p. 3084-93.
213. Faouzi, M., et al., The TRPM7 channel kinase regulates store-operated calcium entry. *J Physiol*, 2017. **595**(10): p. 3165-3180.
214. Zholos, A., et al., TRPM channels in the vasculature. *Advances in experimental medicine and biology*, 2011. **704**: p. 707-29.
215. Touyz, R.M., et al., Differential regulation of transient receptor potential melastatin 6 and 7 cation channels by ANG II in vascular smooth muscle cells from spontaneously hypertensive rats. *American journal of physiology. Regulatory, integrative and comparative physiology*, 2006. **290**(1): p. R73-8.
216. Levitsky, D.O. and M. Takahashi, Interplay of Ca(2+) and Mg (2+) in sodium-calcium exchanger and in other Ca(2+)-binding proteins: magnesium, watchdog that blocks each turn if able. *Advances in experimental medicine and biology*, 2013. **961**: p. 65-78.
217. Helpern, J.A., et al., Acute elevation and recovery of intracellular [Mg2+] following human focal cerebral ischemia. *Neurology*, 1993. **43**(8): p. 1577-81.
218. Vande Linde, A.M., et al., Chronic changes in the brain Mg2+ concentration after forebrain ischemia in the rat. *Metabolic brain disease*, 1991. **6**(4): p. 199-206.
219. Demougeot, C., et al., Effect of diets with different magnesium content in ischemic stroke rats. *Neuroscience letters*, 2004. **362**(1): p. 17-20.
220. Zhao, L., et al., Electroacupuncture regulates TRPM7 expression through the trkA/PI3K pathway after cerebral ischemia-reperfusion in rats. *Life sciences*, 2007. **81**(15): p. 1211-22.
221. Jiang, H., et al., TrkA pathway(s) is involved in regulation of TRPM7 expression in hippocampal neurons subjected to ischemic-reperfusion and oxygen-glucose deprivation. *Brain research bulletin*, 2008. **76**(1-2): p. 124-30.
222. Wei, W.L., et al., TRPM7 channels in hippocampal neurons detect levels of extracellular divalent cations. *Proc Natl Acad Sci U S A*, 2007. **104**(41): p. 16323-8.
223. Sun, H.S., et al., Suppression of hippocampal TRPM7 protein prevents delayed neuronal death in brain ischemia. *Nature neuroscience*, 2009. **12**(10): p. 1300-7.
224. Bae, C.Y. and H.S. Sun, TRPM7 in cerebral ischemia and potential target for drug development in stroke. *Acta pharmacologica Sinica*, 2011. **32**(6): p. 725-33.
225. Huang, H. and H.J. Vogel, Structural basis for the activation of platelet integrin alphaIIb beta3 by calcium- and integrin-binding protein 1. *J Am Chem Soc*, 2012. **134**(8): p. 3864-72.
226. Bynagari, Y.S., et al., Mechanism of activation and functional role of protein kinase Ceta in human platelets. *J Biol Chem*, 2009. **284**(20): p. 13413-21.
227. Bynagari-Settipalli, Y.S., et al., Protein kinase C isoform epsilon negatively regulates ADP-induced calcium mobilization and thromboxane generation in platelets. *Arterioscler Thromb Vasc Biol*, 2012. **32**(5): p. 1211-9.
228. Bousquet, S.M., M. Monet, and G. Boulay, Protein kinase C-dependent phosphorylation of transient receptor potential canonical 6 (TRPC6) on serine 448 causes channel inhibition. *J Biol Chem*, 2010. **285**(52): p. 40534-43.
229. Pula, G., et al., PKCdelta regulates collagen-induced platelet aggregation through inhibition of VASP-mediated filopodia formation. *Blood*, 2006. **108**(13): p. 4035-44.
230. Torres, L.M., et al., Defective translocation of PKCepsilon in EtOH-induced inhibition of Mg2+ accumulation in rat hepatocytes. *Alcohol Clin Exp Res*, 2010. **34**(9): p. 1659-69.
-

- 
231. Molee, P., et al., Up-regulation of AKAP13 and MAGT1 on cytoplasmic membrane in progressive hepatocellular carcinoma: a novel target for prognosis. *Int J Clin Exp Pathol*, 2015. **8**(9): p. 9796-811.
232. Unsworth, A.J., et al., Protein kinase Cepsilon and protein kinase Ctheta double-deficient mice have a bleeding diathesis. *J Thromb Haemost*, 2012. **10**(9): p. 1887-94.
233. Lee, E.J., et al., Delayed treatment with magnesium: reduction of brain infarction and improvement of electrophysiological recovery following transient focal cerebral ischemia in rats. *J Neurosurg*, 2005. **102**(6): p. 1085-93.
234. Izumi, Y., et al., Reduction of infarct volume by magnesium after middle cerebral artery occlusion in rats. *J Cereb Blood Flow Metab*, 1991. **11**(6): p. 1025-30.
235. Spaargaren, M., et al., The B cell antigen receptor controls integrin activity through Btk and PLCgamma2. *J Exp Med*, 2003. **198**(10): p. 1539-50.
236. Numaga, T., et al., Ca<sup>2+</sup> influx and protein scaffolding via TRPC3 sustain PKCbeta and ERK activation in B cells. *Journal of cell science*, 2010. **123**(Pt 6): p. 927-38.
237. Hu, Y., et al., Drosophila MagT1 is upregulated by PKC activation. *Biochem Biophys Res Commun*, 2013. **436**(2): p. 140-4.
238. Huang, W., et al., Increases in intracellular calcium dephosphorylate histone H3 at serine 10 in human hepatoma cells: potential role of protein phosphatase 2A-protein kinase Cbeta11 complex. *J Cell Physiol*, 2005. **205**(1): p. 37-46.
239. Keranen, L.M., E.M. Dutil, and A.C. Newton, Protein kinase C is regulated in vivo by three functionally distinct phosphorylations. *Curr Biol*, 1995. **5**(12): p. 1394-1403.
240. Song, J.S., et al., Tyrosine phosphorylation-dependent and -independent associations of protein kinase C-delta with Src family kinases in the RBL-2H3 mast cell line: regulation of Src family kinase activity by protein kinase C-delta. *Oncogene*, 1998. **16**(26): p. 3357-68.
241. Leitges, M., et al., Protein kinase C-delta is a negative regulator of antigen-induced mast cell degranulation. *Mol Cell Biol*, 2002. **22**(12): p. 3970-80.
242. Rahman, M.T. and M. De Ley, Metallothionein in human thrombocyte precursors, CD61+ megakaryocytes. *Cell biology and toxicology*, 2008. **24**(1): p. 19-25.
243. Sugiura, T. and H. Nakamura, Metallothionein in platelets. *International archives of allergy and immunology*, 1994. **103**(4): p. 341-8.
244. Heijnen, H. and P. van der Sluijs, Platelet secretory behaviour: as diverse as the granules ... or not? *J Thromb Haemost*, 2015. **13**(12): p. 2141-51.
245. Kambe, T., et al., The Physiological, Biochemical, and Molecular Roles of Zinc Transporters in Zinc Homeostasis and Metabolism. *Physiol Rev*, 2015. **95**(3): p. 749-84.
246. Swieringa, F., et al., Rate-limiting roles of the tenase complex of factors VIII and IX in platelet procoagulant activity and formation of platelet-fibrin thrombi under flow. *Haematologica*, 2015. **100**(6): p. 748-56.

## 6. Appendix

### 6.1 List of abbreviations

Arachidonic acid	AA
Acid-citrate-dextrose	ACD
Adenosine diphosphate	ADP
Adenosine triphosphate	ATP
Bone marrow chimeric	BM
Bovine serum albumin	BSA
Carboxyfluorescein succinimidyl ester	CFSE
Collagen-related peptide	CRP
Convulxin	Cvx
C-type lectin-like receptor 2	CLEC-2
Cytosolic free calcium concentration	$[Ca^{2+}]_i$
Cytosolic free magnesium concentration	$[Mg^{2+}]_i$
Cytosolic free zinc concentration	$[Zn^{2+}]_i$
Cytotoxic T cells	CTLs
Diacylglycerol	DAG
Epstein-Barr virus	EBV
G protein coupled receptor	GPCR
Glycoprotein VI	GPVI
Inositol 1,4,5-trisphosphate	IP <sub>3</sub>
Immunoreceptor tyrosine-based activation motif	ITAM
Immunoreceptor tyrosine-based inhibition motif	ITIM
Inositol-1,4,5-trisphosphate	IP <sub>3</sub>
Inductively coupled plasma mass spectrometry	ICP-MS
IP <sub>3</sub> receptor	IP <sub>3</sub> R
Linker for activation of T cells	LAT
Megakaryocytes	MKs
Magnesium transporter 1	MAGT1
Natural killer	NK
N,N,N',N'-tetrakis 2-pyridinylmethyl-1,2-ethanediamine	TPEN
Protease-activated receptor	PAR
Protein kinase C	PKC
Phospholipase C	PLC
Phosphate-buffered saline	PBS
Platelet endothelial cell adhesion molecule	PECAM

---

Platelet-rich plasma	PRP
Phosphatidylinositol-4, 5-bisphosphate	PIP <sub>2</sub>
Store-operated calcium entry	SOCE
Receptor-operated calcium entry	ROCE
Rhodocytin	RC
Room temperature	RT
Storage pool disease	SPD
Stromal interaction molecule 1	STIM1
Serotonin	5-HT
Sarco/endoplasmic reticulum Ca <sup>2+</sup> -ATPase	SERCA
Src family kinase	SFK
Spleen tyrosine kinase	Syk
Src family kinase	SFK
T cell receptor	TCR
Transient middle cerebral artery occlusion	tMCAO
Thromboxane A <sub>2</sub>	TXA <sub>2</sub>
Thromboxane B <sub>2</sub>	TXB <sub>2</sub>
Thromboxane receptor	TP
Thapsigargin	TG
Transient receptor potential nelastatin-like 7 channel	TRPM7
<i>WT</i>	Wild type
X-linked immunodeficiency with magnesium defect, Epstein-Barr virus infection, and neoplasia syndrome	XMEN

## 6.2 Publications

### 6.2.1 Original articles

**Gotru SK**, Chen W, Kraft P, Becker I, Wolf K, Stritt S, Zierler S, Hermanns H.M, Rao D, Perraud AL, Schmitz C, Zahedi R, Noy PJ, Tomlinson MG, Dandekar T, Matsushita M, Chubanov V, Gudermann T, Stoll G, Nieswandt B, Braun A. TRPM7 kinase controls calcium responses in arterial thrombosis and stroke in mice. *Arteriosclerosis, Thrombosis, and Vascular Biology*. 2017.

**Gotru SK<sup>#</sup>**, Gil-Pulido J<sup>#</sup>, Beyersdorf N, Diefenbach A, Becker I, Remer K, Chubanov V, Gudermann T, Nieswandt B, Kerkau T, Zerneck A, and Braun A. Imbalanced cation homeostasis in MAGT1 deficient B cells dysregulates B cell development and signaling in mice. *Journal of Immunology*, 2017.

**Gotru SK**, Schuhmann M, Beyersdorf N, Kerkau T, Wolf K, Kraft P, Herterich S, Vögtle T, Becker I, Stritt S, Remer K, Zierler S, Chubanov V, Gudermann T, Heemskerk JW, Stoll G, Nieswandt B and Braun A. Impaired crosstalk between MAGT1 and TRPC6 accelerates thrombosis and stroke in mice. **(Manuscript in preparation)**.

**Gotru SK<sup>\*</sup>**, van Geffen JP<sup>\*</sup>, Nagy M, Eilenberger J, Manukjan G, Schulze H, Eber S, Schambeck C, Deppermann C, Mammadova-Bach E, Nurden P, Greinacher A, Sachs U, Nieswandt B, Hermanns HM, Heemskerk JH, and Braun A. Defective Zn<sup>2+</sup> homeostasis of human and mouse platelets with  $\alpha$ - and  $\delta$ -storage pool disorders. **(Manuscript in preparation)**.

**Gotru SK**, Schuhmann M, Wolf K, Chubanov V, Gudermann T, Stoll G, Nieswandt B, and Braun A. Genetic depletion of TRPM7 in mouse platelets dysregulates cation homeostasis without altering thrombosis and stroke development in mice. **(Manuscript in preparation)**.

Stritt S, Nurden P, Favier R, Favier M, Ferioli S, **Gotru SK**, van Eeuwijk JM, Schulze H, Nurden AT, Lambert MP, Turro E, Burger-Stritt S, Matsushita M, Mittermeier L, Ballerini P, Zierler S, Laffan MA, Chubanov V, Gudermann T, Nieswandt B, and Braun A. Defects in TRPM7 channel function deregulate thrombopoiesis through altered cellular Mg<sup>2+</sup> homeostasis and cytoskeletal architecture. *Nature Communications*, 2016.

Wolf K, Braun A, Haining EJ, Tseng YL, Kraft P, Schuhmann MK, **Gotru SK**, Chen W, Hermanns HM, Stoll G, Lesch KP, Nieswandt B. Partially defective store-operated calcium entry and hem(ITAM) signaling in platelets of serotonin transporter deficient mice. *PLoS One*, 2016.

### 6.2.2 Oral presentations

Defective  $Mg^{2+}$  transport enhances  $Ca^{2+}$  responses in B cells and platelets thereby accelerating immunothrombotic effects in mice - Gesellschaft für Thrombose- und Hämostaseforschung (GTH) 2018, Vienna, Austria.

Defective  $Zn^{2+}$  homeostasis of human and mouse platelets in storage pool disorders - Gesellschaft für Thrombose- und Hämostaseforschung (GTH) 2018, Vienna, Austria.

Defects in TRPM7 function result in abnormal  $Ca^{2+}$  dependent platelet signaling in mice. - European Congress on Thrombosis and Haemostasis (ECTH) 2016, The Hague, the Netherlands.

Genetic ablation of TRPM7 induces multiple defects in platelet activation. - Gesellschaft für Thrombose- und Hämostaseforschung (GTH) 2016, Münster, Germany.

Magnesium transporter MAGT1 plays a critical role in thrombo-inflammatory diseases and hemostasis in mice. - International Society on Thrombosis and Haemostasis (ISTH) 2015, Toronto, Canada.

Magnesium transporter Magt1 is a key regulator of thrombus formation and ischemic stroke in mice. - Gesellschaft für Thrombose - und Hämostaseforschung (GTH) 2015, Düsseldorf, Germany.

### 6.2.3 Poster presentations

Defective magnesium transport enhances receptor-operated calcium entry in platelets thereby accelerating thrombosis and stroke. - European Congress on Thrombosis and Haemostasis (ECTH) 2016, The Hague, the Netherlands.

Magnesium transporter MAGT1 plays a critical role in thrombo-inflammatory diseases and hemostasis in mice. - Mosbacher Kolloquim 2015, Mosbach, Germany.

The role of magnesium transporter MagT1 in murine platelets. - Gesellschaft für Thrombose- und Hämostaseforschung (GTH) 2014, Vienna, Austria.

### 6.3 Acknowledgement

I take the opportunity to thank my Ph.D. supervisor Dr. Attila Braun for the opportunity to work on his projects, which are funded by the Sonderforschungsbereich 688 (SFB 688), Teilprojekt (TP) A18. As an active member of this scientific network, I received his permanent support, guidance, feedback and positive criticism. Without our collaboration partners within the SFB

688 (Bernhard Nieswandt TP A1, Thomas Dandekar TP A2, Thomas Kerkau TP A10, Alma Zerneck TP A12, Heike Hermanns TP A20, Harald Schulze TP A21 and Guido Stoll TP B1), the achievements during my Ph.D. would not have been possible. I also thank Dr. Vladimir Chubanov and Prof. Thomas Gudermann who supported the TRPM7 projects with materials, animals, technics and regular scientific discussions (Walther-Straub-Institut für Pharmakologie und Toxikologie, Munich).

I also take the opportunity to thank my primary supervisor Prof. Dr. Bernhard Nieswandt, for providing excellent feedback during the annual Ph.D. meetings, group meetings, and institute retreats. I thank each member of his group for providing a good working environment. Here, I would especially thank Dr. Simon Stritt for his active contribution in some projects and his extensive help in various other scientific areas. I like to thank our technician Birgit Midloch for mouse genotyping. I would also like to thank Ms. Isabelle Becker and Ms. Katja Aurbach for proofreading this thesis.

I would like to thank the other members of my Ph.D. committee, Prof. Dr. Guido Stoll, from the Department of Neurology, University of Würzburg, Germany, for his excellent feedback during the annual Ph.D. meetings, and for the stroke experiments. Prof. Dr. Johan W. M. Heemskerk, from the Department of Biochemistry, CARIM, Maastricht University, the Netherlands for providing extensive scientific support in various projects and allowing an active collaboration in some projects. I also thank him for providing excellent feedback in the annual Ph.D. meetings. I thank PD Dr. rer. nat. Heike Hermanns, from the Medizinische Klinik und Poliklinik II, Hepatologie Departement, University Hospital, Würzburg, Germany, for providing extensive support, active contribution in few projects and excellent feedback in the annual Ph.D. meetings.

I would also like to thank Prof. Dr. Katrin Heinze for giving the permission, and her Expert Engineers Mr. Mike Friedrich and Mr. Oğuzhan Angay, for the excellent training to use the imaging facility at the Rudolf Virchow Center, University of Würzburg, Germany.

I thank Prof. Dr. Harald Schulze (Würzburg, Germany), Prof. Dr. Ulrich Sachs (Gießen, Germany), Prof. Dr. med. Andreas Greinacher (Greifswald, Germany) and Prof. Dr. med. Stefan Eber (München, Germany) for providing support, human blood samples and the associated clinical data as part of a collaborative project.

I also take the opportunity to thank Prof. Dr. med. Thomas Kerkau, from the Institute for Virology and Immunobiology, the University of Würzburg for providing necessary equipment and resources to carry out part of the research in my Ph.D. Here, I would like to especially thank PD. Dr. med. Niklas Beyersdorf and his technician Mrs. Sandra Werner for extensive support and active contribution. I would also like to thank Prof. Dr. med. Alma Zerneck-



Madsen, from the Institut für Experimentelle Biomedizin Lehrstuhl II, Universitätsklinikum Würzburg, Germany for providing necessary equipment and resources to carry out part of the research in my Ph.D. Here, I would like to thank Mr. Jesus Gil-Pulido for being an active collaborator in one of the projects. A special thanks to the Graduate School of Life Sciences (GSLs) for organizing various courses and for the financial support to actively participate in scientific conferences on multiple occasions. Finally, I thank my family for the constant support and encouragement during the time of my Ph.D.

## 6.4 Curriculum Vitae

### Education

2012 – Present	<p>Doctoral thesis for Dr. rer. nat. in Biomedical research</p> <p>Theme: Cation homeostasis in platelets in thrombosis and stroke Institute</p> <p>for Experimental Biomedicine/Rudolf Virchow Center, University of Wuerzburg, Germany</p>
2010 – 2012	<p>M. Sc. Agrobiotechnology</p> <p>Justus-Liebig-University, Giessen, Germany</p>
2004 – 2008	<p>B. Tech. (Engineering) in Biotechnology</p> <p>SRM University, Chennai, India</p>
2000 – 2002	<p>Intermediate (Abitur-Equivalent)</p> <p>Board of Intermediate Education, A.P. State Govt., India</p>



### Practical experience

11/2009 - 08/2010	<p>Master thesis: Epithelial-mesenchymal transition (EMT) in cancer progression and its governance by tumor stroma,</p> <p>Max Planck Institute for Heart and Lung Research, Bad Nauheim, Germany</p>
01/2008	<p>Quality control internship at Aurobindo Pharma Ltd., Visakhapatnam, India</p>

### Technical skills

- Biochemical and functional characterization of megakaryocytes, platelets and immune cells
- Immunoblotting, platelet and immune cell isolation, adhesion and activation assays under static and flow conditions, platelet aggregation assays, ELISA, Flow Cytometry (FACS Canto and FACS Calibur)
- Divalent cation flux measurements using fluorescent dyes
- Histological and anatomic characterization of tissues
- Confocal microscopy (SP5), Transmission electron microscopy (TEM)
- MS Office, GraphPad Prism, SigmaPlot, Fiji and Imaris (Image analysis)

### Awards

2015	<p>Young Investigator Award – International Society on Thrombosis and Haemostasis (ISTH)</p>
2014, 2015, 2016	<p>Travel fellowship – Graduate School of Life Sciences (GSLs), Wuerzburg, Germany</p>

**Conferences**

- 2014-2018 Gesellschaft für Thrombose und Hämostaseforschung (GTH) conferences across Europe – oral and poster presentations
- 2015 International Society on Thrombosis and Haemostasis (ISTH) conference, Toronto, Canada, oral presentation
- 2016 European Congress on Thrombosis and Haemostasis (ECTH) conference, The Hague, The Netherlands, oral and poster presentation

**Membership**

- 2014-2016 International Society on Thrombosis and Haemostasis (ISTH)
- 2014-2016 Gesellschaft für Biochemie und Molekularbiologie (GBM)

**Personal details**

- Name Sanjeev Kiran Gotru
- Date of birth 21.05.1985
- Current position Doctoral candidate in Biomedical Research
- Residence Permit Niederlassungserlaubnis (Germany)
- Languages Deutsch (B2), English (Bilingual), Hindi (C2), Tamil (C2),  
Telugu (Mother tongue)
- Telephone +49 (0)152 21862783
- E-Mail sanjeevkiran\_21@yahoo.co.in

**6.5 Affidavit**

I hereby confirm that my thesis entitled "Cation homeostasis in platelets" is the result of my research work, unless otherwise stated collaboratively. I did not receive any help from commercial consultants.

This thesis has not been presented at any other University or commercial body as it stays here or in similar form.

Würzburg

Date

Signature

**6.6 Eidesstattliche Erklärung**

Ich bestätige hiermit, dass meine Dissertation mit dem Titel "Cation homeostasis in platelets" das Ergebnis meiner Forschungsarbeit ist, sofern nicht anders angegeben. Ich habe keine Hilfe von kommerziellen Beratern erhalten.

Diese These wurde an keiner anderen Universität oder Handelsstelle präsentiert, da sie hier oder in ähnlicher Form vorliegt.

Würzburg

Datum

Unterschrift